Acid-Catalyzed Reactions for the Production of Platform Chemicals from Cellulosic Biomass in Liquid Phase Systems

By

Ronen Weingarten

A dissertation submitted in partial fulfillment of

the requirements for the degree of

Doctor of Philosophy

(Chemical Engineering)

at the

UNIVERSITY OF WISCONSIN-MADISON

2014

Date of final oral examination: March 31, 2014

The dissertation is approved by the following members of the Final Oral committee:

George W. Huber, Professor, Chemical Engineering
James A. Dumesic, Professor, Chemical Engineering
Manos Mavrikakis, Professor, Chemical Engineering
Christos T. Maravelias, Associate Professor, Chemical Engineering
Shannon S. Stahl, Professor, Chemistry

To my beloved wife, Dorit, and our two little angels, Eitan and Adam

יפה שלי, אני אסיר תודה על כל ההקרבות במשך השנים האלה. אוהב אותך עד השמיים, נשמה...

ACKNOWLEDGMENTS

I am indebted to several people who have taken part in this journey with me through graduate school. First and foremost, none of this would be possible without the love and support of my family. I owe everything to my wife, Dorit, who has sacrificed so much the last six years to help me fulfill my dreams. Now words can describe how much I love you! Thank you for being a wonderful wife and best friend. Thank you for giving me the greatest gift of all, which is becoming a father to our two boys, Eitan and Adam, who are without a doubt my two best accomplishments in my graduate school career.

I would like to thank my parents and sisters for their love and support and for reminding me what is important in life. Mom, thank you for your never-ending love and positive attitude towards life, two attributes which have molded me to the person I am today. Dad, thank you for pushing me to excel all those years and for showing me between right and wrong. I strive to be as good of a father as you are to us. Einab and Liat, thank you for always being around (even when I was a little distant) and for being the best aunties ever. Special thanks to my extended family in Israel, especially my in-laws Rachel and Nelo, for all their love and support and for letting their daughter fly halfway across the world to be with me. I truly couldn't have asked for a better extended family. I also dedicate this degree to Sabta who sadly passed away in 2010. You will always be in my heart.

I am by and large indebted to my advisor, Professor George W. Huber, for his guidance throughout all the years and for being a wonderful mentor and friend. In particular, I will remember his renowned phrase: "So, what have you learned today?" His motto has motivated me to learn something new every day and I thank him for that. Thank you for showing me how

to set new trends in research and not be a follower. Most of all, thank you for always letting me put my family first. I am also very thankful to Professor Curt Conner, Jr. who served as my co-advisor at UMass Amherst. His sincere character and unique drive for research will always be embedded in my memory. I also enjoyed the spur-of-the-moment barbecues and croquet on Friday afternoons next to Goessmann.

I would like to thank past and present members of the Huber group for making every day in the lab an enjoyable one. It was a pleasure working alongside such a devoted group of people day in and day out. I would like to especially thank all the collaborators who made this research possible. They include: Dr. Joungmo Cho, Dr. Geoffrey A. Tompsett, Dr. Rong Xing, Dr. Wenqin Shen, Dr. Ayyagari V. Subrahmanyam (Subbu) and Dr. Yong Tae Kim. I thank them all for their thoughtful discussions and great friendships. The move to Madison was quite an adventure, and it wouldn't have been possible without the effort of the original Huber group (Ani, Chris, Pranav, Yong, Jechan and Hyung Ju). This whole experience definitely brought us closer together as friends.

I would like to thank the members of my thesis committee for their guidance and suggestions in completing my degree. A special thanks to Professor James A. Dumesic with whom I was able to collaborate before graduating. It was a very humbling experience working with such a pioneer in this field.

I am extremely grateful to the entire faculty and staff in the Chemical Engineering Department at UMass Amherst for making the first four years of graduate school so memorable. In particular, I would like to thank the Department Head, Professor T.J. (Lakis) Mountziaris, for his warm welcome to the department and for being so humble. I would also like to express my

deep appreciation to Gary Czupkiewicz and Joseph Smith for their help during senior lab and their relentless technical assistance whenever we needed them in the research labs. Many thanks to Marie Wallace and Sheilagh Hanley for their tireless help, especially prior to our move to Madison.

Accordingly, I would also like to express my deepest gratitude to the faculty and staff in the Department of Chemical and Biological Engineering at UW-Madison for welcoming us with open arms. Special thanks go to Professor Sean P. Palecek, Andrew Greenberg, Christi Balas Levenson, Kathy Heinzen, Heidi Udelhoven, Roger Packard, Joel Lord and Eric Codner for easing the transition to the department. Many thanks to Michelle McCrumb and Beth Brandl for being so friendly and helpful. I would also like to acknowledge help from Bill Goebel from the Chemistry Department for his technical support.

Finally, I am extremely grateful for all the special friendships that I have made throughout the years from Amherst and Madison. Special thanks to the Lesmes Family who became like our family during our stay in Amherst. Your lasting friendship throughout the years has been unsurpassable and we are truly thankful. Many special thanks to Hakan Olcay and Gonca Şeber for their close and long lasting friendship. Thank you to all the Israeli couples who made it feel more like home.

The research projects presented in this thesis were supported by grants from NSF-CBET (Grant # 0756663) and NSF MRI (Grant # 0722802). A part of this research was also supported as part of the Institute for Atom-efficient Chemical Transformations (IACT), an Energy Frontier Research Center funded by the US Department of Energy, Office of Science, Office of Basic Energy Sciences. I gratefully acknowledge financial support from these funding agencies.

TABLE OF CONTENTS

LIST OF TABLES

Table **Page**

LIST OF FIGURES AND SCHEMES

Figure **Page**

ABSTRACT

Acid catalysts are used in many applications focused on biomass conversion. Liquid phase processing serves as one of the primary routes to produce platform chemicals from cellulosic biomass. However, there are still many challenges to overcome before commercialization of these processes can be realized. The fundamental challenge with producing products by acid catalyzed reactions is that undesired carbonaceous species (*i.e.* humins) form by both parallel and series reactions, which limit the selectivity to desired products.

The goal of this research is to study the fundamental acid-catalyzed chemistry to produce biomass-derived platform chemicals in liquid phase systems. We use an integrated approach that includes: (1) understanding the fundamental chemistry and reaction pathways through kinetic studies with homogeneous acid catalysts and (2) elucidating the relationship between the properties of solid acid catalysts and their correlation with activity and selectivity of acid catalyzed reactions.

We have developed kinetic models for the aqueous phase production of furfural and hydroxymethylfurfural (HMF) from xylose and glucose respectively using homogeneous catalysts. The dehydration chemistry to form these furanic derivatives from carbohydrates is distinguished by a relatively high activation energy step (*ca.* 120-160 kJ mol^{-1}). Undesired humins also form, which typically have lower activation barriers (*i.e.* 50-70 kJ mol^{-1}). Accordingly, a higher selectivity to furfural and HMF is obtained at increased temperatures and relatively short reaction times. HMF and furfural selectivity can also be improved by using a biphasic regime to extract the desired products before they undergo further degradation

reactions. According to our kinetic model, we estimate that furfural yields in a biphasic system can reach 85%, whereas at these same conditions in a monophase aqueous system furfural yields are only 30%.

Product selectivity can also be tuned by altering the Brønsted to Lewis acid site ratio of the acid catalysts. We examined the role of Lewis and Brønsted sites of acid catalysts for the dehydration of xylose and glucose in aqueous media. Lewis acid sites decrease furfural and HMF selectivity, as they mainly catalyze the formation of isomerization byproducts and humins. Brønsted acid sites catalyze the dehydration step to produce furfural and HMF. These findings are true for both heterogeneous and homogeneous catalysts. Catalysts with high Brønsted to Lewis acid ratios, such as zirconium phosphate (ZrP) and Amberlyst 70 (ion resin), exhibit furfural selectivities as much as 30 times higher than catalysts with higher Lewis acid site concentrations.

In our studies of levulinic acid production from glucose with solid acid metal(IV) phosphate catalysts, we show that the Brønsted to Lewis acid site ratio can be controlled by the adjusting the metal(IV) oxide to phosphorus ratio. Zirconium phosphate (ZrP) has a higher concentration of total acid sites and Brønsted acid sites compared to tin phosphate (SnP). ZrP with a P/Zr molar ratio of 2 is favorable for levulinic acid production due to its inherently high surface area and enhanced Brønsted acidity. Solid-state NMR spectroscopy reveals that ZrP has four different phosphate species, with polyphosphates being the predominant species. The three other species are comprised of tetrahedral phosphates bonded to zirconia and hydroxyl groups at varying ratios.

We have also discovered that HMF can selectively be produced from cellulose under mild reaction conditions in polar aprotic solvents (*i.e.* tetrahydrofuran) without the presence of water. This pathway goes through a levoglucosan intermediate. With high concentrations of water in the system the levoglucosan will hydrolyze to produce glucose. In contrast, at low water concentrations the levoglucosan will undergo dehydration to produce HMF. The turnover frequency for cellulose conversion increases as the water content in the solvent decreases, with conversion rates in tetrahydrofuran being more than twenty times higher than those in water. We believe that the acid sites are stabilized in an aprotic solvent to a less extent than in water, leading to higher reactivity of the acid proton. The highest HMF yield from cellulose we obtained was 44%, which is comparable to yields obtained in ionic liquids or biphasic systems.

CHAPTER 1

Introduction

A worldwide initiative has been set forth to decrease our dependence on petroleum-based fuels and develop new renewable sources of energy. Particularly, the use of agricultural and forest residues and other lignocellulosic crops is a viable option compared to first generation biomass, which demonstrate several drawbacks including competition with food crops and water.[1] Lignocellulosic biomass is a renewable feedstock that has received considerable attention as a sustainable alternative for the production of fuels and chemicals.[2-11] In contrast to other renewable energies, biomass is the only renewable source of fixed carbon, which is essential for the production of liquid hydrocarbon fuels and chemicals.[12-14]

The production of biomass-derived fuels and chemicals calls for the defunctionalization of highly oxygenated compounds which make up lignocellulosic biomass. Hence, the transformation of biomass to fuels primarily calls for the decrease of the effective oxygen to carbon molar ratio. The initial step in liquid-phase biomass upgrading is often hydrolysis, which suffers from relatively poor selectivity. The major challenge in the commercialization of cellulosic fuels and chemicals is the development of efficient technologies to attain high product selectivity and improve carbon balances. This in turn will facilitate the overall objective to achieve process sustainability and convert high volumes of biomass feedstock to displace crude oil as the primary source of fuels.[15]

Further improvement of conversion and selectivity by liquid phase processing is essential to overcome these challenges. Acid catalysts play fundamental roles in many applications focused on biomass upgrading and promising results have already been obtained with homogeneous acid catalysts.[16] Nevertheless, due to their economic and environmental *via*bility,

it would be desirable to obtain solid acid catalysts that exhibit activities and selectivities at least comparable to their homogeneous counterparts.

As the major component of lignocellulosic biomass (40-80 wt%[12]), cellulose offers great potential as a model compound for the production of renewable fuels and commodity chemicals. Compared to hemicellulose and lignin, cellulose is more difficult to decompose due to its ordered crystalline structure consisting of glucose monomer units joined together *via* β-1,4-glycosidic bonds. Its recalcitrant nature is increased by intramolecular and intermolecular hydrogen bonding networks. With that being said, cellulose can be subjected to various thermochemical techniques to promote decomposition, including hydrolysis with homogeneous and solid acid catalysts to produce soluble sugars.[17-19] Pang *et al.* reported a glucose yield as high as 74.5% from cellulose over sulfonated carbons at 150 °C for 24 h with a feedstock concentration of 1 wt%.[20] Luterbacher *et al.* recently published a study on the production of soluble carbohydrates from cellulosic biomass at high yields (70 to 90%) in a solvent mixture of biomass-derived γ-valerolactone (GVL), water, and dilute acid (0.05 wt% H_2SO_4).[16]

In addition, the use of ionic liquids as solvents for cellulose decomposition has recently received much attention due to their solvation capabilities. Bell and co-workers have done extensive work on this topic including kinetic and thermodynamic studies of cellulose solvation and decomposition in ionic liquids such as 1-butyl-3-methylimidazolium chloride.[21-23] Binder and Raines developed a process to convert cellulose and biomass to glucose at yields as high as 90% in mixtures of an ionic liquid and water with HCl.[24] Nevertheless, many challenges still remain that hinder the potential application of ionic liquids in industrial settings. Relative low

cellulose solubility, high costs, recovery and reuse are currently the major drawbacks of using ionic liquids.[25, 26]

Acid-catalyzed aqueous phase reactions including hydrolysis and dehydration have been the focal point of many research studies in the recent years.[10, 27] Using water as the reaction solvent is particularly promising due to the inherently large amounts of water found in cellulosic biomass. Hydrolysis of cellulose and hemicellulose lead to the formation of monosaccharides. The acid-catalyzed dehydration of these monomers including pentoses and hexoses leads to the formation of 2-furancarboxaldehyde (furfural) and 5-hydroxymethylfurfural (HMF) respectively. It has been shown that these furanic derivatives can serve as intermediates for production of liquid alkanes and other furan-based chemicals.[5, 28-33] Dehydration reactions have also been shown to play vital roles in liquid phase catalytic processing and aqueous-phase reforming to produce jet and diesel fuel range alkanes from biomass-derived oxygenated hydrocarbons.[4, 12, 34, 35]

Scheme 1 shows the overall reaction pathways to produce platform chemicals from cellulosic biomass with acid catalysts in liquid phase systems. The challenge is to selectively produce furfural and HMF at high sugar conversions, as undesirable oligomerization reactions can occur which lead to humin formation. Several approaches have been suggested to increase product selectivity. These include reactions in non-aqueous media to prevent subsequent rehydration reactions, mixed solvent systems and novel catalytic systems. A review has been written by Corma *et al.* reporting the various catalytic systems and processes available for dehydration reactions.[14]

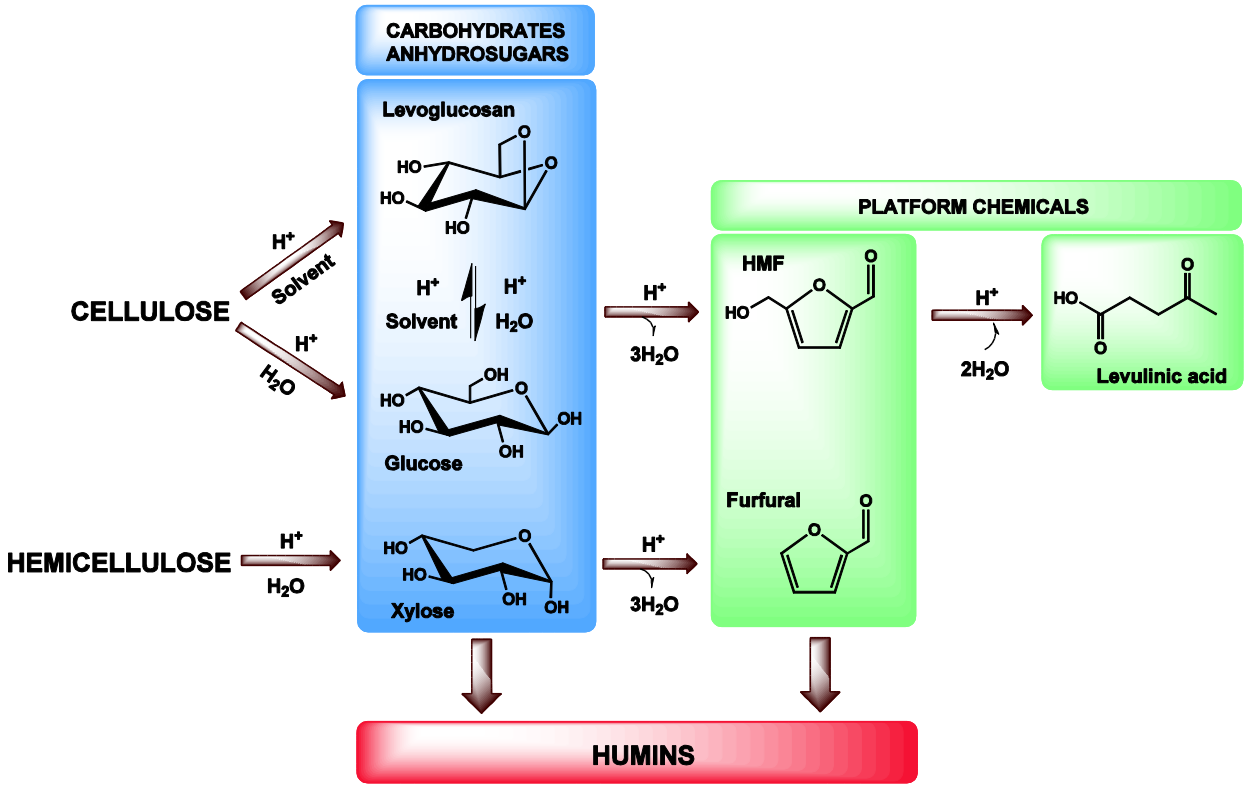

Scheme 1. Reaction scheme for the acid-catalyzed conversion of cellulosic biomass to produce platform chemicals in liquid phase systems.

Furfural is a renewable biochemical produced from lignocellulosic biomass that has many different uses. It is considered an excellent solvent for many organic materials, such as resins and polymers. It is also a precursor to other desired compounds such as furfuryl alcohol (*via* hydrogenation), furan (*via* decarbonylation) and tetrahydrofuran (*via* hydrogenation of furan).[36] Likewise, it can serve as the starting material for the production of HMF (by way of hydroxymethylation with formaldehyde).[37] A comprehensive assessment of the various applications for furfural was published by Bir Sain *et al.*[38] Furfural can also be used as a feedstock to make gasoline, diesel or jet fuel. Huber *et al.* showed that furfural can serve as a precursor for production of liquid alkanes.[39] It has also been shown that methyl-tetrahydrofuran

(MTHF, produced from hydrogenation of furfural) can directly serve as a gasoline blendstock.[40] The US-DOE has approved MTHF as a component of P Series type fuels.[12]

Furfural was first produced industrially in the beginning of the twentieth century by the Quaker Oats Company.[36] Today commercially, furfural is produced in an energy intensive process using batch or continuous reactors with a mineral acid (*i.e.* sulfuric acid) serving as the reaction catalyst.[36] Current production of furfural uses high pressure steam to heat the reaction. The steam also serves as an extractant to continuously remove the furfural from the reaction media. Downstream, the furfural-water vapor mixture is condensed and fed through a stripping column to form a furfural-rich vapor mixture which is then condensed. Due to the limited solubility of furfural in water (8.3% at 20 °C)[36], phase splitting occurs and the furfural-rich lower phase is separated in a decanter. Further dehydration and distillation take place to purify the commercial product. The water-rich upper layer is recycled from the decanter back to the stripper column as reflux. It is highly likely that furfural demand will continue to grow as the price of petroleum based feedstocks continues to rise.

HMF is an alternative nonpetroleum precursor which can be used as a building block chemical for the production of various high-volume organic chemicals with numerous potential industrial applications.[41] Its versatility is attributed to its unique chemical structure consisting of hydroxyl and aldehyde functional groups situated symmetrically in the 2,5 positions on the molecule. As a result, HMF can serve as a precursor to an array of 2,5-disubstituted furan derivatives. These include 2,5-furandicarboxylic acid (FDCA) which can serve as a precursor in the polymer industry[42], and 2,5-dimethylfuran (DMF) which can be used as a liquid

transportation fuel.[30, 43, 44] DMF can also be used to produce *p*-xylene *via* cycloaddition with ethylene combined with dehydration over acidic zeolites and acidic oxides.[45-49] Alamillo *et al.* have shown quantitative yields of 2,5-di-hydroxy-methyl-tetrahydrofuran (DHMTHF) from HMF with ruthenium-supported oxide catalysts.[50] Huber *et al.* showed that distillate range liquid alkanes (ranging from C_7 to C_{15}) can be produced from HMF.[39] In aqueous systems, HMF is readily converted to levulinic acid and formic acid *via* rehydration.

Levulinic acid is also a versatile building block which for decades has been considered a basic chemical raw material thanks to its high chemical reactivity.[51] This unique feature is attributed to its two highly reactive keto and carboxyl groups. This renewable biochemical can be used as a platform for the production of various high-volume organic chemicals with numerous potential industrial applications.[52] For example, levulinic acid can serve as a feedstock for the production of transportation fuels (gasoline and diesel). Esterification of levulinic acid with C_1-C_2 alcohols produces levulinic esters which can be used as diesel additives.[15] Elliott and Frye have also shown that levulinic acid can be hydrogenated in the presence of a bifunctional catalyst to produce MTHF in one step at relatively high yields.[53]

The increased relevance of levulinic acid is in part due to its potential capability to serve as a biobased chemical intermediate to produce fuels *via* conventional petrochemical technology.[54] Levulinic acid can be converted into GVL *via* hydrogenation with molecular hydrogen or formic acid.[55, 56] GVL has been shown to be a sustainable liquid transportation fuel suitable of replacing ethanol in gasoline-ethanol blends.[57] Lange *et al.* have shown that continued hydrogenation of GVL produces valeric acid which can be esterified with alcohols to produce a new class of cellulosic transportation fuels, “valeric biofuels”.[58] Blends of these

valeric esters with gasoline have showed promising results in engine testing. Dumesic and co-workers have developed an integrated catalytic process to convert GVL to liquid alkenes (ranging from C_8 to C_{24}) which could be blended with gasoline or jet fuels.[59] Butene and carbon dioxide are initially produced by decarboxylation of the GVL. The products are then fed to an oligomerization reactor where butene monomers are coupled to form condensable alkenes. A comprehensive review of levulinic acid applications is given by Alonso *et al.*[9]

The formation of levulinic acid from carbohydrates consists of a series of consecutive reactions, which includes a hexose triple dehydration step to produce 5-hydroxymethylfurfural (HMF) and the rehydration of HMF with two molecules of water to produce levulinic acid and formic acid. Furfuryl alcohol, a product of hemicellulose depolymerization and hydrogenation, can also serve as an alternative source of levulinic acid.[60] Levulinic acid production greater than 80% can be achieved from conversion of aqueous solutions of furfuryl alcohol with hydrochloric acid.[61] Extensive studies have been reported on the conversion of biomass feedstock to levulinic acid using homogeneous catalysts, including mineral acids and metal chlorides.[62-66] An overview of levulinic acid synthesis using various feedstocks and acid catalysts is given by Girisuta,[67] as well as by Rackemann and Doherty.[68]

The overall objective of this research is to better understand the fundamental reactions and chemistry for acid-catalyzed reactions for the production of platform chemicals from biomass-derived feedstocks in liquid phase systems. The following chapters will lay the groundwork to better understand some of the main challenges that are faced in biomass upgrading. These fundamental studies will set the stage to further improve the low product selectivity to biomass-derived platform chemicals, which is currently one of the impeding factors

to commercialize these processes. This research combines the following disciplines: reaction kinetic studies; detailed characterization and testing of solid acid catalysts; reaction engineering and conceptual process design. This unique combination will allow us to uncover the most proficient means of converting renewable feedstocks to target chemicals in liquid phase systems.

SECTION I: AQUEOUS PHASE FURFURAL STUDIES

CHAPTER 2

Furfural kinetics in a biphasic reaction system

Weingarten, R.; Cho, J.; Conner, W. C.; Huber, G. W., Kinetics of Furfural Production by Dehydration of Xylose in a Biphasic Reactor with Microwave Heating. *Green Chemistry* **2010,** *12* (8), 1423-1429

2.1. Background

The objective of this study was to develop a kinetic model for the dehydration of xylose to furfural in a biphasic reactor system heated with microwave energy. Methyl isobutyl ketone (MIBK) was chosen as the extracting solvent. There are four key steps in our kinetic model: (1) xylose dehydration to form furfural; (2) furfural reaction to form degradation products; (3) furfural reaction with xylose to form degradation products, and (4) mass transfer of furfural from the aqueous phase into the organic phase. We use our model to describe the optimal reaction conditions for furfural production from xylose.

A number of kinetic studies on the production of furfural from xylose dehydration have appeared in the literature. The undesired products produced as a byproduct with furfural are humins, which are a solid carbonaceous species.[69-72] Product furfural yields in industrial batch processes are between 45% and 50% due to formation of degradation products like humins.[73] It has been proposed that the humins are produced by a reaction between furfural and xylose.[74]

Several studies have suggested ways to inhibit the formation of humins and subsequently increase the furfural yield. One approach is to selectively extract the furfural from the aqueous solution into an organic phase. This technique has been reported to be the most promising in terms of yield and flexibility.[75] Trimble and Dunlop[76] originated this concept using ethyl acetate as the extracting media. Subsequent research included studies on various organic solvents such as MIBK.[77-79] Alternatives to organic solvents have been studied as well, such as supercritical carbon dioxide.[80] Dumesic and co-workers have shown viable promise in using a biphasic system.[29, 31] They have demonstrated this concept with a variety of feedstocks, high feedstock concentration, and recycling of organic phase.

Similarly, they have shown that applying a low-boiling solvent system, such as MIBK, is energetically more advantageous.

It has also been suggested that microwave heating may increase the yield of dehydration products from carbohydrates.[81, 82] Microwave-assisted organic synthesis was introduced nearly 30 years ago by Gedye *et al.*[83] This alternative heating method offers a means of rapid and efficient heating which minimizes temperature gradients within the reaction sample due to selective heating of the reaction media. In turn, microwave irradiation can result in accelerated reaction rates, higher yields and lower amounts of by-products for certain reactions.[84, 85] Hence, this non-conventional energy source has since evolved into a very popular and useful technology in the world of organic chemistry.

Recent studies have investigated the production of biomass-derived chemicals *via* microwave heating. Qi *et al.* studied the dehydration of fructose to HMF in a microwave-assisted reaction system in acetone-water media with ion-exchange resin as catalyst.[81] Under their reaction conditions, fructose conversion and HMF yields by microwave heating (91.7% and 70.3%, respectively) greatly surpassed those by sand bath heating (22.1% and 13.9%, respectively). The same authors also developed a process to efficiently convert fructose to HMF by combining the use of ion-exchange resins as catalysts with ionic liquid.[86, 87] The application of ionic liquids in carbohydrates (lignocellulosic biomass) chemistry is relatively new and further studies combining these two fields are presented by Zakrzewska *et al.*[88] Additionally, Qi *et al.* also reported promising results when they studied the production of HMF from glucose and fructose catalyzed by TiO_2 and ZrO_2 under microwave irradiation.[81] When taking energy efficiency into consideration, Gronnow *et al.* have reported up to an 85-

fold reduction in energy consumption on switching from a conventional oil bath to microwave-assisted set up for a heterogeneous Suzuki reaction.[89]

2.2. Experimental

2.2.1. Reaction kinetics measurements

Mono and biphase batch reactions were performed by way of microwave heating. Reactions were carried out in the Discover™ System (CEM Corporation) with an 80 mL batch reactor. Monophase reactions consisted of an aqueous solution of 10 wt% xylose (Acros Organics), unless otherwise stated. Biphasic systems consisted of 1:1 wt/wt aqueous solution and MIBK (Fisher Scientific). In all experiments, the acid concentration was constant at 0.1 M HCl (relative to aqueous phase). All solutions were mixed at a maximum constant rate using a magnetic stir bar. Temperatures in the reactor were measured by way of a fiber optic sensor. The reaction vessel was pressurized autogenously due to the vapor pressure of the solution at the defined reaction temperature. A dip tube was inserted into the reaction media for sampling purposes. Samples were immediately quenched with ice and filtered with a 0.2 μm syringe filter prior to analysis. Conventional reactions took place in a 100 mL Parr reactor with a sampling port. Sample handling was as described above.

2.2.2. Analysis

Each phase of the reaction mixture was analyzed separately by high-pressure liquid chromatography (HPLC) with a Shimadzu© LC-20AT. Xylose was detected with a RI detector (RID-10A) and products were detected with a UV-Vis detector (SPD-20AV) at

wavelengths of 210 and 254 nm. The column used was a Biorad© Aminex HPX-87H sugar column. The mobile phase was 0.005 M H_2SO_4 flowing at a rate of 0.6 mL/min. The column oven was set to 30 °C. Total organic carbon (TOC) measurements were performed with a Shimadzu© TOC-VCPH Analyzer. Any experimental errors associated with the measurements reported below pertain solely to the calibraton technique used to quantify the concentrations of the reagents and products.

2.2.3. Modeling

Experimental data were collected and used to compare with the proposed kinetic model to estimate rate parameters of the reaction paths in a xylose dehydration system. The kinetic model for the overall reaction path was a set of coupled nonlinear ordinary differential equations (ODEs) and rate constants were correlated by the Arrhenius equation to include temperature dependency. A complete set of concentration data of reactants and products at different temperatures was used to numerically adjust the rate parameters of the overall governing reaction equations. Matlab and Athena Visual Studio v14.0 were used for the numerical integration of ODEs and parameter estimations.

In the model, it was assumed that the furfural decomposition occurred only in the aqueous phase and was not significantly dependent on the concentration of xylose and other derived products. Separate experiments with 0.16 M furfural (1.5 wt%) as feedstock were executed in order to determine the rate parameters for furfural decomposition. A value of 0.74 M xylose (10 wt%) was used as the initial conditions of rate equations in the numerical integration and the sum of absolute errors between estimated and observed values at

experimental sampling points was minimized to find the optimal prediction for the rate of xylose decomposition and furfural formation. All kinetic data at temperatures between 130 and 170^{o}C (5-15 points for each temperature) obtained from monophase experiments were included in the kinetic parameter estimation. Rate parameters determined from monophase data were used further to estimate the furfural distributions between organic and aqueous layers in the biphasic system.

2.3. Results

2.3.1. Comparison of microwave and conventional heating

Initial tests were performed to compare the efficiency of the reaction with microwave and conventional heating at three different temperatures as shown in Figure 1. This figure reveals that microwave heating slightly enhanced xylose decomposition, as well as furfural yield. Nonetheless, the results obtained with both heating sources were comparable to each other.

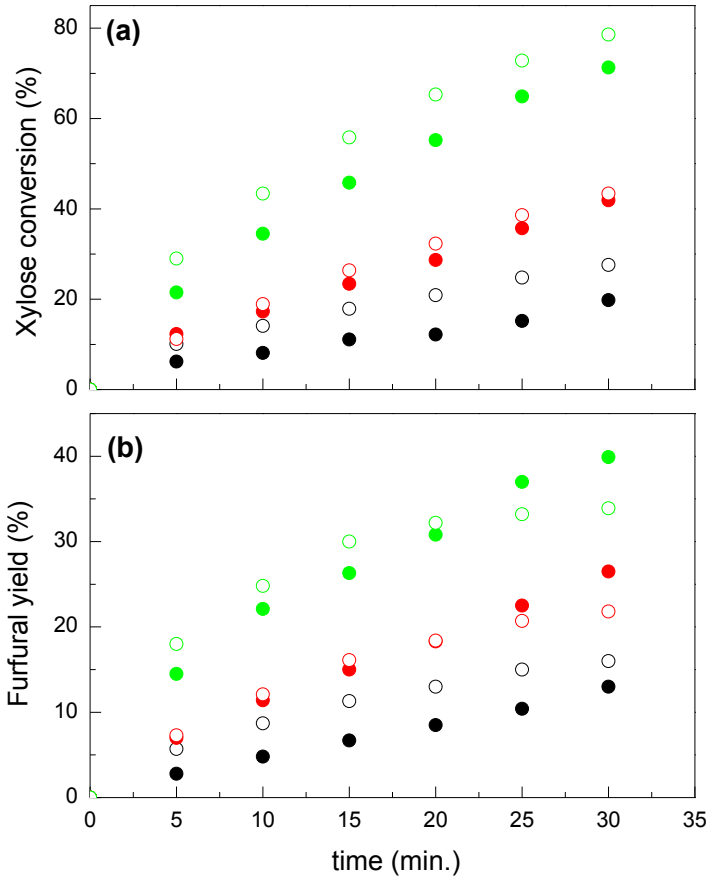

Figure 1. Comparison between microwave (open symbols) and conventional (closed symbols) heating in a monophase system for 10 wt% xylose and 0.1 M HCl. T (°C) = 150 (●), 160 (●), 170 (●). (**a**) xylose conversion; (**b**) furfural yield. Reproduced from ref.[90] by permission of The Royal Society of Chemistry.

2.3.2. Effect of xylose concentration

The effect of xylose concentration on the dehydration of xylose was studied at a temperature of 160 °C as shown in Figure 2. The furfural yield was found to be independent of the xylose concentration. However, the xylose degradation rate increased with increasing xylose concentration. The furfural selectivity also showed dependency on the xylose concentration as shown in Figure 3. The furfural selectivity decreased with increased xylose

(and furfural) concentration. This coincides with the concept stated earlier that byproducts (humins) could be formed from a reaction between xylose and furfural.[74] The remaining portion of this study was performed with a xylose concentration of 10 wt%.

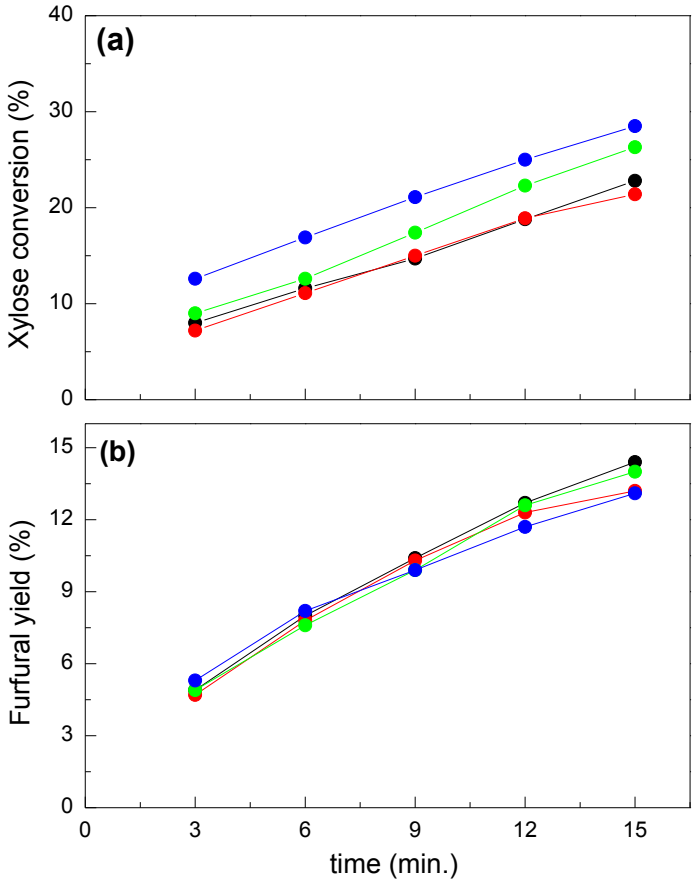

Figure 2. Effect of initial xylose concentration on (**a**) xylose conversion and (**b**) furfural yield in a monophase system at 160 °C and 0.1 M HCl. $[X]_o$ (wt%) = 1 (●), 5 (●), 10 (●), 15 (●). Reproduced from ref.[90] by permission of The Royal Society of Chemistry.

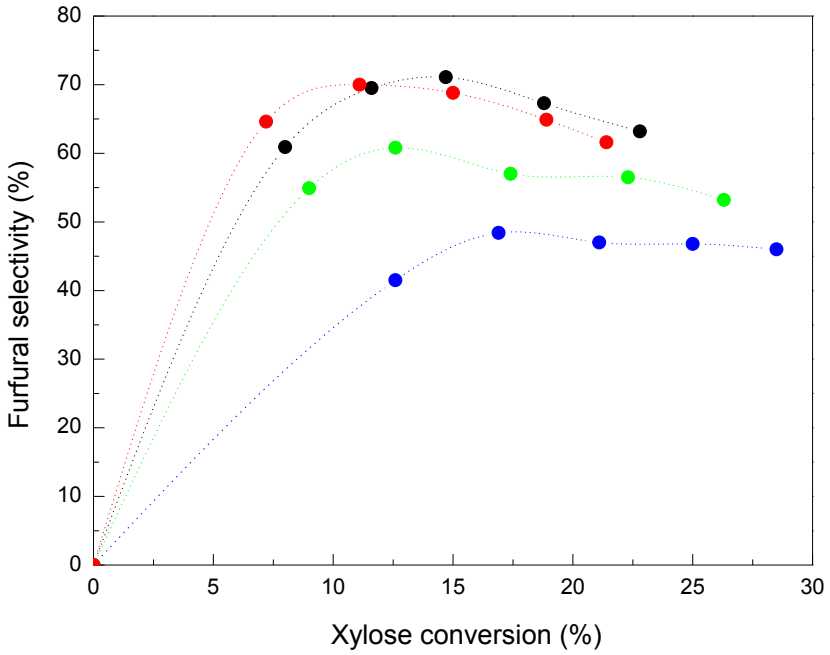

Figure 3. Effect of initial xylose concentration on furfural selectivity in a monophase system at 160 °C and 0.1 M HCl. $[X]_o$ (wt%) = 1 (●), 5 (●), 10 (●), 15 (●). Reproduced from ref.[90] by permission of The Royal Society of Chemistry.

2.3.3. Xylose dehydration and furfural degradation in a monophase system

Dehydration of xylose was performed in a single (aqueous) phase at temperatures between 130-170 °C. In order to measure the decomposition rate of furfural in the aqueous phase, experiments were also performed with furfural as the feedstock (1.5 wt%) in acidic media (0.1 M HCl). Reaction times of up to 8 hours were required to detect any considerable decomposition of furfural. This finding also coincides with previous investigations,[71, 91] which found furfural degradation to be relatively slow compared to xylose dehydration. It is notable to mention that quantifiable amounts of formic acid were also detected as a by-product of this reaction. Williams and Dunlop suggested that this was a result of hydrolytic fission of the furfural aldehyde group.[69, 91]

2.3.4. Xylose dehydration in a biphasic system

Biphasic experiments were performed by employing two immiscible liquid phases in the reactor. A 1:1 wt/wt ratio of MIBK to aqueous xylose solution was used. The MIBK served as the upper phase and the aqueous xylose solution constituted the bottom phase. The xylose was only soluble in the aqueous phase. Biphasic studies with MIBK were conducted at temperatures 140-160 °C. The rate of xylose decomposition was found to be higher in the monophase system compared to the biphasic as shown in Figure 4(a). Additionally, as expected, the overall furfural yield in the biphasic system surpassed the values obtained in the monophase system (Figure 4(b)).

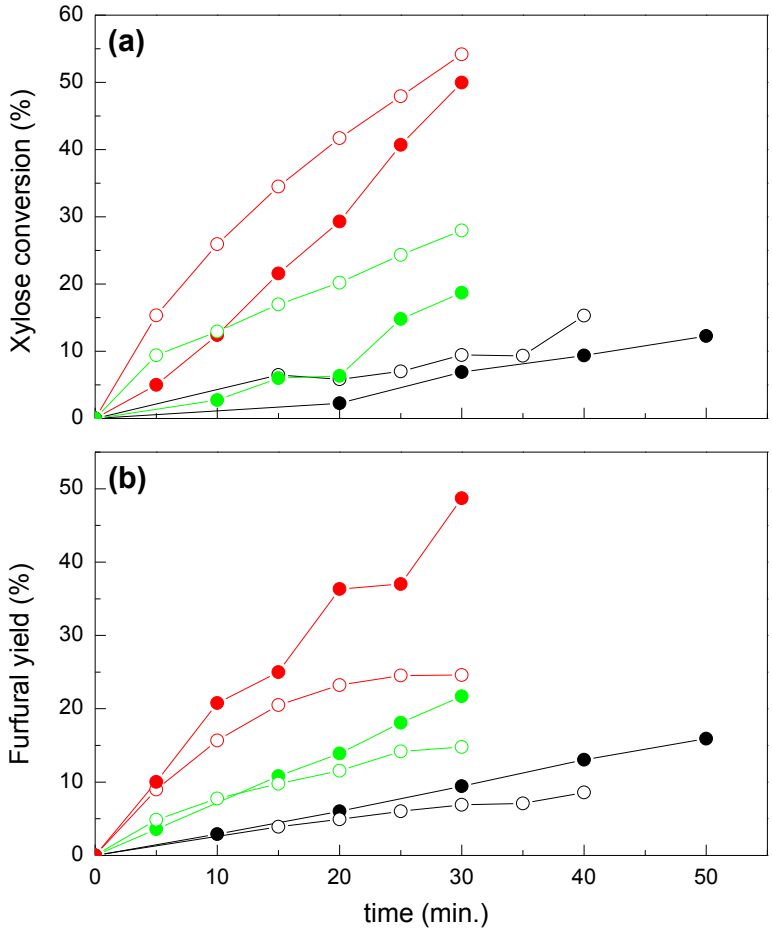

Figure 4. Effect of monophase (open symbols) and biphase (closed symbols) reaction systems on (**a**) xylose conversion and (**b**) furfural yield for 10 wt% xylose and 0.1 M HCl. Biphase system consisted of 1:1 wt/wt aqueous solution and MIBK. T (°C) = 140 (●), 150 (●), 160 (●). Reproduced from ref.[90] by permission of The Royal Society of Chemistry.

The furfural distribution ratio $[F]_{org}/[F]_{aq}$ was also calculated and plotted as a function of reaction time as shown in Figure 5. This ratio did not significantly vary with temperature. All temperatures approached a $[F]_{org}/[F]_{aq}$ value of 7.1 as the time of reaction increased. Consequently, separate extraction experiments showed the furfural distribution to be constant and equal to 7.1. These tests were performed with furfural in a biphasic system at different temperatures. Furfural aqueous solutions (with no acid) were mixed with MIBK

for a fixed time. The two phases were then left to phase separate and samples were taken at the mixing temperature.

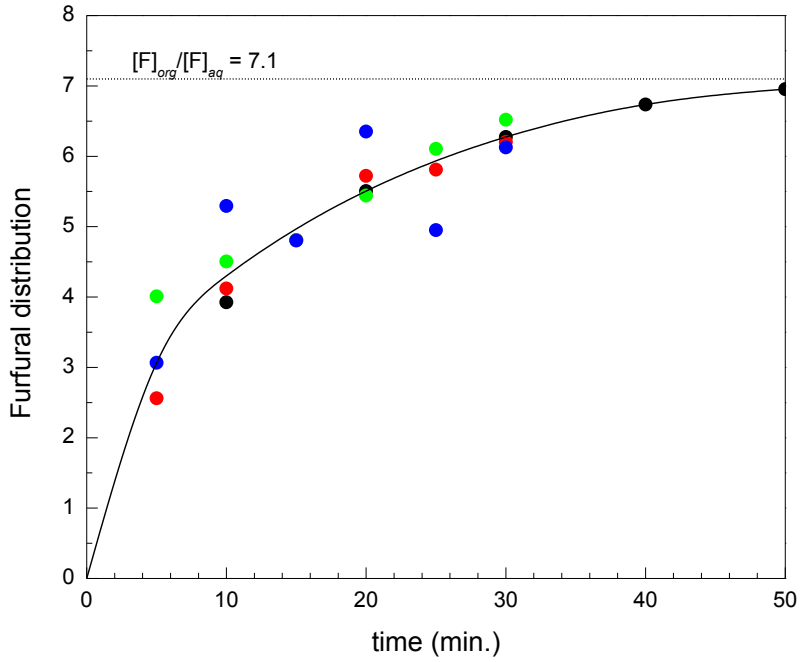

Figure 5. Effect of temperature on furfural distribution between organic and aqueous phase for 10 wt% xylose and 0.1 M HCl. Biphase system consisted of 1:1 wt/wt aqueous solution and MIBK. $[F]_{org}$ and $[F]_{aq}$ denote furfural concentrations in the organic and aqueous phase respectively. T (°C) = 140 (●), 150 (●), 160 (●), 170 (●). Reproduced from ref.[90] by permission of The Royal Society of Chemistry.

2.3.5. Kinetic model for xylose dehydration in a monophase system

The adopted reaction scheme for monophase dehydration of xylose is shown below in Scheme 2. All three of these reactions are irreversible. Xylose can undergo two parallel reactions Eq. 1 and Eq. 2. The first reaction is the dehydration of xylose to produce furfural. The second reaction involves the reaction of xylose and furfural to produce humins and other decomposition products. The third reaction is the degradation of furfural to produce humins.

Reaction 1 is reported to be pseudo first order with respect to xylose.[71, 72, 91, 92] This coincides with the kinetic data we reported in Figure 2(b). Furfural decomposition as depicted by Eq. 3 is found to be first order with respect to furfural. This is also similar to previous studies.[69, 70, 72, 92] Reaction 2 is first order with respect to xylose and first order with respect to furfural.

$$X \xrightarrow[k_1]{} F + 3H_2O \tag{1}$$

$$X + F \xrightarrow[k_2]{} D_1 \tag{2}$$

$$F \xrightarrow[k_3]{} D_2 \tag{3}$$

$$X \equiv xylose;\ F \equiv furfural;\ \ D_1, D_2 \equiv decomposition\ products.$$

Scheme 2. Xylose dehydration in a monophase system.

Other researchers have suggested that Reaction 2 takes place between furfural and a xylose intermediate.[91, 92] Root *et al.* based this claim by citing that the quantity of furfural added to a xylose solution did not affect its disappearance rate.[92] However, as shown in Figure 4(a), there is a visible distinction between xylose disappearance in the monophase and biphasic systems. Qi *et al.*[71] postulated a side reaction which involves xylose; however it was defined as a unimolecular decomposition reaction. The rate equations for xylose consumption and furfural production can be written as:

$$d[X]/dt = -k'_1[X][H_3O^+] - k'_2[X][F][H_3O^+] \tag{4}$$

$$d[F]/dt = k'_1[X][H_3O^+] - k'_2[X][F][H_3O^+] - k'_3[F][H_3O^+] \tag{5}$$

All three reactions are a function of the acid catalyst concentration and their rate constants have the appropriate dimensions. All experimental data for the monophasic reactions were fit to the model to estimate the three rate parameters. The best correlated values with their standard errors are tabulated in Table 1. Figure 6 shows the experimental data in a monophase reacting system with the fitted model.

Table 1. Estimated kinetic parameters for xylose dehydration in a monophase system.[c]

	$\log_{10}A$	E_A(kJ mol^{-1})
[b]k_1(min^{-1})	13.17 ± 0.72 [a]	123.91 ± 6.00
[b]k_2(M^{-1} ·min^{-1})	7.63 ± 1.97	72.47 ± 16.28
[b]k_3(min^{-1})	5.44 ± 1.18	67.58 ± 9.66

[a] 95% confidence interval in parameter estimation.
[b] 1st and 2nd order rate parameters that are lumped with acid concentration; $k_n = k'_n[H_3O^+]$
[c] Reproduced from ref.[90] by permission of The Royal Society of Chemistry.

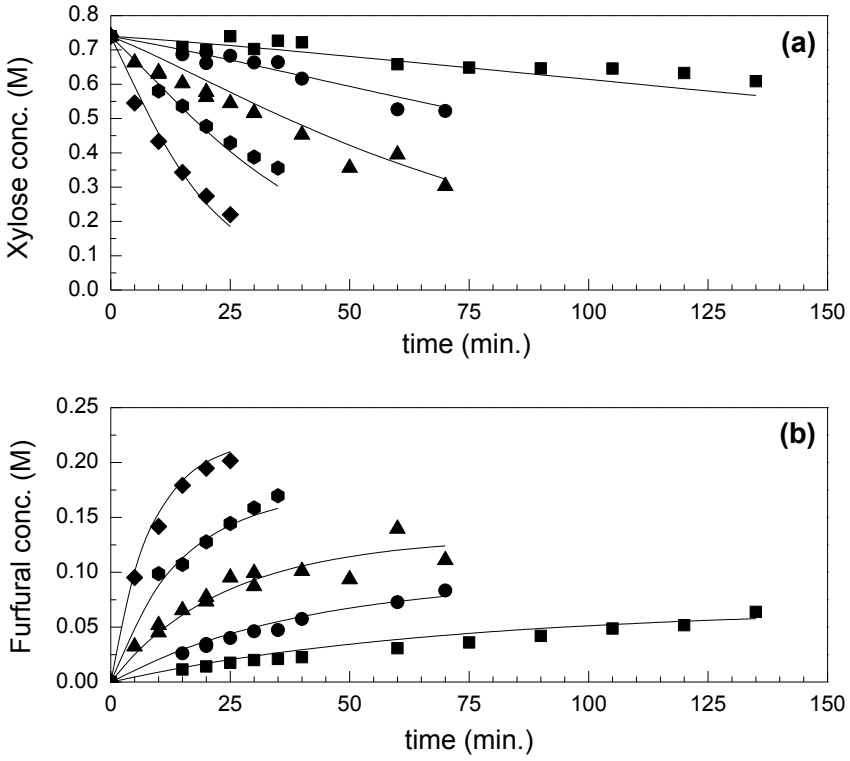

Figure 6. Kinetic model fit for (**a**) xylose decomposition and (**b**) furfural formation in a monophase system for 10 wt% xylose and 0.1 M HCl. T (°C) = 130 (■), 140 (●), 150 (▲), 160 (⬢), 170 (◆); Model prediction (—). Reproduced from ref.[90] by permission of The Royal Society of Chemistry.

The furfural decomposition data is plotted in Figure 7 along with its kinetic model fit. The disappearance rate was relatively slow and observed to follow a first order decomposition. TOC measurements were performed to predict the overall carbon balance. We accounted for over 90% of the carbon. This balance does not include formic acid which was detected as a by-product and not quantified. The correlated values for activation energy and pre-exponential factor for Reaction 3 in our kinetic model are listed in Table 1. These results are consistent with previously reported values for unimolecular furfural degradation in a single phase.[69, 71]

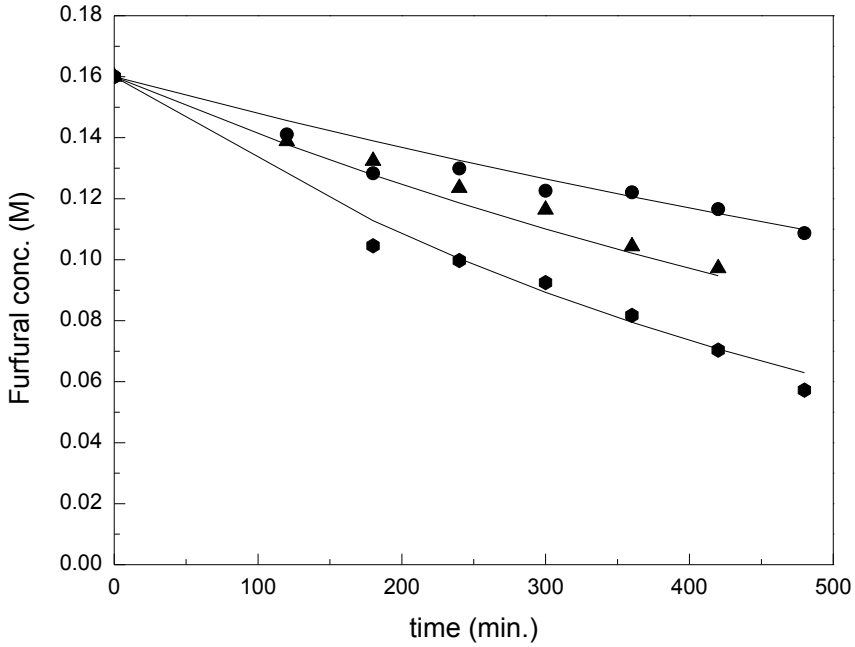

Figure 7. Kinetic model fit for furfural decomposition in a monophase system for 1.5 wt% furfural and 0.1 M HCl. T (°C) = 140 (●), 150 (▲), 160 (⬢); Model prediction (—). Reproduced from ref.[90] by permission of The Royal Society of Chemistry.

2.3.6. Kinetic model for xylose dehydration in a biphasic system

The suggested reaction scheme for dehydration of xylose in a biphasic system is shown in Figure 8. This one is similar to our previously proposed scheme for a monophase system with the exception that the furfural can be extracted into a separate organic phase.

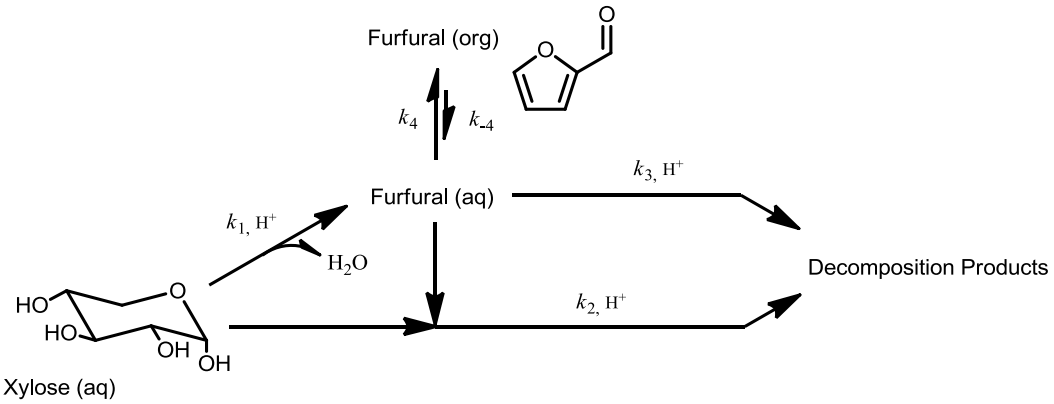

Figure 8. Overall reaction scheme including furfural extraction to the organic phase in a biphasic system. Reproduced from ref.[90] by permission of The Royal Society of Chemistry.

Based on experimental observation, the following kinetic model was established to depict xylose decomposition in the two-phased system:

$$X(aq) \xrightarrow[k_1]{} F(aq) + 3H_2O \tag{6}$$

$$X(aq) + F(aq) \xrightarrow[k_2]{} D_1 \tag{7}$$

$$F(aq) \xrightarrow[k_3]{} D_2 \tag{8}$$

$$F(aq) \xrightarrow[k_4]{} F(org) \tag{9}$$

$$F(org) \xrightarrow[k_{-4}]{} F(aq) \tag{10}$$

Scheme 3. Xylose dehydration in a biphase system.

In this model estimation, the same values estimated from monophase experiments were used for the rate parameters of k_1, k_2, and k_3. Reaction 4 depicts furfural transport between the organic and aqueous layers. The mass transfer coefficients, k_4 and k_{-4}, were

assumed constant values, as the furfural distribution between aqueous and organic phases was considered to be constant and not temperature dependent of the Arrhenius equation under the reaction conditions (Table 2). In the modeling, it was assumed that the furfural distribution was solely dependent on the bidirectional mass transfer rates and other kinetics or paths were not disturbed by thermodynamic instability.

Table 2. Estimated mass transfer coefficients derived for a biphasic system.[a]

k_4/k_{-4}	7.1

[a] Reproduced from ref.[90] by permission of The Royal Society of Chemistry.

Additional tests showed that the organic phase served solely as "storage" for furfural where no additional decomposition reactions occurred. This is most likely due to the negligible solubility of the acid catalyst in this phase. The organic phase only contained furfural and MIBK. The overall rate equations for a biphasic system are:

$$d[X]/dt = -k'_1[X][H_3O^+] - k'_2[X][F]_{aq}[H_3O^+] \quad (11)$$

$$d[F]_{aq}/dt = k'_1[X][H_3O^+] - k'_2[X][F]_{aq}[H_3O^+]$$

$$-k'_3[F]_{aq}[H_3O^+] - k_4[F]_{aq} + k_{-4}[F]_{org} \quad (12)$$

$$d[F]_{org}/dt = k_4[F]_{aq} - k_{-4}[F]_{org} \quad (13)$$

When the rates of mass transfer are much faster than the rate of furfural formation, their parameters can be related by the distribution coefficient of furfural at equilibrium.

$$k_4/k_{-4} \approx K_{eq} = [F]_{org}/[F]_{aq} = 7.1$$

The best fit was achieved when $\log(k_4)$ was approximately 7.4, which is much larger than the other kinetic parameters (k_4 or $k_{-4} \gg k_1, k_2, \text{or } k_3$).

Figure 9 exhibits the biphasic model fit to the experimental data for xylose decomposition and furfural formation. The model shows a good fit for all temperatures apart from 170 °C. The model underestimates the xylose degradation rate at this temperature, as well as the furfural presence in the organic phase.

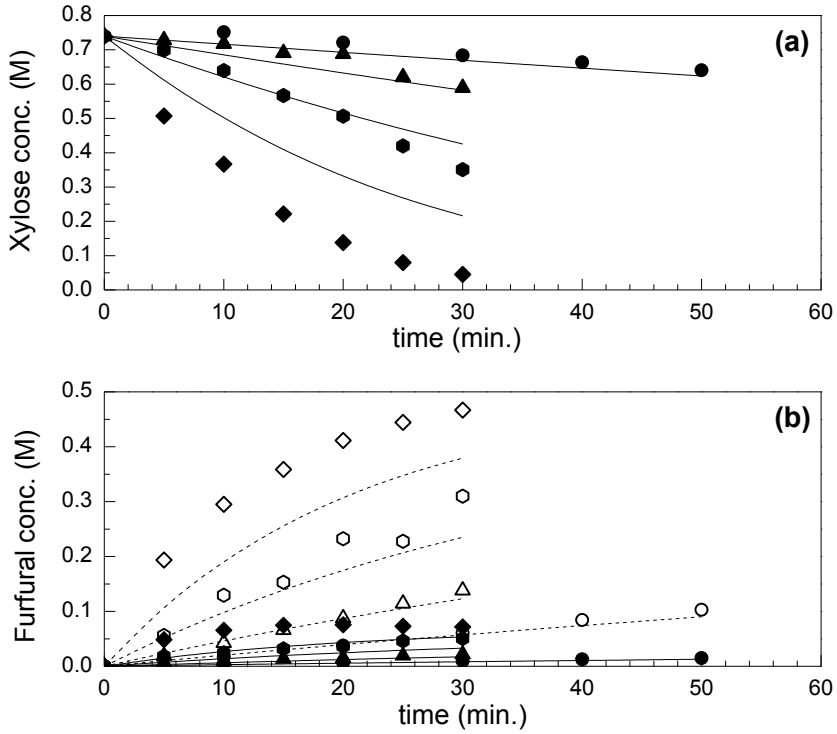

Figure 9. Kinetic model fit for (**a**) xylose decomposition and (**b**) furfural formation in a biphase system for 10 wt% xylose and 0.1 M HCl. Biphase system consisted of 1:1 wt/wt aqueous solution and MIBK. T (°C) = 140 (●), 150 (▲), 160 (⬢), 170 (◆). Open and closed symbols denote furfural concentrations in the organic and aqueous phase respectively. Dashed (---) and solid (—) lines represent model predictions for furfural in the organic and aqueous phase respectively. Reproduced from ref.[90] by permission of The Royal Society of Chemistry.

2.4. Discussion

2.4.1. Kinetic model calculations

The apparent rate parameters introduced here allow for theoretical calculations of furfural yield in both a single and two-phase system. Figure 10 plots the calculated values at various temperatures as a function of reaction time for both systems. These results show that a biphasic reaction system is essential to maximize the yield of furfural. The optimal yield also occurs at high temperatures and short reaction times. The kinetic parameters in Table 1 show that the dehydration of xylose to furfural is the highest activation energy step. As this is the desired reaction, a higher yield is expected at increased temperatures since the ratio of k_1 to k_2 and k_1 to k_3 increase with elevated temperatures. Likewise, shorter reaction times are preferred to maximize the furfural yield. Implementing a biphasic system presents a distinct advantage with a theoretical furfural yield of 85% at 170 °C compared to a single aqueous phase system which yields only 30% at the same temperature.

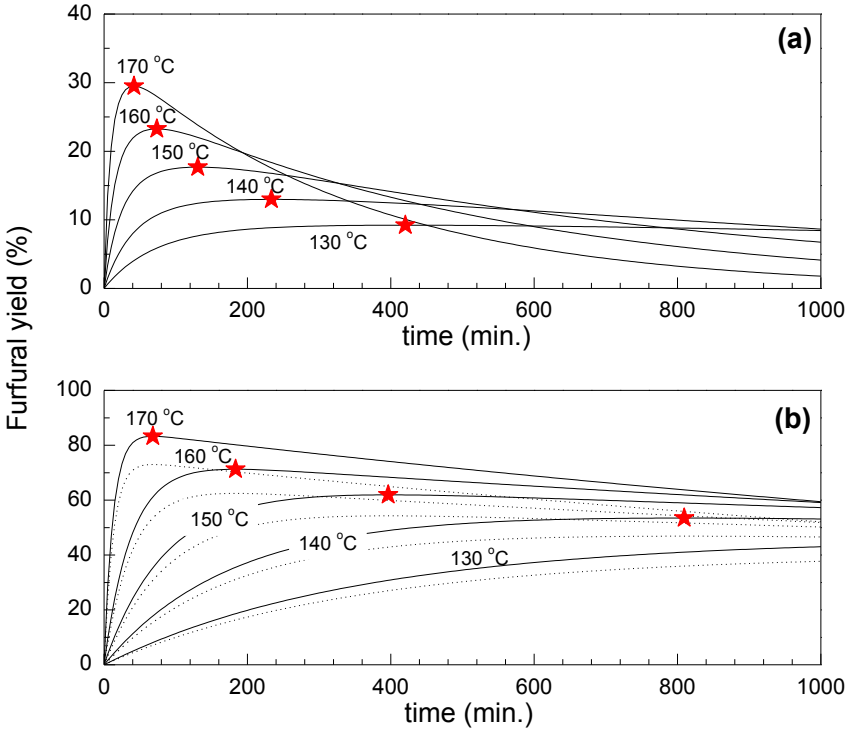

Figure 10. Calculated furfural yield as a function of reaction time and temperature for a (**a**) monophase and a (**b**) biphase system at 10 wt% xylose and 0.1 M HCl. Biphasic system consisted of 1:1 wt/wt aqueous solution and MIBK. Dotted lines (…) represent furfural yield in the organic phase. Solid lines (—) represent total furfural yield. Symbol (★) represents maximum furfural yield. Reproduced from ref.[90] by permission of The Royal Society of Chemistry.

2.4.2. Microwave effect on rate parameters

The kinetic parameters derived from our model (Table 1) are in good agreement with those obtained in previous studies that used conventional heating methods. The literature reports activation energies for xylose dehydration in the range 111 to 125 kJ mol^{-1}.[71, 72, 93] Values for furfural degradation range from 48 to 90 kJ mol^{-1}.[69-72] These comparable rate parameters confirm the lack of any considerable effects arising from microwave heating. Our finding is contrary to others who report enhanced results due to microwave irradiation[81].

A plausible cause for the discrepancy lies in the nature of the catalyst. The enhanced microwave effects were reported for reaction systems with solid acid catalysts. Accordingly, it has been emphasized that microwave absorption at the solid interface can advantageously influence the overall reaction kinetics.[94]

2.4.3. Kinetic model comparison to proposed mechanism

Antal *et al.* proposed a detailed mechanism of the formation of furfural from xylose.[95] According to this work, it can be assumed that the rate-determining step for xylose dehydration is the formation of the protonated xylopyranose intermediate (refer to step no. 5 in scheme II in ref.[95]). To determine the credibility of our kinetic model, a comparison was made between their reported rate constant and our rate constant k'_1 calculated at their reaction temperature of 250 °C. The calculated rate constant from our model (1.04 $M^{-1} \cdot s^{-1}$) was found to be comparable to that cited in the literature by Antal *et al.* (5.58 $M^{-1} \cdot s^{-1}$). Different reaction conditions (temperature, catalyst) are a probable cause for the slight dissimilarity.

CHAPTER 3

Design of solid acid catalysts for aqueous phase dehydration of carbohydrates

Weingarten, R.; Tompsett, G. A.; Conner Jr, W. C.; Huber, G. W., Design of solid acid catalysts for aqueous-phase dehydration of carbohydrates: The role of Lewis and Brønsted acid sites. *Journal of Catalysis* **2011,** *279* (1), 174-182.

3.1. Background

This chapter discusses a study wherein we prepared a series of well characterized solid acid catalysts, including zirconium phosphate (ZrP), silica alumina (SiO_2-Al_2O_3), tungstated zirconia (WO_X/ZrO_2), gamma alumina (γ-Al_2O_3), and HY zeolite, and tested them for aqueous phase dehydration of xylose. The objective of this study was to examine the role of Lewis and Brønsted sites of solid acid catalysts for the dehydration of carbohydrates in aqueous media. These results will allow us to deduce the optimal design of solid acid catalysts for this class of reactions.

Many studies have reported on the dehydration of xylose to form furfural with homogeneous acid catalysts.[29, 31, 38, 96] Even though promising results have been attained, it would be desirable to obtain solid catalysts that exhibit activities and selectivities at least comparable to homogeneous catalysts for aqueous phase dehydration. Solid catalysts are advantageous due to their economic and environmental *via*bility. Industrially, they are preferred due to the ease of post reaction catalyst separation. Valente and co-workers have reported various studies on the design of solid acid catalysts for the dehydration of xylose to produce furfural. Their work spans over a broad range of catalytic materials including modified mesoporous silicas,[97-100] exfoliated transition metal oxides,[101] sulfated metal oxides [102] and microporous silicoaluminophosphates.[103] Gürbüz *et al.* reported a study on the conversion of hemicellulose into furfural using solid acid catalysts.[104] They obtained furfural yields of up to 80% in the presence of H-Mordenite in a solvent system containing GVL and 10 wt% water. Similarly, Gallo *et al.* used H-Beta zeolite to produce furfural from biomass-derived compounds in a solvent system containing GVL.[105] The combination of Lewis and Bronsted acid

functionality of H-Beta was shown to be effective for the isomerization of xylose and arabinose, followed by dehydration. It has also been shown that modified mesoporous catalysts, such as arenesulfonic SBA-15, are highly active and selective for xylose dehydration to produce furfural.[106] A comprehensive review of furfural production with solid acid catalysts is given by Karinen *et al.*[107]

There are still many unanswered questions pertaining to the behavior of solid catalysts in aqueous solutions. An area of particular focus is the interfacial interactions between aqueous solutions and metal oxides. The metal oxide-water interface is reactive due to a range of chemistries, including acid-base, ligand exchange, and/or redox.[108] In general, the exposure of solid oxides to water gives rise to electrical charges on the solid surface. This is due to hydration effects which can involve H^+ and OH^- ions from the bulk aqueous phase. Incomplete coordination of the exposed metal or oxide ions at the solid surface is the cause of this phenomenon.[109] As a result, positive and negative sites are present on the solid surface and the excess of one type of site determines the net charge. For aqueous solutions this is a function of the pH. The solution pH at which the net charge on the surface is zero is known as the point of zero charge (PZC). The surface has a net positive charge when the *s*olution pH is below the PZC and a net negative charge when the solution pH is above the PZC.[110] Comprehensive studies on the PZC of various metal oxides and hydroxides have been reported by Parks and Kosmulski.[111-116]

On the catalyst surface, Brønsted acid sites (proton donors) can be generated from highly polarized hydroxyl groups. They can also form on oxide-based catalysts *via* proton balance of a net negative charge introduced by substituting cations with a lower valence charge.[117]

Alternatively, Lewis acid sites form from coordinatively unsaturated cationic sites, which leave M^{n+} exposed to interact with guest molecules as an acceptor of an electron-pair.[26] Exposure of the catalysts to a polar solvent such as water can potentially alter the intrinsic nature of the acid surface due to solvation effects. For instance, the hydroxyl ion from the water molecule (Lewis base) can react with a Lewis site on the surface to generate Brønsted sites.[118-121] Davis and co-workers have shown that tin-containing zeolites behave as Lewis acids in water and are highly active catalysts for the isomerization of glucose.[122] Others have reported that the primary effect of water is displacement of strongly adsorbed basic probe molecules from the acid sites.[123, 124] Poisoning of the acid sites by water may also occur depending on the surface hydrophilicity/hydrophobicity of the catalyst.[125]

This reality in turn poses difficulties in determining the acidity of solid acids in aqueous media. One approach is to determine the number of Brønsted sites in water from the number of free protons arising from cation exchange with a salt in aqueous solution at the surface of the solid.[126-130] Aqueous phase titration is a common method used for quantification purposes. The concentration of acid sites can also be estimated by *poisoning* of the active sites with a base and measuring the catalytic activity versus poison concentration.[119] Other techniques for acid site characterization have been reviewed by Tanabe.[131]

3.2. Experimental

3.2.1. Catalyst Preparation

The ZrP catalyst was prepared following procedures previously reported in the literature,[132] which consisted of precipitation of $ZrCl_2O \cdot 8H_2O$ (Sigma Aldrich, 1 mol L^{-1}, 70

mL) and $NH_4H_2PO_4$ (Sigma Aldrich, 1 mol L^{-1}, 140 mL) at a molar ratio of P/Zr = 2. The solution was stirred and then filtered, washed with de-ionized (DI) water and dried overnight at 373 K. The catalyst was calcined at 673 K for 4 h in air prior to reaction. This ZrP was confirmed to be amorphous by X-ray diffraction (XRD). The SiO_2-Al_2O_3 catalyst (Sigma Aldrich grade 135, Si/Al = 5.0) was calcined at 773 K for 16 h in air. HY catalyst (Zeolyst CBV 720, Si/Al = 30) was calcined at 813 K for 16 h in air. Tungstated zirconia catalyst (WO_X/ZrO_2, XZO 1251) with WO_3 content 15 wt% was supplied by MEL Chemicals. This catalyst was calcined in air at 873 K for 4 h to remove water and organic contaminants. The γ-Al_2O_3 catalyst was obtained by calcining alumina boehmite CATAPAL B supplied by Sasol at 873 K for 4 h in air. The crystal structure was confirmed by XRD. The Nafion SAC-13 (Sigma Aldrich) and Amberlyst 70 (Rohm and Haas) were dried overnight at 383 K and crushed. The latter was sieved to a particle size of $\leq$ 125 μm. Hydrochloric acid was supplied by Fisher Scientific. Ytterbium (III) trifluoromethanesulfonate hydrate, $Yb(OTf)_3$, was supplied by Strem Chemicals. The Brønsted and Lewis acid sites for each solid catalyst are portrayed in Table 3.

Table 3. Illustration of the Brønsted and Lewis acid sites for each solid catalyst.[b]

Catalyst [a]	Brønsted sites	Lewis sites
ZrP [133, 134]	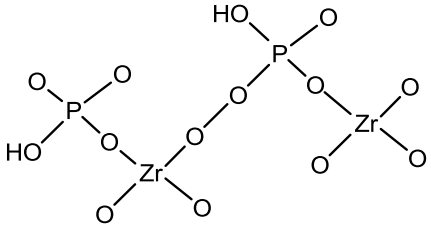	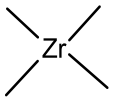
SiO_2-Al_2O_3 [119, 125] HY	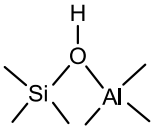	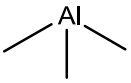
WO_X/ZrO_2 [135-137]	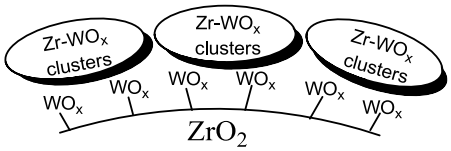	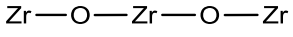
γ-Al_2O_3 [118]	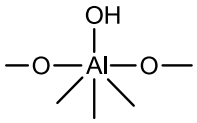	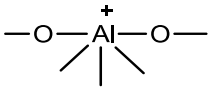
Nafion SAC-13 [138]	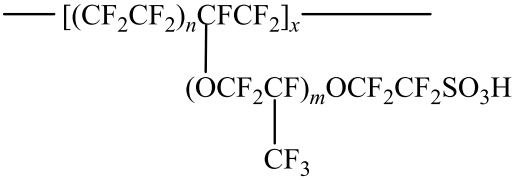	N/A
Amberlyst 70 [139]	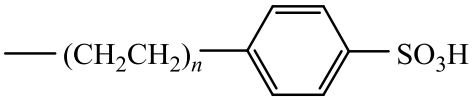	N/A

[a] references to figures
[b] Reprinted from ref.[140], Copyright(2011), with permission from Elsevier.

3.2.2. Catalyst Characterization

Total acid sites were determined by ammonia-temperature programmed desorption (NH_3-TPD)[141] with a Quantachrome ChemBET Pulsar™ TPR/TPD Automatic Chemisorption Analyzer coupled with a thermal conductivity detector (TCD) to quantify the ammonia desorbed

from the sample. A sample of 300 mg was initially degassed at 773 K for 1 h under a constant helium flow of 60 mL min^{-1} (Airgas, UHP). The sample was cooled and ammonia (Airgas, electronic grade) was adsorbed at 373 K. After saturation, the ammonia supply line was shut off and helium was purged at 60 mL min^{-1} to remove any physically adsorbed ammonia. The sample was then heated linearly at a rate of 10 K min^{-1} from 373 to 873 K (973 K for ZrP) under a constant helium flow of 60 mL min^{-1}. The sample was held at the temperature set point for an additional 1 h.

The Brønsted to Lewis acid site ratio of the catalysts were determined by FTIR spectroscopy with ammonia as a probe molecule.[142, 143] The spectra were recorded on a Bruker Equinox 55 spectrometer at a resolution of 4 cm^{-1} (averaging 50 scans). A Harrick Scientific "Praying Mantis" Diffuse Reflectance Infrared cell (DRIFTS) allowed for *in situ* recording of the spectra at ambient temperature and catalyst activation at higher temperatures. The cell was equipped with a heater and connected to a gas flow system. The temperature was monitored with a thermocouple placed in direct contact with the sample. Powder samples (~20 mg) were loaded into the DRIFTS cell for FTIR spectroscopy studies. A spectrum of KBr (taken at ambient temperature before) was used as a background reference. Before the surface characterization was performed, the samples were activated by heating at 673 K for 2 h under helium (Airgas, UHP) flow of 20 mL min^{-1}, cooled down to 373 K and saturated with ammonia (Airgas, anhydrous 99.99%) for 20-30 min. The gas flow was then switched back to helium (20 mL min^{-1}) to remove physically adsorbed ammonia and the spectrum monitored until no change was observed (*ca.* 30 min). The samples were then heated in helium flow (20 mL min^{-1}) to various temperatures. The spectra were recorded at each temperature up to 873 K. All of the

spectra were obtained by subtraction of the corresponding background reference spectra. Data analysis and peak fitting were carried out using GRAMS/AI® software (ThermoScientific). The ion-exchange polymer resins were analyzed by FTIR spectroscopy according to a previously reported method with pyridine as a probe molecule.[144]

The BET surface areas and pore volumes were determined by nitrogen adsorption at 77 K using a Quantachrome Autosorb®-1-C automated gas sorption system. The samples were evacuated before each experiment at 523 K for 24 h (423 K for ion-exchange resins). As the BET method overestimates the surface area of microporous material, an empirical estimation technique was used. This consisted of subtracting the adsorbed volume of adsorbate in the microporous region (typically $P/P_o < 10^{-4}$) from the remaining adsorption points and recalculating the surface area by using the BET method and obtaining the appropriate "C" constant.

Liquid adsorption experiments with aqueous solutions of xylose and furfural were performed in accordance with the literature.[124] A known amount of catalyst (0.15 g) was mixed with 10 g of a 2 wt% solution of DI water and the adsorbate. The mixture was stirred for 19-22 h at room temperature to ensure that equilibrium was reached, followed by filtration with a 0.2 μm syringe filter to remove the catalyst. Desorption studies were carried out by separating the catalyst from the liquid phase with a centrifuge following the adsorption procedure. DI water was then added to the retained catalyst and the mixture was stirred for additional 22 h at room temperature to ensure that equilibrium was reached. The mixture was finally filtered with a 0.2 μm syringe filter to remove the catalyst. The amounts of adsorbate/desorbate present in the liquid phase were determined with the analysis method stated below.

The catalytic acid sites in the aqueous phase were determined by a titration method previously reported in the literature.[145] A sodium hydroxide aqueous solution (0.01 mol L^{-1}, 20 mL) was mixed with a known amount of catalyst for 2 h at room temperature. The solution was then filtered with a 0.2 μm syringe filter and titrated by a hydrochloric acid solution (0.1 mol L^{-1}). The equivalence point (EQP) was detected by using a Mettler-Toledo© T50 auto-titrator. Phenolphthalein indicator was used as well for qualitative purposes.

3.2.3. Catalyst Activity

Reactions were carried out in the Discover™ System (CEM Corporation) with an 80 mL batch reactor. Xylose dehydration reactions consisted of an aqueous solution of 10 wt% xylose (Acros Organics) unless otherwise stated. Furfural decomposition reactions consisted of 1.5 wt% furfural (Acros Organics) unless otherwise stated. All of the aqueous solutions were prepared with DI water. Throughout all of the experiments, the total number of acid sites was held constant at 0.500 mmoles (determined by NH_3-TPD) unless otherwise stated and the amount of loaded reaction solution was kept constant at 30 g. All solutions were mixed at a maximum constant rate using a magnetic stir bar. Temperatures in the reactor were measured by way of a fiber optic sensor. The reaction vessel was pressurized due to the vapor pressure of the solution at the defined reaction temperature. A dip tube was inserted into the reaction media for sampling purposes. Samples were immediately quenched with ice and filtered with a 0.2 μm syringe filter prior to analysis.

3.2.4. Analysis

Samples were analyzed by high pressure liquid chromatography (HPLC) with a Shimadzu© LC-20AT. Xylose was detected with a RI detector (RID-10A) and products were detected with a UV-Vis detector (SPD-20AV) at wavelengths of 210 and 254 nm. The column used was a Biorad© Aminex HPX-87H sugar column. The mobile phase was 0.005 M H_2SO_4 flowing at a rate of 0.6 mL/min. The column oven was set to 30 °C. Total organic carbon (TOC) measurements were performed with a Shimadzu© TOC-VCPH Analyzer. Calibrations were performed with carbon standards supplied by SpectroPure.

3.3. Results

3.3.1. Characterization of solid acid catalysts

The solid acid catalysts were characterized both in the gaseous and aqueous phase. The characterization data appear in Table 4 in descending order of Brønsted to Lewis acid site ratio. Adsorption experiments were performed with both xylose and furfural as adsorbates at room temperature in the aqueous phase. Xylose did not adsorb on any of the catalysts at room temperature. Furfural adsorption uptakes were found to be similar for all of the catalysts with the exception of HY which had an uptake of up to 7 times the amount of the other catalysts on a per gram basis. This result is higher than that reported by Tsapatsis and co-workers for furfural adsorption on faujasite zeolite (Si/Al = 30).[124] Additional desorption experiments with HY showed that only 27% of the adsorbed furfural on the catalyst desorbed back into the aqueous phase.

The number of acid sites calculated from the aqueous phase titration was different than those calculated by ammonia-TPD. The aqueous phase method showed an increased number of acid sites compared to the number of acid sites obtained with the gaseous sorption technique. This could be due to the adsorption of sodium hydroxide (titrant) on inactive sites, as well as on the active acid sites of the catalysts throughout the titration process.[119] Even so, the concentration of acid sites measured by aqueous phase titration increased with the ratio of Brønsted to Lewis acid sites determined by ammonia FTIR spectroscopy in the gas phase.

The acid concentrations obtained from the aqueous (titration) and gaseous techniques (NH_3-TPD) were not comparable to each other. With the exception of γ-Al_2O_3, the results obtained from aqueous phase titration are higher than those from the gas phase sorption technique. Several studies have been reported on titration techniques, with some stating that aqueous phase titration solely quantifies Brønsted sites.[131, 145] To validate these claims, we carried out additional titration experiments at constant Brønsted sites (according to NH_3-TPD). Similarly, we also performed titrations while keeping the total number of acid sites constant (according to NH_3-TPD). Arbitrary and inconsistent results on both attempts raise doubts about the validity of this aqueous phase characterization technique (refer to Table A.1 in the Appendix). Similar conclusions have been previously reported.[120, 121, 131]

Table 4. Characterization of solid acid catalysts.[b]

	Gas Phase Characterization					Aqueous Phase Characterization	Furfural Adsorption
Catalyst	BET Surface Area (m^2 g^{-1})	Micropore Volume (cm^3 g^{-1})	Brønsted : Lewis ratio	Total acid sites (mmol g^{-1})	Brønsted sites (mmol g^{-1})	Acid sites (mmol g^{-1})	Uptake (g g^{-1})
ZrP	168	0	27.00	1.413	1.362	4.250	0.07
SiO_2-Al_2O_3	585	0	3.78	0.432	0.342	1.450	0.06
HY	303 [a]	0.028	1.50	0.520	0.312	1.047	0.30
WO_X/ZrO_2	149	0	0.74	0.324	0.138	0.875	0.05
γ-Al_2O_3	262	0	0.67	0.428	0.171	0.124	0.04

[a] Estimated using microporous subtraction method. BET "C" constant is 68.
[b] Reprinted from ref.[140], Copyright(2011), with permission from Elsevier.

3.3.2. Xylose dehydration and furfural degradation

Xylose dehydration was studied with the different solid acid catalysts in the aqueous phase at 160 °C with the total acid sites held constant at 0.500 mmoles (according to NH_3-TPD). Figure 11 depicts xylose conversion as a function of reaction time for the various catalysts. The catalytic activity was found not to be a function of the total number of acid sites as measured by NH_3-TPD. However, the catalysts with the highest number of Lewis acid sites were found to be the most active. On a per site basis, the catalytic activity decreased as follows: γ-Al_2O_3 ~ WO_X/ZrO_2 > SiO_2-Al_2O_3 ~ HY > ZrP ~ HCl. Increasing the relative number of Brønsted to Lewis acid sites decreased the catalytic activity.

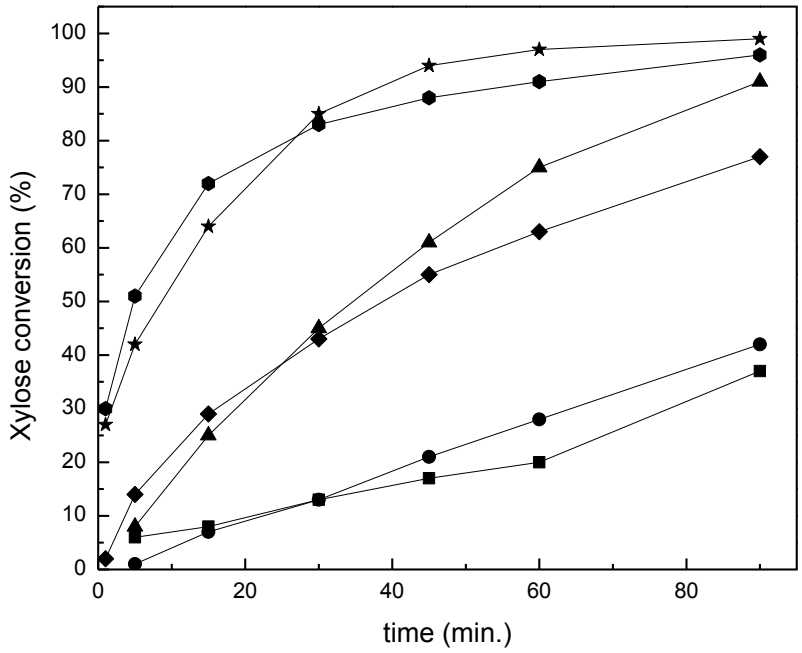

Figure 11. Aqueous phase xylose dehydration at 160 °C with different solid acid catalysts. Total acid sites were kept constant at 0.500 mmoles (determined by NH_3-TPD). Feed was 10 wt% xylose aqueous solution. Catalysts: HCl (■), ZrP (●), SiO_2-Al_2O_3 (▲), HY (◆), WO_X/ZrO_2 (⬢), γ-Al_2O_3 (★). Reprinted from ref.[140], Copyright(2011), with permission from Elsevier.

The furfural selectivity as a function of conversion is shown in Figure 12. The furfural selectivity decreased as follows: ZrP ~ HCl >> SiO_2-Al_2O_3 > WO_X/ZrO_2 > HY > γ-Al_2O_3. This follows the opposite trend compared to catalyst activity. Thus, the catalysts that are most active demonstrate the lowest selectivity for furfural production. The ZrP and HCl catalysts have significantly higher furfural selectivities than the other four catalysts. The furfural selectivity increases with xylose conversion for the other four catalysts. These experiments show that the furfural selectivity is dependent on the type of acid catalyst site.

Additional stability studies with ZrP, SiO_2-Al_2O_3 and WO_X/ZrO_2 have shown that the catalysts retain their total acid concentrations after exposure to water at 160 °C (refer to Table

A.2 in the Appendix). This was confirmed by NH_3-TPD following filtration and recalcination of the catalysts. Further testing was performed on ZrP which consisted of mixing ZrP in DI water for 1.5 h at 160 °C, followed by hot filtration to separate the catalyst. Xylose was then added to the filtrate to produce an aqueous solution of 10 wt% xylose. We then proceeded to dehydrate the xylose in a blank experiment (no additional catalyst). A comparable blank study was also carried out for an aqueous solution of 10 wt% xylose consisting of clean DI water. Results from both experiments were practically identical, indicating that that the acid sites on ZrP do not leach in aqueous media. This agrees with conclusions made by Li *et al.* who found ZrP to be stable in aqueous media at high temperatures (245 °C).[146] They found that for aqueous-phase hydrodeoxygenation of sorbitol no deactivation occurred for Pt/ZrP after 200 h time-on stream. ICP studies confirmed that no leaching occurred.

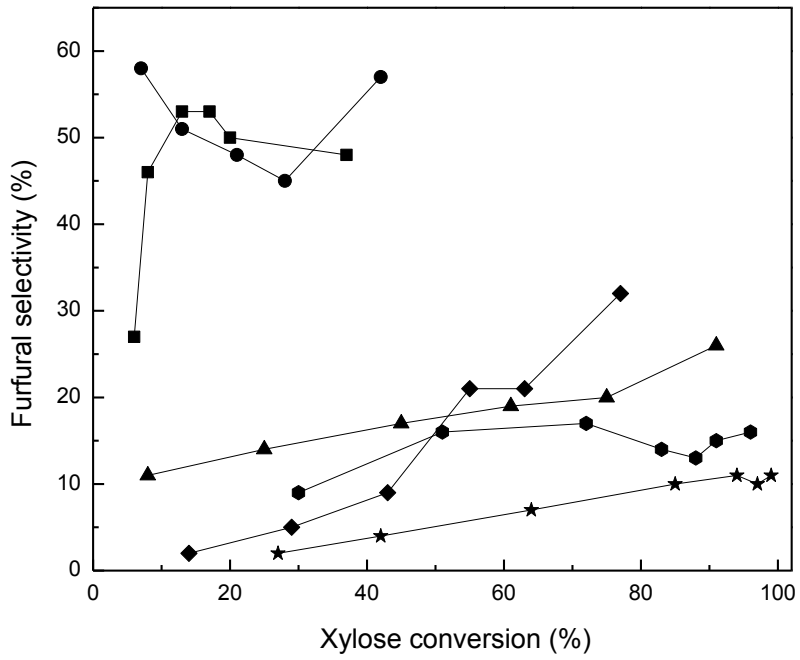

Figure 12. Furfural selectivity as a function of xylose conversion for different solid acid catalysts at 160 °C. Total acid sites were kept constant at 0.500 mmoles (determined by NH_3-TPD). Feed was 10 wt% xylose aqueous solution. Catalysts: HCl (■), ZrP (●), SiO_2-Al_2O_3 (▲), HY (◆), WO_X/ZrO_2 (⬢), γ-Al_2O_3 (★). Reprinted from ref.[140], Copyright(2011), with permission from Elsevier.

Furfural itself can undergo degradation reactions to form humins.[90] Separate experiments were performed with furfural as the feedstock (1.5 wt%) to study the effect of the catalysts on furfural degradation as shown in Figure 13. Reactions took place at 160 °C with total acid sites held constant at 0.500 mmoles (according to NH_3-TPD). In these experiments furfural was converted into a water insoluble humin phase that could not be detected by HPLC analysis. The catalyst activity was determined by measuring the residual amount of furfural in the aqueous phase. TOC measurements were performed to predict the overall carbon balance and results showed that we can account for all of the carbon. Formic acid was also detected as a minor by-

product of this reaction. Williams and Dunlop suggested that the presence of formic acid is a result of hydrolytic fission of the furfural aldehyde group.[69, 91]

Furfural degradation (disappearance) was found to be fairly independent of the catalyst used, with the exception of HY which had a significantly higher rate of furfural disappearance. This concurs with the HY adsorption/desorption data which showed a relatively high uptake of furfural. Further reactions with furfural as the feedstock and HY at various mixing rates confirmed that the reaction with this catalyst was not limited by external mass transfer.

HY behaves differently from the other catalysts as it has a microporous structure (see Table 4). Furfural irreversibly adsorbs in the HY pores and polymerizes to form humic substances. With that being said, Gürbüz *et al.* showed high yields of furfural (*ca.* 80%) from hemicellulose in the presence of H-Mordenite in GVL/water mixtures.[104] It is reasonable to believe that these conflicting results are as a result of differences in the pore dimensionality of HY and H-Mordenite. The former has a three-dimensional channel structure, whereas the latter is considered to be one-dimensional.[147]

Overall, these experiments show that the furfural degradation is a function of the amount of acid sites on the catalyst surface. Humins can also form from reactions between xylose and furfural, which we have previously shown to be the dominant pathway for humin formation for the aqueous phase dehydration of xylose with HCl.[90]

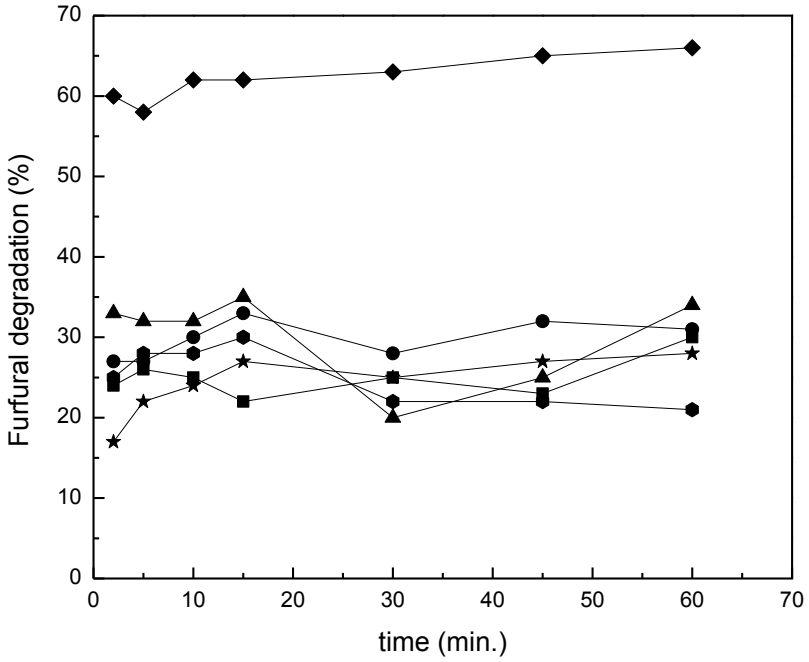

Figure 13. Furfural degradation (disappearance) with different acid catalysts at 160 °C. Total acid sites were kept constant at 0.500 mmoles (determined by NH_3-TPD). Feed was 1.5 wt% furfural aqueous solution. Catalysts: HCl (■), ZrP (●), SiO_2-Al_2O_3 (▲), HY (◆), WO_X/ZrO_2 (⬢), γ-Al_2O_3 (★). Reprinted from ref.[140], Copyright(2011), with permission from Elsevier.

3.3.3. Dehydration reactions with homogeneous Brønsted and Lewis acids

Water-soluble Brønsted and Lewis acids were used for xylose dehydration reactions in the aqueous phase. Hydrochloric acid and ytterbium (III) trifluoromethanesulfonate hydrate, $Yb(OTf)_3$, were used respectively. The latter is considered a stable water-soluble Lewis acid.[125, 148] Reactions were performed at varying Brønsted to Lewis ratios by combining the two acids accordingly, while holding the total amount of acid constant at 0.500 mmoles. Figure 14 shows the conversion of xylose for the different ratios of catalysts. The pure $Yb(OTf)_3$ catalyst had the highest activity for xylose disappearance while the pure HCl showed the lowest activity. A

mixture of $Yb(OTf)_3$ and HCl had a moderate catalyst activity. This result indicates that the Lewis acid sites have a higher catalytic activity towards xylose disappearance compared to the Brønsted acid sites, which is consistent with the results from the heterogeneous catalysts.

The furfural selectivity as a function of conversion is shown in Figure 15. HCl has a significantly higher furfural selectivity compared to $Yb(OTf)_3$. This signifies that the nature of the acid site can significantly affect the furfural selectivity, with Brønsted acid sites being more selective towards furfural production than Lewis acid sites. Again, these results are consistent with those of the heterogeneous catalysts.

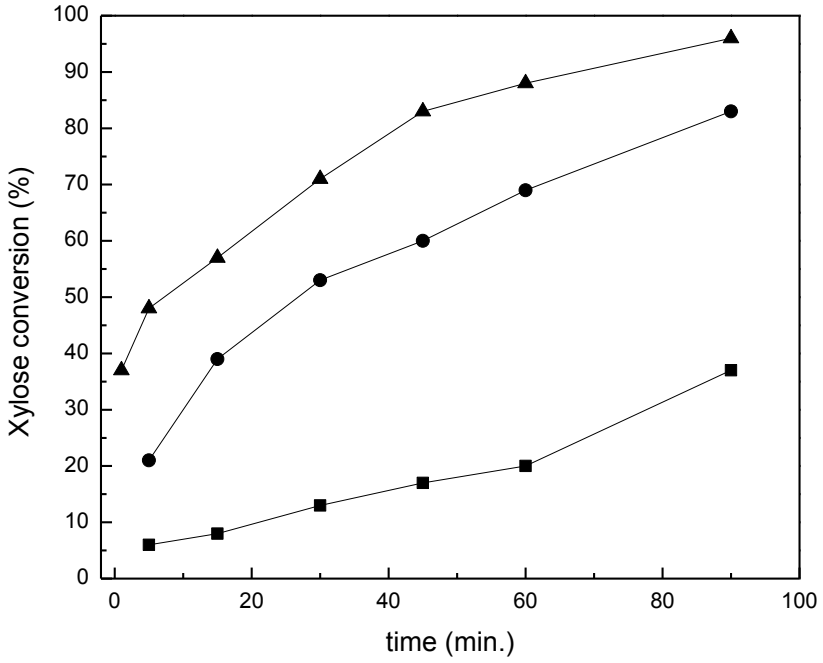

Figure 14. Effect of Brønsted to Lewis acid ratio on xylose conversion in a homogeneous regime at 160 °C. Total acid sites were kept constant at 0.500 mmoles. Feed was 10 wt% xylose aqueous solution. Brønsted : Lewis ratio = 1:0 (■), 1:1 (●), 0:1 (▲). Reprinted from ref.[140], Copyright(2011), with permission from Elsevier.

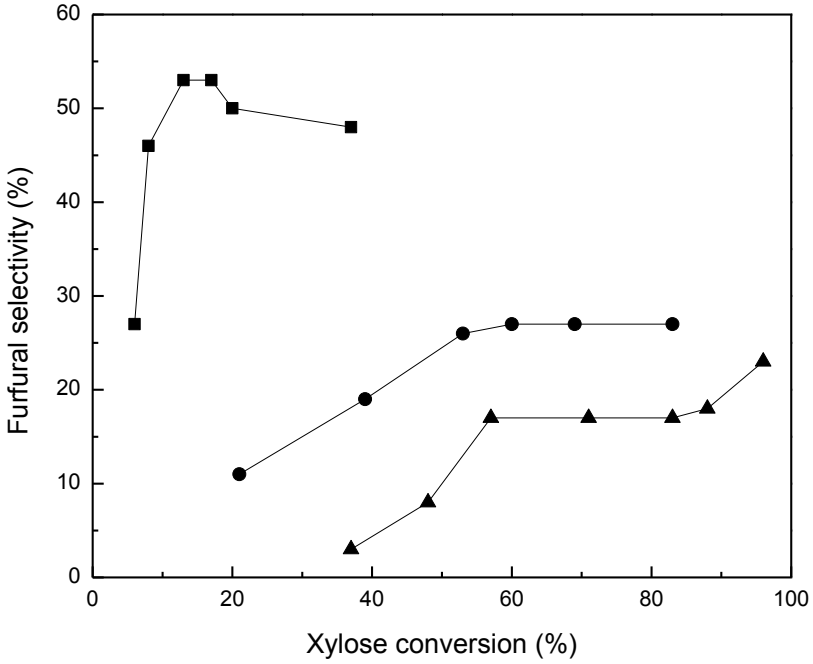

Figure 15. Effect of Brønsted to Lewis acid ratio on furfural selectivity from xylose in a homogeneous regime at 160 °C. Total acid sites were kept constant at 0.500 mmoles. Feed was 10 wt% xylose aqueous solution. Brønsted : Lewis ratio = 1:0 (■), 1:1 (●), 0:1 (▲). Reprinted from ref.[140], Copyright(2011), with permission from Elsevier.

Additional studies were performed at lower temperatures using a feedstock comprised of a mixture of xylose and furfural. Reactions were carried out with HCl and $Yb(OTf)_3$ separately. A 1:1 molar ratio of xylose and furfural was used with the total number of acid sites held constant at 0.750 mmoles. The results appear in Table 5.

Table 5. Results from dehydration reactions with homogeneous acid catalysts at 88 °C. Feeds were 3 wt% xylose, 2 wt% furfural or a mixture of the both (1:1 molar ratio). Total acid sites were kept constant at 0.750 mmoles. Reaction time was 90 min.[a]

Catalyst	Feedstock	Xylose conversion (%)	Furfural conversion (%)	Furfural yield (%)	Humins yield (%)
HCl	xylose	5.7	-	0.4	5.3
	furfural	-	11.4	-	10.4
	xylose + furfural	4.9	6.6	-	5.3
$Yb(OTf)_3$	xylose	28.5	-	0.5	27.5
	furfural	-	7.4	-	7.4
	xylose + furfural	27.1	13.9	-	17.4

[a] Reprinted from ref.[140], Copyright(2011), with permission from Elsevier.

The results obtained with HCl coincide with the reaction scheme in Figure 8. Reaction 1 (xylose dehydration) did not occur at the low reaction temperature due to its relatively high activation energy compared to Reactions 2 and 3. The latter reactions were suppressed as a result of the negligible amounts of furfural present. This is confirmed by the negligible xylose conversion and furfural yield. A similar outcome was attained with a feedstock composed of xylose and furfural.

Reactions with the homogeneous Lewis acid catalyst $Yb(OTf)_3$ resulted in relatively high xylose conversions and humins yields. The low reaction temperature and negligible furfural yield reduce the likelihood that this was due to xylose dehydration to produce furfural (Reaction 1). Rather, this was due to a new reaction pathway with xylose reacting with itself to produce humins.

3.3.4. Furfural production with ion resin catalysts

Xylose dehydration reactions were performed with acidic ion-exchange polymer resins to show the significance of Brønsted acid sites on furfural selectivity. Resins such as Nafion and Amberlyst have been shown to be effective catalysts for a wide range of acid-catalyzed reactions.[138, 149] Dumesic and co-workers used Nafion SAC-13 and Amberlyst 70 in part to produce liquid hydrocarbon transportation fuels. The catalysts were found to be particularly active for the dehydration of 5-nonanol to form nonenes with subsequent oligomerization to form C_9-derived alkenes.[150] This is primarily due to their relatively high concentrations of Brønsted acid sites. Likewise, Amberlyst 70 was found to be highly active and selective for butene oligomerization to form condensable alkenes.[59] A general overview of solid acid catalysis using ion-exchange resins is given by Harmer and Sun.[151] The characterization data for the ion resins appear in Table 6.

Table 6. Characterization of acidic ion-exchange polymer resins.[c]

	Gas Phase Characterization					Aqueous Phase Characterization	Furfural Adsorption
Catalyst	BET Surface Area (m^2 g^{-1})	Micropore Volume (cm^3 g^{-1})	Brønsted : Lewis ratio	Total acid sites (mmol g^{-1})	Brønsted sites (mmol g^{-1})	Acid sites (mmol g^{-1})	Uptake (g g^{-1})
Nafion SAC-13	231	0	∞ [b]	0.140 [a]	0.140	0.881	0.10
Amberlyst 70	0.32	0	∞	2.860 [a]	2.860	3.176	0.13

[a] Data provided by manufacturer.
[b] FTIR spectroscopic analysis detected weak Lewis acid sites originating from the silica matrix.[144] These sites were inactive in xylose dehydration.
[c] Reprinted from ref.[140], Copyright(2011), with permission from Elsevier.

Xylose conversion was measured as a function of time for Nafion SAC-13, Amberlyst 70, ZrP and HCl as shown in Figure 16. The catalytic activity of ZrP was found to be the highest compared to the ion resins and HCl. This coincides with our previous results which found catalyst activity to increase with the concentration of Lewis acid sites. The ion resins and HCl contain only Brønsted acid sites, whereas ZrP contains Lewis sites as well. Nafion SAC-13 showed lower xylose conversions than Amberlyst 70 and HCl. We believe that this is due to mass transfer limitations in the reactor due to inadequate mixing of the catalyst. Figure 17 compares the furfural selectivities as a function of xylose conversion for Nafion SAC-13, Amberlyst 70, ZrP and HCl. The results were found to be comparable for all of the catalysts.

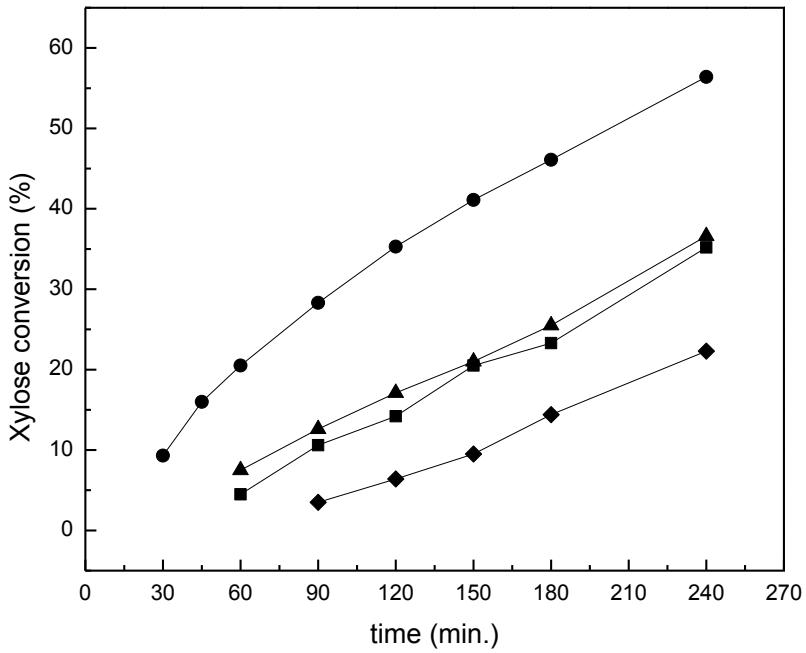

Figure 16. Xylose conversion as a function of time for different solid acid catalysts at 160 °C. Total acid sites were kept constant at 0.150 mmoles (data determined by NH_3-TPD or taken from manufacturer). Feed was 3 wt% xylose aqueous solution. Catalysts: HCl (■), ZrP (●), Amberlyst 70 (▲), Nafion SAC-13 (◆). Reprinted from ref.[140], Copyright(2011), with permission from Elsevier.

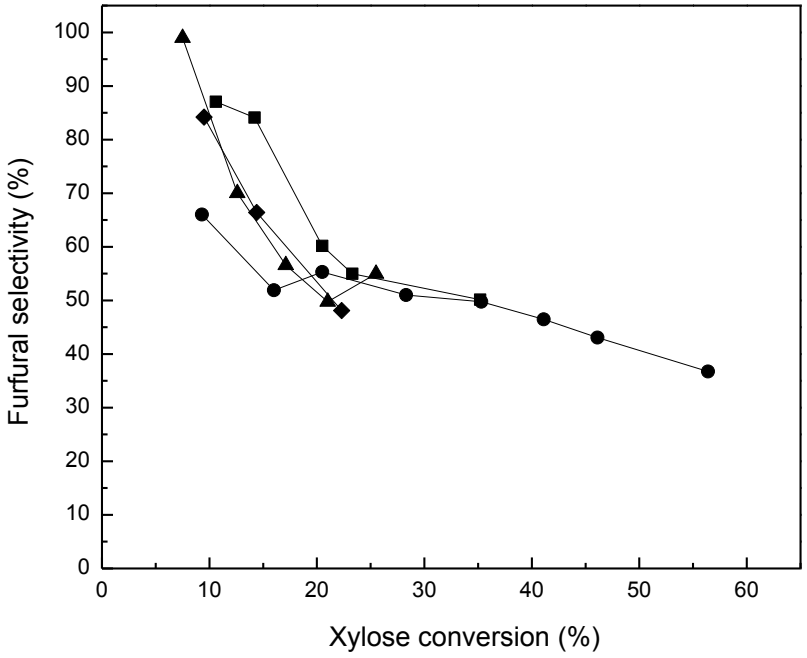

Figure 17. Furfural selectivity as a function of xylose conversion for different solid acid catalysts at 160 °C. Total acid sites were kept constant at 0.150 mmoles (data determined by NH_3-TPD or taken from manufacturer). Feed was 3 wt% xylose aqueous solution. Catalysts: HCl (■), ZrP (●), Amberlyst 70 (▲), Nafion SAC-13 (◆). Reprinted from ref.[140], Copyright(2011), with permission from Elsevier.

3.4. Discussion

The reaction chemistry for furfural production is comprised of three key reactions (refer to Figure 8). Xylose undergoes dehydration to lose three water molecules and produce furfural (Reaction 1); xylose reacts with furfural to produce humins (Reaction 2), and furfural undergoes a mono-degradation reaction to produce humins (Reaction 3). We have demonstrated here that Lewis and Brønsted sites share different functions as related to our proposed reaction scheme for xylose dehydration. Our studies show that both types of acid sites catalyze the dehydration of xylose to produce furfural (Reaction 1). Similarly, furfural decomposes on both Brønsted and Lewis sites to form humins (Reaction 3). Reaction 2, on the other hand, is predominantly catalyzed by Lewis sites. Consequently, a higher rate of xylose disappearance and lower furfural selectivity are observed for catalysts with increased Lewis sites. We have also showed that Lewis sites catalyze xylose mono-decomposition at lower temperatures. This reaction pathway could potentially be significant at higher temperatures as well.

Similar conclusions have been deduced by Song-Hai *et al.* in their study of acrolein production by gas-phase dehydration of glycerol with solid acid catalysts.[152] They found Brønsted acid sites to be advantageous over Lewis acid sites in selectively producing acrolein. They did not attempt to explain the cause of the undesired degradation reactions leading to lower acrolein selectivity. Likewise, in their study of furfural formation by acid hydrolysis of rice-hulls, Islam *et al.* found the addition of metal chlorides (Lewis acids) to have a negative effect on the furfural yield.[153] In regard to furfural, it has been suggested that the formation of black resinous products, *i.e.* humins, is a result of the furfural furan ring as well as the aldehyde group participating in polymerization reactions.[154] Accordingly, given the favorable conditions, Lewis

acids can form stable adducts with furfural which can possibly lead to the further formation of highly complex structures.

Initial reaction rates were deduced from the experimental plots of concentrations versus time using OriginPro® 7.5 software. The relative reaction rates for humin formation by furfural degradation (Reaction 3) and humin formation by reaction of furfural with xylose (Reaction 2) are shown in Table 7. For this purpose humins were considered all non-detectable soluble and insoluble compounds. These reaction rates are reported in reference to Reaction 1, which is furfural production. The relative rate of Reaction 2 increases with the concentration of Lewis acid sites. The relative rate of Reaction 3 is similar for all catalysts except for the HY and WO_X/ZrO_2. The high relative rate of Reaction 3 observed for HY, as depicted in Table 7, confirms that induced degradation reactions occur due to the irreversible adsorption of furfural in the catalyst pores. This concurs with previous conclusions made by Lourvanij *et al.* in their studies of glucose dehydration to oxygenated hydrocarbons with microporous materials.[155-157] They claim that microporous catalysts such as HY-zeolite induce molecular sieving reactions within the pores to promote the formation of coke. In comparison, they showed that a considerable less amount of decomposition reactions occurred with mesoporous MCM catalysts.

Table 7. Relative reaction rates calculated in accordance with xylose dehydration scheme.[b]

		Relative Rates	
Catalyst	Fraction of Brønsted acid sites	$rate_2 / rate_1$ [a]	$rate_3 / rate_1$ [a]
HCl	1.00	7.52	39.02
ZrP	0.96	3.73	46.94
SiO_2-Al_2O_3	0.79	20.42	54.12
HY	0.60	54.05	140.56
WO_X/ZrO_2	0.43	25.26	5.71
γ-Al_2O_3	0.40	167.93	20.84

[a] Reaction 1corresponds to furfural production from xylose; Reaction 2 corresponds to humin formation from furfural reacting with xylose; Reaction 3 corresponds to humin formation by furfural degradation.
[b] Reprinted from ref.[140], Copyright(2011), with permission from Elsevier.

Figure 18 shows the furfural selectivity as a function of the fraction of Brønsted acid sites for the heterogeneous and homogeneous catalysts tested in this study. These results clearly show that the furfural selectivity is a function of the Brønsted to Lewis acid site ratio as measured by the gas phase characterization. Thus, solid acid catalysts with high Brønsted to Lewis acid site ratios are necessary in order to obtain high furfural selectivities. A low concentration of Lewis acid sites minimizes the undesirable formation of humins *via* Reaction 2. Furthermore, dehydration reactions with acidic ion-exchange polymer resins show comparable furfural selectivities with ZrP and HCl. Similarly, Dias *et al.* showed that furfural can be produced from xylose at high selectivities (70%) and conversions (90%) with Amberlyst 15.[97] These results confirm that furfural selectivity is a direct function of the Brønsted acid sites concentration and not necessarily the nature of the acid sites.

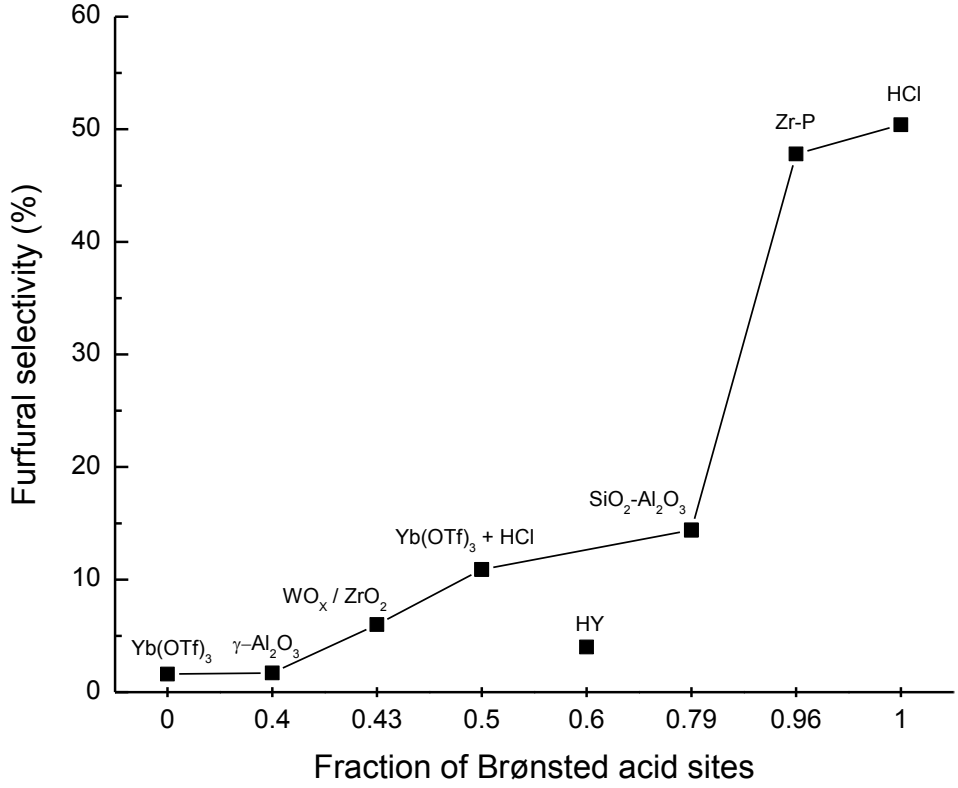

Figure 18. Furfural selectivity as a function of the fraction of Brønsted acid sites at 20% xylose conversion and 160 °C. Total acid sites were kept constant at 0.500 mmoles. Feed was 10 wt% xylose aqueous solution. Reprinted from ref.[140], Copyright(2011), with permission from Elsevier.

CHAPTER 4

Conclusions and Future work (I)

4.1. Conclusions

In Chapter 2 we developed a kinetic model for the dehydration of xylose in a biphasic reaction system using microwave heating and hydrochloric acid. Microwave heating shows no prominent effect on the dehydration chemistry with homogeneous acid catalysts and therefore it is likely that our model can also be valid for conventional heating. Our kinetic model involves three reactions and a phase equilibrium relationship. The kinetic steps consist of (1) xylose dehydration to form furfural, (2) formation of degradation products *via* reaction of xylose with furfural, and (3) furfural degradation. In a two-phase system, the furfural is extracted into the organic phase. The proposed kinetic model is consistent with the experimental data and can be used for both mono and biphasic systems.

The biphasic system does not alter the fundamental kinetics of its monophase analogue. The only role of the second phase is to extract the furfural. We have demonstrated that a two-phase system is favorable with the calculated product yield being more than twofold of that obtained in the single aqueous phase system. The apparent rate parameters derived from our kinetic model can be used to recognize the optimal conditions to achieve maximum furfural yield in this system. Accordingly, the apparent activation energy for xylose dehydration is higher (almost by two-fold) than the apparent activation energy for the degradation reactions. Thus, the maximum yields are obtained in a biphasic system, at high temperature, and short reaction times. Furfural yields of over 80% should be achieved in this type of system which is significantly higher than industrially obtained furfural yields of 40-50%.[73]

Chapter 3 discusses our work on the design of solid acid catalysts for aqueous phase dehydration of carbohydrates. Xylose dehydration to furfural was used as a model reaction. The catalytic activity of the various solid acid catalysts for xylose dehydration in the aqueous phase is

not a function of the total number of acid sites as measured by NH_3 adsorption. Increasing the relative number of Brønsted to Lewis acid sites decreases the catalytic activity. On a per site basis, γ-Al_2O_3 shows the highest activity, whereas ZrP and HCl demonstrate the lowest. Furfural selectivity follows the opposite trend with ZrP and HCl having considerably higher furfural selectivities than the other four catalysts. This finding confirms that furfural selectivity is dependent on the type of acid catalyst site. This has been confirmed with both heterogeneous and homogeneous acids (*i.e.* hydrochloric acid and ytterbium triflate).

The function of Lewis and Brønsted acid sites has been established in reference to the kinetic model that we developed for xylose dehydration. Lewis and Brønsted sites are responsible for catalyzing the dehydration reaction of xylose to form furfural (Reaction 1), as well as the degradation of furfural to form humins (Reaction 3). Lewis sites are principally accountable for the decrease in furfural selectivity due to the reaction between xylose and furfural to form humins (Reaction 2). Lewis sites can also potentially decrease the furfural selectivity by catalyzing the mono-decomposition of xylose to form humic compounds.

Furfural selectivity increases with an increase in the Brønsted to Lewis acid site ratio of the catalyst. Catalysts with high Brønsted to Lewis acid site ratios, such as ZrP, show selectivities as much as 30 times higher than catalysts with increased Lewis acid sites at 20% xylose conversion. These results are comparable with those obtained from dehydration reactions with acidic ion-exchange polymer resins and HCl. Additionally, ZrP shows viable promise for dehydration reactions due to its catalytic stability in the aqueous phase at high temperatures.

4.2. Future work

In our kinetic model we encountered an inconsistency with the experimental data at elevated temperatures for the two-phase system. The experimental data show an unpredicted increase in xylose decomposition, as well as an increased presence of furfural in the organic phase, as shown in Figure 9. This raises the question: Why does our model fall apart at elevated temperatures in a biphasic system? Hence, a modified kinetic model is necessary to accurately represent the biphasic system at higher temperatures. An additional kinetic term(s) which is prominent at higher temperatures is required to explain this behavior. One of the simplest, for instance, would be an additional term that depicts the decomposition of xylose to produce furfural directly in the organic phase. This would explain the observed rate increase of xylose decomposition and the elevated furfural concentration in the organic layer. However, this concept is difficult to realize for xylose is not found in the upper phase under these reaction conditions. Nonetheless, it would be reasonable to conceive that this term describes the chemistry that occurs in the interfacial region between the aqueous and organic phase.

For clarification purposes, a comparable term was indeed proposed to the existing kinetic model and the revised version showed to be consistent with the experimental data at all temperatures. The activation energy for this additional theoretical term was found to be threefold of E_{A_1}. Hence, this high energy barrier step becomes relevant only at higher temperatures. Pressure limitations in the reaction vessel prohibited further studies at elevated temperatures to attempt to validate this hypothesis. In fact, Vlachos and co-workers have proposed a method to produce furfural from xylose at relatively mild conditions (100-

145 °C) using a cascade of reactions, wherein xylose is first isomerized to xylulose and lyxose with a Lewis acid followed dehydration to furfural with a Brønsted acid.[158, 159] They were able to achieve furfural yields of up to 76% in a biphasic system with toluene as the extracting phase in combination with $CrCl_3$ (Lewis acid) and HCl (Brønsted acid).[160]

In our kinetic model study we also realized that equilibrium between furfural in the organic and aqueous phase is not sustained throughout the reaction. The mass transfer between the phases is limiting in our system compared to furfural formation. As the reaction proceeds and the rate of furfural formation decreases, the relative rate of mass transfer consequently intensifies and the system approaches phase equilibrium. Xing *et al.* used a continuous two zone biphasic reactor to produce furfural from waste aqueous hemicellulose solutions.[161] Furfural was continuously extracted from the aqueous phase to an immiscible organic layer during the reaction. They report partition coefficients which are predominantly higher than the value of 7.1 which we report in our system. This indicates that reactor design is critical in obtaining high yields of furfural. Consequently, a model to account for the hydrodynamics will be important as the process is scaled-up. Román-Leshkov *et al.* have shown that the use of phase modifiers can enhance the partitioning of furan derivatives (*i.e.* furfural and HMF) into the extracting phase.[29, 33] Further studies with different reactor configurations and perhaps phase modifiers would be essential to improve the rate of furfural extraction to the organic phase in these types of biphasic systems.

We determined the concentration of both Brønsted and Lewis acid sites of these catalysts with gas phase techniques and compared the results with those obtained with a titration technique in the aqueous phase. For four out of the five catalysts tested, the titration studies resulted in

higher acid concentrations compared to the gas phase technique. These inconsistent results raise questions about the reliability of the aqueous phase titration to measure acid sites. Moreover, Shanks and co-workers have found that the conditions under which aqueous phase titrations are performed can have a significant effect on the measured values.[162]

The consistent data that we have obtained from dehydration reactions in aqueous solutions with the solid acid catalysts suggest that gas phase characterization of acid sites can be used to predict catalytic activity in the aqueous phase. Even so, as the field of aqueous phase biomass conversion continues to advance, it will be imperative to further study how acid catalysts are affected by water under hydrothermal conditions.

On another note, it is also notable to mention that all of the reactions that we performed in Chapter 3 were carried out by way of microwave heating. As mentioned in Chapter 2, when HCl was used as a catalyst no differences in the rate of xylose conversion or furfural selectivity were observed with microwave and conventional heating. However, when ZrP was used as a catalyst the rate of xylose conversion with microwave heating was between 1.92-3.32 times that of conventional heating depending on reaction time (refer to Figure A.21 in the Appendix). Conventional reactions took place in a Parr reactor and identical heating rates were employed for all reactions in this comparison. The furfural selectivity was slightly higher for microwave heating than conventional heating with the ZrP catalyst (refer to Figure A.22 in the Appendix). Our current findings agree with those reported by Qi *et al.* who showed enhanced production of 5-hydroxymethylfurfural (HMF) from fructose and glucose due to microwave irradiation.[81] Accordingly, it has been emphasized that microwave absorption at the solid interface can

advantageously influence the overall reaction kinetics.[94] Further studies are necessary to fully understand the enhanced microwave effects reported for systems with heterogeneous catalysts.

Overall, there are still many unanswered questions pertaining to the behavior of solid acid catalysts in liquid phase systems. Some of the key fundamental questions include:

- How do we design solid acid catalysts with more Brønsted acid sites?
- What makes a solid acid catalyst hydrothermally stable?
- Is catalytic activity in the gas-phase analogous to that observed in the liquid phase (effect of solvation)?
- What are the differences in the reaction mechanism with homogeneous and heterogeneous acids?
- What are the reaction intermediates and why can't we detect them?
- What is the fundamental chemistry for humins formation and what are the determining factors that influence the chemistry (*i.e.* feedstock and solvent)?

SECTION II: AQUEOUS PHASE LEVULINIC ACID STUDIES

CHAPTER 5

Levulinic acid kinetics and reaction engineering

Weingarten, R.; Cho, J.; Xing, R.; Conner, W. C.; Huber, G. W., Kinetics and Reaction Engineering of Levulinic Acid Production from Aqueous Glucose Solutions. *Chemsuschem* **2012,** *5* (7), 1280-1290.

5.1. Background

The purpose of this study was to develop a kinetic model for the conversion of glucose to levulinic acid in aqueous media with HCl by fitting kinetic data collected in a batch reactor, a plug flow reactor (PFR) and a continuously stirred-tank reactor (CSTR). The kinetic model consists of four key steps: (1) glucose dehydration to form 5-hydroxymethylfurfural (HMF); (2) glucose reversion/degradation reactions to produce humins; (3) HMF rehydration to form levulinic acid and formic acid, and (4) HMF degradation to form humins.

Levulinic acid is currently not produced in commercial quantities. This is due to a number of impeding factors which include high cost of raw material, complex conversion routes, energy intensive downstream processing, high operating costs due to the use of homogeneous acid catalysts and low selectivity.[68] HMF rehydration is fairly selective to levulinic acid and form acid, thus the bottleneck in the production of levulinic acid from carbohydrates lies in the dehydration step to produce HMF from hexose sugars. The apparent rate parameters derived in this model will be used to predict the optimal operating conditions for HMF and levulinic acid production from glucose. This model also predicts the optimal reactor design in a continuous reactor system, which is instrumental from a process perspective.

One current process for production of levulinic acid was developed by Biofine Incorporated (presently Biofine Renewables). The Biofine process claims to produce levulinic acid at yields higher than 70% of the theoretical (58% carbon yield), based on the hexose content of the cellulosic feedstock, in a two-reactor system.[163, 164] The carbohydrate-containing feedstock is initially hydrolyzed in the first reactor (PFR) at 210-230 °C for 13-25 seconds in the presence of 1-5 wt% sulfuric acid. The product, HMF, is then continuously removed and

supplied to a second reactor (CSTR) where it is further hydrolyzed at 195-215 °C for 15-30 minutes to produce levulinic acid. The production of 1 ton of levulinic acid from cellulose, assuming a theoretical yield of 76% and a 3.5 wt% acid concentration, requires 3.5 tons of sulfuric acid. A schematic of the Biofine process appears in Figure 19.

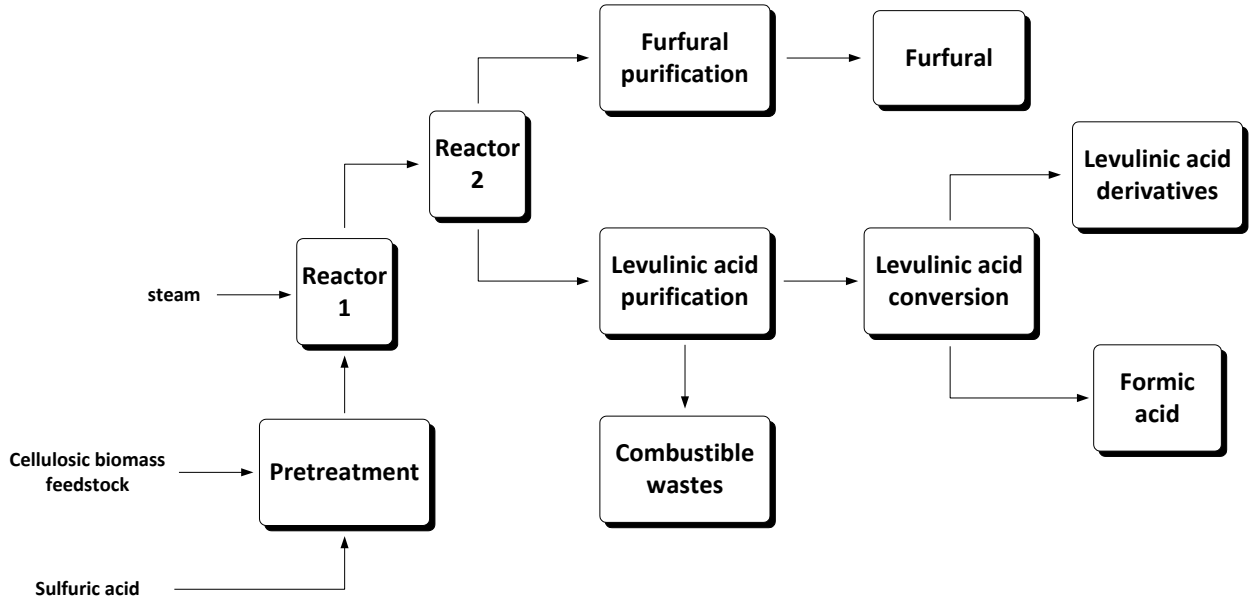

Figure 19. The Biofine process. Reprinted from ref.[52], Copyright(2000), with permission from Elsevier.

Vast interest in levulinic acid applications has lead to numerous kinetic studies on the decomposition of carbohydrates to produce HMF and levulinic acid. Some studies have also incorporated a hydrolysis step into their models to produce glucose from cellulose or woody biomass. The formation of humins has been reported in the literature since the early stages of this research.[165-167] It has also been postulated that discoloration of sugar solutions is attributed to the polymerization of HMF to yield colored products of varying degrees of solubility.[168] Nonetheless, early kinetic studies only obtained kinetic parameters for the dehydration and

rehydration steps leading to levulinic acid. More recent kinetic studies have incorporated undesired byproduct formation steps to enhance the accuracy of their models.[169-174]

5.2. Experimental

5.2.1. Reaction kinetics measurements

Batch reactions were carried out in a 100 mL reactor vessel provided by Parr Instrument Company, series 4560. The feedstock solutions were prepared with DI water at the specified concentrations. Acidic solutions were prepared with hydrochloric acid (Fisher Scientific). Glucose was provided by Fisher Scientific. HMF (99%) was provided by Sigma Aldrich. Levulinic acid (98%) and formic acid (98%) were provided by Acros Organics. Temperatures in the reactor were measured by a thermocouple in the solution. All reaction solutions were mixed at a maximum constant rate of 600 rpm using an internal stirrer. The temperature and stirring were controlled by a 4848 Controller provided by Parr. The reaction vessel was initially pressurized to 800 psi with industrial grade helium (Airgas). Samples were taken periodically by way of a sampling port. The samples were immediately quenched in an ice water bath and filtered with a 0.2 μm syringe filter prior to analysis. The reactor was repressurized with helium after each sampling.

Continuous reactions were carried out in both a PFR and a CSTR. The PFR reactor was made with a stainless steel tube of 0.25 inch O.D. A Varian HPLC pump (Prostar 210) was used to introduce the feedstock into the reactor at flow rates ranging from 0.065-1.293 mL/min. The reactor was heated by a heating tape (McMaster-Carr) and insulation tape was used to minimize

heat losses. A thermocouple was placed adjacent to the reactor wall to measure the temperature and connected to a temperature controller. The reactor system was initially pressurized to 600 psi with UHP grade helium (Airgas). Liquid products were recovered in a sample vessel at room temperature. The samples were filtered with a 0.2 μm syringe filter prior to analysis.

The CSTR with a 100 mL reactor vessel was modified from a Parr batch reactor, allowing continuous liquid flow in and out of the reactor. A Varian HPLC pump (Prostar 210) was used to introduce the feedstock into the reactor through a port on the reactor cap. The flow rates ranged from 0.300-2.400 mL/min. A dip tube was used as the outlet of the reactor. The temperature and stirring were controlled as described for the batch reactions. The reaction vessel was initially pressurized to 800 psi with industrial grade helium (Airgas). A back pressure regulator was used to monitor the pressure of the system. Liquid products were recovered in a sample vessel at room temperature. The samples were filtered with a 0.2 μm syringe filter prior to analysis.

5.2.2. Analysis

Samples were analyzed by high pressure liquid chromatography (HPLC) with a Shimadzu© LC-20AT. Carbohydrates were detected with a RI detector (RID-10A) and products were detected with a UV-Vis detector (SPD-20AV) at wavelengths of 210 and 254 nm. The column used was a Biorad© Aminex HPX-87H sugar column. The mobile phase was 0.005 M H_2SO_4 flowing at a rate of 0.6 mL/min. The column oven was set to 30 °C. The total organic carbon (TOC) measurements were performed with a Shimadzu© TOC-VCPH Analyzer. Calibrations were performed with carbon standards supplied by SpectroPure.

5.2.3. Modeling

Experimental data were collected and used to compare with the proposed kinetic model to estimate rate parameters of the reaction pathways for levulinic acid production from glucose. The kinetic model for the overall reaction paths was a set of coupled ordinary differential equations (ODEs) and rate constants were correlated by the Arrhenius equation to include temperature dependence. The pre-exponential factors and activation energies were set as adjustable parameters to simultaneously correlate a complete set of concentration data for reactants and products at different temperatures (120-180 °C). The sum of absolute errors between estimated and observed values was minimized to find the best fit with the observed reaction rates of glucose dehydration and levulinic acid formation. Matlab and Athena Visual Studio (v14.0) were used for the numerical integration of ODEs and parameter estimations.

5.3. Results

5.3.1. Kinetic model for HMF rehydration

Aqueous-phase HMF rehydration experiments were carried out in a batch reactor at temperatures 120-150 °C in acidic media (0.1 M HCl) with an initial concentration of 4 wt% HMF. Similarly, additional experiments were carried out at 130 °C with initial HMF concentrations ranging 4-16 wt% to study the effect of both feedstock and water concentration. Figure 20 shows that comparable HMF conversions and levulinic acid yields were obtained for the range of initial HMF concentrations in the current study.

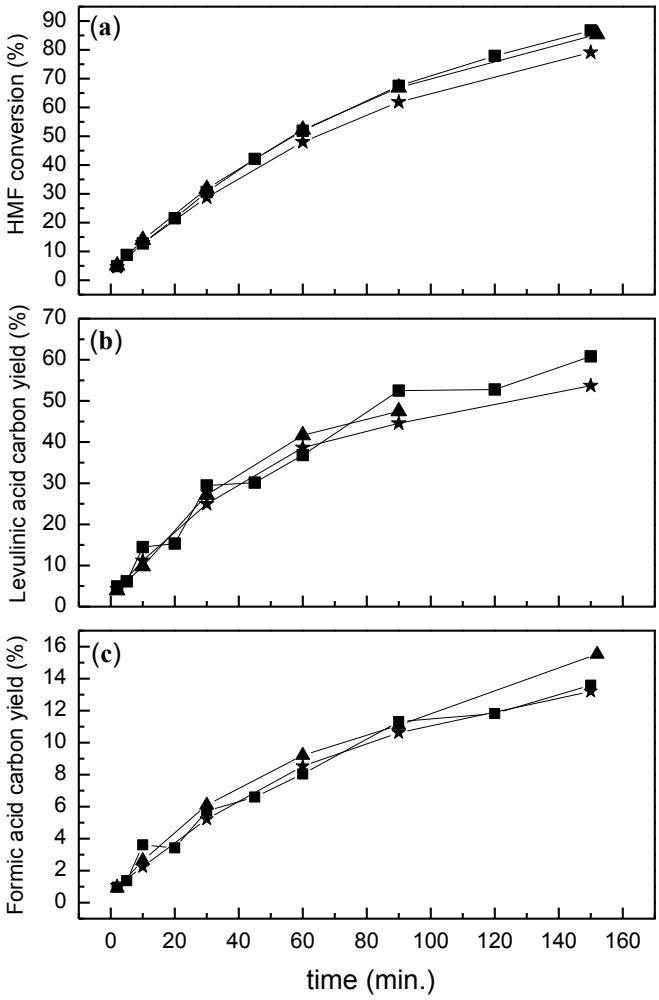

Figure 20. Aqueous-phase acid-catalyzed HMF rehydration in a stirred batch reactor. Effect of initial HMF concentration on (**a**) HMF conversion; (**b**) levulinic acid carbon yield and (**c**) formic acid carbon yield at 130 °C and 0.1 M HCl. $[HMF]_o$ (wt%) = 4 (■), 8 (▲), 16 (★). Reprinted from ref.[175], Copyright(2012), with permission from John Wiley and Sons.

$$HMF + 2H_2O \xrightarrow{k_3} LA + FA \quad (14)$$

$$HMF \xrightarrow{k_4} D \quad (15)$$

LA ≡ levulinic acid; FA ≡ formic acid; D ≡ decomposition products (humins)

Scheme 4. Aqueous-phase HMF rehydration.

The reaction scheme for HMF rehydration consists of two irreversible parallel reactions of Equations (14) and (15), as shown in Scheme 4. The first reaction (Eqn. 14) is the rehydration of HMF with two molecules of water to produce levulinic acid and formic acid. The second reaction (Eqn. 15) is the degradation of HMF to produce humins. This proposed reaction scheme is consistent with the mechanism proposed by Horvat *et al.* for levulinic acid formation from HMF.[176, 177] They claimed that the addition of water to the 2, 3-carbon position on HMF resulted in undesired polymerization reactions, whereas the 4, 5 addition of water gave way to levulinic acid formation *via* decarboxylation to produce formic acid. Both reactions fit equations that are pseudo first order with respect to HMF. This is in agreement with previous kinetic studies on HMF decomposition.[167, 178] Furthermore, within our range of concentrations, water is considered to be in excess (zero order) in the rehydration step (see Figure 20). Some kinetic studies have also proposed an additional reaction pathway to produce humins from levulinic acid.[173, 174] However, our separate studies with equimolar concentrations of levulinic acid and formic acid at 180 °C with 0.1 M HCl concluded that levulinic acid did not degrade after 120 min. This is in agreement with other studies.[167, 170]

All experimental data for HMF rehydration were fit to the proposed kinetic model to estimate the rate parameters. Our model assumed a first order dependence with respect to the acid concentration and the activation energies were determined for experiments carried out at a constant acid concentration of 0.1 M HCl. The best correlated values with their standard errors appear in Table 8. The estimated values of the activation energies were assumed to be independent of the acid concentration and were used for the remaining of the model fitting. On this note, it has been reported that activation energy can be a function of acid concentration.

However, this claim is valid when a reaction is governed by a slow proton transfer step.[179] It is also notable to mention that small amounts of furfural were detected as a by-product of this reaction, at less than 0.04% yield. It has been reported that the formation of furfural from HMF proceeds *via* loss of formaldehyde.[180-183] Figure 21 shows the experimental data for HMF rehydration and levulinic acid production with the fitted model at 0.1 M HCl.

Table 8. Estimated kinetic parameters for aqueous-phase HMF conversion.[c]

Rate constants [a]	$\log_{10}[A\ (\text{min}^{-1})]$	E (kJ mol^{-1})
k_3	10.31 ± 0.71 [b]	94.72 ± 5.54
k_4	15.69 ± 3.22	141.94 ± 25.72

Kinetic parameters fit experimental data at: T = 120-150 °C; $[HMF]_o$ = 4-16 wt%; $[H^+]$ = 0.1 M.
[a] 1st order rate parameters are lumped with acid concentration.
[b] 95% confidence interval in parameter estimation.
[c] Reprinted from ref.[175], Copyright(2012), with permission from John Wiley and Sons.

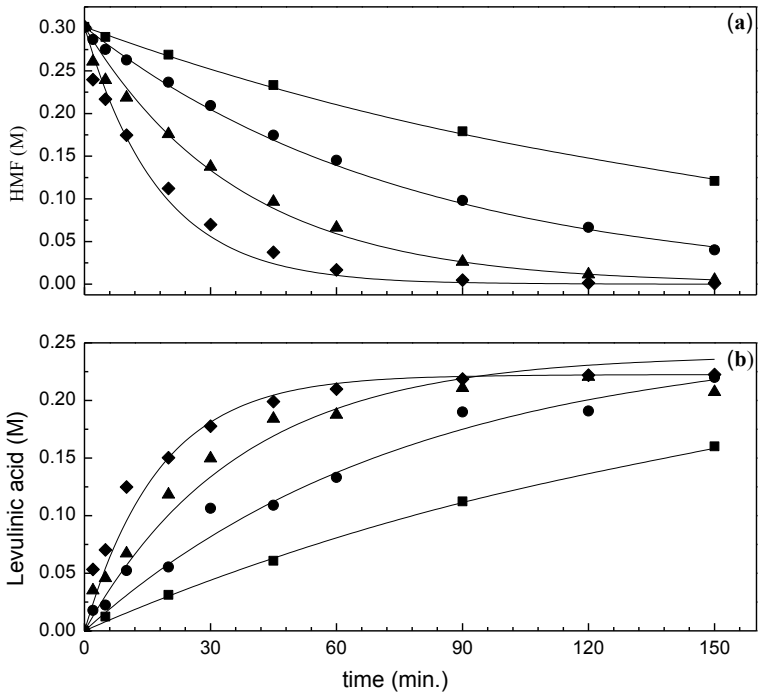

Figure 21. Aqueous-phase acid-catalyzed HMF rehydration to levulinic acid in a stirred batch reactor. Kinetic model fit for (**a**) HMF rehydration and (**b**) levulinic acid formation for 4 wt% HMF and 0.1 M HCl. T (°C) = 120 (■), 130 (●), 140 (▲), 150 (◆); Model prediction (—). Reprinted from ref.[175], Copyright(2012), with permission from John Wiley and Sons.

5.3.2. Kinetic model for glucose dehydration

Glucose dehydration experiments were carried out in a batch reactor at temperatures 140-180 °C in 0.1 M HCl with an initial glucose concentration of 10 wt%. The overall reaction scheme for aqueous-phase levulinic acid production from glucose appears in Figure 22.

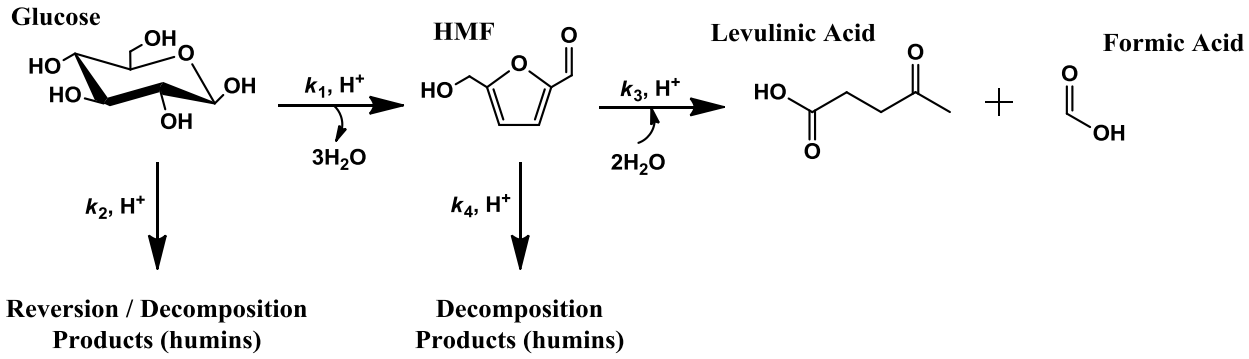

Figure 22. Overall reaction scheme for the aqueous-phase acid-catalyzed production of levulinic acid from glucose. Reprinted from ref.[175], Copyright(2012), with permission from John Wiley and Sons.

Glucose undergoes two irreversible parallel reactions which consist of a triple dehydration step to produce HMF, or a degradation reaction to form humins. Both reactions have been reported to be pseudo first order with respect to glucose.[171] This was also confirmed with reactions that were carried out at various initial glucose concentrations ranging from 2-20 wt% at 160 °C in 0.1 M HCl. Glucose conversions, HMF yields and levulinic acid yields were found to be predominantly independent of the initial glucose concentration, as illustrated in Figure 23.

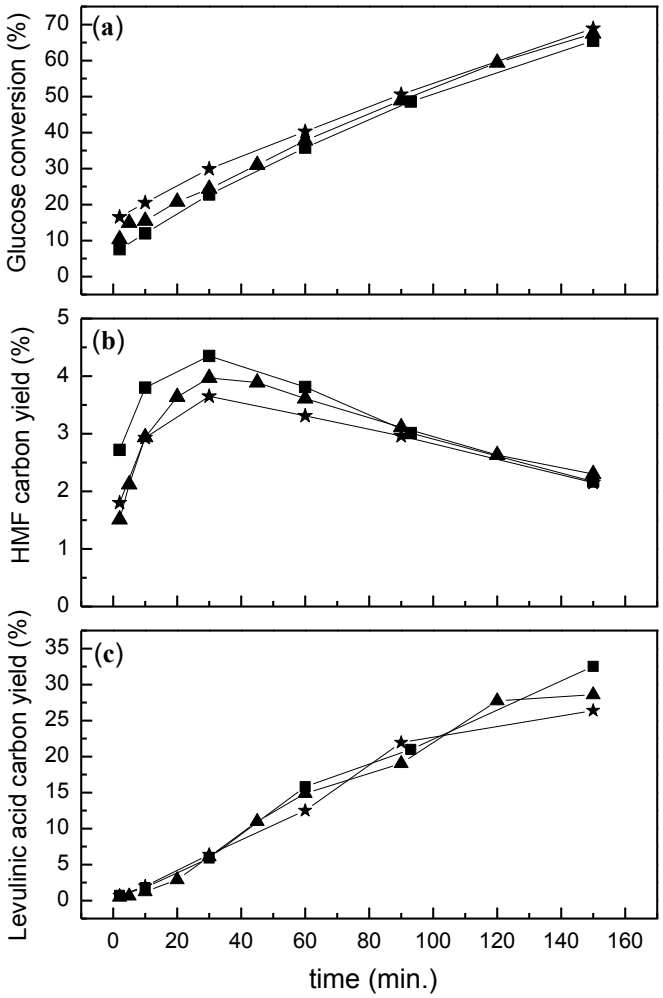

Figure 23. Aqueous-phase acid-catalyzed glucose dehydration reactions in a stirred batch reactor. Effect of initial glucose concentration on (**a**) glucose conversion; (**b**) HMF carbon yield and (**c**) levulinic acid carbon yield at 160 °C and 0.1 M HCl. $[Glucose]_o$ (wt%) = 2 (■), 10 (▲), 20 (★). Reprinted from ref.[175], Copyright(2012), with permission from John Wiley and Sons.

The rate parameters obtained for glucose dehydration appear in Table 9. Reactions 3 and 4 (HMF rehydration and HMF decomposition respectively) were assumed independent of Reactions 1 and 2 (glucose dehydration and glucose decomposition respectively). Therefore, the same rate parameters obtained for HMF rehydration (refer to Table 8) were combined with those derived for glucose dehydration to fit the experimental data to our proposed model for levulinic

acid production from glucose. The experimental data for glucose dehydration, HMF and levulinic acid production appear in Figure 24 along with the fitted kinetic model.

Table 9. Estimated kinetic parameters for aqueous-phase glucose conversion.[c]

Rate constants [a]	$\log_{10}[A\ (\text{min}^{-1})]$	E (kJ mol^{-1})
k_1	17.12 ± 0.62 [b]	160.16 ± 5.15
k_2	3.33 ± 0.29	50.68 ± 2.38

Kinetic parameters fit experimental data at: T = 140-180 °C; $[\text{Glucose}]_o$ = 2-20 wt%; $[H^+]$ = 0.1 M.
[a] 1st order rate parameters are lumped with acid concentration.
[b] 95% confidence interval in parameter estimation.
[c] Reprinted from ref.[175], Copyright(2012), with permission from John Wiley and Sons.

The overall rate equations for glucose conversion are shown as Equations 16, 17 and 18.

$$\frac{d[\text{G}]}{dt} = -(k_1 + k_2)[\text{G}] \tag{16}$$

$$\frac{d[\text{HMF}]}{dt} = k_1[\text{G}] - (k_3 + k_4)[\text{HMF}] \tag{17}$$

$$\frac{d[\text{LA}]}{dt} = k_3[\text{HMF}] \tag{18}$$

As with the HMF rehydration study, the activation energies for glucose dehydration (Reactions 1 and 2) were determined for experiments carried out at a constant acid concentration of 0.1 M HCl. Likewise, it was initially assumed that a first order dependence exists with respect to the acid concentration.

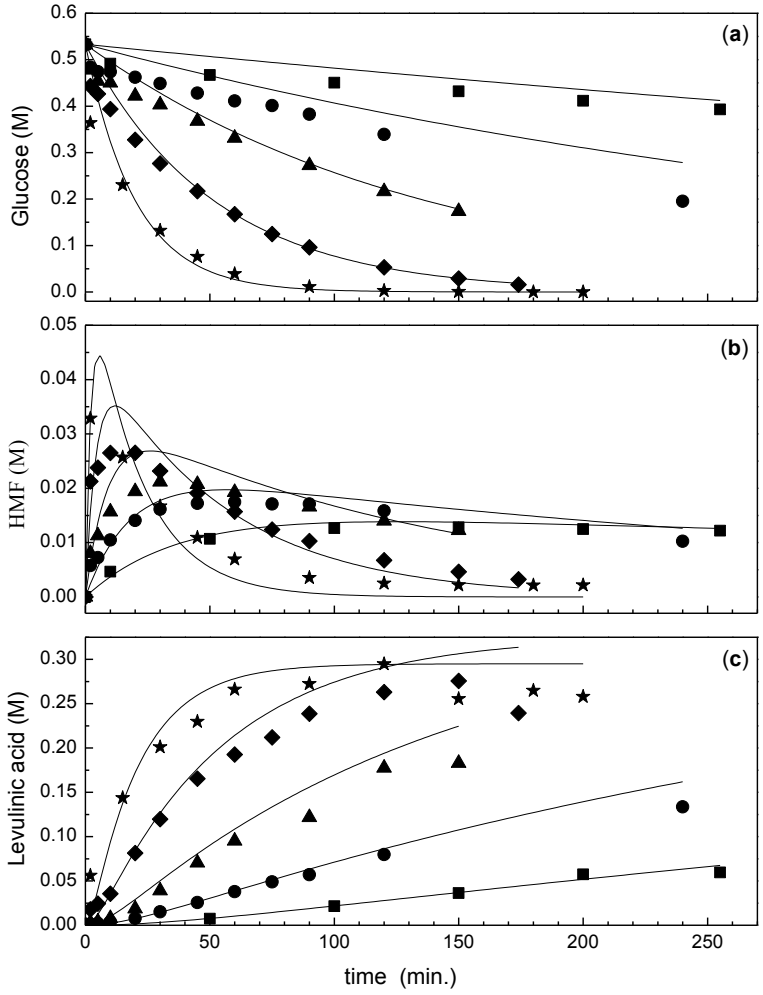

Figure 24. Aqueous-phase acid-catalyzed glucose dehydration in a stirred batch reactor. Kinetic model fit for (**a**) glucose dehydration, (**b**) HMF formation and (**c**) levulinic acid formation for 10 wt% glucose and 0.1 M HCl. T (°C) = 140 (■), 150 (●), 160 (▲), 170 (◆), 180 (★); Model prediction (—). Reprinted from ref.[175], Copyright(2012), with permission from John Wiley and Sons.

Glucose can also undergo reversion and epimerization reactions to produce oligosaccharides, anhydro sugars and fructose respectively.[166, 171, 184] The reversion products are mainly disaccharides, which are formed by way of a coupling reaction of the anomeric hydroxyl group of one glucose molecule with any hydroxyl group of a second molecule.[185] It has also been suggested that products from reversion reactions can be subject to degradation reactions, in

which the disaccharides react further to form oligosaccharides.[186] Consequently, the presence of cellobiose confirmed the occurrence of reversion reactions in this study. Levoglucosan (1, 6-anhydro-β-D-glucopyranose) and fructose were also detected in the reaction samples in qualitative amounts. Fructose was present at less than 0.1% yield. Previous studies have shown that the formation of fructose from glucose in acidic solution proceeds by way of a C_2 to C_1 intramolecular hydrogen transfer.[187] The role of the acid catalyst is to protonate the carbonyl oxygen atom to facilitate a hydride shift mechanism.[188] Similar conclusions were deduced by Davis and co-workers in their study of aqueous-phase glucose isomerization to fructose with a solid Lewis acid catalyst.[122, 189, 190]

Hence, one theory suggests that the formation of HMF from glucose proceeds *via* fructose[185]; and the near nil presence of fructose can be attributed to its high reactivity compared to glucose.[187, 191] Conversely, others claim that glucose can be converted directly to HMF through cyclization of a 3-deoxyglucosone intermediate formed from the open-ring form of glucose.[192, 193] In this respect, relatively low conversion of glucose to HMF is caused by its low affinity to exist in the open-ring form due to stabilization of the glucose pyranose forms in aqueous solution.[194] Overall, there are two schools of thought with regard to the mechanism of HMF formation from C_6 carbohydrates. One theory postulates that the reaction proceeds by way of the acyclic 1, 2-enediol intermediate.[187, 195] The other takes into account a fructofuranosyl cyclic intermediate in the formation of HMF from fructose.[192, 196] Recent computational studies have also reported the use of fructofuranosyl intermediates in the formation of levulinic acid and HMF from glucose and fructose respectively.[194, 197] Caratzoulas and Vlachos studied the energetics of the acid-catalyzed dehydration of fructose to HMF *via* the closed-ring

mechanism.[198] They found that the reaction proceeds by way of intramolecular proton and hydride transfers.

Furfural was also detected as a final by-product of the dehydration reaction from glucose, at less than 0.61% yield. As mentioned previously, it is possible that HMF is the precursor for its formation. However, some have also postulated alternative pathways to produce furfural from hexoses *via* a pentose unit with formaldehyde or formic acid as by-products.[182, 199, 200] Incidentally, formic acid can also be produced directly from C_6 monosaccharides,[200] as well as from furfural.[69, 91] Regardless, it is reasonable to assume that formic acid was produced *via* multiple routes, besides the conventional pathway from HMF rehydration. Accordingly, an excess of formic acid was detected throughout the entire study relative to the kinetic model data, as depicted in Figure 25. Consequently, the levulinic acid to formic acid carbon molar ratio was lower than its stoichiometric value of 5 in this study.

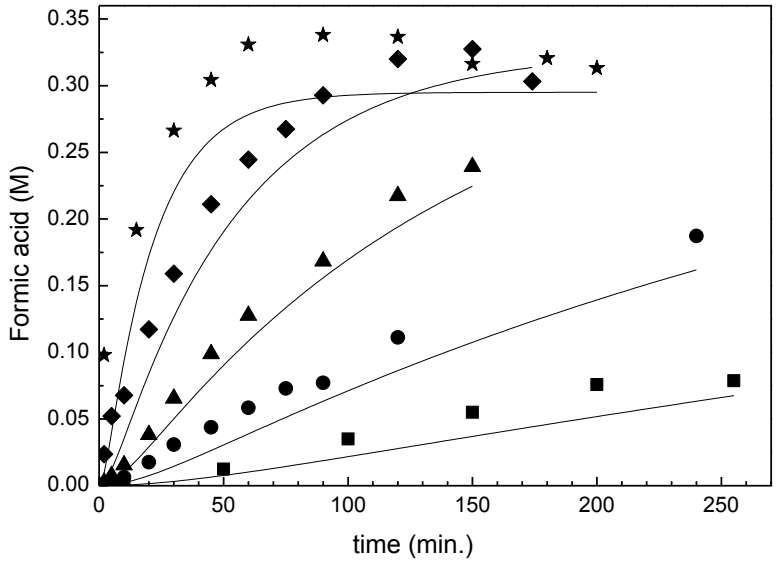

Figure 25. Aqueous-phase formic acid production from glucose in a stirred batch reactor. Comparison between experimental and kinetic model data. Feed was 10 wt% glucose and 0.1 M HCl. T (°C) = 140 (■), 150 (●), 160 (▲), 170 (◆), 180 (★); Model (—). Reprinted from ref.[175], Copyright(2012), with permission from John Wiley and Sons.

5.3.3. Effect of acid concentration

Further glucose dehydration experiments were carried out at acid concentrations with 0.5 and 1.0 M HCl and temperatures 140-180 °C. The initial glucose concentration was kept constant at 10 wt%. The kinetic model fits for glucose dehydration at 0.5 M HCl and 1.0 M HCl appear in the Appendix (refer to Figures A.1-A.2). As mentioned beforehand, activation energies were calculated for reactions at 0.1 M HCl and assumed to be constant for all other acid concentrations. The pre-exponential factors were calculated for each reaction step *i* (refer to Figure 22) at every acid concentration and a power law function was derived, as shown in Eqn. 19. This approach was similar to those used by Saeman[165] and Kuster.[191] The best fit kinetic parameters with their standard errors are tabulated in Table 10.

$$A_i = A_{i,\mathrm{o}} \times \left(\mathrm{H}_{i,\mathrm{o}} + \left[\mathrm{H}^+\right]^{n_i}\right) \tag{19}$$

$i \equiv$ reaction number; $\mathrm{A}_{i,\mathrm{o}}$, $\mathrm{H}_{i,\mathrm{o}}$, $n_i \equiv$ constants

Table 10. Estimated kinetic parameters for aqueous-phase glucose dehydration to levulinic acid with dependence on acid concentration.[b]

i	$\log_{10}\left[A_{i,o}\ \left(\mathrm{M}^{-n_i}\ \mathrm{min}^{-1}\right)\right]$	$E_i\left(\mathrm{kJ\ mol}^{-1}\right)$	$\mathrm{H}_{i,\mathrm{o}}$	n_i
1	18.44 ± 0.98 [a]	160.16 ± 5.15	0	1.290 ± 0.062
2	3.86 ± 0.52	50.68 ± 2.38	0.29 ± 0.01	2.764 ± 0.213
3	11.50 ± 0.83	94.72 ± 5.54	0	1.176 ± 0.103
4	16.83 ± 3.43	141.94 ± 25.72	0	1.176 ± 0.114

Kinetic parameters fit experimental data at: T = 140-180 °C; $[\mathrm{Glucose}]_o$ = 2-20 wt%; 0 M < $[\mathrm{H}^+]$ ≤ 1.0 M.

[a] 95% confidence interval in parameter estimation.

[b] Reprinted from ref.[175], Copyright(2012), with permission from John Wiley and Sons.

Non-catalyzed reactions were also performed at various temperatures to study the effect of glucose decomposition without HCl in the aqueous solutions. As shown in Figure 26(a), the rate of glucose disappearance increased with temperature, and nearly full disappearance was reached at 180 °C after 150 min. Figure 26(b) reveals that the maximum attainable carbon yield of HMF is 7.5% at 180 °C after 60 min. Levulinic acid was detected only at 180 °C after 60 min., and a maximum carbon yield of 12% was obtained after 150 min. TOC analysis confirmed that at high temperatures only 50% of the water soluble organic carbon was accounted for. Up to 50% of the overall organic carbon went to form insoluble humic species. This finding agrees with Figure 26(c) which plots the total humins carbon yield. For this purpose, humins were considered all non-detectable soluble and insoluble compounds.

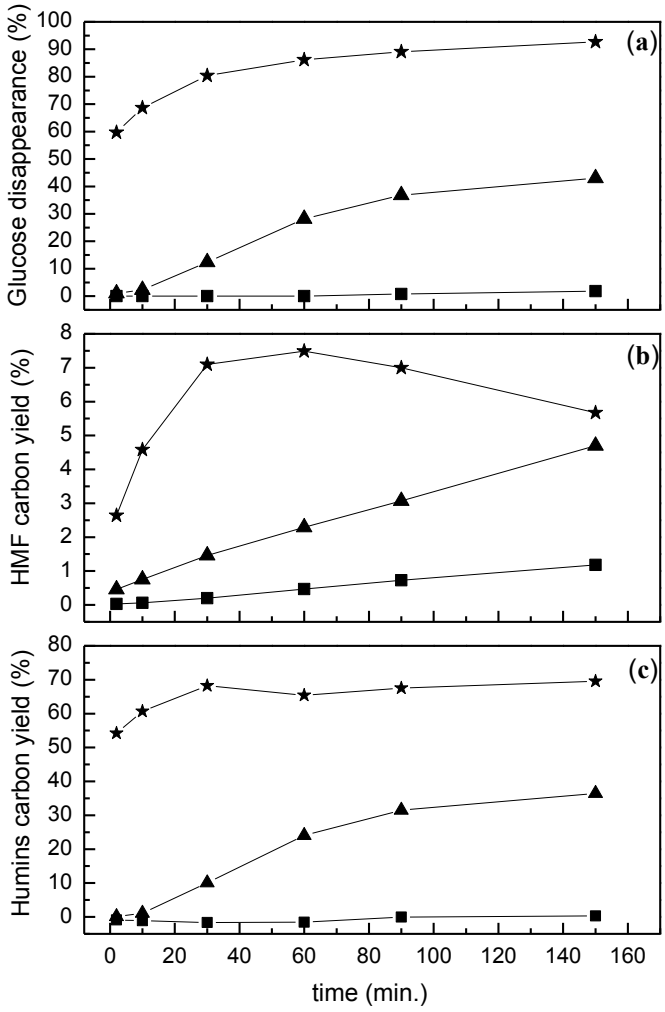

Figure 26. Aqueous-phase non-catalyzed thermal decomposition of glucose in a stirred batch reactor. T (°C) = 140 (■), 160 (▲), 180 (★). Feed was 10 wt% glucose. (**a**) Glucose disappearance; (**b**) HMF carbon yield; (**c**) Humins carbon yield. Reprinted from ref.[175], Copyright(2012), with permission from John Wiley and Sons.

5.3.4. Continuous reactor systems

The kinetic model that was derived above can further be used to model data from continuous reactor systems. These can be divided into two reactor types based on the mixing of reactant – plug flow reactor (PFR) and continuous stirred-tank reactor (CSTR). Under steady-state operating conditions, their design equations are described as Equations 20 and 21:

PFR: $$\tau = C_{i,\mathrm{o}} \int_0^X \frac{dX}{-r_i} \quad (20)$$

CSTR: $$\tau = \frac{C_{i,\mathrm{o}} X}{-r_i} \quad (21)$$

$\tau \equiv$ residence time; $C_{i,\mathrm{o}} \equiv$ initial concentration of species *i*
$r_i \equiv$ reaction rate; X ≡ conversion

The above equations were combined with the kinetic model (Eqns. 16-19) to simulate continuous production of levulinic acid. The key process variables include initial concentration of glucose, acid concentration, temperature, and residence time. The variables can be manipulated to maximize throughput, conversion of glucose and yields of HMF and levulinic acid. Experimental studies were also carried out with a PFR and CSTR at temperatures 160-180 °C with 0.5 M HCl. Steady state conditions were attained after a period corresponding to 4-5 times the residence time of the reactor. This was confirmed by sampling multiple times at each steady state condition and taking the average value along with its standard de*via*tion. The experimental data along with the fitted models appear in Figure 27.

The kinetic model shows that the rate of glucose conversion is higher in a PFR compared to a CSTR. Likewise, maximum HMF carbon yields of 10% are obtained in a PFR at 180 °C and short residence times (less than 1 minute). A maximum levulinic acid yield of 55% is obtained in a PFR at 160 °C and a residence time of 100 minutes. This is compared to 46% levulinic acid carbon yield obtained in a CSTR at the same temperature and residence time.

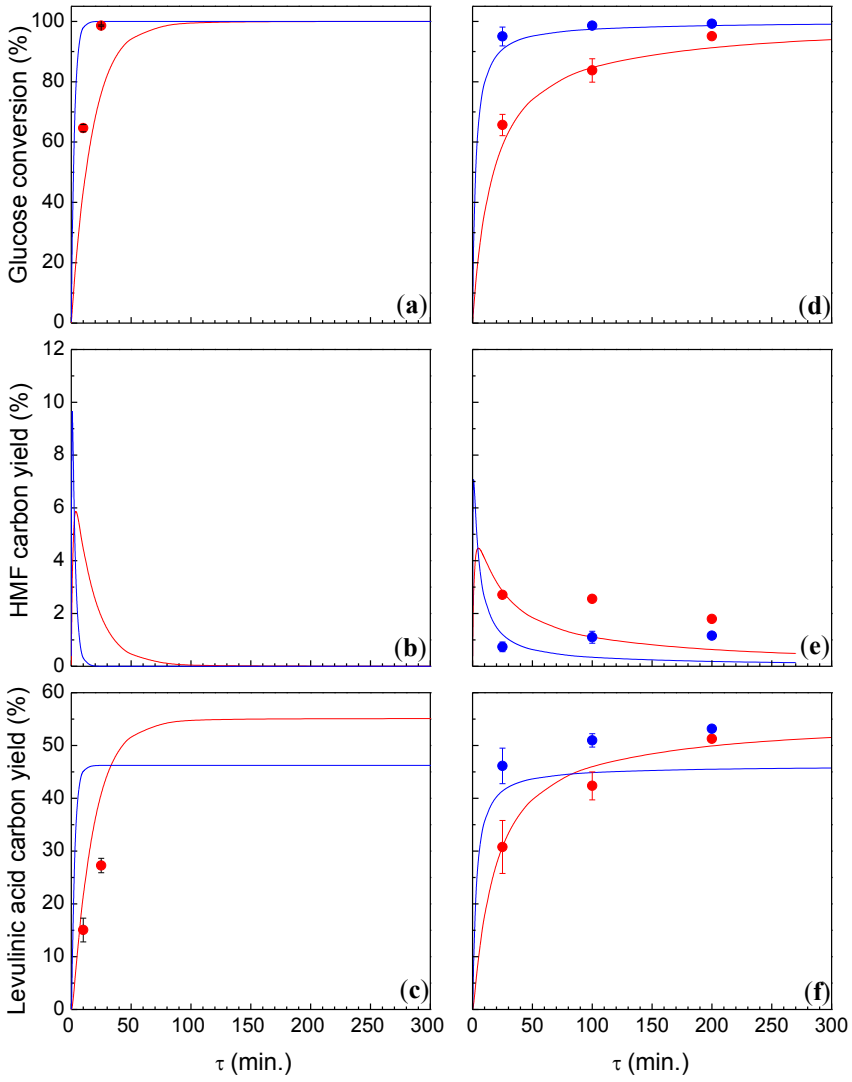

Figure 27. Aqueous-phase acid-catalyzed glucose dehydration in continuous reactors. Kinetic model fit with a single PFR (plots **a**, **b**, **c**) and single CSTR (plots **d**, **e**, **f**) for glucose conversion, HMF carbon yield and levulinic acid carbon yield. Experimental reaction conditions: 3-5 wt% glucose and 0.5 M HCl. T (°C) = 160 (●), 180 (●); Model prediction for 160 °C (—). Model prediction for 180 °C (—). Reprinted from ref.[175], Copyright(2012), with permission from John Wiley and Sons.

5.4. Discussion

5.4.1. Comparison with previous kinetic models

The kinetic parameters derived from our model (Table 10) are in fairly good agreement with those obtained in previous studies. The literature reports activation energies for acid-catalyzed glucose dehydration (Reaction 1) in the range 121 to 152 kJ mol^{-1} (see Table 11 for references). Our study reported a value of 160 kJ mol^{-1} with a 95% confidence interval of ± 5, which is in the range of previous studies. The majority of the literature values for acid-catalyzed HMF rehydration (Reaction 3) range from 95 to 111 kJ mol^{-1}. This is in agreement with our reported value of 95 ± 6 kJ mol^{-1}. Girisuta *et al.* claimed activation energies of 165 and 111 kJ mol^{-1} for humins formation from glucose and HMF respectively.[171] For humins formation from glucose (Reaction 2) we obtained a value of 51 ± 2 kJ mol^{-1}. We obtained a value of 142 ± 26 kJ mol^{-1} for humins formation from HMF (Reaction 4). In their study of non-catalyzed glucose decomposition, Qi *et al.* reported values of 136 and 109 kJ mol^{-1} to form humins from glucose and HMF respectively.[173] Wyman and Shen reported a value of 147 kJ mol^{-1} for humins formation from HMF.[174] The latter value agrees well with our calculated value of 142 kJ mol^{-1}. On the other hand, our derived value of 51 kJ mol^{-1} for humins formation from glucose does not coincide with those reported above.

A power-law approach was used to derive the reaction orders with respect to acid concentration in the rate equations (n_i in Table 10). All reactions were found to demonstrate a near first order dependence to the acid concentration, with the exception of Reaction 2 (glucose

to humins) which exhibits close to a third order dependence. This differs from the values reported by Girisuta *et al.*[171]

A plausible cause for these observed de*via*tions lies in the methods used to develop the kinetic models. For example, unlike our model, Girisuta *et al.*[170, 171] employed a modified Arrhenius equation to determine temperature dependence of the rate constants, and a rate selectivity parameter to maximize the rate of the desired reactions. They also took into account the dissociation constant of their catalyst, as they used sulfuric acid. Our model prediction has been made for a wide range of acid concentration extended to zero acid concentration to assure systematic dependence of rate constants on the concentration of the catalyst, *i.e.* infinite dilution, where some of the reaction rates become negligible. Table 11 summarizes the kinetic studies that appear in the literature for glucose conversion to levulinic acid.

Table 11. Proposed kinetic models for aqueous-phase acid-catalyzed glucose conversion to levulinic acid.[b]

Proposed Model	Reaction Conditions [a]	Activation Energy (kJ mol^{-1})	Reference
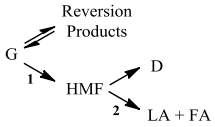	T = 100-150 °C [HCl] = 0.35 M $[Glucose]_o$ = 1 wt%	Ea_1 = 133 Ea_2 = 95	Heimlich[166], 1960
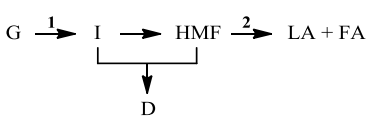	T = 140-250 °C $[H_2SO_4]$ = 0.0125-0.4 M $[Glucose]_o$ = 5-17 wt% $[HMF]_o$ = 1-2 wt%	Ea_1 = 137 Ea_2 = 97	McKibbins[167], 1962
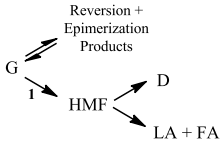	T = 180-224 °C $[H_2SO_4]$ = 0.05-0.4 M $[Glucose]_o$ = 0.4-6 wt%	Ea_1 = 128	Smith[184], 1982
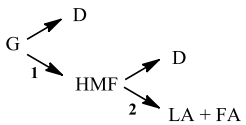	T = 170-230 °C $[H_3PO_4]$: pH 1-4 $[Glucose]_o$ = 0.6-6 wt% $[HMF]_o$ = 0.3 wt%	Ea_1 = 121 Ea_2 = 56	Baugh[178], 1988
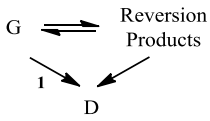	T = 200-230 °C $[H_2SO_4]$ = 0.005-0.02 M $[Glucose]_o$ = 2 wt%	Ea_1 = 139	Xiang[186], 2004
	T = 170-190 °C $[H_2SO_4]$ = 0.1-0.5 M $[Glucose]_o$ = 5 wt%	Ea_1 = 86 Ea_2 = 210 Ea_3 = 57	Chun[169], 2006
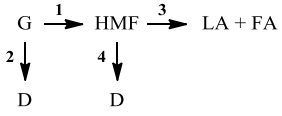	T = 98-200 °C $[H_2SO_4]$ = 0.05-1 M $[Glucose]_o$ = 2-15 wt% $[HMF]_o$ = 1-11 wt%	Ea_1 = 152 Ea_2 = 165 Ea_3 = 111 Ea_4 = 111	Girisuta[170, 171], 2006
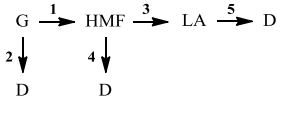	T = 180-280 °C Non-catalyzed $[Glucose]_o$ = 1 wt% $[HMF]_o$ = 0.75 wt% $[Levulinic\ Acid]_o$ = 0.5wt%	Ea_1 = 108 Ea_2 = 136 Ea_3 = 89 Ea_4 = 109 Ea_5 = 31	Qi[173], 2008
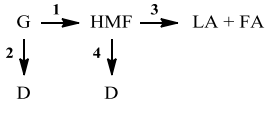	T = 140-180 °C 0 M < [HCl] ≤ 1.0 M $[Glucose]_o$ = 2-20 wt% $[HMF]_o$ = 4-16 wt%	Ea_1 = 160 ± 5 Ea_2 = 51 ± 2 Ea_3 = 95 ± 6 Ea_4 = 142 ± 26	this study

G ≡ glucose; ; HMF ≡ 5-hydroxymethylfurfural; LA ≡ levulinic acid; FA ≡ formic acid; I ≡ intermediate; D ≡ decomposition products (humins).[a] Units of feedstock and acid concentrations were converted for consistency. Values were rounded to the nearest unit.

[b] Reprinted from ref.[175], Copyright(2012), with permission from John Wiley and Sons.

5.4.2. Reactor design for production of HMF and levulinic acid

The apparent rate parameters introduced here allow for kinetic modeling of HMF and levulinic acid yields. The type of reactor and its operating conditions can be modified to maximize the yields of these desired products. The kinetic model fit in Figure 27 shows that at a constant residence time higher glucose conversions and levulinic acid yields can be obtained in a PFR relative to a CSTR. Likewise, higher temperatures and short residence times are essential to maximize HMF yield. These conditions are favored in a PFR type reactor. This finding also agrees with our previous work on furfural production from xylose in Chapter 2. In contrast, lower temperatures are necessary to obtain optimal levulinic acid yields. This is due to the induced HMF degradation reaction (Reaction 4) that occurs at relatively higher temperatures ($Ea_4 > Ea_3$).

Figure 28 shows the calculated HMF and levulinic acid yields as a function of glucose conversion for an ideal PFR and CSTR. On a conversion basis, HMF yield is maximized in a PFR at high temperatures. This is because the dehydration step to form HMF (Reaction 1) is favored at increased temperatures due to its higher activation energy compared to the degradation step to form humins from glucose (Reaction 2). At similar feedstock conversions shorter residence times are obtained in a PFR compared to a CSTR. This shorter residence time minimizes the further decomposition of HMF and maximizes the HMF production. Calculations show that a HMF yield of 14% can be obtained at 200 °C in a PFR at 34% glucose conversion. This conversion corresponds to a residence time of 10 seconds.

At equal glucose conversions a slightly higher yield of levulinic acid can be obtained in a CSTR compared to a PFR (11.6% *vs.* 10.5% respectively, at 25% glucose conversion and 160

°C), as shown in Figure 28(b). Lower temperatures (140-160 °C) are also favorable to maximize levulinic acid production, as these conditions minimize the formation of humins due to the relatively higher activation energy associated with Reaction 4 (humins from HMF) compared with the rehydration reaction to produce levulinic acid (Reaction 3). Longer residence times are required in a CSTR compared to a PFR in order to obtain equivalent glucose conversions. As shown in Figure 28(b), the longer residence times achieved in a CSTR are favorable in the case of levulinic acid production, as we have shown that it does not undergo degradation reactions under the reaction conditions in this study.

This behavior agrees with those reported by Girisuta *et al.*[171] However, their kinetic model calculations show a bigger de*via*tion between CSTR and PFR with increased glucose conversion. They report a levulinic acid carbon yield of 70% in a CSTR at 140 °C and complete glucose conversion. Our model predicts a levulinic acid carbon yield of 54% at the same temperature and conversion for both reactor types, as shown in Figure 28(b). This result is comparable to that reported by Girisuta *et al.* in a PFR, however there is an inconsistency with the levulinic acid yield reported in a CSTR at complete glucose conversion. To further determine the credibility of our model, we calculated the projected glucose conversion and levulinic acid yield obtained in a CSTR with the kinetic parameters reported by Girisuta *et al.*[171] These calculations resulted in a glucose conversion of 89.8% and a levulinic acid carbon yield of 50.4% at 160 °C, 0.5 N acid concentration and retention time of 200 min. These results are quite similar to those reported in this study, as shown in Figure 27(d, f). Experimentally, at the same reaction conditions, we obtained a glucose conversion of 95.1% and a levulinic acid carbon yield

of 51.3%. Likewise, our kinetic model projected a glucose conversion of 92.0% and a levulinic acid carbon yield of 50.4%.

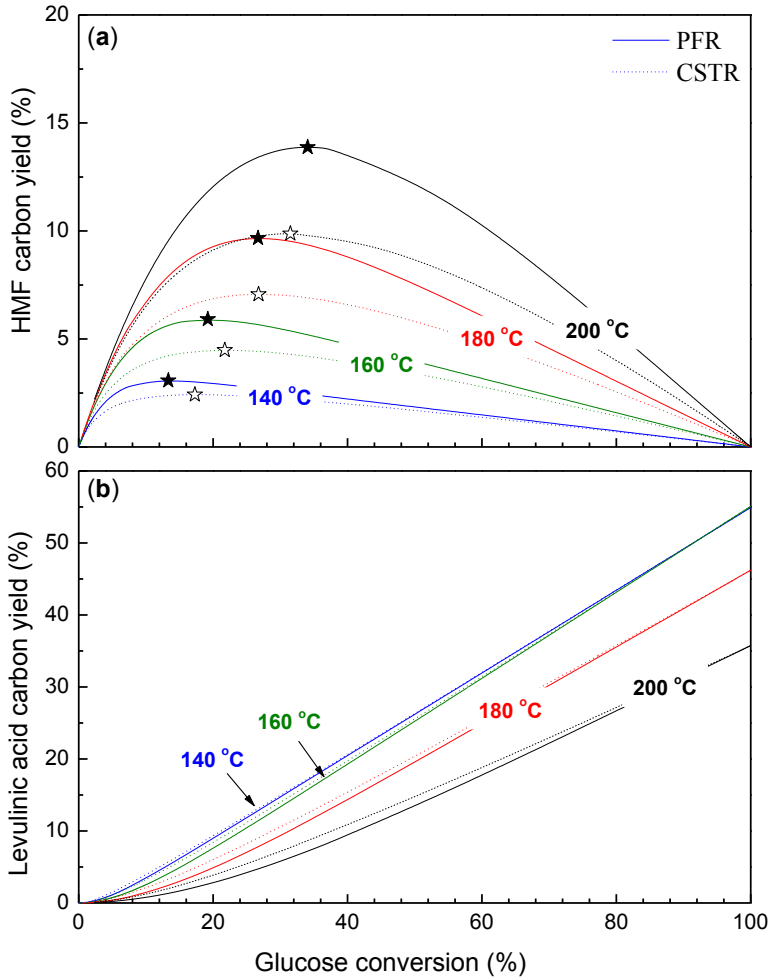

Figure 28. Continuous reactor modeling for acid-catalyzed glucose dehydration in a single continuous reactor. Calculated values for (**a**) HMF carbon yield and (**b**) levulinic acid carbon yield as a function of glucose conversion and temperature for 10 wt% glucose and 0.5 M HCl. PFR (—); CSTR (····). Symbols (★) and (☆) represent maximum HMF yields in a PFR and CSTR respectively. Reprinted from ref.[175], Copyright(2012), with permission from John Wiley and Sons.

The calculated levulinic acid carbon yield, plotted as a function of temperature and residence time in a PFR, is shown in Figure 29. In a PFR 56% carbon yield can be achieved at 153 °C after 200 min. The carbon yield rises to 57% with an increase in residence time to 500 min. at 149 °C. However, a further increase to 1000 min. shows no improvement in the results. If the residence time in the PFR decreases then a higher temperature is required to maximize levulinic acid production. This in turn results in lower yields of levulinic acid due to induced humins formation from HMF (Reaction 4). The levulinic acid yield has an optimum with regard to temperature and residence time. On the one hand, HMF production from glucose (Reaction 1) is maximized at elevated temperatures ($Ea_1 > Ea_2$). Conversely, high temperatures are unfavorable for levulinic acid production from HMF (Reaction 3) due to a parallel degradation step with a higher activation energy ($Ea_4 > Ea_3$).

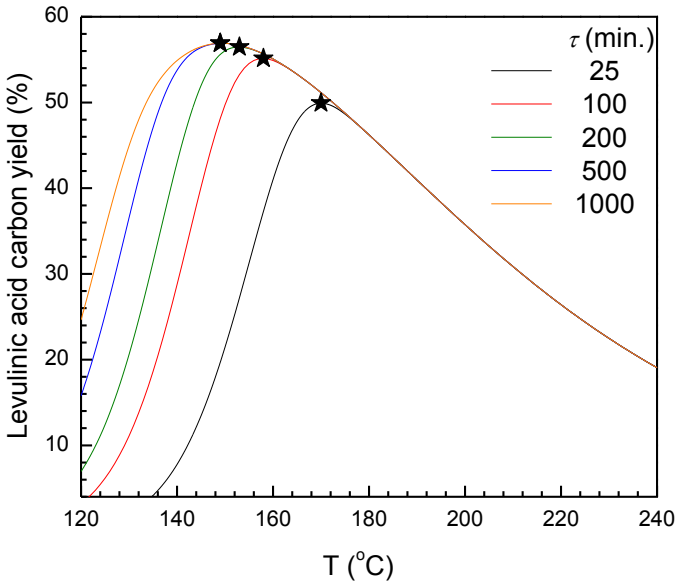

Figure 29. Continuous reactor modeling for acid-catalyzed glucose dehydration in a PFR. Calculated levulinic acid carbon yield as a function of temperature for 10 wt% glucose and 0.5 M HCl at varying residence times. τ (min.) = 25 (—), 100 (—), 200 (—), 500 (—), 1000 (—). Symbol (★) represents maximum levulinic acid yield. Reprinted from ref.[175], Copyright(2012), with permission from John Wiley and Sons.

In addition to operating parameters, a variety of reactor configurations can be examined, including a combination of two reactors in series. Figure 30 plots the overall calculated levulinic acid yield for two reactors in series as a function of the temperature and residence time of the second reactor (T_2 and τ_2 respectively). The first reactor is a PFR, as we have shown that this reactor type is favorable to maximize levulinic acid yield. Its operational conditions were set to maximize the levulinic acid yield in the first reactor. The second reactor depicts a PFR or CSTR as shown in Figure 30(a) and (b) respectively. As can be seen, a combination of two PFR reactors in series is preferred relative to a PFR/CSTR combination. The former gives rise to a higher levulinic acid yield (52.5% *vs.* 47.5%) at shorter residence times in the second reactor (55 min. *vs.* 93 min.). The contour plots demonstrate that a decrease in the temperature of the second reactor subsequently requires an increase in its residence time to maintain equivalent levulinic acid yields. The combination of two PFRs in series shows nearly the same results as a single PFR. According to Figure 27, a single PFR at 160 °C and residence time of 50 minutes can yield 51.7% levulinic acid, which is similar to the maximum yield of 52.5% obtained with two PFRs in series at 160 °C and residence time of 60 minutes.

Our proposed model for levulinic acid production from glucose differs from that employed by the Biofine Process. As mentioned previously, this process consists of two acid-catalyzed steps: (1) hydrolysis of the lignocellulosic biomass feedstock to monosaccharides and subsequent dehydration to produce HMF; (2) rehydration of the HMF to produce levulinic and formic acid. Furfural is also produced during the process. The first stage takes place in a PFR reactor between 210-230 °C within 13-25 seconds. The second stage consists of using a CSTR reactor at temperatures ranging 195-215 °C and residence times of 15-30 minutes.

The general operating trend realized by the Biofine Process agrees with our model, in that initially higher temperatures are necessary to maximize the hydrolysis/dehydration step and then lower temperatures should be employed to maximize levulinic acid yield. However, a discrepancy arises with respect to the optimal reactor configuration. The Biofine Process uses a PFR followed by a CSTR, whereas our model predicts a single PFR as the most favorable. This inconsistency could be due to that, unlike the Biofine Process, a biomass hydrolysis step was not included in our proposed model. This preliminary depolymerization step has a high energy barrier and requires relatively high temperatures,[165, 201] which could necessitate a multi-stage process.[68] Hayes *et al.* have suggested that higher yields are obtained in a CSTR in the Biofine Process because this reactor minimizes the "higher-order" degradation reactions, compared to the first order rehydration of HMF to produce levulinic acid.[202] Their claim differs from our proposed kinetic model which suggests that all four of the reactions are first order with respect to the reactants (refer to Eqns. 16-18). A CSTR may also be beneficial compared to a PFR because of the operational issues associated with the formation of solid humins during the reaction. As observed in this study, it may well be easier to operate a CSTR amid the formation of solid humins compared to a PFR.

According to the Biofine process, levulinic acid production can reach carbon yields higher than 58% (70% of the theoretical yield) from cellulosic biomass.[163, 164] Similarly, in this study we project a maximum carbon yield of 57% (68% of the theoretical yield) levulinic acid from glucose, as shown in Figure 29. Likewise, in their kinetic study of levulinic acid production from cellulose, Wyman and Shen report a maximum levulinic acid carbon yield of

50% (60% of the theoretical) at an initial cellulose concentration of 99.6 mM, acid concentration of 0.927 M and temperatures between 180-200 °C.[174]

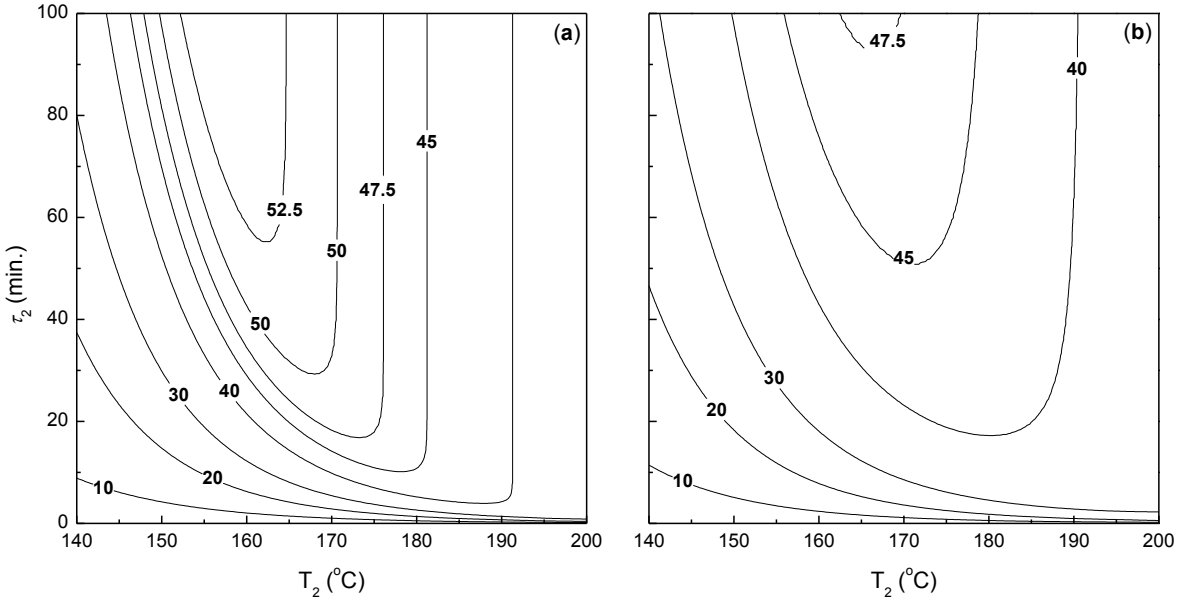

Figure 30. Continuous reactor modeling for acid-catalyzed glucose dehydration in a system of two reactors in series. Calculated total levulinic acid carbon yield as a function of the residence time (τ_2) and temperature (T_2) of the second reactor for 10 wt% glucose. For both cases the first reactor is a PFR at: T_1 = 200 °C, τ_1 = 5 sec and 0.5 M HCl. The second reactor is (**a**) PFR or (**b**) CSTR, both at 0.5 M HCl. Reprinted from ref.[175], Copyright(2012), with permission from John Wiley and Sons.

CHAPTER 6

Levulinic acid production with solid metal(IV) phosphate catalysts

Weingarten, R.; Kim, Y. T.; Tompsett, G. A.; Fernandez, A.; Han, K. S.; Hagaman, E. W.; Conner, W. C.; Dumesic, J. A.; Huber, G. W., Conversion of glucose into levulinic acid with solid metal(IV) phosphate catalysts. *Journal of Catalysis* **2013,** *304*, 123-134.

6.1. Background

In this chapter we discuss the design of solid acid catalysts for the aqueous phase production of levulinic acid from glucose. The objective of this study was to characterize the different catalytic sites on supported metal(IV) phosphate solid acid catalysts and identify their roles in this reaction. The nature of the metal(IV) and phosphorus loading was investigated, as well as the role of Lewis and Brønsted acid sites. The catalysts that we tested include zirconium (ZrP) and tin (SnP) phosphates with varying ratios of phosphorus to metal(IV).

As mentioned previously, levulinic acid is produced from glucose by way of a two-step acid-catalyzed reaction (Figure 31). Overall there are four parallel pathways in which glucose can react: (1) reversion reactions can lead to the formation of cellobiose and levoglucosan;[166, 184, 185] (2) degradation reactions to form highly polymerized carbonaceous species (*i.e.* humins); (3) epimerization reactions to form fructose and mannose,[184] and (4) dehydration to produce HMF. It has been reported that reversion and epimerization products can also decompose to form humins.[186] The humins are both water soluble and water insoluble. Water-soluble humins polymerize with time to form water-insoluble compounds. The isomerization of glucose into fructose has been reported to be favored by the presence of Lewis acid sites.[122, 189, 190] Recent studies have reported the efficient conversion of glucose to HMF using a combination of Lewis and Brønsted acid catalysts in a biphasic reactor system with 2-*sec*-butylphenol as the extracting solvent.[203, 204] The reaction proceeds through a tandem pathway including isomerization of glucose to fructose followed by dehydration of fructose to HMF. Subsequently, HMF can rehydrate to produce levulinic acid and formic acid. HMF can also decompose to produce humins and produce furfural *via* loss of formaldehyde.[180-183] As depicted in Chapter 2, furfural

can also undergo degradation reactions to form humins. Formic acid is also a byproduct of furfural degradation by way of hydrolytic fission of the furfural aldehyde group.[69, 91]

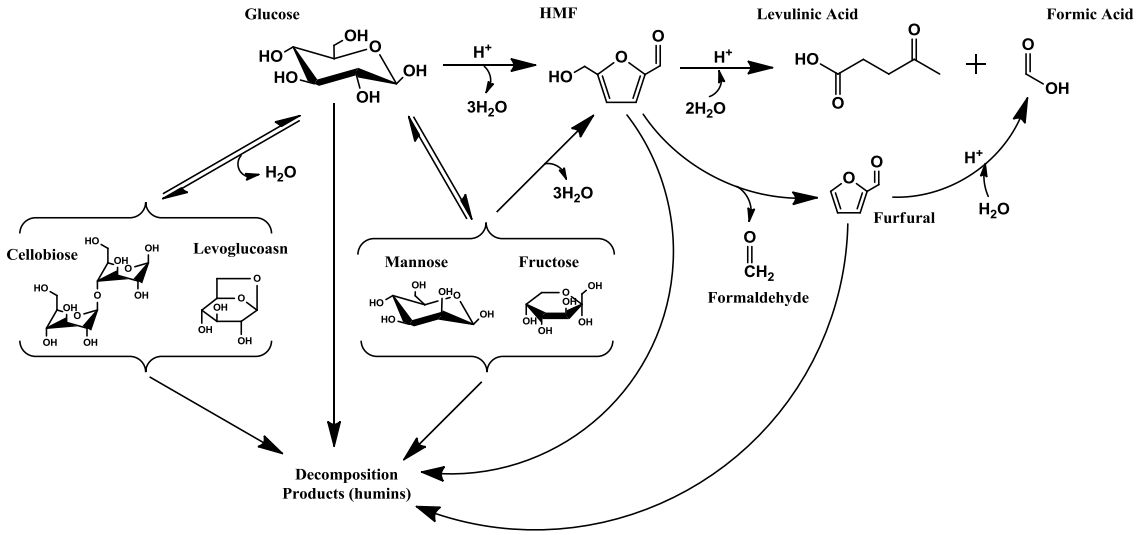

Figure 31. Reaction pathway scheme for the conversion of glucose to levulinic acid. Reprinted from ref.[205], Copyright(2013), with permission from Elsevier.

Extensive studies have reported on the conversion of biomass feedstocks to levulinic acid using homogeneous catalysts, including mineral acids and metal chlorides.[62-66] Many have also attempted to utilize recyclable solid acid catalysts for this reaction. Jow *et al.* studied the production of levulinic acid production from fructose over a LZY zeolite (Y-type Faujasite) catalyst.[206] Levulinic acid molar carbon yield of 56% (67% of the theoretical) was obtained after 15 h in a batch reactor at 140 °C. They reasoned that this was due to the strong Lewis acidity of the silica/alumina support, as well as the molecular sieving capability of the Y-type zeolite. Wang *et al.* studied the production of levulinic acid from cellulose with sulfated TiO_2 as a solid acid catalyst.[207] They claimed a levulinic acid molar carbon yield of 32% (38% of the theoretical) at their optimal reaction conditions. The catalyst stability was found to be a concern, as a loss in activity was observed after two consecutive runs. Others have reported the use of

solid acid catalysts to produce esters of levulinic acid in non-aqueous solutions from glucose and cellulose.[208, 209]

In particular, metal(IV) phosphate catalysts have shown to be selective and active for aqueous phase acid-catalyzed dehydration and isomerization reactions.[210-213] Extensive investigations have been carried out to determine the physicochemical and acidic properties of these catalysts.[214, 215] Studies have shown that the amorphous form of these catalysts demonstrate higher activity due to increased overall acidity and surface area compared to their crystalline analogue.[132, 216] In addition, metal(IV) phosphates are beneficial as catalyst supports for metal oxides due to their textural and acid properties.[133, 217, 218]

In the field of biomass conversion various studies have been reported on the selective production of HMF from carbohydrates in the aqueous phase using metal phosphates as solid acid catalysts.[219-222] In Chapter 3 we showed that amorphous zirconium phosphate containing a high Brønsted to Lewis acid site ratio exhibits high selectivity for furfural production from xylose. The activity and selectivity for furfural production of the zirconium phosphate were comparable to those obtained from dehydration reactions with HCl. The dehydration of sorbitol to produce isosorbide with metal(IV) phosphates has also been reported.[223] Li *et al.* have found that platinum supported on zirconium phosphate serves as a stable, selective and active catalyst for aqueous phase hydrodeoxygenation of aqueous sugar solutions to produce high-octane gasoline.[146, 224] They found the catalyst to be stable in aqueous media at high temperatures (245 °C) and no deactivation occurred after 200 h time-on stream. ICP studies confirmed that no leaching occurred. This coincides with a study by Asghari *et al.* who also found zirconium phosphate to be stable under sub-critical water conditions.[225] Niobium based catalysts have also

received much consideration as solid acid catalysts due to their hydrothermal stability and high activity for aqueous phase dehydration of alcohols to olefins.[226, 227]

Zirconium phosphate has unique properties as a solid acid catalyst in that it is compatible in aqueous media. Various studies have investigated the source of the active sites on this class of catalysts. In their study of crystalline zirconium phosphate, Hattori *et al.* concluded that the catalyst possesses weak and strong acid sites, both of which are derived from P(OH) groups.[228] Clearfield and Thakur observed a decrease in the activity of zirconium phosphate after poisoning the catalyst with quinoline or following proton exchange with Cs^+ on the catalyst surface.[210, 214] They correlated the active sites to surface hydroxyl groups but also associated some of the activity to Lewis-type sites. La Ginestra *et al.* used a similar surface poisoning technique to conclude that the catalytic activity of zirconium phosphate was solely from Brønsted acid sites on the surface of the catalyst.[211] Sinhamahapatra *et al.* observed both Brønsted and Lewis acid sites in their study on mesoporous zirconium phosphate.[229] They postulated that the Brønsted acid sites possibly arise from geminal P(OH) groups. The Lewis acid centers could be attributed to Zr^{4+}, as suggested by Spielbauer *et al.*[230]

6.2. Experimental

6.2.1. Catalyst Preparation

The zirconium phosphate catalysts (ZrP) were prepared following procedures previously reported,[132] which consisted of precipitation of $ZrCl_2O \cdot 8H_2O$ (Sigma Aldrich, 1 mol L^{-1}, 140 mL) and $NH_4H_2PO_4$ (Sigma Aldrich, 1 mol L^{-1}, 280 mL) at a molar ratio of P/Zr = 2 (ZrP2). The solution was stirred at room temperature and then filtered, washed with de-ionized (DI) water until pH 5 and dried overnight at 373 K. The catalyst was powdered and calcined at 673 K for 4 h in air prior to reaction. The other two zirconium phosphate catalysts (ZrP1 and ZrP3) were prepared following the same procedure but varying the molar ratio of P/Zr to 1 and 3 respectively.

The tin phosphate catalyst (SnP1) was obtained following a procedure reported by Patel *et al.*[213] A 0.1 M aqueous solution of disodium hydrogen phosphate (Sigma Aldrich, ReagentPlus^{TM} ≥ 99%) was added drop wise to an equimolar, equivolume, stirred aqueous solution of tin tetrachloride ($SnCl_4 \cdot 5H_2O$, Fisher Scientific). The resulting gel was stirred at 50ºC for 2 h and at room temperature for 24 h. It was then filtered and dried at room temperature. The dried material was powdered and converted to the hydrogen form by treatment with a 1 M aqueous solution of HNO_3 (Fisher Scientific) for 3 h, the acid being intermittently replaced with a fresh batch. It was then washed several times with de-ionized water to remove the excess acid until pH of 3, and finally dried at room temperature. Tin phosphate (SnP2) was prepared following the same procedure but varying the molar ratio of P/Sn to 2, and then washed thoroughly until pH 3.

Zirconium oxide was obtained by calcining zirconium hydroxide (supplied by MEL chemicals-(XZO 880/01)) at 673 K for 2 h in air. Hydrochloric acid was supplied by Fischer Scientific. Ytterbium (III) trifluoromethanesulfonate hydrate, Yb $(OTf)_3$, was supplied by Strem Chemicals.

6.2.2. Catalyst Characterization

Total acid sites were determined by temperature programmed desorption of ammonia (NH_3-TPD) with a Quantachrome ChemBET Pulsar^{TM} TPR/TPD Automatic Chemisorption Analyzer coupled with a TCD to quantify the ammonia desorbed from the sample. A sample of approximately 300 mg was initially degassed at 673 K for 1.5 h under a constant helium flow of 12 mL min^{-1} (Airgas, UHP). The sample was cooled and ammonia (Airgas, electronic grade) was adsorbed at 373 K for 30 min. to reach saturation. Afterwards, the ammonia supply line was shut off and helium was purged at 12 mL min^{-1} for 2 h to remove any physically adsorbed ammonia. The sample was then heated linearly at a rate of 10 K min^{-1} from 373 to 973 K (773 K for the tin phosphate samples) under a constant helium flow of 12 mL min^{-1}. The sample was held at the temperature set point for an additional 2 h.

The concentration of Brønsted acid sites was determined by temperature programmed desorption of isopropylamine (IPA-TPD) with thermogravimetric analysis-mass spectrometry (TA instruments SDT Q600 system), as reported by Gorte *et al.*[231-233] Approximately 50–60 mg of sample was loaded and degassed at 673 K for 1.5 h under a constant helium flow of 100 mL min^{-1} (Airgas, UHP). The sample was then cooled to 318 K, at which point isopropylamine was bubbled with helium and adsorbed for 15-20 min. After saturation, the isopropylamine supply

line was shut off and helium was purged at 100 mL min^{-1} to remove any physically adsorbed isopropylamine. The sample was then heated linearly at a rate of 10 K min^{-1} from 318 to 973 K (773 K for the tin phosphate samples) under a constant helium flow of 100 mL min^{-1}. During the TPD analysis, the signal m/z 39 (propylene) was monitored by the mass spectrometer. The mass spectrometer was calibrated for propylene (Sigma Aldrich, ≥ 99%) for quantification purposes.

Adsorption and desorption isotherms (40 points each) of nitrogen were obtained for all of the samples at 77 K using a Quantachrome Autosorb® iQ2 automated gas sorption system. The surface areas were calculated using BET analysis ranging from 0.05 to 0.3 relative pressure P/P_o on the adsorption branch and the BET "C" constants were recorded. The samples were degassed before each experiment at 523 K for 12 h.

X-ray photoelectron spectroscopy (XPS) measurements were performed using a Physical Electronics Quantum 2000 Scanning ESCA Microprobe equipped with a monochromatic Al Kα anode (1486.6 eV). Samples were prepared by dusting them on double sided adhesive tape. They were then evacuated and placed on the stage of the instrument. Charging was neutralized using the turnkey electron/ion system so that the C1s peak was fixed at 284.0 eV. Analysis was performed by taking sequential spectra from a 5 degree take-off angle increasing the angle by 3 degrees per spectrum until the C1s line increased. Since this indicated that the substrate tape was detected, the angle was then decreased to that before the tape was detected. This proved to be a 15 degree take-off angle which provided excellent signal to noise for quality spectra, acquired using a 200 micron spot at 50 Watts. All quantitative calculations used atomic sensitivity factors tailored to the instrument by the manufacturer.

Solid-state ^{31}P magic angle spinning (MAS) nuclear magnetic resonance (NMR) spectra were obtained on a 9.4 T Bruker Avance® spectrometer at a resonance frequency of 161.97 MHz. Powdered samples were spun at 12 kHz in a 4 mm CP/MAS probe under ambient temperature and humidity conditions. Samples were not dried prior to examination. Spectra were acquired using a single pulse excitation pulse sequence (zg) with a 5 μs (90 degree) pulse length and 120 s recycle delay. The ^{31}P spin- lattice relaxation time estimated from progressive saturation experiments is *ca.* 30 s and does not show marked differences between the partially resolved resonance bands. ^{31}P chemical shifts were referenced to external 85% H_3PO_4 (0 ppm).

The structures of the catalysts were determined by XRD. The XRD patterns were obtained with a Philips X'Pert Pro diffractometer equipped with a X'Celerator detector operated at 45 kV and 40 mA using Cu Kα radiation ($\lambda = 0.15406$ nm) at a scan rate of 0.1° (2θ) s^{-1}.

The amounts of phosphorous, zirconium and tin present in the solid acid catalysts were determined by elemental analysis by way of inductively coupled plasma (ICP) analysis. The samples were not degassed prior to analysis. The analyses were performed by Galbraith Laboratories, Inc.

6.2.3. Catalyst Activity

Batch reactions were carried out in a 100 mL reactor vessel provided by Parr Instrument Company, series 4560. Glucose (Fisher Scientific) solutions were prepared with de-ionized water at the specified concentration. Throughout all of the experiments, the amount of loaded reaction solution was kept constant at 70 g. Temperatures in the reactor were measured by means of a thermocouple in contact with the solution. All reaction solutions were mixed at a

maximum constant rate of 600 rpm using an internal stirrer. The temperature and stirring were controlled by a 4848 Controller provided by Parr. The reaction vessel was initially pressurized to 800 psi with industrial grade helium (Airgas). Samples were taken periodically through a sampling port. The samples were immediately quenched in an ice water bath and filtered with a 0.2 μm syringe filter prior to analysis. The reactor was repressurized with helium after each sampling. The dip tube was covered with a stainless steel woven wire cloth, mesh size 400x400 provided by McMaster-Carr. This was done to prevent clogging and loss of catalyst during sampling.

6.2.4. Analysis

Reaction product samples were analyzed by high pressure liquid chromatography (HPLC) with a Shimadzu© LC-20AT. Carbohydrates were detected with a RI detector (RID-10A) and reaction products were detected with a UV-Vis detector (SPD-20AV) at wavelengths of 210 and 254 nm. The column used was a Biorad© Aminex HPX-87H sugar column. The mobile phase was 0.005 M H_2SO_4 flowing at a rate of 0.6 mL/min. The column oven was set to 30 °C.

6.3. Results

6.3.1. Characterization of solid acid catalysts by adsorption and ICP

The characterization for the solid acid catalysts by adsorption and ICP appear in Table 12. Zirconia was used as a reference material due to its high Lewis acidity.[234] All of the phosphate catalysts in this study were confirmed to be amorphous by XRD (Figure A.3 in the Appendix). Previous studies have shown that the presence of phosphate stabilizes the amorphous zirconia phase.[235] It has also been reported that amorphous zirconium phosphate is thermally stable even after calcination at 800 ^{o}C.[229] The phosphorous to metal(IV) molar ratios obtained from ICP analysis were different than the phosphorous to metal(IV) molar ratios used in the precipitation solutions with the exception of ZrP2. The sample ZrP3 had the same phosphorus content as ZrP2 despite the additional loading of the phosphorus precursor during synthesis. The molar ratios for the two tin phosphate samples were comparable to each other, but lower than the phosphorus to tin ratio used in the prescription solution.

Table 12. Characterization of solid acid catalysts by adsorption and ICP studies.[e]

Catalyst	BET surface area [a] (m^2 g^{-1})	Metal(IV) [b] (molar %)	Phosphorus [b] (molar %)	P / metal(IV) molar ratio	Total acid sites [c] (mmol g^{-1})	Brønsted acid sites [d] (mmol g^{-1})	Fraction of Brønsted acid sites
ZrP1	173	9.45	12.07	1.28	1.942	0.240	0.12
ZrP2	276	8.29	16.60	2.00	2.146	0.818	0.38
ZrP3	123	8.07	15.95	1.98	1.834	0.388	0.21
SnP1	11	9.20	6.64	0.72	0.463	0.031	0.07
SnP2	142	11.03	7.20	0.65	1.260	0.068	0.05
ZrO_2	143	-	N/A	N/A	0.905	0.087	0.10

[a] BET "C" constants for the catalysts in descending order are 88, 89, 73, 44, 185 and 80.
[b] Determined from elemental analysis (Galbraith Laboratories, Inc.).
[c] Determined from ammonia TPD.
[d] Determined from isopropylamine TPD.
[e] Reprinted from ref.[205], Copyright(2013), with permission from Elsevier.

Zirconium phosphate samples ZrP1 and ZrP3 had similar BET surface areas to that reported by Kamiya *et al.* (130 m^2 g^{-1}).[132] The highest surface area was obtained for ZrP2 (276 m^2 g^{-1}). In contrast, tin phosphate SnP1 had the lowest surface area (11 m^2 g^{-1}), which was appreciably lower than that reported by Patel *et al.* following the same preparation procedure (141 m^2 g^{-1}).[213]

Ammonia TPD revealed a higher concentration of total acid sites for the zirconium phosphates compared to the tin phosphate catalysts. The three zirconium phosphate samples showed similar concentrations of total acid sites as measured by NH_3-TPD (Figure A.4 in the Appendix). Sample ZrP2 showed the highest total acid concentration despite equivalent P/Zr molar ratios to sample ZrP3. This higher total acid concentration for ZrP2 could be due to its higher surface area. SnP1 had a comparable acid concentration to that reported in the literature.[213] In contrast, an increased amount of acid sites was observed for SnP2 despite the

similar amounts of phosphorous incorporated in the framework. The two tin phosphate samples showed similar acid strength according to the NH_3-TPD profiles.

Brønsted acid sites were quantified according to isopropylamine TPD.[231-233] The concentrations of Brønsted acid sites obtained for the zirconium phosphate samples were at least 3 times higher than the concentration of Brønsted acid sites for the tin phosphates (Figure A.5 in the Appendix). ZrP2 showed the highest Brønsted acid concentration among all of the catalysts tested, containing more than 26 times the amount of Brønsted sites observed with SnP1. In this respect, extensive studies have been reported on the use of ^{1}H MAS NMR spectroscopy to determine the strength of Brønsted acid sites. Acid sites of increasing acid strength are characterized by higher ^{1}H NMR chemical shifts.[236] Fraissard and co-workers have measured the acid strength of several types of acid catalysts by two ^{1}H NMR techniques in the presence of water.[237-242] As part of this study, the zirconium phosphate samples were characterized by solid-state ^{1}H MAS NMR spectroscopy. Results reveal that all three samples showed a broad resonance at 7.3 ppm. The placement is downfield of the shift for water (4.8 ppm) and represents a weighted average of the acid proton chemical shifts and water.[240] The chemical shift of all three materials is the same implying that their acid strengths are comparable. This corresponds with results obtained from NH_3-TPD. It is also notable to mention that the fraction of Brønsted acid sites for ZrP2 in this study was somewhat lower than that reported by us in Chapter 3. This could be due to a number of factors including differences in the catalyst washing routine during the synthesis procedure or different characterization techniques. NH_3 FTIR spectroscopy was used to quantify the ratio of Brønsted to Lewis sites in our previous study. Isopropylamine TPD was used in this study. This could also lead to inconsistencies in the

quantification of the Brønsted acid sites by different techniques, as different adsorption techniques quantify sites differently.

6.3.2. Solid-state ^{31}P MAS NMR spectroscopy

The zirconium phosphate samples were characterized by solid-state ^{31}P MAS NMR spectroscopy. This characterization method serves as a useful technique to identify the coordination states of the phosphorus atoms in the bulk phase. Generally, a transition of the chemical shift (δ_P) to more negative values is indicative of both an increase in the number of P-O-Zr bonds,[243, 244] as well as an increase in the chain length of the phosphorus atoms.[230] The latter corresponds to progressive deprotonation and subsequent condensation of phosphate species (P-O-P bonds), typically during calcination.[243] Figure 32 shows the NMR spectra for the three zirconium phosphate samples. All of the samples showed relatively broad peaks due to their amorphous nature.[229, 245] Samples ZrP2 and ZrP3 showed very similar spectra which were characterized by four different resonance peaks. The resonance peak at -7 ppm is attributed to tetrahedral phosphates bonded to one zirconia group and two hydroxyl groups (Zr-O)-PO(OH)$_2$. This coordination gives way to geminal P-(OH) groups. The signal at -14 ppm signifies the presence of two zirconia and one hydroxyl group bonded to the phosphate (Zr-O)$_2$-PO(OH). Similarly, a peak at -21 ppm can be assigned to a tetrahedral phosphate connected with three zirconia groups (Zr-O)$_3$-PO. The high intensity peak at -27 ppm implies relatively high amounts of polyphosphates, P-O-P, due to condensation of phosphate species.[133, 229] The resonance peaks associated with zirconium phosphate ZrP1 were broader and less discrete than those for the other two samples.

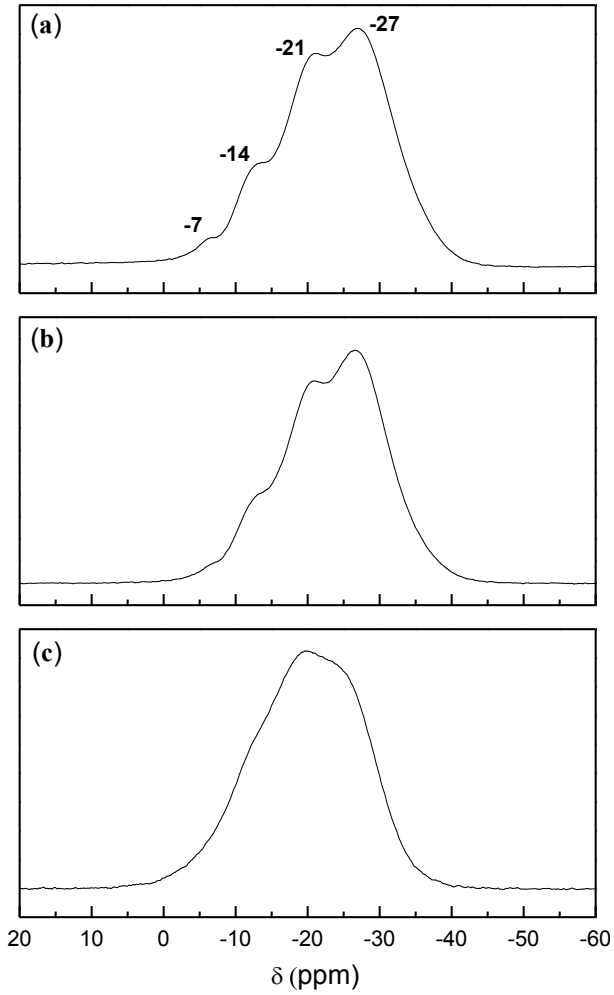

Figure 32. Solid-state ^{31}P MAS NMR spectra of the zirconium phosphate catalysts. (**a**) ZrP3, (**b**) ZrP2, (**c**) ZrP1. Reprinted from ref.[205], Copyright(2013), with permission from Elsevier.

The NMR spectra were deconvoluted using Origin software. The four resonance bands were fit with Gaussian line shapes. The band areas were normalized according to the sample weight, assuming equal density for the samples. Table 13 shows the relative amounts of the different phosphate species for each catalyst. The spectrum of ZrP1 has just three inflections and gave unreasonable fitting results until (Zr-O)-$PO(OH)_2$ was constrained to a small value. Overall, from these results it can be concluded that ZrP2 and ZrP3 are quite similar materials

with respect to their bulk properties. In contrast, ZrP1 showed a higher amount of $(Zr\text{-}O)_2$-PO(OH) species at -14 ppm and less polyphosphates at -27 ppm compared to ZrP2 and ZrP3. Panda *et al.* reasoned that the Brønsted acid sites in their study of mesoporous zirconium phosphate came primarily from geminal P(OH) groups.[229] This corresponds to the coordination state detected at -7 ppm. Others have postulated that the Brønsted acid sites come from the phosphate species on the surface bonded to two and three zirconia groups (chemical shifts -14 ppm and -21 ppm respectively).[244, 246] It is unlikely that these former conclusions are valid for this study, as the samples with the highest concentration of Brønsted acid sites (ZrP2 and ZrP3) are predominantly comprised of polyphosphate species. Consequently, even though the formation of polyphosphates species is attributed with deprotonation, their increased amount in the bulk phase could be a primary cause of the higher Brønsted acidity observed for ZrP2 and ZrP3 in relation to ZrP1. According to Segawa *et al.*, P-O-P species in the bulk phase can withdraw electrons from the residual phosphate groups on the surface, thus enhancing the acidic properties of P-OH groups on the surface.[247, 248]

Table 13. Relative amounts of the different phosphate species for the zirconium phosphate catalysts from solid-state ^{31}P MAS NMR spectroscopy.[c]

Chemical shift (ppm)	-7	-14	-21	-27
Coordination state [a]	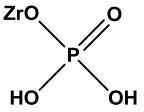	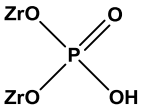	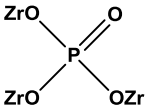	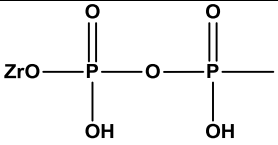
Catalyst	Relative amount (%)			
ZrP1	2.3 [b]	30.9	15.7	51.1
ZrP2	3.6	12.9	11.8	71.7
ZrP3	5.0	11.3	13.5	70.2

[a] Adapted from ref. [229].
[b] This value was constrained. Any small value is acceptable.
[c] Reprinted from ref.[205], Copyright(2013), with permission from Elsevier.

6.3.3. XPS Analysis

The zirconium phosphate catalysts were characterized by XPS in order to study their surface composition and oxidation states. Figure 33 shows the high resolution XPS spectra of zirconium, phosphorus and oxygen for the three zirconium phosphate catalysts. The Zr*3d* line is composed of two peaks assigned to Zr$3d_{5/2}$ at 183 eV and Zr$3d_{3/2}$ at roughly 185 eV. This is characteristic of tetravalent zirconium Zr^{4+}.[249] All samples had typical P*2p* binding energies of 133 eV, characteristic of pentavalent tetracoordinated phosphorus (P^{5+}).[249, 250] The O*1s* line shows a broad peak which could correspond to oxygen bonded to both zirconium and phosphorus.[249] The O*1s* component characteristic of the P-O bond is dominant for all samples with an average binding energy of 531 eV.

The surface atomic compositions of the zirconium phosphate catalysts appear in Table 14. These values were determined by the XPS line areas of Zr*3d*, P*2p* and O*1s* and the

phosphorus to zirconium atomic ratios on the surface were calculated accordingly. There is a gradual increase of phosphorus on the surface in agreement with the increase in phosphorus loading in the preparation procedure. The P/Zr molar ratio on the surface increased as follows: ZrP1 < ZrP2 < ZrP3. The atomic compositions on the surfaces showed only slight differences to the bulk compositions (see Table 12 and Table 14). Catalyst ZrP1 showed practically identical P/Zr surface and bulk molar ratios, as determined by XPS and ICP respectively. However, higher zirconium and phosphorus contents were observed on the surface than in the bulk (Table 12). The relatively higher amount of zirconium on the surface of ZrP1 could be a plausible cause for its relatively higher concentration of Lewis acid sites compared to ZrP2 and ZrP3. For sample ZrP2, the phosphorus content on the surface was slightly lower than in the bulk. The opposite trend was found for zirconium. The highest P/Zr molar ratio on the surface was observed for ZrP3. Nevertheless, this value was lower than the theoretical ratio predetermined in the preparation procedure (P/Zr = 3).

Electron binding energy shifts observed for Zr, P and O can reflect variations in the polarity of the bonds on the surface of zirconium phosphate catalysts. A slight downward shift in the Zr*3d* binding energies was observed for sample ZrP1 compared to ZrP2 and ZrP3. This indicates a reduced polarization of the Zr-O bonds in the ZrP1 sample, which could be due to fewer hydroxyl groups on the surface relative to the other samples.[251] As for the P*2p* binding energies, the shifts increased as follows: ZrP1 < ZrP2 < ZrP3. Higher P*2p* binding energies are a result of increased polarity of the P-O bonds on the surface which can be enhanced by the hydroxyl groups bonded to the phosphorus atoms.[251] This suggests that higher P*2p* binding energies are indicative of increased amounts of acid sites on the surface, as shown with ZrP2 and

ZrP3. The O*1s* binding energies increase according to: ZrP1 < ZrP3 < ZrP2. Higher O*1s* binding energy suggests an increased amount of surface hydroxyl groups.[251]

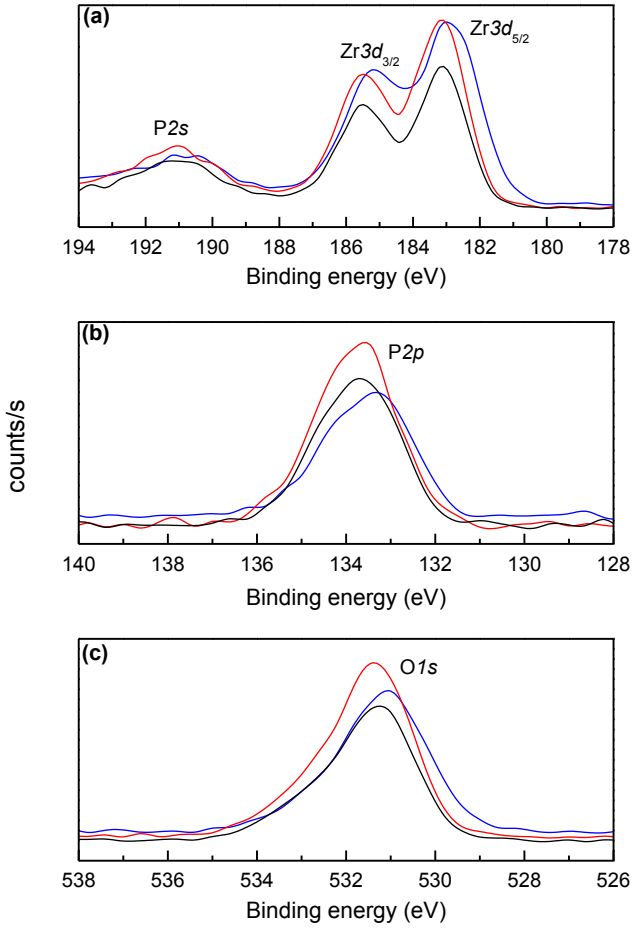

Figure 33. High-resolution XPS spectra of the (**a**) Zr*3d*, (**b**) P*2p* and (**c**) O*1s* regions for the catalysts: ZrP1 (—); ZrP2 (—); ZrP3 (—). Reprinted from ref.[205], Copyright(2013), with permission from Elsevier.

Table 14. Electron binding energies and atomic surface composition determined by XPS for the zirconium phosphate catalysts.[b]

Catalyst	Binding energy (eV)				Surface atomic composition [a] (%)			P/Zr ratio
	Zr*3d*$_{3/2}$	Zr*3d*$_{5/2}$	P*2p*	O*1s*	Zr	P	O	
ZrP1	185.2	183.0	133.3	531.1	11.1	13.6	75.3	1.26
ZrP2	185.5	183.1	133.6	531.4	8.8	16.3	75.0	1.85
ZrP3	185.5	183.1	133.7	531.3	8.1	16.6	75.2	2.05

[a] Based on XPS line areas of Zr*3d*, P*2p* and O*1s*.
[b] Reprinted from ref.[205], Copyright(2013), with permission from Elsevier.

6.3.4. Aqueous phase glucose dehydration studies with solid metal(IV) phosphate catalysts

Glucose dehydration studies were carried out at 160 ºC with the different solid acid catalysts in the aqueous phase. The concentration of the catalysts was kept constant at 5 wt%. Figure 34 depicts glucose conversion as a function of reaction time for the various catalysts. The tin phosphate catalysts showed a higher activity compared to the zirconium phosphate catalysts. As part of this study, a run without any catalyst was also carried out and showed that glucose underwent hydrothermal decomposition. Similar observations were noted in our previous study where we studied the kinetics of levulinic acid production from glucose.[175] There we found that nearly full glucose disappearance was attained at 180 °C after 150 min. without an acid catalyst and 75% of the overall carbon content went to form water soluble and insoluble humic species. In this study, the catalyst activity obtained from sample ZrP3 was lower than that from the hydrothermal reactions with glucose at longer reaction times. This suggests that zirconium phosphate suppresses some of the undesired reactions encountered under hydrothermal conditions. Figure 35 shows the initial turnover frequency (TOF) of glucose disappearance for

the different catalysts in this study. The TOF calculations are based on the total concentration of acid sites as determined by NH_3-TPD. On a per site basis, the catalytic activity increased as follows: ZrP3 < ZrP2 < ZrP1 < SnP2 < SnP1. As mentioned previously, results from the NH_3-TPD and ^1H MAS NMR studies showed that the acid strengths for each series of metal(IV) phosphates were similar. Therefore, it is reasonable to assume that acid strength does not play a significant role in determining the catalyst activity. For calculation purposes, the homogeneous (blank) glucose reactions were subtracted out of the TOF estimations.

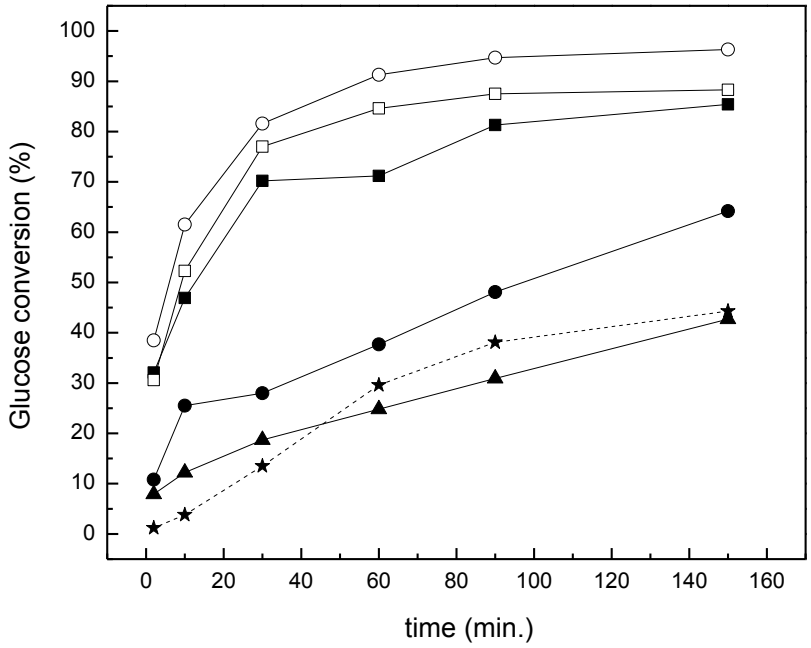

Figure 34. Aqueous phase glucose dehydration at 160 ºC in a stirred batch reactor with different solid acid catalysts. Feed was 10 wt% glucose aqueous solution. The solid catalyst loading was constant at 5 wt%. Catalysts: ZrP1 (■), ZrP2 (●), ZrP3 (▲), SnP1 (□), SnP2 (○). Blank run (dashed line) (★). Reprinted from ref.[205], Copyright(2013), with permission from Elsevier.

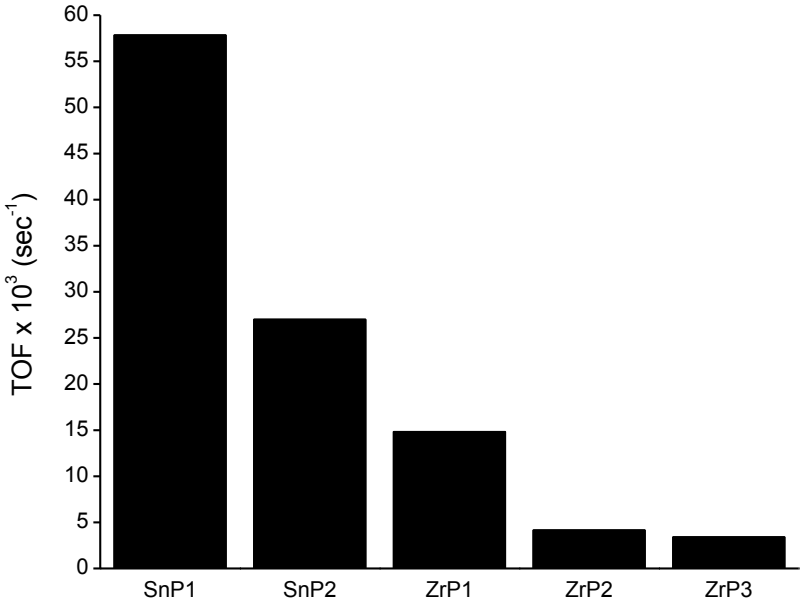

Figure 35. Aqueous phase glucose dehydration at 160 ºC in a stirred batch reactor. Initial turn-over frequency (according to total acid sites concentration determined from NH_3-TPD) based on glucose disappearance for the different solid acid catalysts. Feed was 10 wt% glucose aqueous solution. The solid catalyst loading was constant at 5 wt%. The homogeneous glucose reactions were subtracted out for calculation purposes. Reprinted from ref.[205], Copyright(2013), with permission from Elsevier.

Figure 36 shows the carbon selectivities of the major products as a function of glucose conversion. The tin phosphate catalysts had a higher fructose selectivity compared to the zirconium phosphates, as shown in Figure 36(a). This is in agreement with the work of Davis and co-workers,[122, 189, 190] and Dumesic and co-workers,[203, 204, 252] where they find that Lewis acid sites catalyze the isomerization reaction of glucose to fructose. The fructose selectivity increased as follows: blank < ZrP3 < ZrP2 < ZrP1 < SnP1 ~ SnP2. In all cases the fructose selectivity decreased with increased glucose conversion. It is notable to mention that lactic acid was also detected as a by-product of this reaction. The amounts were not quantified, but were observed for all of the solid catalysts tested here due to the presence of Lewis acid sites. Chambon *et al.*

published a study on the production of lactic acid from cellulose with solid Lewis acid catalysts.[253] They found that Lewis sites improve the extent of cellulose depolymerization compared to Brønsted acid sties. Holm *et al.* also discovered that solid Lewis acid catalysts, such as Sn-Beta, are able to convert pentose and hexose sugars to methyl lactate in methanol.[252, 254]

Figure 36(b) depicts the HMF selectivity for the different metal(IV) phosphates. Initially the HMF selectivity increased as it was being produced from glucose and fructose. The HMF selectivity then decreased as it reacted to produce levulinic acid, formic acid and decomposition products. Higher HMF selectivities were observed for ZrP2 and ZrP3 at relatively low glucose conversions. This coincides with the trend that was observed for catalysts with relatively high Brønsted to Lewis ratios.[140] The HMF selectivity reached a maximum of 38% with ZrP2 at a glucose conversion of 38%. Similar selectivities were achieved with the tin phosphate catalysts at a glucose conversion of 80%. The lowest selectivity was observed for non-catalyzed glucose decomposition (blank run).

A relatively high levulinic acid selectivity was observed for the zirconium phosphate catalysts ZrP2 and ZrP3 compared to the tin phosphates, as shown in Figure 36(c). For the tin phosphates, levulinic acid was detected only at glucose conversions above 80%. The catalyst ZrP2 showed the highest levulinic acid selectivity of 22% at a glucose conversion of 64%. In contrast, catalyst ZrP1 showed no production of levulinic acid. No levulinic acid was observed when only water was used. The levulinic acid selectivity increased as follows: blank ~ ZrP1 < SnP2 < SnP1 < ZrP3 < ZrP2. In all cases the levulinic acid selectivity increased with increasing glucose conversion.

In addition to the major products mentioned earlier, quantifiable amounts of cellobiose, levoglucosan and furfural were also detected as by-products for all of the catalysts tested in this study. Cellobiose was detected primarily for catalysts with relatively high Brønsted to Lewis ratios, such as ZrP2 and ZrP3. Carbon selectivity to cellobiose decreased with glucose conversion. The maximum carbon selectivity was 36% at 8% glucose conversion for ZrP3. Similar trends were observed for levoglucosan with a maximum carbon selectivity of 13% at 8% at glucose conversion for ZrP3. Furfural was also detected, but at carbon selectivities no higher than 4%. Higher selectivities to furfural were observed for catalysts with higher amounts of Lewis acid sites.

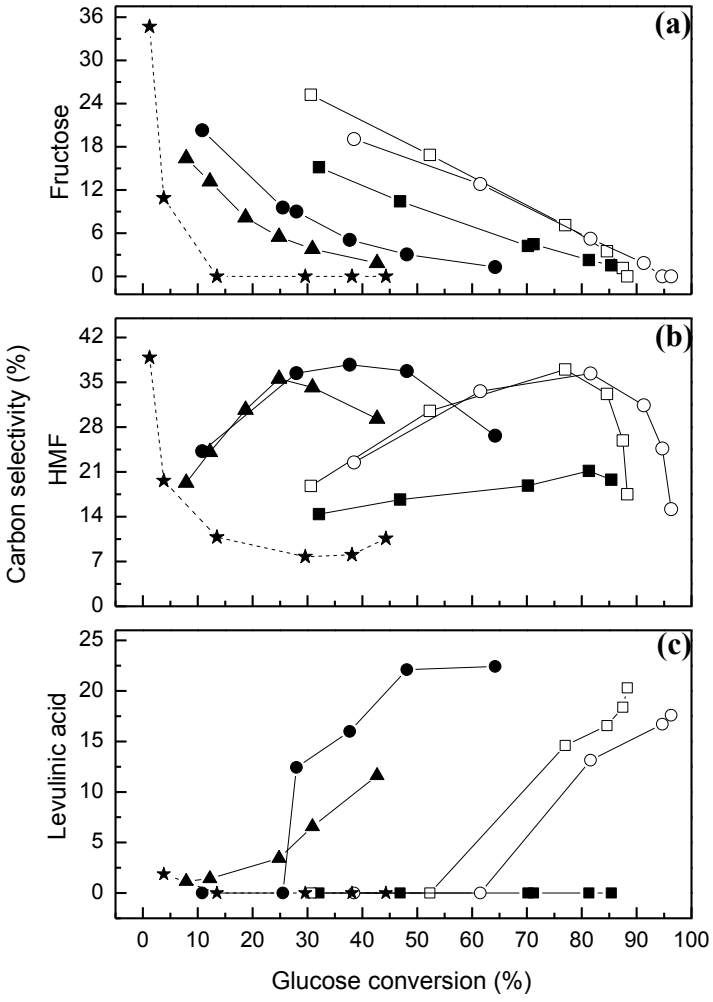

Figure 36. Carbon selectivity of the major products as a function of glucose conversion for the different metal phosphate catalysts at 160 ºC. (**a**) fructose, (**b**) HMF, (**c**) levulinic acid. Feed was 10 wt% glucose aqueous solution. The solid catalyst loading was constant at 5 wt%. Catalysts: ZrP1 (■), ZrP2 (●), ZrP3 (▲), SnP1 (□), SnP2 (○). Blank run (dashed line) (★). Reprinted from ref.[205], Copyright(2013), with permission from Elsevier.

6.3.5. Aqueous phase dehydration of glucose with homogeneous acid catalysts

Aqueous phase glucose dehydration studies were carried out with water-soluble Lewis and Brønsted acids. Ytterbium (III) trifluoromethanesulfonate hydrate, $Yb(OTf)_3$, and hydrochloric acid were used respectively. The former is considered a stable water-soluble Lewis acid.[125, 148] Reactions were performed at varying Brønsted to Lewis ratios by combining the two acids accordingly, while holding the total acid concentration constant at 0.1 M. Figure 37 shows the results of glucose conversion for the different ratios of the homogeneous catalysts. The activity for glucose disappearance increased systematically as the relative amount of Lewis sites increased. Pure $Yb(OTf)_3$ showed the highest glucose conversion whereas pure HCl had the lowest catalytic activity. These results indicate that the Lewis acid sites have a higher catalytic activity towards glucose disappearance compared to the Brønsted acid sites, which is consistent with the results from the heterogeneous catalysts.

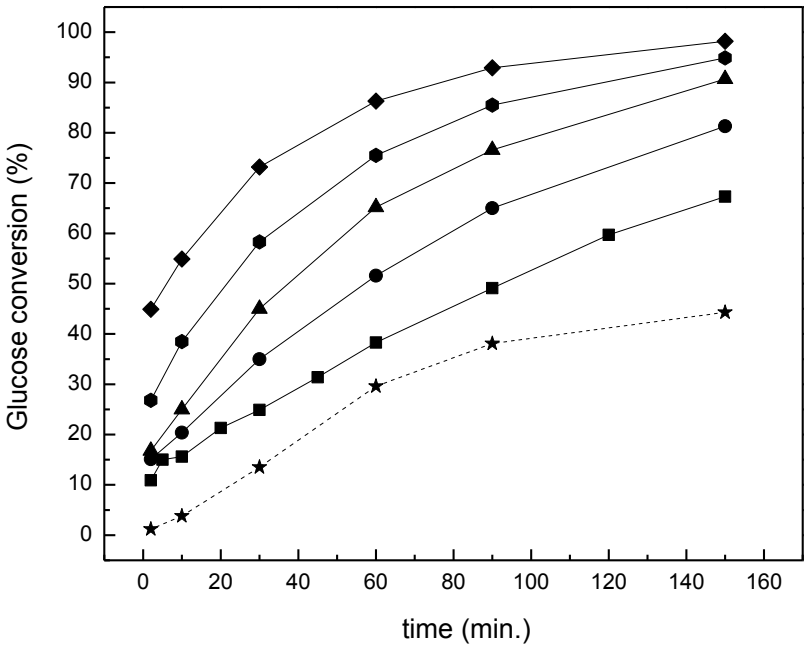

Figure 37. Aqueous phase glucose dehydration in a stirred batch reactor. Effect of the Brønsted to Lewis acid ratio on glucose conversion with homogeneous acid catalysts at 160 ºC. Feed was 10 wt% glucose aqueous solution. Total acid concentration was kept constant at 0.1 M. Brønsted to Lewis acid ratio = 1:0 (■), 3:1 (●), 1:1 (▲), 1:3 (⬢), and 0:1 (◆). Blank run (dashed line) (★). Reprinted from ref.[205], Copyright(2013), with permission from Elsevier.

Figure 38 depicts the carbon selectivities of the major compounds as a function of glucose conversion for the various Brønsted to Lewis ratios in the homogeneous regime. The selectivity for fructose production increased with the concentration of Lewis sites, as shown in Figure 38(a), reaching a maximum of 34% at 45% conversion with pure $Yb(OTf)_3$ as a catalyst. Figure 38(b) shows the HMF selectivity for the different Brønsted to Lewis ratios in the homogeneous regime. As with the solid acid catalysts, a maximum selectivity was observed for all ratios. This maximum value shifts toward higher glucose conversions as the relative amount of Lewis acid sites increases. At lower glucose conversions, HMF was selectively produced by catalysts with more Brønsted acid sites. Lewis acid sites showed a higher selectivity for HMF

production at higher glucose conversions. The selectivity towards levulinic acid production from glucose systematically increases with the concentration of Brønsted sites, as depicted in Figure 38(c). Pure HCl showed a significantly higher levulinic acid selectivity compared to $Yb(OTf)_3$, with a maximum selectivity of 46% at 60% glucose conversion. These results are consistent with those reported for the heterogeneous catalysts.

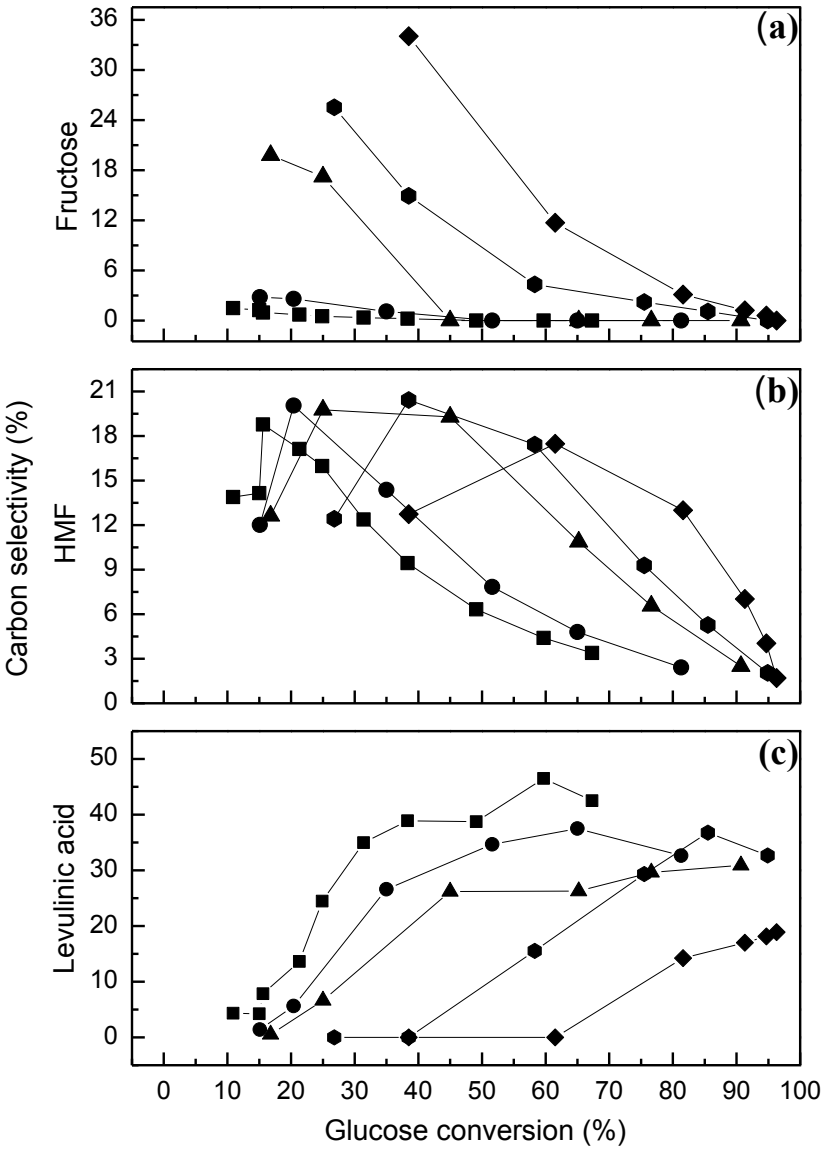

Figure 38. Effect of the Brønsted to Lewis acid ratio on the carbon selectivity of major products from glucose dehydration with homogeneous acid catalysts at 160 ºC. (**a**) fructose, (**b**) HMF, (**c**) levulinic acid. Feed was 10 wt% glucose aqueous solution. Total acid concentration was kept constant at 0.1 M. Brønsted to Lewis acid ratio = 1:0 (■), 3:1 (●), 1:1 (▲), 1:3 (⬢), and 0:1 (◆). Reprinted from ref.[205], Copyright(2013), with permission from Elsevier.

6.4. Discussion

The reaction chemistry for levulinic acid production from glucose consists of three key steps which generate products that can easily be quantified. Glucose undergoes isomerization to produce fructose and mannose; hexoses undergo dehydration to form HMF, and HMF undergoes a rehydration reaction to produce levulinic acid and formic acid. Additional undesirable decomposition reactions can also come about from glucose, fructose and HMF to ultimately form humins. For this study, humins were considered as all unidentified water soluble and insoluble compounds. Further characterization of humic species was not carried out here, as this goes beyond the scope of this thesis. Table 15 shows the product distribution of all identified products for the metal(IV) phosphates. The values were interpolated to correspond with a glucose conversion of 40%. The results show that the formation of humins was predominant for the reaction with ZrP1. The catalyst ZrP2 showed the lowest selectivity towards these undesired compounds, which is consistent with its high selectivity toward HMF and levulinic acid. The tin phosphate catalysts showed similar trends to each other for humins formation. Following the reactions in this study, it was observed that solid humins were deposited on all of the solid acid catalysts. The amounts of carbon deposited on the catalysts were not determined and regeneration was not carried out as part of this study. However, we have shown in the previous chapters that we can obtain a satisfactory carbon balance for these aqueous dehydration reactions based on various characterization techniques.[175, 255] This indicates that the method used in this study to calculate the product selectivities is valid.

Table 15. Product distribution at 40% glucose conversion for the metal(IV) phosphate catalysts at 160 ºC. Feed was 10 wt% glucose aqueous solution. The solid catalyst loading was constant at 5 wt%.[b]

Catalyst	Carbon selectivity (%)							
	Fructose	Cellobiose	Levoglucosan	HMF	Furfural	Levulinic acid	Formic acid	Humins [a]
ZrP1	12.6	1.8	0.6	15.6	2.3	0.0	4.1	63.0
ZrP2	4.6	6.2	3.8	37.5	1.5	17.3	5.4	23.7
ZrP3	2.3	6.3	4.0	30.4	1.0	10.5	3.9	41.6
SnP1	21.6	3.7	1.7	23.9	2.4	0.0	1.2	45.5
SnP2	18.7	3.3	1.4	23.2	2.2	0.0	1.8	49.4

[a] Considered as all unidentified water soluble and insoluble products.
[b] Reprinted from ref.[205], Copyright(2013), with permission from Elsevier.

Figure 39 shows the carbon selectivity of the major products as a function of the fraction of Brønsted acid sites for the three zirconium phosphate catalysts. The values were interpolated to correspond with a glucose conversion of 40%. There is a direct correlation between the product distribution and the fraction of Brønsted sites as determined by TPD measurements with ammonia and isopropylamine. HMF and levulinic acid production increase with the amount of Brønsted acid sites. Isomerization to produce fructose from glucose is predominant at higher Lewis acid concentrations, as shown for sample ZrP1. The formation of humic species is greatest at lower Brønsted to Lewis ratios. Consequently, a higher rate of glucose disappearance and lower selectivities to HMF and levulinic acid are observed for catalysts with increased Lewis sites.

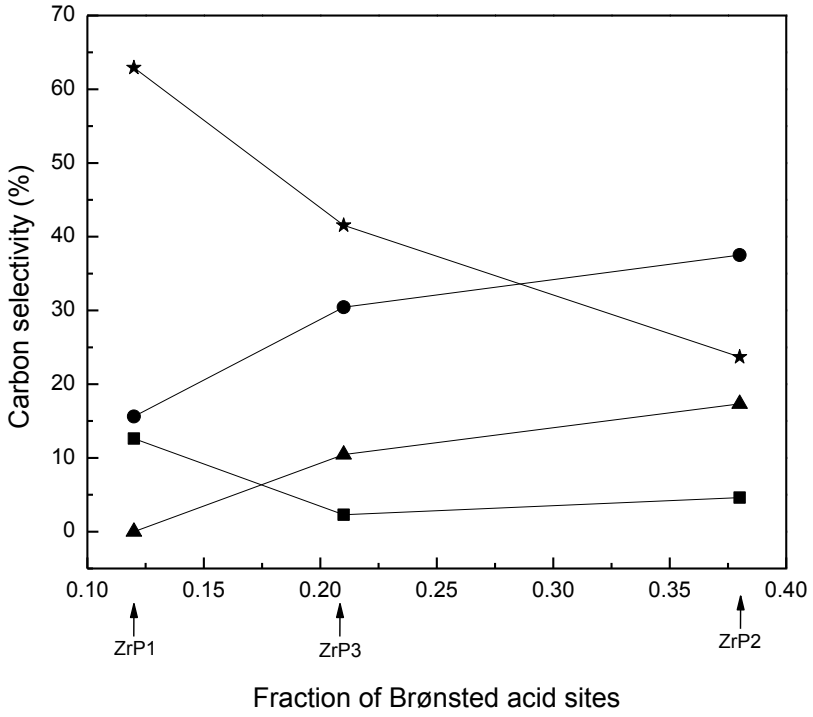

Figure 39. Carbon selectivity of major products at 40 % glucose conversion as a function of the fraction of Brønsted acid sites (determined by NH_3 and isopropylamine TPD) for the zirconium phosphate catalysts at 160ºC. Feed was 10 wt% glucose aqueous solution. The solid catalyst loading was constant at 5 wt%. Major products: fructose (■), HMF (●), levulinic acid (▲), total humins (★). Reprinted from ref.[205], Copyright(2013), with permission from Elsevier.

This claim is further supported by the studies carried out with homogeneous Brønsted and Lewis acid catalysts. Figure 40 shows the carbon selectivities of all the identified products as a function of the fraction of Brønsted acid sites for the homogeneous acid catalysts. These calculated values were interpolated to correspond with a glucose conversion of 50%. Levulinic acid and formic acid selectivities increase as the fraction of Brønsted sites increases. A minimal HMF selectivity is observed with pure Brønsted acid sites suggesting this type of acid site predominantly catalyzes the rehydration of HMF to form levulinic acid and formic acid. In contrast, Lewis acid sites favor the isomerization reaction of glucose to fructose. Similar

conclusions have been reported in the past by Davis and co-workers in their studies of tin-containing zeolites as highly active solid Lewis acid catalysts,[122, 189, 190] and by Dumesic and Shanks.[203, 204] As with the dehydration step, it is apparent from the results that both Brønsted and Lewis acid sites catalyze the production of HMF from glucose and fructose, reaching a maximum carbon selectivity of 19% at 50% glucose conversion with a Brønsted acid site fraction of 0.25. The selectivity to humins does not vary much as a function of the Brønsted to Lewis acid site ratio, however a slight decrease is observed at higher fractions of Brønsted sites.

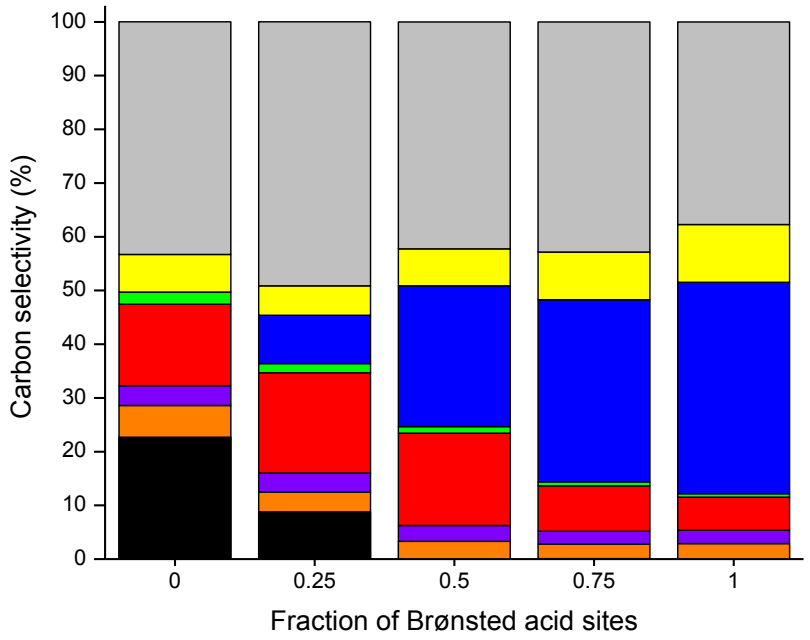

Figure 40. Carbon selectivity of water-soluble products as a function of the fraction of Brønsted acid sites for the homogeneous acid catalysts at 50 % glucose conversion and 160ºC. Total acid concentration was kept constant at 0.1 M. Feed was 10 wt% glucose aqueous solution. ■ fructose; ■ cellobiose; ■ levoglucosan; ■ HMF; ■ furfural; ■ levulinic acid; ■ formic acid; ■ humins. Reprinted from ref.[205], Copyright(2013), with permission from Elsevier.

Two classes of metal(IV) phosphates have been prepared based on tin and zirconium precursors. Despite the same phosphorus to metal(IV) molar loadings in the preparation procedure, the tin phosphates have lower phosphorus concentrations than the zirconium phosphates according to elemental analysis. The phosphorus to metal(IV) ratios obtained for the zirconium phosphates are more than two fold the amount obtained for the tin-based analogues. Consequently, the zirconium phosphates all have higher total acid and Brønsted acid concentrations according to ammonia and isopropylamine TPD respectively. Prior studies which have compared different types of metal(IV) phosphates have reported conflicting results. Patel *et al.* [213, 216] compared tin, zirconium and titanium phosphates for cyclodehydration of 1,*n*-diols. They found tin phosphate to be the most active and selective catalyst, which they attributed to its relatively high surface area and strong acid sites. Similar conclusions were deduced by Gu *et al.* [223] in their study of sorbitol dehydration to produce isosorbide. It is notable to mention that the catalysts tested in these previous studies were not calcined. The discrepancy with our study could be attributed to the differences in catalyst preparation procedures. Similarly, Tran *et al.* have shown a direct correlation between the acidic and catalytic properties of sulfated zirconia and its calcination temperature.[256] It has been reported in the literature that the concentration of Brønsted acid sites for crystalline zirconium phosphate is maximized at a calcination temperature of 400 °C.[228]

The bulk and surface properties of the zirconium phosphate catalysts differ according to their phosphorus loadings. Results from elemental analysis and ^{31}P solid-state NMR spectroscopy show that catalysts ZrP2 and ZrP3 are quite similar in the bulk phase. Despite different phosphorus loadings in the preparation procedure, both catalysts contain nearly

identical phosphorus amounts in the bulk phase, as well as on the surface. The highest attainable phosphorus to zirconium molar ratio is 2 to 1. This is similar to the maximum P/Zr ratio of 2.21 reported by Sinhamahapatra *et al.* who studied the effect of phosphate concentration and calcination temperature on the catalytic properties of mesoporous zirconium phosphate.[229]

Characterization techniques carried out in this study show noticeable differences in surface properties among the three zirconium phosphate catalysts. As shown with ZrP1 and ZrP2, increased phosphorus loading results in higher phosphorus content in the bulk and on the surface. This in turn increases the total acidity and Brønsted acidity.[229] Conversely, a higher zirconium loading increases the Lewis acidity due to increased amounts of tetravalent zirconium (Zr^{4+}), as shown for ZrP1. Further increasing the phosphorus loading in the preparation step from a P/Zr molar ratio of 2 to 3 does not increase the phosphorus content in the bulk or on the surface, as shown for ZrP2 and ZrP3. Among the three zirconium phosphate catalysts, ZrP2 has the highest surface area, as well as the highest overall acid and Brønsted acid concentrations. Consequently, ZrP2 was found to contain the highest amount of hydroxyl groups on its surface, as confirmed with XPS analyses. This could explain its high concentration of Brønsted acid sites.[210] Kellum and Hahn found a direct correlation between the concentration of surface hydroxyl groups and the surface area for a series of trimethylsiloxy-treated ammonium silicates.[257] Therefore, the increased amount of surface hydroxyl groups on ZrP2 could also be a cause for its relatively high surface area. On the other hand, other studies have claimed that the preparation conditions have a strong effect on the structure and surface properties of zirconia catalysts. Specifically, the nature of the zirconium precursor, the pH of the solution during precipitation, temperature and time of digestion and calcination temperature all play key roles

that influence these properties.[258-261] In this study, the zirconium phosphate catalysts differ by the P/Zr molar ratios in the preparation step. This was achieved by varying the relative amounts of phosphorus and zirconium precursors (ammonium phosphate monobasic and zirconium oxychloride octahydrate respectively). This in turn alters the pH of the solution during precipitation, which could be a cause for varying surface areas observed for the different samples.

Various groups have studied the effect of phosphate and sulphate loading on different acid catalysts. Sinhamahapatra *et al.* discovered that a phosphate to zirconium ratio of 2 yields the highest surface area as well as the highest concentration of total acid sites and Brønsted acid sites as determined by NH_3-TPD and DRIFTS spectra for pyridine adsorption respectively.[229] A further increase in phosphate loading (P/Zr ratio 3) resulted in a decrease in total acidity and Brønsted acidity. They reasoned the decrease in Brønsted acidity was due to the formation of polyphosphate, which in turn diminishes the P-OH groups. It is unlikely that these conclusions are entirely valid for this study, as the relative amounts of the polyphosphate species for ZrP2 and ZrP3 are nearly identical (Table 13), whereas ZrP2 shows a higher concentration of acid sites compared to ZrP3. However, it has been reported in the literature that the length of the polyphosphate chain is a function of the metal oxide to phosphate ratio.[262] An increase in the polyphosphate chain length is observed with increased amounts of P_2O_5. Determining the composition and chain length of the polyphosphate species was not a focus of this study, however differences in these parameters between ZrP2 and ZrP3 could be a reason for the discrepancies in their catalytic properties. Another analogous study was reported by Mishra and Parida who examined the effect of sulphate loading on sulphated zirconia catalysts.[234]

According to their results, increasing the sulphate loading from 10 wt% to 15 wt% resulted in decreased sulphur content as determined by elemental analysis. The increase in sulphate loading also resulted in inferior catalytic properties including lower surface area, lower overall acidity and decreased surface hydrophilicity. Another study was carried out by Ahmed *et al.* on the effect of sulphate loading with sulphated zirconia.[263] They incorporated SO_4^{2-} in zirconia ranging from 5 to 30 wt% and found the catalyst with a loading of 15 wt% sulphate to possess the highest surface area, as well as highest total acidity and Brønsted to Lewis ratio. Consequently, this catalyst was found to exhibit optimal catalytic activity for ethanol dehydration.

CHAPTER 7

Aqueous phase production of levulinic acid from cellulose

Weingarten, R.; Conner Jr, W. C.; Huber, G. W., Production of levulinic acid from cellulose by hydrothermal decomposition combined with aqueous phase dehydration with a solid acid catalyst. *Energy and Environmental Science* **2012,** *5*, 7559-7574.

7.1. Background

Herein, we introduce a process to produce levulinic acid from cellulose without the use of a homogeneous acid catalyst. The first step consists of cellulose hydrothermal decomposition followed by conversion of the water-soluble organics to produce levulinic acid with a solid acid catalyst. Amberlyst 70 was used as a solid acid catalyst for conversion of the water soluble organics into HMF, levulinic acid and formic acid.

The transformation of cellulosic biomass in aqueous media offers an environmentally friendly and economical route to produce targeted chemicals. One distinct advantage of this technology is that the biomass feedstock can be directly converted without the need for an energy intensive pre-drying step.[264] During hydrothermal treatment, water acts both as a reactant and catalyst.[265] In particular, it has been shown that exposure to water at elevated temperatures and pressures can cause the cellulose crystalline structure to become amorphous.[266] Glucose oligomers with a wide range of degrees of polymerization have also been detected during exposure of cellulose in hot-compressed water.[267]

Promising results have been reported for levulinic acid production from cellulosic biomass. In their recent publication, Hongzhang and co-workers described the use of a solid superacid ($S_2O_8^{2-}/ZrO_2–SiO_2–Sm_2O_3$) to produce levulinic acid from rice straw.[268] At their optimal conditions they obtained a molar carbon yield of 58% (70% of the theoretical) from the cellulose portion of the rice straw following a pretreatment procedure that included exposure to steam and superfine grinding of the rice straw. These results were achieved for a solid acid catalyst concentration of 13.3 wt%, which corresponds to more than four times the cellulose weight content in the feedstock. Likewise, they performed catalyst recycle studies

which resulted in a 50% and 67% loss of activity following the second and third use of the catalyst respectively. The decrease in activity was attributed to the loss of active sties on the solid acid catalyst. Catalytic activity was not fully recovered despite regeneration of the catalyst. Van de Vyver *et al.* showed that levulinic acid can be produced directly from cellulose at 25% carbon molar yield (30% of the theoretical) at mild temperatures using sulfonated hyperbranched poly(arylene oxindole)s.[269] These are a new class of water-soluble acid catalysts which can be separated post-reaction by ultrafiltration. Another interesting concept was reported by Lai *et al.* in which they used sulfonated mesoporous silica modified with magnetic iron oxide particles (Fe_3O_4-SBA-SO_3H) to produce levulinic acid from cellulose.[270] They obtained a carbon molar yield of 38% (45% of the theoretical) after 12 h at 150°C with a feedstock concentration of 10 wt%. They were able to separate and recycle the magnetic catalyst after reaction when a magnetic field was applied.

Acidic ion-exchange polymer resins such as Nafion and Amberlyst have been shown to be effective catalysts for a wide range of acid-catalyzed reactions due their relatively high concentrations of Brønsted acid sites.[138, 149] As we have shown in Chapter 3, dehydration reactions using Amberlyst 70 and Nafion SAC-13 showed similar selectivities to HCl due to their inherently high concentration of Brønsted sites. Early work with acidic ion exchange resins to produce levulinic acid from carbohydrates showed relatively low levulinic acid yields of 8% (9% of the theoretical) and 30% molar carbon (36% of the theoretical) from glucose and fructose respectively.[271] These studies were carried out at relatively low temperatures, and thus endured relatively low reaction rates, due to the limited thermal stability of the ion resins.[272] Lucht and co-workers have been able to produce glucose and

levulinic acid from cellulose with Nafion SAC-13.[273] They studied the effect of NaCl on these reactions and found the yield of levulinic acid to increase five-fold from 14% (of the theoretical) with just water as the solvent to 72% (of the theoretical) in a 25% NaCl solution.[274]

7.2. Experimental

7.2.1. Catalyst preparation and characterization

The zirconium phosphate catalyst (ZrP) was prepared as mentioned in the previous chapters. The Amberlyst 70 (Dow Chemical) was prewashed with DI water to remove any excess acid (pH of filtrate was 5) and then used in its wet form. Hydrochloric acid was supplied by Fisher Scientific. Ytterbium trifluoromethanesulfonate hydrate, $Yb(OTf)_3$, was supplied by Strem Chemicals.

Total acid sites were determined by ammonia-temperature programmed desorption (NH_3-TPD)[141] with a Quantachrome ChemBET Pulsar^{TM} TPR/TPD Automatic Chemisorption Analyzer coupled with a TCD to quantify the ammonia desorbed from the sample. A sample of 300 mg was initially degassed at 673 K for 2 h under a constant helium flow of 12 mL min^{-1} (Airgas, UHP). The sample was cooled to room temperature and ammonia (Airgas, electronic grade) was adsorbed at 373 K for 30 min. to reach saturation. Afterwards, the ammonia supply line was shut off and helium was purged at 12 mL min^{-1} for 1.5 h to remove any physically adsorbed ammonia. The sample was then heated at a rate of 10 K min^{-1} from 373 to 973 K under a constant helium flow of 12 mL min^{-1}. The sample was held at the temperature set point for an additional 1.5 h. The total acidity of Amberlyst 70

was taken from the manufacturer.

The BET surface areas were determined by nitrogen adsorption at 77 K using a Quantachrome Autosorb® iQ2 automated gas sorption system. Initially, the Amberlyst 70 was dried overnight at 383 K, crushed and sieved to a particle size of ≤ 125 μm. ZrP was degassed at 523 K for 24 h and Amberlyst 70 was degassed at 423 K for 24 h prior to analysis. An eleven-point BET analysis was performed ranging from 0.05 to 0.3 relative pressure P/P_o and the BET "C" constant recorded.

X-ray diffraction patterns were obtained using a Philips X'Pert Pro diffractometer equipped with a X'Celerator detector. An accelerating voltage of 45 kV was used at 36 mA. Powder samples were placed on a glass slide sample holder.

7.2.2. Reaction experiments

Batch reactions were carried out in 100 and 160 mL reactor vessels provided by Parr Instrument Company, series 4560. The feedstock solutions were prepared with DI water at the specified concentrations. Microcrystalline cellulose (Avicel® PH-101) with a particle size of approximately 50 μm was provided by Sigma Aldrich. Glucose was provided by Fisher Scientific. Temperatures in the reactor were measured by a thermocouple in the solution. Time zero in the reaction was defined as the time when the reactor reached the desired temperature. Depending on the reaction temperature, the heat up time ranged from 10 to 40 minutes. All reaction solutions were mixed at a maximum constant rate of 600 rpm using an internal stirrer. The temperature and stirring were controlled by a 4848 Controller provided by Parr. The reaction vessel was initially pressurized to 600-750 psi with industrial

grade helium (Airgas). Liquid samples were taken periodically by way of a sampling port with a dip tube immersed in the reaction mixture. A stainless steel woven wire cloth, mesh size 400x400 provided by McMaster-Carr, was wrapped around the dip tube to prevent loss of solids and clogging during sampling. The samples were immediately quenched in an ice water bath and filtered with a 0.2 μm syringe filter prior to analysis. The reactor was repressurized with helium after each sampling. In cases when sampling was not feasible, the entire reactor was immersed in an ice bath to rapidly quench the reaction.

7.2.3. Analysis

Liquid samples were analyzed by high pressure liquid chromatography (HPLC) with a Shimadzu© LC-20AT. Carbohydrates were detected with a RI detector (RID-10A) and products were detected with a UV-Vis detector (SPD-20AV) at wavelengths of 210 and 254 nm. The column used was a Biorad© Aminex HPX-87H sugar column. The mobile phase was 0.005 M H_2SO_4 flowing at a rate of 0.6 mL/min. The column oven was set to 30 °C. The total organic carbon (TOC) measurements were performed with a Shimadzu© TOC-VCPH Analyzer. TOC calibration standards were prepared with carbon standards supplied by SpectroPure. For the purpose of this study, humins were considered all non-detectable compounds. These undesired compounds can be further distinguished as water-soluble and insoluble humins.

Solid samples were pyrolized in a DSC–TGA (TA instruments SDT Q600 system). Approximately 15–30 mg of initial solid was loaded for each run and degassed at 383 K for 1 h under a constant helium flow of 100 mL min^{-1} (Airgas, UHP). Samples were cooled and

then heated linearly at a rate of 15 K min^{-1} from 333 to 1073 K under a constant helium flow of 100 mL min^{-1}. TGA was used to measure the weight changes of the residual mass.

In this study, conversion was defined as the ratio of moles of feed (n_{feed}) that reacted, obtained from HPLC analysis, divided by the initial moles of feed loaded in the reactor:

$$Conversion\ (\%) = 100 \times \frac{n_{feed_{initial}} - n_{feed_{final}}}{n_{feed_{initial}}} \tag{22}$$

Unless otherwise mentioned, carbon selectivity of product *i* was defined as the ratio of moles of product *i* (n_i), as determined by HPLC analysis, multiplied by the number of carbon atoms of product *i* (C_i), divided by the moles of feed (n_{feed}) that reacted multiplied by the number of carbon atoms of feed (C_{feed}):

$$[Carbon\ selectivity]_i\ (\%) = 100 \times \frac{C_i \times n_i}{C_{feed} \times \left(n_{feed_{initial}} - n_{feed_{final}}\right)} \tag{23}$$

Carbon yield of product *i* was defined as the ratio of moles of product *i* (n_i) multiplied by the number of carbon atoms of product *i* (C_i), divided by initial moles of feed (n_{feed}) loaded in the reactor multiplied by the number of carbon atoms of feed (C_{feed}):

$$[Carbon\ yield]_i\ (\%) = 100 \times \frac{C_i \times n_i}{C_{feed} \times n_{feed_{initial}}} \tag{24}$$

7.3. Results

7.3.1. Production of levulinic acid from aqueous glucose solutions with solid acid catalysts

Aqueous-phase glucose dehydration studies were carried out in a batch reactor with solid acid catalysts, including ZrP and Amberlyst 70, at 160 °C with the concentration of total acid sites held constant at 0.1 M (determined by NH_3-TPD or taken from manufacturer). The characterization data for the solid acid catalysts appear in Table 16.

Table 16. Characterization of solid acid catalysts.[d]

Catalyst	BET surface area (m^2 g^{-1}) [a]	Total acid sites (mmol g^{-1})
ZrP	313	2.15 [b]
Amberlyst 70	0.54	2.86 [c]

[a] BET "C" constant is 101 for ZrP and 46 for Amberlyst 70.
[b] Determined by NH_3-TPD.
[c] Data provided by manufacturer.
[d] Reproduced from ref.[255] by permission of The Royal Society of Chemistry.

Figure 41 depicts glucose conversion and yields of the key products as a function of reaction time. Experiments were also carried out with a homogeneous acid catalyst (HCl) for comparison. As shown in Figure 41(a), the catalytic activity based on glucose conversion was found to be comparable for all of the catalysts tested, homogeneous and heterogeneous alike. The blank run (without a catalyst) showed a lower rate of glucose conversion. With respect to HMF production, the most selective catalyst was ZrP, with a maximum attainable carbon yield of 21% after 120 min. ZrP showed the lowest selectivity towards levulinic acid production. This could be due to the presence of Lewis acid sites on the ZrP, as suggested by separate studies that we performed with homogeneous Brønsted and Lewis acid catalysts (refer to Figure A.6 in the Appendix). With respect to levulinic acid production, HCl had the highest yield, followed by Amberlyst 70. As shown in Figure 41(c), levulinic acid yield

increased with reaction time with the Amberlyst 70 catalyst and reached a 33% carbon yield after 4 h.

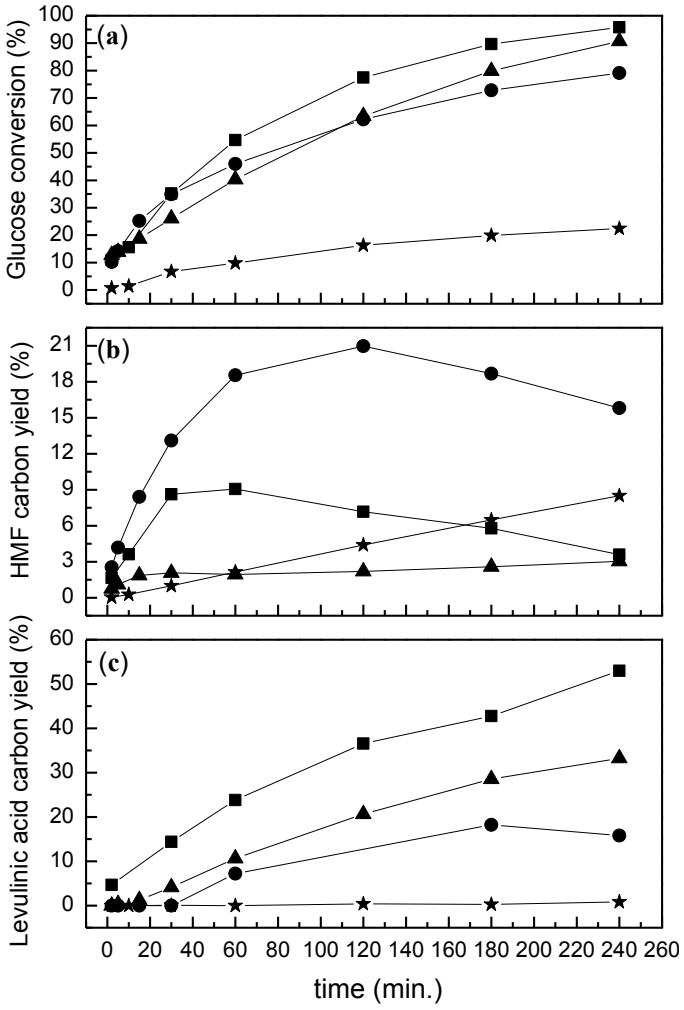

Figure 41. Aqueous phase acid-catalyzed glucose dehydration in a stirred batch reactor at 160 °C. Effect of catalyst on (**a**) glucose conversion; (**b**) HMF carbon yield; (**c**) levulinic acid carbon yield. Feed was 10 wt% glucose aqueous solution. Catalyst concentration was 0.1 M total acid sites (for solid acid catalysts this was determined by NH_3-TPD or taken from manufacturer). Catalysts: HCl (■), ZrP (●), Amberlyst 70 (▲), blank (★). Reproduced from ref.[255] by permission of The Royal Society of Chemistry.

Amberlyst 70 was selected as a solid acid catalyst for further studies due to its higher

rate of levulinic acid production compared to ZrP. The effect of reaction temperature on the conversion of glucose to HMF and levulinic acid is shown in Figure 42. As shown in Figure 42(a), the HMF selectivity increases with temperature. The reason is that glucose dehydration to HMF has a relatively higher apparent activation energy barrier step compared to HMF conversion to levulinic acid, as shown in Chapter 5. Levulinic acid selectivity increased with glucose conversion and was similar for all temperatures. Nevertheless, a closer look at Figure 42(b) shows that the highest levulinic acid selectivity at high glucose conversion was obtained at 160 °C. The selectivity to total humins production (soluble and insoluble) at nearly full glucose conversion was the lowest at 160 °C. Accordingly, all additional acid-catalyzed aqueous phase reactions were performed with Amberlyst 70 as a solid acid catalyst at 160 °C.

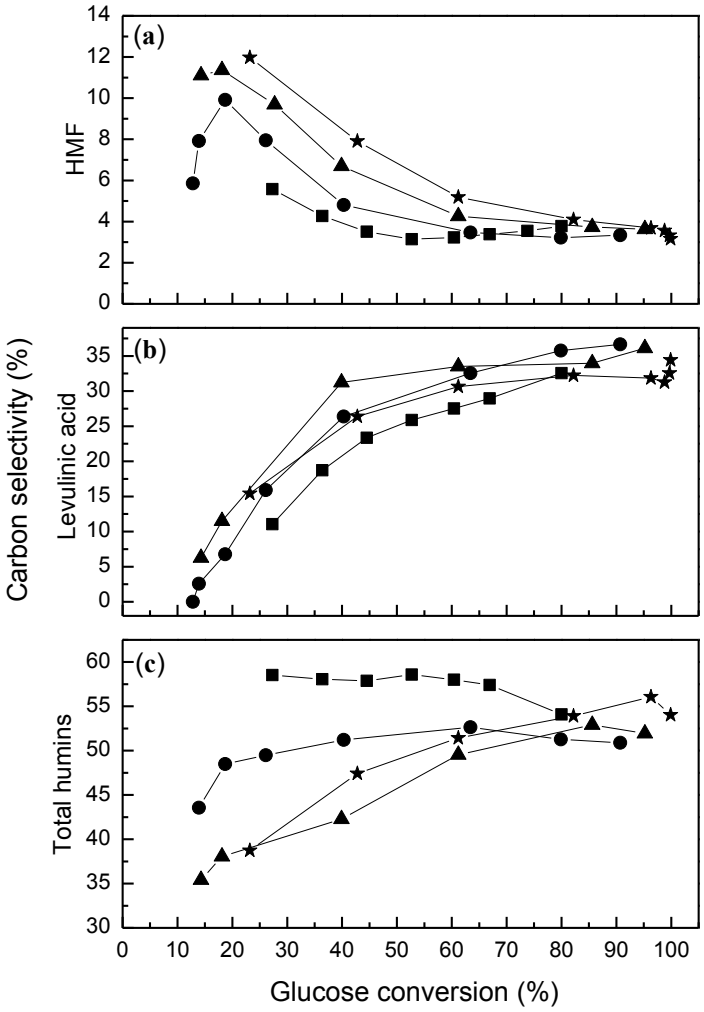

Figure 42. Aqueous phase glucose dehydration in a stirred batch reactor with Amberlyst 70. Effect of temperature on carbon selectivity for (**a**) HMF; (**b**) levulinic acid; (**c**) total humins. Feed was 10 wt% glucose aqueous solution. Catalyst concentration was 0.1 M total acid sites (concentration of acid sites was taken from manufacturer). T (°C) = 150 (■), 160 (●), 170 (▲), 180 (★). Reproduced from ref.[255] by permission of The Royal Society of Chemistry.

As part of the additional studies conducted with Amberlyst 70, we tested for leaching of acid sites from the ion resin into the aqueous phase. This consisted of exposing the ion resin to DI water at 160 °C for two 4 h cycles, followed by hot vacuum filtration to separate the catalyst. The catalyst was then immersed in a fresh glucose solution for further reaction.

The catalytic activity as well as the selectivity toward HMF and levulinic acid were retained, as compared with reaction with fresh (not pre-exposed to hot DI water) Amberlyst 70 (refer to Figure A.7 in the Appendix). The filtrate from the original test was mixed with glucose to produce an aqueous solution of 10 wt% glucose. We then proceeded to dehydrate the glucose in a blank experiment (no additional catalyst). An equivalent blank study was also carried out for an aqueous solution of 10 wt% glucose consisting of clean DI water. Figure A.8 in the Appendix shows that comparable product yields were obtained for both blank experiments. Overall, these results indicate that Amberlyst 70 was stable under the reaction conditions tested in this study.

Further studies were also carried out to test for the recyclability and regeneration of Amberlyst 70. The used catalyst was recovered with vacuum filtration and prewashed with DI water (pH of filtrate was 5) before it was recycled. The regeneration process consisted of washing the fouled catalyst with excess solution of 1 N sodium hydroxide at 50 °C to remove solid humins deposited on the catalyst. The catalyst was then washed with DI water at 50 °C to remove any excess base and reprotonated with 2 N sulfuric acid solution at room temperature. The regenerated catalyst was washed with DI water (pH of filtrate was 5) before the reaction. Figure A.9 in the Appendix shows the catalytic activity based on glucose conversion for the fresh, recycled and regenerated catalyst. The recycled catalyst showed higher conversion rates than the fresh catalyst. We suspect that this is due to residual acids on the catalyst that were not removed during the prewashing step. Likewise, the catalytic activity was not fully recovered after regeneration. The recycled catalyst showed lower carbon selectivity towards levulinic acid production, as shown in Figure A.10

in the Appendix. Levulinic acid selectivity increased after catalyst regeneration, though it remained lower than that of the fresh batch. It is notable to mention that the volume of the sodium hydroxide solution used may vary according to the degree of fouling on the resin. Therefore, insufficient washes with the basic solution during the regeneration process could be a plausible cause to the irrecoverable activity and selectivity.

7.3.2. Aqueous phase decomposition of cellulose with ZrP

Hydrothermal decomposition studies of cellulose were carried out in a batch reactor at temperatures 190-270 °C with initial cellulose loadings of 4 wt% (concentration calculated according to cellulose and water content). The solid acid catalyst ZrP (4 wt% loading according to catalyst and water content) was used due to its increased thermal stability compared to Amberlyst 70.[146] Amberlyst 70 is known to decompose at temperatures above 190 °C. Figure 43 shows the total water-soluble organic carbon yield of the products. This was defined as the ratio of water-soluble organic carbon obtained by TOC analysis divided by the initial carbon content from the glucosyl units (molecular weight of 162) present in the cellulose feedstock. Cellulose solubilization increased with temperature at short reaction times. The carbon yield decreased with increasing reaction times for all temperatures above 220 °C. This decrease in water-soluble organic carbon is caused by the formation of water-insoluble humins. At higher temperatures only decreases in the yields were detected, suggesting that in these cases the cellulose hydrolyzed during the reactor heat up. It typically took 10 to 40 minutes for the reactor to heat to the reaction temperature. The maximum yield of water-soluble organics was 61% at 250 °C at time 0 (time when the reactor reached the

desired temperature). Overall, a higher yield of water-soluble products can be achieved at relatively higher temperatures and shorter reaction times. Solid humins were deposited on the solid acid catalyst for all of the reactions performed with ZrP.

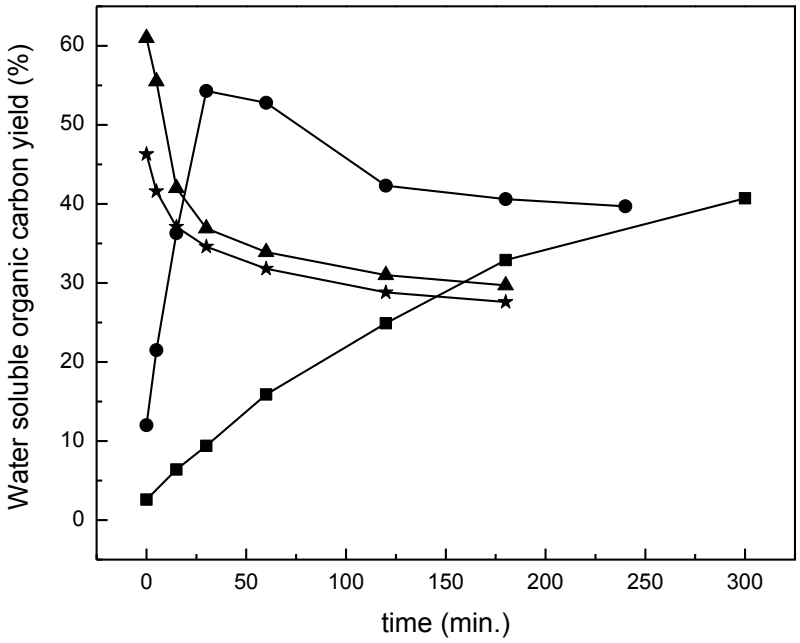

Figure 43. Aqueous phase cellulose decomposition with ZrP in a stirred batch reactor. Total water-soluble organic carbon yield as a function of reaction time. Initial cellulose and catalyst loadings were 4 wt% of total. T (°C) = 190 (■), 220 (●), 250 (▲), 270(★). Reproduced from ref.[255] by permission of The Royal Society of Chemistry.

Figure 44 depicts the carbon yield of the major products from cellulose hydrolysis with ZrP as a solid acid catalyst. These included glucose, HMF, levulinic acid and water-soluble humins. Glucose and HMF showed similar trends in which optimum yields were obtained at 250 °C and relatively short reaction times. This is consistent with our kinetic model that we derived for levulinic acid production from glucose in Chapter 5. In this model HMF production is maximized at relatively higher temperatures and shorter reaction times.

A sharp decrease in glucose and HMF content was observed at 270 °C due to the increased formation of humins, which was attributed to the rather long heat up stage of the reactor (approximately 40 minutes to reach 270 °C). The highest yields of glucose and HMF obtained from cellulose with ZrP were 9 and 20% respectively, at 250 °C at time 0.

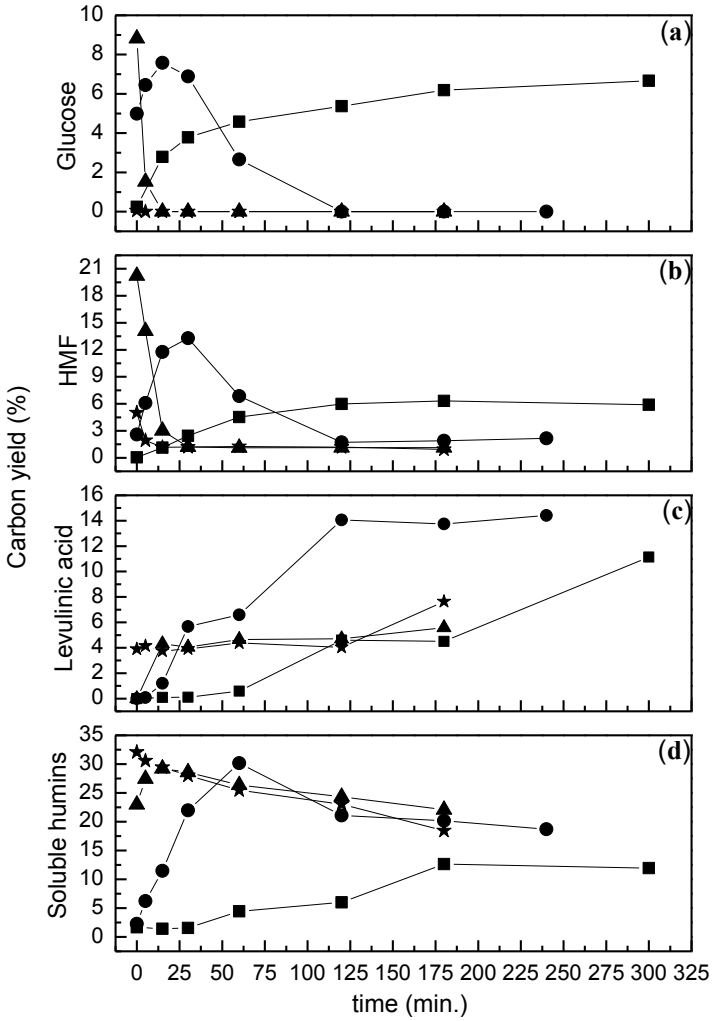

Figure 44. Aqueous phase cellulose decomposition with ZrP in a stirred batch reactor. Water-soluble organic carbon yield of (**a**) glucose, (**b**) HMF, (**c**) levulinic acid, (**d**) soluble humins. Initial cellulose and catalyst loadings were 4 wt% of total. T (°C) = 190 (■), 220 (●), 250 (▲), 270(★). Reproduced from ref.[255] by permission of The Royal Society of Chemistry.

Levulinic acid yield production increased systematically with reaction time, reaching a plateau at 14% carbon yield at 220 °C. At 190 °C there was a continuous increase of levulinic acid carbon yield throughout the entire reaction time. Consequently, according to Figure 44(b), HMF content was the highest for 190 °C at prolonged reaction times. We have shown in previous studies that HMF rehydration to produce levulinic acid is favorable at relatively lower temperatures ranging from 150-160 °C due to a parallel high activation energy step for HMF decomposition to produce humins.[175] Consistent with this observation, Figure 44(d) reveals that the yield of soluble humins decreases at lower temperatures. Patil and Lund have proposed that the acid-catalyzed conversion of HMF to form humins is primarily by way of aldol addition and condensation reactions.[275]

The product distribution of water-soluble organic carbon as a function of reaction time appears in Figure 45 for temperatures 190-270 °C. This was defined as the ratio of carbon content attributed to each detectable product, as determined by HPLC analysis, to the total water-soluble organic carbon obtained by TOC analysis. In general, the selectivity toward desirable products (glucose, HMF, levulinic acid, formic acid) increases as the reaction temperature decreases. Additional byproducts including fructose, cellobiose, levoglucosan and furfural were also detected. Furfural has been reported to come from HMF *via* loss of formaldehyde.[180-183] The carbon yield to furfural was less than 5% in this study. Cellobiose was present at less than 1% carbon yield and its presence could be attributed to the depolymerization of cellulose *via* cellooligomers[17, 276, 277] and/or reversion reactions from glucose.[166, 184, 185] Levoglucosan (present at less than 2% carbon yield) has also been reported to be formed from glucose reversion reactions.[166] Finally, small amounts of

fructose were also accounted for at less than 1% carbon yield. It has been proposed that epimerization reactions with glucose could lead to its formation.[184] The presence of qualitative amounts of mannose in this study supports this last claim.

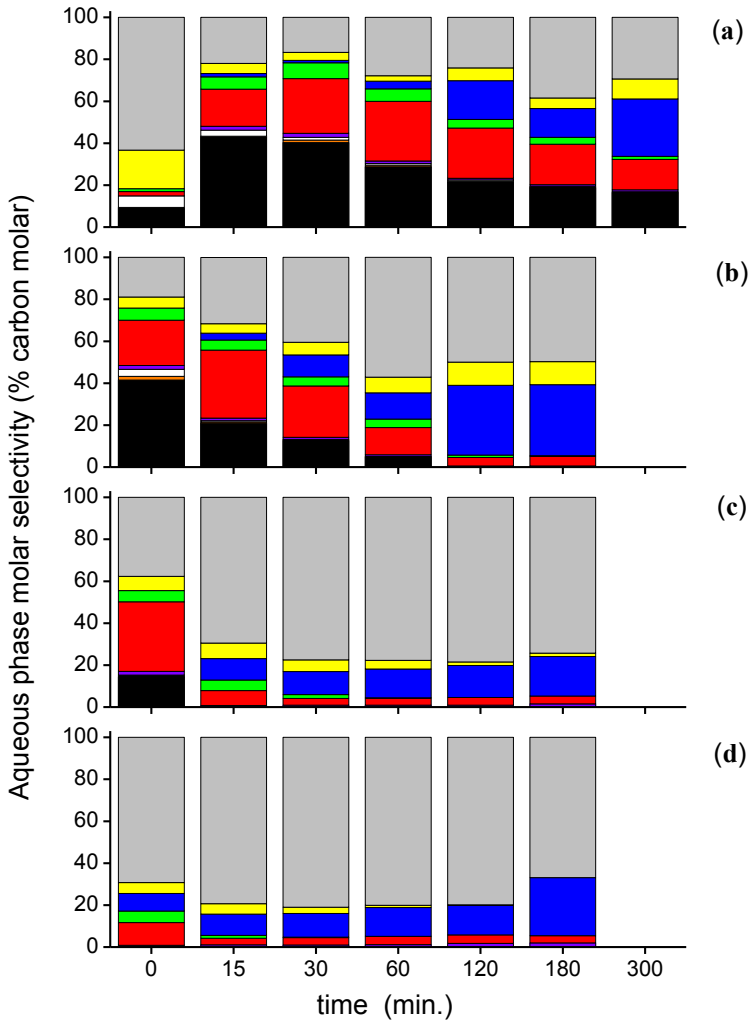

Figure 45. Water-soluble organic carbon product selectivity for the aqueous phase cellulose decomposition with ZrP in a stirred batch reactor for T (°C) = (**a**) 190 (**b**) 220, (**c**) 250, (**d**) 270. Initial cellulose and catalyst loadings were 4 wt% of total. ■ glucose; ■ fructose; □ cellobiose; ■ levoglucosan; ■ HMF; ■ furfural; ■ levulinic acid; ■ formic acid; ■ humins. Reproduced from ref.[255] by permission of The Royal Society of Chemistry.

7.3.3. Non-catalyzed hydrothermal decomposition of cellulose

Equivalent experiments to those with ZrP were carried out for cellulose hydrothermal decomposition without the presence of an acid catalyst. Figure A.11 in the Appendix shows the total water-soluble organic carbon yield, as determined by TOC analysis. Similar trends to those in Figure 43 were observed without an acid catalyst. However, it is apparent that the total water-soluble carbon yield was higher with ZrP at lower temperatures (*i.e.* 190 °C). Conversely, at temperatures 250-270 °C, a slightly higher yield was obtained for the reactions without a catalyst with a maximum value of 65% of water-soluble organics at 270 °C at the initial time. The maximum yield of water-soluble organic carbon obtained with ZrP was 61% at 250 °C at time 0. This suggests that degradation reactions are enhanced by the acid catalyst ZrP at temperatures above 220 °C.

Figure A.12 in the Appendix depicts the carbon yield of the major products from cellulose hydrothermal decomposition without a solid acid catalyst. More glucose was obtained without the solid acid catalyst for all temperatures, with a maximum glucose carbon yield of 16%. HMF yields were also higher throughout the entire reaction time without the solid catalyst with a maximum HMF yield of 22% carbon. Lower levulinic acid concentrations were observed without an acid catalyst (maximum 7% yield at 220 °C after 3 h), signifying that HMF rehydration to form levulinic acid has a higher rate of reaction with the solid acid than without. This is consistent with our findings in Figure 41(c).

Product distribution of the water-soluble organic carbon for non-catalyzed cellulose hydrothermal decomposition appears in Figure A.13 in the Appendix. Similar to its acid-catalyzed counterpart (Figure 45), the selectivity toward desirable products (glucose, HMF,

levulinic acid, formic acid) is favorable at relatively lower temperatures. The same byproducts were observed as in the acid-catalyzed decomposition. The highest combined selectivity of detectable compounds for both acid-catalyzed and non-catalyzed cellulose decomposition was 80% at 190 and 220 °C respectively for an initial cellulose loading of 4 wt%. Nevertheless, the product distribution for non-catalyzed cellulose decomposition favors more glucose and HMF and less levulinic acid compared to cellulose decomposition catalyzed by ZrP.

As mentioned earlier, in this study, water-soluble humins were considered as all non-detectable compounds in the aqueous phase. These include any water-soluble cellulose oligosaccharides not detected with HPLC analysis, which could potentially be converted to valuable products. Therefore, a separate study was carried out on selected samples from both series of experiments (acid-catalyzed and non-catalyzed) to account for oligosaccharides produced from cellulose decomposition. Various studies have suggested that the cellulose decomposition pathway begins first with a hydrolysis step that produces water-soluble compounds.[265, 278] The procedure to convert the oligosaccharides to monosaccharides was taken from the literature[279] and consisted of hydrolyzing the product solutions in a 0.5 M sulfuric acid solution at 100 °C for 3 h. The resulting solutions were filtered with a 0.2 μm syringe filter and analyzed by way of HPLC and TOC. For all hydrolyzed samples, the carbon yield of water-soluble humins decreased while the carbon yield of glucose increased, thus confirming the presence of cellulose oligosaccharides in the samples. Additionally, the HMF content decreased and levulinic acid increased. TOC analysis revealed a lower organic carbon content for all hydrolyzed samples, indicating the formation of insoluble humins

during the hydrolysis procedure. The latter could be due to acid-catalyzed decomposition reactions associated with glucose and/or HMF.[175] As a result of these undesired reactions, quantitative assessments of the cellulose oligosaccharides could not be determined.

The overall reaction scheme for aqueous phase levulinic acid production from cellulose appears in Figure 46. This is complementary to the reaction scheme for levulinic acid production from glucose which appears in Figure 31. Cellulose initially hydrothermally decomposes to form water-soluble compounds, including glucose and oligosaccharides. These water-soluble oligosaccharides can further hydrolyze to form cellobiose. Humins are both water soluble and water insoluble. Water-soluble humins polymerize with time to form water-insoluble compounds. A detailed description of the reaction scheme appears in Chapter 6.

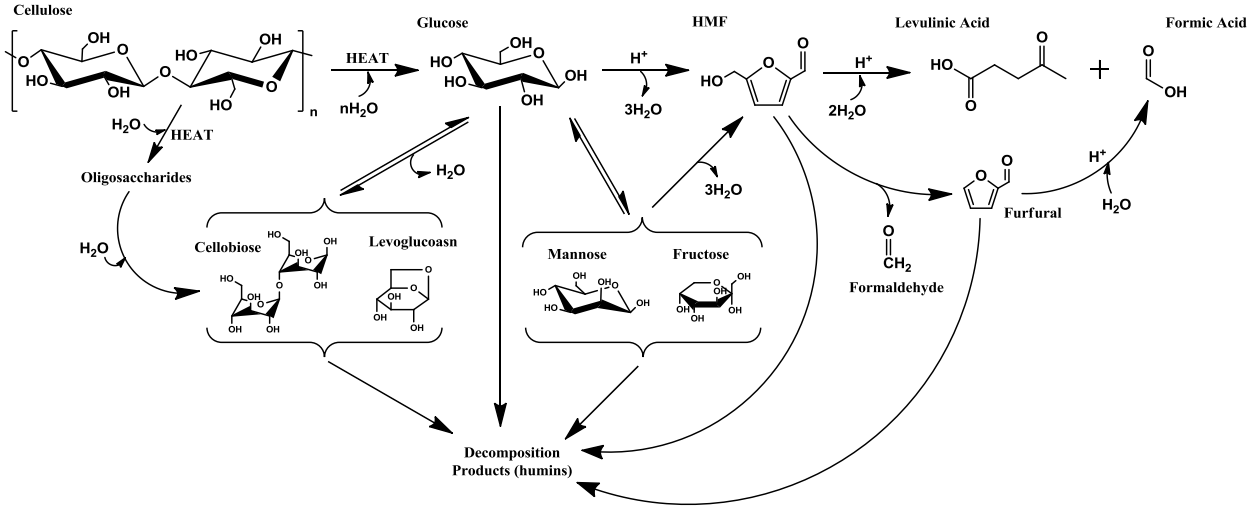

Figure 46. Overall reaction scheme for aqueous phase acid-catalyzed production of levulinic acid from cellulose by hydrothermal decomposition. Reproduced from ref.[255] by permission of The Royal Society of Chemistry.

Further cellulose decomposition studies were performed without a solid acid catalyst to investigate the effect of initial cellulose loading. Based on the results shown earlier, the use of a solid acid catalyst, such as ZrP, was not found to be advantageous compared to non-catalyzed cellulose decomposition, in terms of maximizing the amount of water-soluble organic carbon. In addition, increased formation of humins was observed with ZrP. Therefore, not using a solid catalyst for cellulose depolymerization also avoids the need to regenerate the solid acid catalyst prior to reuse. Figure 47 shows the total water-soluble organic carbon yield and product distribution as a function of initial cellulose loading at a constant reaction condition of 220 °C and 30 minutes. The total carbon yield was comparable for all cellulose loadings up to 17 wt%, with an average of 21%. A cellulose loading of 29 wt% resulted in the highest total carbon yield (32%) along with the highest selectivity of non-humin products in the aqueous phase (around 90%). This increase in yield at cellulose loading of 29 wt% could be attributed to a relatively higher concentration of organic acids present in the aqueous solution which might catalyze the hydrolysis reaction.[280] This could also be the reason for the higher selectivities of levulinic acid observed at the higher cellulose loadings. Further increasing the cellulose concentration to 38 wt% caused a decrease in the yield along with a decrease in the combined selectivity. This could be due to insufficient water which could hinder the decomposition of cellulose and also cause inadequate mixing of the solids in the reactor.

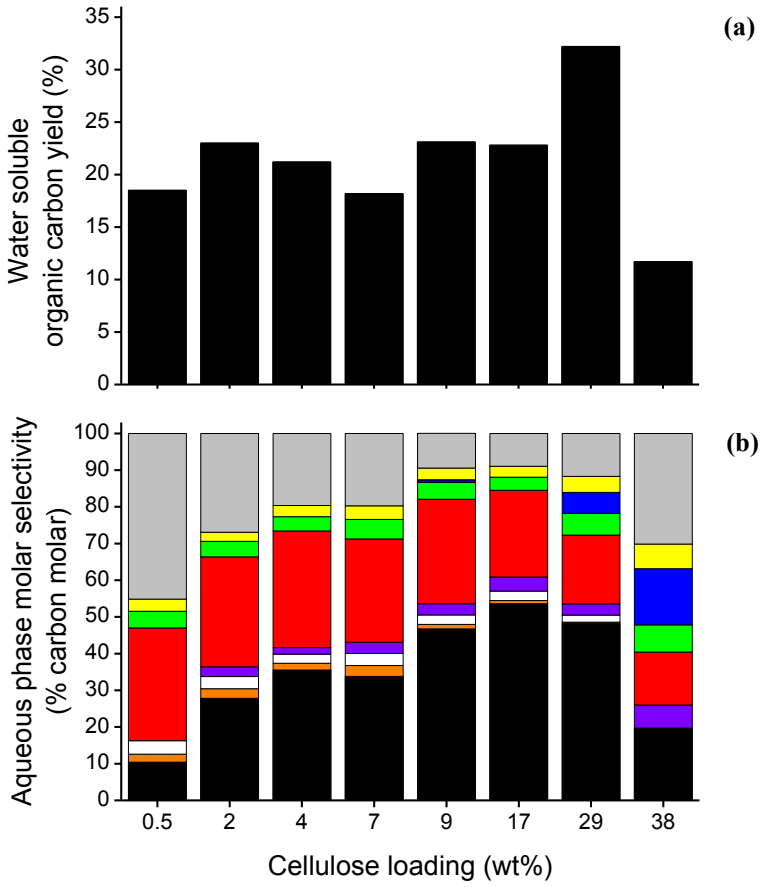

Figure 47. Non-catalyzed hydrothermal decomposition of cellulose in a stirred batch reactor at 220 °C and 30 min. Effect of initial cellulose loading on (**a**) total water-soluble organic carbon yield and (**b**) water-soluble organic carbon product selectivity. ■ glucose; ■ fructose; □ cellobiose; ■ levoglucosan; ■ HMF; ■ furfural; ■ levulinic acid; ■ formic acid; ■ humins. Reproduced from ref.[255] by permission of The Royal Society of Chemistry.

7.3.4. Two-step process to produce levulinic acid from cellulose

The major water-soluble compounds produced from non-catalyzed hydrothermal decomposition of cellulose are glucose and HMF, as shown in Figure 47. Hence, in order to produce levulinic acid, the aqueous phase from the decomposition step was subsequently subjected to a dehydration/rehydration step with Amberlyst 70. In this study both steps were

carried out in a batch reactor. The reaction conditions chosen for the first step (cellulose decomposition) were 220 °C for 30 min. at an initial cellulose loading of 29 wt%. These conditions showed the highest selectivity and yield of water-soluble compounds, as shown in Figure A.13(b) and Figure 47. The reaction was quenched by immersing the entire reactor into an ice bath, as sampling through the sample port was not feasible due the high loading of cellulose. DI water was used to dilute the reactor contents and the solids were separated with vacuum filtration. The solids were then washed with acetone to remove any acetone-soluble humins and dried overnight at 110 °C. The final solid phase, which consisted of unreacted cellulose and insoluble humins, was then reloaded to the reactor with clean DI water (29 wt% solids loading) to further decompose the unreacted cellulose.

The product distribution and yields of the key water-soluble products obtained from the cellulose decomposition step appear in Tables 17 and 18 respectively. Cellulose conversion was calculated based on the weight of unreacted cellulose in the residual solid phase. Pyrolysis experiments were carried out in a DSC-TGA instrument to determine the weight fraction of cellulose in the solid phase. Initially, the weight change of the residual mass of the sample was recorded as a function of time and normalized according to the mass of the sample at time zero. Time zero was considered at 100 °C during the pyrolysis segment of the method. The derivative weight was then calculated, defined as the ratio of the change in normalized mass to the change in temperature. Figure 48 depicts the derivative weight and solids conversion as a function of temperature in the range of 500-700 K. As shown in Figure 48(a), pyrolysis of pure cellulose generates a distinct derivative peak within this range. Pyrolysis of recycled samples results in the broadening and shifting of this

characteristic peak. This is due to a decrease in the crystallinity of the cellulose. XRD measurements of pure cellulose and the recycled samples confirm this claim, as shown in Figure 49.[281, 282] The cellulose weight fraction in the solid phase was proportional to the ratio of the peak area corresponding to the sample and pure cellulose.

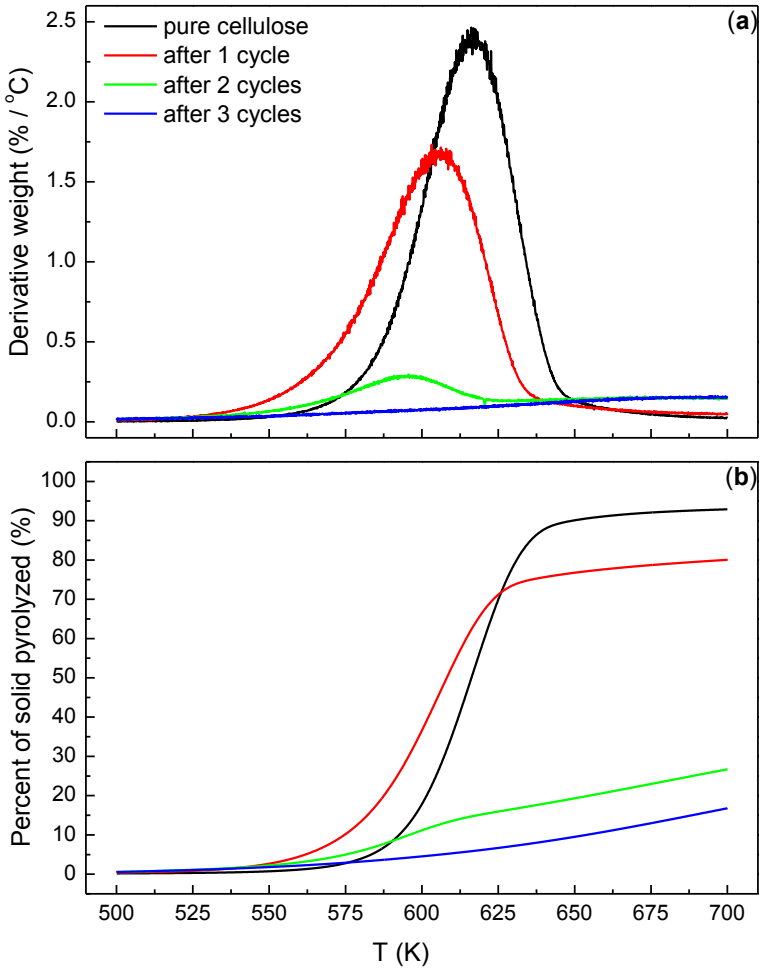

Figure 48. Pyrolysis of solid samples recovered from non-catalyzed hydrothermal decomposition of cellulose at 220 °C with recycling of solids. Each cycle reaction time was 30 min. **(a)** weight derivative; **(b)** percent of solid pyrolyzed. Reproduced from ref.[255] by permission of The Royal Society of Chemistry.

Alternatively, conversion data (percent of solid pyrolyzed), as shown in Figure 48(b), can also be used to determine the cellulose weight fraction. This was calculated as the ratio of the conversion obtained with a solid sample to that of pure cellulose. This technique is accurate under the assumption that only the cellulose portion of the solid is pyrolyzed. This was true for all samples, except for the solid sample recovered after 3 cycles. Otherwise, the calculated weight fractions of cellulose using both techniques were comparable. Figure 50 depicts the product distribution of the water-soluble products for each separate cycle run. Comparable selectivities were obtained for the first two cycle studies. The third cycle showed a lower selectivity, apparently due to the negligible conversion of cellulose during this cycle.

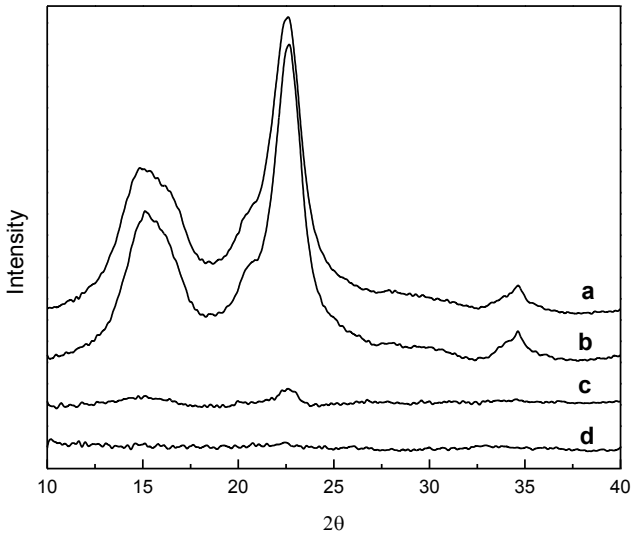

Figure 49. X-ray diffraction patterns of solid samples recovered from hydrothermal decomposition of cellulose without a solid acid catalyst at 220 °C with recycling of solids. Each cycle reaction time was 30 min. **(a)** pure cellulose; **(b)** after 1 cycle; **(c)** after 2 cycles; **(d)** after 3 cycles. Reproduced from ref.[255] by permission of The Royal Society of Chemistry.

Table 17. Product distribution from non-catalyzed hydrothermal decomposition of cellulose in a stirred batch reactor at 220 °C with recycling of solids. Initial solids loading for each cycle was 29 wt%. Each cycle reaction time was 30 min.[b]

		Cumulative carbon selectivity (%)			Cumulative carbon yield (%)		
Cycle	Cumulative cellulose conversion (%)	Usable organics [a]	Water-soluble humins	Insoluble humins	Usable organics [a]	Water-soluble humins	Insoluble humins
1	51.8	64.7	7.2	28.1	33.5	3.7	14.6
2	93.3	48.0	5.8	46.2	44.7	5.4	43.2
3	100.0	44.9	5.5	49.6	44.9	5.5	49.6

[a] includes: glucose, fructose, cellobiose, levoglucosan, HMF, furfural, levulinic acid, formic acid.
[b] Reproduced from ref.[255] by permission of The Royal Society of Chemistry.

Table 18. Carbon yields of key water-soluble products from non-catalyzed hydrothermal decomposition of cellulose in a stirred batch reactor at 220 °C with recycling of solids. Initial solids loading for each cycle was 29 wt%. Each cycle reaction time was 30 min.[a]

	Cumulative carbon yield (%)					
Cycle	Glucose	HMF	Levulinic acid	Formic acid	Water-soluble humins	Total water-soluble compounds
1	19.29	7.17	1.58	1.34	3.7	37.3
2	24.54	9.92	2.89	2.25	5.4	50.2
3	24.57	9.93	2.93	2.26	5.5	50.4

[a] Reproduced from ref.[255] by permission of The Royal Society of Chemistry.

A separate study for cellulose decomposition along with recycling of solids was also performed at a lower temperature and longer reaction time (170 °C for 4 h each cycle) for comparison purposes. The results appear in Table A.3 and Figure A.14 in the Appendix. The overall cellulose conversion after 6 cycles at these conditions was only 42%, whereas nearly full cellulose conversion was obtained following 2 cycles at 220 °C and 30 min. Consequently, the carbon yield of usable organics (includes: glucose, fructose, cellobiose,

levoglucosan, HMF, furfural, levulinic acid, and formic acid) after 6 cycles at 170 °C and 4 h was half of that obtained at 220 °C and 30 min. (23% and 45% respectively). The product distribution in the aqueous phase was similar for all cycles at 170 °C and 4 h. Lastly, the selectivity to usable organics decreased with cellulose conversion for both reaction conditions, as shown in Figure A.15 in the Appendix. However, the selectivity to usable organics was higher at 220 °C and 30 min. when compared at a constant cellulose conversion.

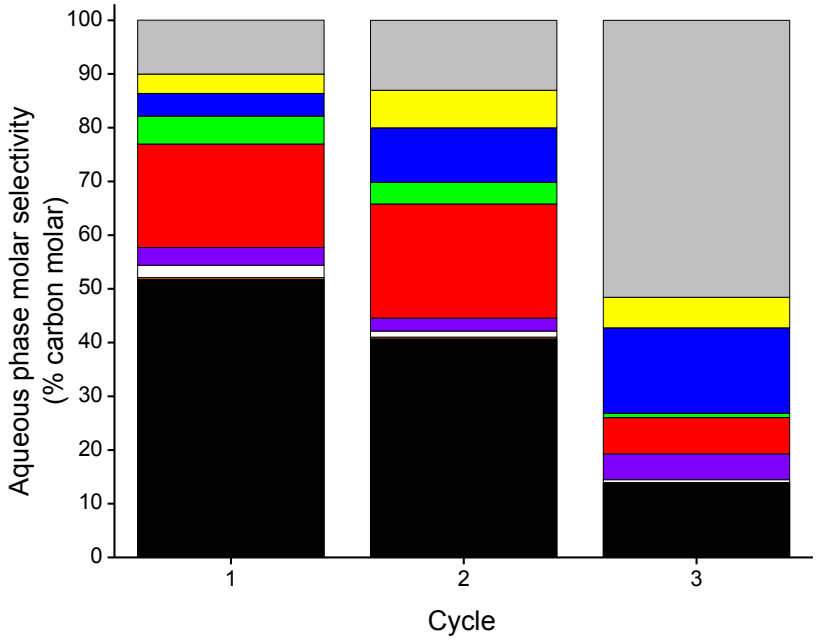

Figure 50. Water-soluble organic carbon product selectivity for each recycle run from non-catalyzed hydrothermal decomposition of cellulose in a stirred batch reactor at 220 °C. Initial solids loading for each cycle was 29 wt%. Each cycle reaction time was 30 min. ■ glucose; ■ fructose; □ cellobiose; ■ levoglucosan; ■ HMF; ■ furfural; ■ levulinic acid; ■ formic acid; ■ humins. Reproduced from ref.[255] by permission of The Royal Society of Chemistry.

The aqueous phase obtained from the cellulose decomposition step at 220 °C and 30 min. was further reacted with Amberlyst 70 to produce levulinic acid from the water-soluble compounds. Figure 51 shows the carbon yield of the key compounds. Glucose and HMF content decrease with time as they react to produce levulinic acid, formic acid and humins. Levulinic acid carbon yield reached 21% after 8 h at 160 °C. This value is 50% higher than that obtained from cellulose decomposition with ZrP at 220 °C (refer to Figure 44(c)).

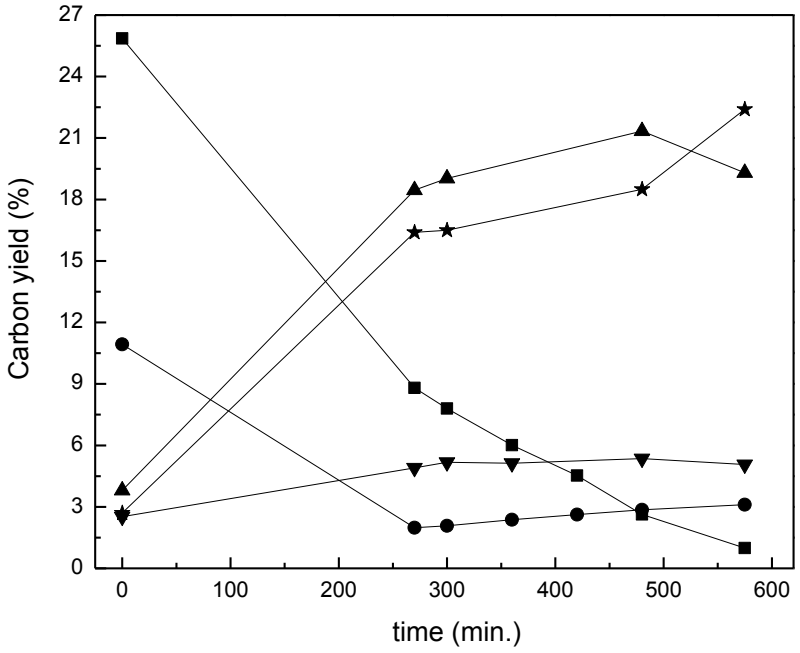

Figure 51. Aqueous phase solid acid-catalyzed conversion of water-soluble organics obtained from hydrothermal decomposition of cellulose with solids recycling at 220 °C. Product yields as a function of reaction time for 160 °C. Catalyst was Amberlyst 70 at a loading of 0.1 M total acid sites (acid sites concentration taken from manufacturer). Products: glucose (■), HMF (●), levulinic acid (▲), formic acid (▼), water-soluble and insoluble humins (★). Reproduced from ref.[255] by permission of The Royal Society of Chemistry.

7.4. Discussion

7.4.1. The effect of water in cellulose hydrothermal decomposition

We have shown in this study that hydrothermal decomposition of cellulose can selectively produce valuable water-soluble compounds at high initial loadings of cellulose and moderate temperatures (190-270 °C). The effect of water on this class of reactions has been studied extensively and has appeared as a central theme of various literature reviews.[18, 283, 284] In addition to solvation effects, water can also behave as a reactant and a catalyst.[283] In part, this phenomenon is due to the distinct properties that water exhibits at elevated temperatures and pressures. For example, the equilibrium constant for the ionization of water ($K_w = [H_3O^+][OH^-] = 1.0 \times 10^{-14}$ at 25 °C) near the critical temperature is about 3 orders of magnitude higher than that for ambient liquid water, which can be advantageous for acid- and base-catalyzed reactions.[283] Vàrhegyi and co-workers studied the effects of water on the reaction mechanism of cellulose thermal decomposition and discovered that cellulose decomposition was enhanced in the presence of water.[265] They derived a kinetic model consisting of two steps for cellulose decomposition in the presence of water applicable for a temperature range of 270-300 °C. According to their model, cellulose is hydrolyzed in the presence of water to produce water-soluble products (intermediates), which can then further decompose to form char, water and gases. Minowa *et al.* proposed a similar model for cellulose decomposition in hot-compressed water under catalyst-free conditions.[278]

An alternative method to decompose cellulose is by pyrolysis where the cellulose is thermally decomposed without water in an oxygen-free environment. Cellulose pyrolysis is governed by three primary reactions depicted by the Broido-Shafizadeh model.[285] An

"initiation" reaction first leads to form "active" cellulose from cellulose. This species subsequently decomposes by way of two parallel routes to form anhydrosugars[286] alongside char, gases and water. Cho *et al.* have measured the kinetic and thermodynamic parameters for this proposed model valid for the temperature range of 240-750 °C.[287] To demonstrate the catalytic effect of water on cellulose decomposition, we compared between the rate constant reported by Cho *et al.* for cellulose pyrolysis and that of Vàrhegyi *et al.* for cellulose decomposition in the presence of water, both at a reaction temperature of 280 °C. Based on these references we can calculate that the rate constant for cellulose decomposition at 280 °C in the presence of water (0.0304 L g^{-1} $min.^{-1}$) is nearly fivefold the rate constant obtained for cellulose pyrolysis at the same temperature without the presence of water (0.0063 $min.^{-1}$). The former consists of a second order reaction with dependence on the amount of water present expressed in units of [g L^{-1}]. This finding agrees with our results for cellulose hydrothermal decomposition. In our studies the cellulose decomposed almost entirely within a time frame of hours, whereas according to the data from Cho *et al.*,[287] cellulose pyrolyzed within days in this same temperature range. This provides clear evidence that the rate of cellulose decomposition is enhanced by the presence of water.

7.4.2. Conceptual design for levulinic acid production from cellulose

A conceptual process for the production of levulinic acid from cellulose is proposed and analyzed based on the experiments carried out in this study. The process flow diagram appears in Figure 52. The material balance for the process is given in Table 19. The data for Streams 1 to 13 were based on experimental results in this study. A water balance was

carried out for the process by performing an oxygen balance around each reactor. For this purpose it was assumed that no gasification occurred during the reaction due to the relatively low temperature of Reactor 1.[278] The oxygen content of the water-soluble and insoluble humins was taken from previous studies.[288, 289]

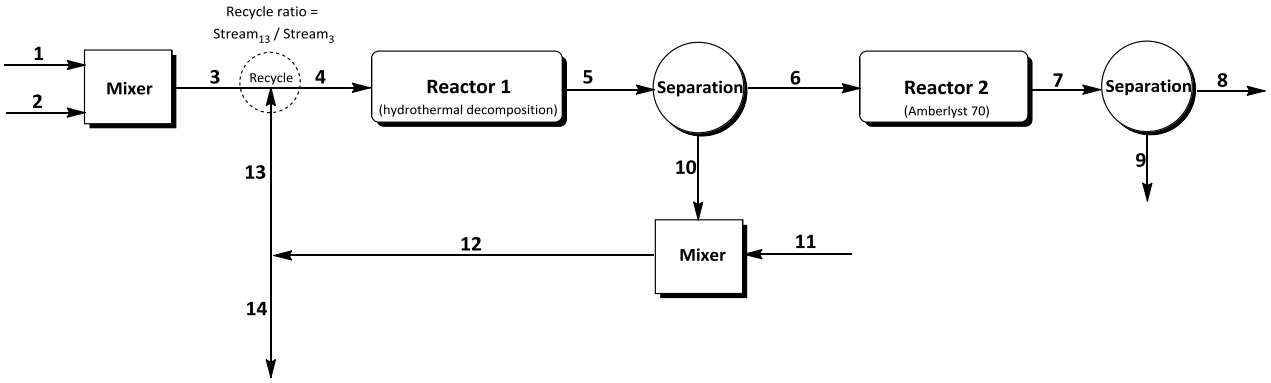

Figure 52. Process flow diagram for the production of levulinic acid from cellulose by way of hydrothermal decomposition in Reactor 1 followed by aqueous phase solid acid catalyzed dehydration in Reactor 2, along with recycling of solids. Reproduced from ref.[255] by permission of The Royal Society of Chemistry.

In this process, water (Stream 1) and fresh cellulose (Stream 2) are mixed to form a slurry solution (Stream 3) containing 29 wt% solids. This stream is then mixed with the recycle stream (Stream 13) to make up Stream 4. The recycle stream consists of a slurry solution containing water, unreacted cellulose and water-insoluble humins, making a combined total of 29 wt% solids. The recycle ratio was defined as the ratio of the recycle stream (Stream 13) to the stream of fresh feedstock (Stream 3). The value was set to 0.56 based on experimental results. The combined slurry solution (Stream 4) is then fed to Reactor 1 where the cellulose is hydrothermally decomposed in the absence of a catalyst. Afterwards, the product stream (Stream 5) is separated to an aqueous stream (Stream 6) and

solids stream (Stream 10) made up of unreacted cellulose and water-insoluble humins. The solids are mixed with water (Stream 11) to form a slurry solution containing 29 wt% solids. The solids are not prewashed with acetone to remove acetone-soluble humins as depicted in the experimental section, seeing that separate studies have shown that this is not a particularly necessary step in the recycle process. A portion of this stream is purged (Stream 14) to prevent accumulation of humins in the system and the remainder serves as the recycle stream (Stream 13). The concentration of cellulose and humins in Streams 12, 13 and 14 are identical. Concurrently, the aqueous stream (Stream 6) is fed to Reactor 2 where the water-soluble compounds are converted to levulinic acid and formic acid with a solid acid catalyst (Amberlyst 70). Water-soluble and insoluble humins are also formed. The product stream (Stream 7) is separated to an aqueous stream containing primarily levulinic acid and formic acid (Stream 8) and a stream made up of water-insoluble humins (Stream 9).

Table 19. Representative mass flow rates (kg h^{-1}) for levulinic acid production from cellulose by hydrothermal decomposition at 220 °C for 30 min. followed by acid catalyzed conversion of the aqueous phase with Amberlyst 70 (0.1 M total acid sites) at 160 °C for 8 h, together with recycling of solids. Concentration of solids in slurry streams was 29 wt%. Results for Streams 1 to 13 were obtained based on experimental results.[b]

				Water-soluble organics							
Stream	Water	Fresh cellulose	Cellulose for recycle/purge [a]	glucose	HMF	LA	FA	soluble humins	Total	Water-insoluble humins	Sum
1	250	–	–	–	–	–	–	–	–	–	250
2	–	100	–	–	–	–	–	–	–	–	100
3	250	100	–	–	–	–	–	–	–	–	350
4	389	100	41	–	–	–	–	–	–	15	545
5	394	–	68	34	9	2	4	5	58	25	545
6	394	–	–	34	9	2	4	5	58	–	452
7	400	–	–	3	2	20	10	1	37	14	452
8	400	–	–	3	2	20	10	1	37	–	437
9	–	–	–	–	–	–	–	–	–	14	14
10	–	–	68	–	–	–	–	–	–	25	93
11	232	–	–	–	–	–	–	–	–	–	232
12	232	–	68	–	–	–	–	–	–	25	325
13	139	–	41	–	–	–	–	–	–	15	195
14	93	–	27	–	–	–	–	–	–	10	130

[a] Recycle ratio = Stream $_{13}$ / Stream $_{3}$ = 0.56 . All values were rounded to the nearest unit. LA = levulinic acid; FA = formic acid.

[b] Reproduced from ref.[255] by permission of The Royal Society of Chemistry.

The maximum attainable carbon yield of water-soluble organics produced from hydrothermal decomposition of cellulose (Reactor 1) is 50%. Only 5% of this water-soluble organics is attributed to soluble humins (Table 17). The glucose and HMF content in the aqueous stream exiting Reactor 1 corresponds to 25% and 10% carbon yield respectively. Further conversion of this aqueous stream in Reactor 2 with Amberlyst 70 produces a reasonably pure aqueous stream of levulinic acid and formic acid at 21% and 5% carbon yield respectively. Therefore, according to the selected reaction conditions, approximately 50% of the organic carbon entering Reactor 2 converts to levulinic acid and formic acid.

7.4.3. Comparisons with other existing processes

Vast interest in levulinic acid applications has led to the realization of a number of viable processes for its production from cellulose and cellulosic biomass. An input-output analysis can be used to compare different processes and make some decisions about the economic *via*bility of different process options. This type of analysis is the first step in the conceptual process design of a process.[290, 291] An input-output analysis compares the total material going into a process with the total material leaving a process. Figure 53 compares the input-output analysis of four different processes for levulinic acid production from cellulose all based on 100 kg cellulose feedstock. All undesired decomposition products were referred to as humins.

The Biofine process (refer to Figure 19 in Chapter 5) depicted in Figure 53(a) has been under development since 1988 and involves the use of sulfuric acid in a two-step continuous process to produce levulinic acid, formic acid and furfural from lignocellulosic biomass.[163, 164, 292] This process claims to produce levulinic acid at yields higher than 70% of the theoretical based on the hexose content of the cellulosic feedstock. According to their reference,[164] the cellulose content in the feedstock is less than 5 wt% of the total and the sulfuric acid concentration ranges from 1.15 to 5 wt% of the aqueous portion. One of the major disadvantages of using a water-soluble acid catalyst for this process is the post-reaction separation and purification of levulinic acid from the acidic aqueous stream. Simple neutralization with a base is not possible due to the acid functionality of levulinic acid. Consequently, levulinic acid must be initially separated from the aqueous stream for further purification. Two feasible options include extraction of levulinic acid with an organic

solvent or evaporation of the final product. By extracting the levulinic acid, the aqueous stream containing the homogeneous acid catalyst can then be neutralized or recycled for further reuse. This requires energy intensive purification steps in stripping columns to purify the acidic aqueous stream from the organic solvent.[293] Further purification steps must also be carried out to separate the levulinic acid from the extracting organic solvent. Recycle of the organic solvent also requires additional purification steps.

In the Biofine process, the levulinic acid is separated from the water and sulfuric acid by evaporation.[293] However, this is an energy intensive route consisting of a two-stage evaporation process. Levulinic acid has a higher boiling point than water (245 °C *vs.* 100 °C); therefore water must first be evaporated from the reaction products, followed by evaporation of levulinic acid from the sulfuric acid. Assuming that process heat is supplied by saturated steam at 250 PSIG, the energy cost associated with water evaporation is 1.28 kg steam per kg water. Evaporating levulinic acid requires 0.24 kg steam per kg levulinic acid produced.[294] Based on the data provided in Figure 53(a), the concentration of levulinic acid exiting the second reactor is approximately 1 wt%, and water makes up 95 wt% of the stream. Accordingly, the total amount of steam required for the dual evaporation step is 130 kg steam per kg of total levulinic acid produced. If higher concentrations of levulinic acid are produced, then this will decrease the steam requirements.

An input-output analysis was also carried out based on the optimal reaction conditions reported by Shen and Wyman[174] to produce levulinic acid production from cellulose with hydrochloric acid as the catalyst, as shown in Figure 53(b). They report a maximum yield of 60% levulinic acid of the theoretical from cellulose with a cellulose content of 1.5 wt% and

acid concentration of 3.2 wt% of the aqueous portion. These values fall in the range reported in the Biofine process. According to their process scheme, the amount of acid catalyst required for the reaction is more than two fold the amount of cellulose on a weight basis. For the sake of comparison, stoichiometric amounts of sodium hydroxide were added to account for neutralization of the hydrochloric acid. On a weight basis, this amount of base is even higher than the amount of acid used for the reaction. The neutralization waste consists of water and sodium chloride. Moreover, without a prior purification step, the levulinic acid and formic acid will also react with the base to form their corresponding salts[295], thus making downstream applications more complex. Disposal of the sodium chloride produced from this step is another drawback that must be accounted for.

Alonso *et al.* have developed a novel route to recycle the aqueous stream containing sulfuric acid after levulinic acid is produced from cellulose. They show that alkylphenol solvents can be used to selectively extract levulinic acid from aqueous solutions of sulfuric acid.[296] The acidic aqueous stream can then be recycled for further cycles of cellulose decomposition with no observed loss of sulfuric acid to the organic phase. Following the extraction step, the levulinic acid in the organic phase is further hydrogenated to produce GVL. Additionally, they have shown that the cellulose decomposition step is facilitated by adding the cellulose to the reactor in progressive stages.[297] As mentioned in their study, this technique ensures a continuous low concentration of glucose in the reactor, thereby minimizing undesirable humins formation. They did however observe a slight decrease in the levulinic acid yield with each recurring cycle of cellulose addition. They also discovered that the levulinic acid partition coefficient was compromised as the amount of GVL in the

organic phase increased. For a cellulose content of 7.7 wt% (for each cellulose deconstruction cycle) with 0.5 M sulfuric acid, they obtained a cumulative levulinic acid yield of 55% of the theoretical after three consecutive cellulose decomposition cycles (Figure 53(c)). It is notable to mention that these results were obtained without recycle of the aqueous stream. Lower yields of levulinic acid were attained with successive recycling of the aqueous stream. The organic solvent used to extract the levulinic acid was 2-*sec*-butylphenol at a ratio of 1:1 wt/wt aqueous solution and organic solvent. Even though promising results have been obtained with this class of organic solvents, vast research has been published on the toxicity of alkylphenolic compounds and their adverse effect on the environment.[298, 299]

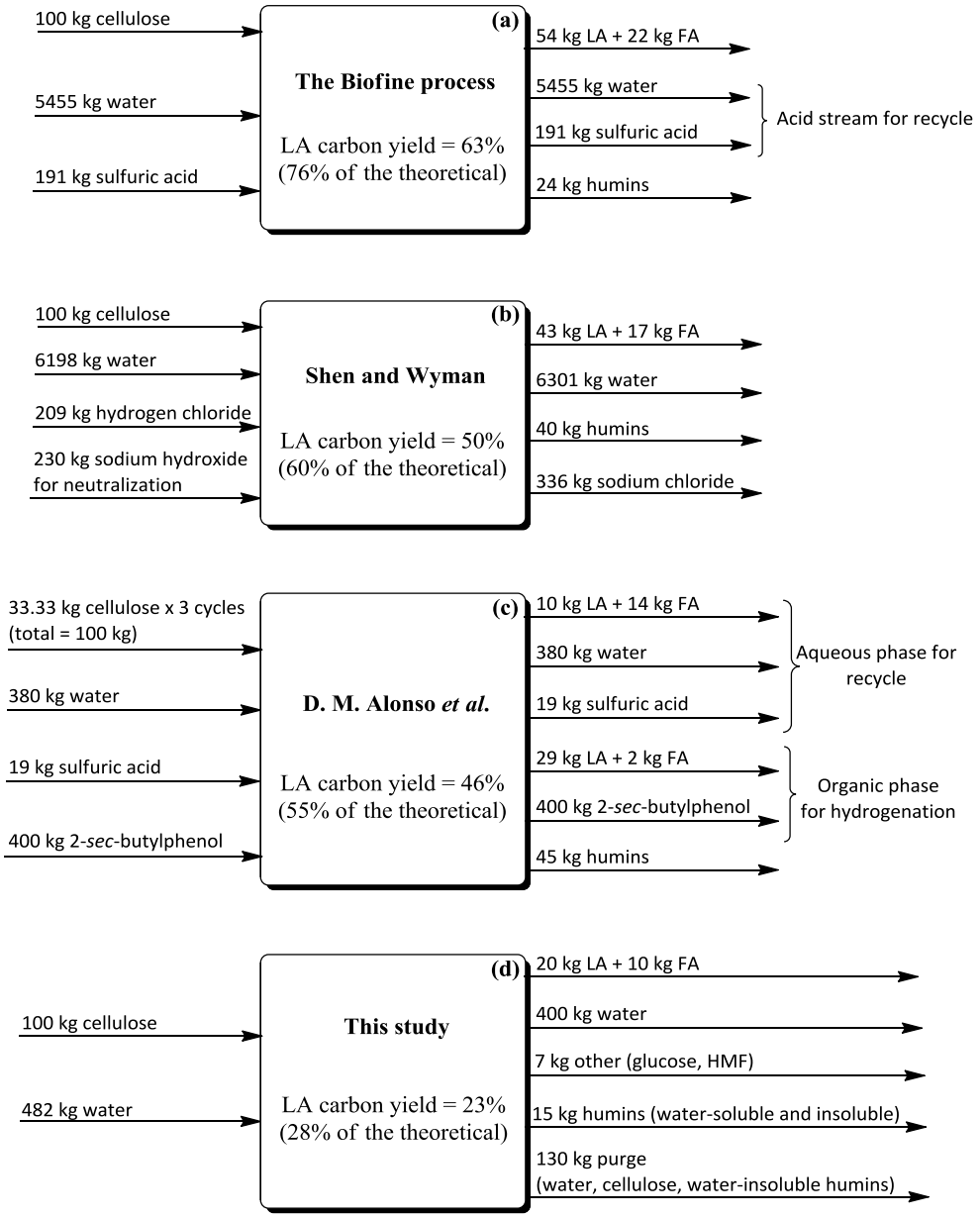

Figure 53. Input-output analysis of levulinic acid production from cellulose for **(a)** the Biofine process[164] (in accordance with Example 1from reference); **(b)** Study by Shen and Wyman[174]; **(c)** process developed by Alonso *et al.*[296] (in accordance with data taken from their supporting information: Table S2, Entry 1); **(d)** this study. LA ≡ levulinic acid; FA ≡ formic acid. Reproduced from ref.[255] by permission of The Royal Society of Chemistry.

The process introduced in this study consists of a two step procedure to produce levulinic acid from cellulose at relatively high initial loadings of 29 wt%, as shown in Figure 53(d). A recycle loop is utilized to treat unreacted feedstock, thereby maximizing the conversion of cellulose while maintaining a high selectivity of water-soluble compounds in the aqueous stream. The non-catalytic route for cellulose decomposition (step 1) facilitates this recycle procedure since there is a recurrent need to regenerate the solid acid catalyst following cellulose decomposition due to the deposition of humins on the catalyst. Regeneration of the solid acid catalyst *via* thermal oxidation is the most widely used technique,[300] but would require the difficult task of separating the catalyst from the unreacted cellulose.[270]

The key advantage of our approach is that it does not use a homogeneous acid catalyst. This greatly simplifies the downstream separation and purification of levulinic acid. It has been shown for furfural production from hemicellulose solutions that the mineral acid accounts for 28% of the total raw materials cost.[161] Additional costs associated with the use of homogeneous acid catalysts include acid recovery, treatment (neutralization) and disposal. The corrosive nature of the acid also calls for more expensive materials in construction of the reactors and piping. Our process also produces a relatively high purity of the final aqueous stream which consists primarily of levulinic acid and formic acid. Consequently, downstream purification steps would require less energy. These factors also simplify downstream processing of converting the levulinic acid into other products, such as GVL,[56] which is a platform chemical for the production of liquid fuels.[58, 59] Additionally, the levulinic acid solution we produce could also be neutralized with a base to form levulinic

acid and formic acid salt mixtures, which in turn can be pyrolized to produce liquid hydrocarbon fuels.[301]

The process proposed by Alonso *et al.* to produce levulinic acid from cellulose is attractive due to the relatively high attainable yield of levulinic acid and the recyclability of the acid stream. However, the use of organic solvents to extract the final product inevitably makes the downstream processing more complex due to extra unit operations. This is not to mention the loss of yield that transpires with every additional post-reaction step in the process due to inefficiencies.[293] The maximum yield of levulinic acid obtained with our process is 28% of the theoretical, demonstrating that the yield in our process must be increased if it is to be competitive with the other processes. However, due to the high cellulose loading in this process, the concentration of levulinic acid in the final aqueous stream is relatively high at 4.5 wt%. This facilitates recovery and purification of the final product downstream.

CHAPTER 8

Conclusions and Future work (II)

8.1. Conclusions

In Chapter 5 we discussed a kinetic model for aqueous-phase glucose dehydration to produce HMF and levulinic acid. Our model involves 4 reactions. Glucose first undergoes a dehydration reaction in which 3 molecules of water are removed to produce HMF (Reaction 1). In a parallel step glucose can undergo reversion and decomposition reactions to form humins, which are highly polymerized insoluble carbonaceous species (Reaction 2). The dehydration step to form HMF (Reaction 1) is favored at increased temperatures due to its higher activation energy compared to the degradation step to form humins from glucose (Reaction 2). Once HMF is formed, it can also undergo parallel reactions. In the presence of water, a rehydration reaction takes place with 2 molecules of water to produce levulinic acid and formic acid (Reaction 3). Likewise, HMF can also decompose to form humic species (Reaction 4). Relatively lower temperatures are favorable to maximize levulinic acid production, as these conditions minimize the formation of humins due to the relatively higher activation energy associated with Reaction 4 compared with the rehydration reaction to produce levulinic acid (Reaction 3).

The proposed kinetic model is consistent with the experimental data for batch reactions within the conditions of this study. In general, higher temperatures (*i.e.* 180-200 °C) and short reaction times of less than 1 min. are essential to maximize the HMF content. On the other hand, low temperatures between 140-160 °C and long residence times of greater than 100 min. are essential for maximum levulinic acid yield.

A PFR type reactor is favorable for the aqueous-phase production of HMF and levulinic acid from glucose, as compared with a CSTR. Higher HMF yields can be obtained in a PFR at relatively shorter residence times. Likewise, compared to a PFR, a CSTR requires longer residence to attain comparable levulinic acid yields. We have shown that a

system of two consecutive PFRs has a higher performance than a PFR/CSTR combination. Compared to a single PFR, for aqueous-phase levulinic acid production from glucose there is no distinct advantage to implement a system of two consecutive reactors.

We also prepared and characterized a series of metal(IV) phosphate catalysts and tested them for aqueous phase dehydration of glucose to levulinic acid. Adsorption studies with ammonia and isopropylamine as probe molecules reveal a higher overall concentration of acid sites for the zirconium phosphates compared to the tin phosphate catalysts. Sample ZrP2 shows the highest amount of total acid sites, as well as the highest concentration of Brønsted sites among all of the catalysts tested. XPS analysis corroborates these findings by revealing a high concentration of surface hydroxyl groups for the zirconium phosphate catalysts, specifically ZrP2. Four phosphorus coordination states have been identified by solid-state ^{31}P MAS NMR spectroscopy, among which the polyphosphate species has the highest relative amount. The other species include tetrahedral phosphates bonded to one zirconia group and two hydroxyl groups, tetrahedral phosphates bonded to two zirconia and one hydroxyl group and tetrahedral phosphates bonded to three zirconia groups. The higher amounts of polyphosphate species detected in ZrP2 and ZrP3 could be a reason for their enhanced acidity compared to ZrP1.

We have demonstrated here that both heterogeneous and homogeneous Lewis and Brønsted sites share different functions as related to the proposed reaction scheme for glucose dehydration. The catalytic activity and selectivity for all of the metal(IV) phosphates tested in this study vary according to the Brønsted to Lewis ratio. Catalysts with high Lewis acidity, such as the tin phosphates, show the highest activity on a per site basis, whereas the zirconium phosphates with relatively high Brønsted acidity (*i.e.* ZrP2 and ZrP3) demonstrate the lowest

activity. Fructose selectivity increases with an increase in the Lewis acid concentration of the catalyst. This is due to induced isomerization reaction catalyzed by Lewis acid sites. Both types of acid sites catalyze the dehydration reaction to produce HMF from glucose. However, the HMF selectivity increases with increased concentration of Brønsted acid sites, particularly at lower glucose conversions for the heterogeneous catalysts. The levulinic acid selectivity is also a function of the relative concentration of Brønsted to Lewis sites. The levulinic acid selectivity increases with an increase in the Brønsted to Lewis ratio for both the heterogeneous and homogeneous acid catalysts. The formation of humic species increases with increased Lewis acidity for the heterogeneous catalysts.

Increase in the P/metal(IV) molar ratio from 1 to 2 in the precursor solution results in a higher surface area, as well as increased overall concentration of acid sites and Brønsted acid sites. However, for the tin phosphates, the fraction of Brønsted sites remains the same for both catalysts in the series (SnP1 and SnP2). Consequently, both catalysts show nearly identical selectivities for the major reaction products. For the zirconium phosphates, a further increase in phosphorus loading to a P/Zr molar ratio of 3 does not alter the bulk phase of the catalyst, rather only the surface properties.

Among the zirconium phosphate catalysts, the catalyst with a P/Zr ratio of 2 (ZrP2) exhibits the highest surface area, as well as the highest amount of total acid sites and fraction of Brønsted sites. This catalyst in turn exhibits the highest selectivity to HMF and levulinic acid. A relatively high concentration of surface hydroxyl groups is most likely the source of the relatively high amounts of Brønsted acid sites, as well as the high surface area.

We also investigated the concept of a two-step process to produce levulinic acid from

cellulose without the use of a homogeneous acid catalyst. The process consists of: (1) non-catalytic hydrothermal decomposition of cellulose at moderate temperatures (190-270 °C) to produce organic water-soluble compounds including glucose and HMF; (2) water-soluble compounds are further reacted with a solid acid catalyst at relatively low temperatures (160 °C) to produce levulinic acid and formic acid. Unreacted cellulose can be recycled back to the first reactor for further decomposition.

Hydrothermal decomposition of cellulose has been compared with and without a solid acid catalyst (ZrP). A higher rate of cellulose decomposition was obtained with ZrP. This was indicated by the higher yield of water-soluble organics in the aqueous phase. However, the solid acid catalyst also induced the formation of solid humins, defined by a sharper decrease in the total organic content in the aqueous phase. The product distribution of the water-soluble organics was comparable for cases with and without a solid acid catalyst. Recycling of the unreacted cellulose is facilitated by not using a solid acid catalyst during the cellulose decomposition step due to deactivation of the solid catalyst. Moreover, we have shown that cellulose can decompose hydrothermally at high initial loadings without jeopardizing the selectivity of the water-soluble compounds. Relatively higher temperatures and shorter residence times (220 °C and 30 min.) are more favorable for the production of usable water-soluble organics from cellulose compared to lower temperatures and longer residence times (170 °C and 4 h).

Amberlyst 70 is a rather promising solid acid catalyst for the conversion of glucose to produce HMF and levulinic acid due to its inherent Brønsted acidity. The ion exchange resin showed comparable activity to HCl, however the selectivity to HMF and levulinic acid were

lower compared to the homogeneous acid catalyst. The recycled ion resin catalyst showed a decrease in the selectivity to levulinic acid due to deposition of solid humins. Regeneration did not fully recover the activity and selectivity. This is most probably due to insufficient removal of the fouling during the regeneration procedure. ZrP showed a predominantly higher HMF selectivity and a lower levulinic acid selectivity compared to Amberlyst 70. This could be due to the presence of Lewis acid sites on ZrP.

We have reported a conceptual design of this process and have compared it to existing processes for the production of levulinic acid from cellulose. The experimentally obtained yield of levulinic acid in this process is 28% of the theoretical with an initial cellulose loading of 29 wt%. This high loading results in a final aqueous stream with a relatively high concentration of levulinic acid, which is favorable for downstream applications. There are clear ecological and economical advantages to this process by avoiding the use of corrosive soluble acid catalysts and toxic organic solvents.

8.2. Future work

In our kinetic model (Chapter 5) we observed some inconsistency between the experimental data and the theoretical model in the continuous regime. This could be due to a number of factors, such as non-ideal mixing patterns in the reactors. From an operational point of view, challenges arise due to the formation of solid humic species in the reactors. This is predominantly encountered in the PFR, which ultimately results in high pressure drops across the reactor and reduction of the reactor volume. Therefore, only experiments at relatively low temperatures and short residence times were feasible in the PFR. Conversely, the formation of solid humins has a negligible effect on the operational aspect of the CSTR and consequently

harsher reaction conditions could be employed. Further studies to minimize the occurrence of solid humins would in turn improve the operational aspect of the continuous reactors and improve the kinetic model fit.

The bottleneck of this tandem reaction scheme is the dehydration step to produce HMF from glucose. One key question that arises from this study is: Would it be more favorable to decouple the dehydration and rehydration reactions to improve the selectivity of levulinic acid from glucose? This concept would be beneficial pending the development of efficient technologies to produce HMF from carbohydrates. Dumesic and co-workers have carried out vast studies on this topic, including the use of biphasic systems to extract HMF from the aqueous phase.[29, 31] As we have shown in Chapter 2, biphasic systems are promising technologies to isolate furanic derivatives. However, in order to carry out the rehydration reaction, HMF would need to be separated from the extracting solvent and react with water to produce levulinic acid. This separation step could be a limiting factor in the process downstream and should be accounted for in future research.

There are still many open questions pertaining to zirconium phosphates and their use as solid acid catalysts for aqueous phase biomass conversion. Zirconium phosphate is comprised of four phosphate species in the bulk phase, as detected with NMR spectroscopy. The samples with the highest concentration of Brønsted acid sites (ZrP2 and ZrP3) are predominantly comprised of polyphosphate species. These results are counter intuitive given that the formation of polyphosphates species is attributed with deprotonation by condensation of (mono) phosphate species. Nevertheless, there are reports in the literature that polyphosphate species can actually enhance the Brønsted acidity on the catalyst surface.[247, 248]

This raises a key question as to what is the active acid site (phosphate species) that converts glucose to levulinic acid. Further studies to investigate the role of the polyphosphate species on the reaction chemistry are necessary to elucidate the nature of the active site/s for these catalysts. Likewise, the length of the polyphosphate chain could also play a key role in determining the concentration of the acid sites. It has been reported in the literature that the length of the polyphosphate chain is a function of the metal oxide to phosphate ratio, and an increase in the polyphosphate chain length is observed with increased amounts of P_2O_5.[262] Therefore, determining the composition and chain length of the polyphosphate species should also be a focus of future work.

One key finding that we reported in Chapter 7 is that the rate of cellulose decomposition is enhanced by the presence of water. Previous studies have shown that the first stage of cellulose decomposition is a hydrolysis step to form water-soluble compounds.[265, 278] This however is a limiting step and suffers from poor selectivity due to side reactions that produce humins. Water has unique attributes because it not only serves as a solvent, but is also a reactant and an acid catalyst under hydrothermal conditions. This raises a key question: What are the intrinsic effects of water on cellulose decomposition chemistry? Understanding this elementary question should be a focus of future studies in this field.

SECTION III: STUDIES IN POLAR APROTIC SOLVENTS

CHAPTER 9

Selective Conversion of Cellulose to Hydroxymethylfurfural in Polar Aprotic Solvents

9.1. Background

This chapter discusses the production of HMF from cellulose in polar aprotic solvents without the presence of water. HMF is an alternative nonpetroleum precursor which can be used as a building block chemical for the production of various high-volume organic chemicals with numerous potential industrial applications.

HMF is produced conventionally from glucose (in low yields) or fructose (in high yields) by a triple dehydration step with mineral acids in water.[174] It would be highly desirable to be able to produce HMF from cellulose, which is a more abundant and lower value feedstock than fructose. However, in aqueous systems, HMF is only produced in low yields (between 8 to 21%) from cellulose because of miscibility limitations and undesired formation of humins.[302, 303] As discussed in Chapters 5-7, HMF production in aqueous systems is maximized at relatively high temperatures (200-300 °C) and short reaction times (order of seconds or minutes), and is readily converted to formic acid and levulinic acid.

The use of ionic liquids (ILs) as solvents for HMF production has been proposed due to the solvation capabilities of the ILs. A HMF yield of 51% from fructose was obtained by Li *et al.* when a high concentration of feed (67 wt%) was used in 1-butyl-3-methylimidazolium chloride ([C4mim]Cl).[304] Binder and Raines demonstrated that lignocellulosic biomass can be converted to HMF using *N*,*N*-dimethylacetamide (DMA) containing lithium chloride (LiCl) as a solvent.[305] HMF yields of up to 54% were obtained with 1-ethyl-3-methylimidazolium chloride ([EMIM]Cl) as an additive and a mixture of $CrCl_2$/HCl as the catalyst. Rinaldi *et al.* showed that solid acid catalysts can be used in 1-butyl-3-methylimidazolium chloride ([BMIM]Cl) to selectively depolymerize cellulose to produce glucose and HMF.[277] Zhang and co-workers have

reported HMF yields of 55% from cellulose with a mixture of $CuCl_2$ and $CrCl_2$ dissolved in [EMIM]Cl at relatively low temperatures.[306, 307] A comprehensive review covering the process chemistry of HMF production from various feedstocks is given by van Putten *et al.*[308]

Significant challenges hinder the industrial use of ILs for production of HMF. Due to their high costs, quantitative recovery and reuse of ILs (at least 98%) is necessary to make the process economically attractive.[309] Relative low cellulose solubility (10-15 wt%) in ILs,[310] high viscosity and high toxicity of ILs are also impeding factors.[311, 312] Thermal and chemical stability of ILs are also in question, as new compounds have been detected derived from side reactions between HMF and imidazolium-based ILs.[313] Extensive work has been reported by Jérôme and co-workers to produce HMF from biomass derived feedstock in alternative solvent systems that are comparable with imidazolium-based ILs.[314, 315] Alternative approaches have also been investigated using biphasic reaction systems with organic solvents that can extract the HMF from the aqueous phase before it undergoes further degradation reactions.[29, 31] Phase modifiers (*i.e.* NaCl) can be added to the aqueous phase to help enhance HMF partitioning into the immiscible organic phase and consequently impede further HMF degradation.[33]

9.2. Experimental

9.2.1. Reaction studies

Batch reactions were carried out in a 100 mL reactor vessel provided by Parr Instrument Company, series 4560. The feedstock solutions were prepared with tetrahydrofuran (THF, Sigma Aldrich, anhydrous, 99.9%, inhibitor free) at the specified concentrations. Microcrystalline cellulose (Avicel® PH-101) with a particle size of approximately 50 μm was

provided by Sigma Aldrich and used as received. Sulfuric acid (A300-500) and glucose were provided by Fisher Scientific. Levoglucosan (99%) and HMF (99%) were provided by Sigma Aldrich. Throughout all of the experiments, the reaction volume was kept constant at 60 mL. Temperatures in the reactor were measured by means of a thermocouple in contact with the solution. Time zero in the reaction was defined as the time when the reactor reached the desired temperature. All reaction solutions were mixed at a maximum constant rate of 600 rpm using an internal stirrer. The temperature and stirring were controlled by a 4848 Controller provided by Parr. The reaction vessel was initially purged with UHP helium (Airgas) five times at room temperature to remove any air from the vessel. The vessel was then heated to the desired reaction temperature and then pressurized to a final pressure of 1000 psig. Samples were taken periodically through a sampling port. The reactor was repressurized with helium after each sampling. Sample *via*ls were cooled beforehand in dry ice to suppress evaporation of the solvent during sampling. The samples were immediately quenched in an ice water bath and filtered with a 0.2 μm syringe filter (IC Millex®-LG, part no. SLLGC13NL). Samples were diluted with water prior to analysis. The dip tube was covered with a stainless steel woven wire cloth, mesh size 400x400 provided by Grainger. This was done to prevent clogging and loss of feed during sampling.

9.2.2. Analysis

Reaction product samples were analyzed by high pressure liquid chromatography (HPLC) with a Shimadzu© LC-20AD. Carbohydrates were detected with a RI detector (RID-10A). Formic acid, levulinic acid, furfural and HMF were detected with a UV-Vis detector

(SPD-M20A) at wavelengths of 207, 207, 240 and 310 nm respectively. The column used was a Biorad© Aminex HPX-87H sugar column. The mobile phase was 0.005 M H_2SO_4 flowing at a rate of 0.6 mL/min. The column oven was set to 30 °C.

9.2.3. Nomenclature

$$Total\ carbon\ yield\ (\%) = 100 \times \frac{total\ moles\ of\ carbon\ from\ all\ detectable\ products^{*}}{initial\ moles\ of\ carbon\ in\ feed}$$

$* \ Detectable\ products: glucose, levoglucosan, formic\ acid, levulinic\ acid, HMF\ and\ furfural$

$$[Relative\ carbon\ selectivity]_i\ (\%) = 100 \times \frac{moles\ of\ carbon\ of\ product\ i}{total\ moles\ of\ carbon\ from\ all\ detectable\ products}$$

$$[Carbon\ yield]_i\ (\%) = 100 \times \frac{moles\ of\ carbon\ of\ product\ i}{initial\ moles\ of\ carbon\ in\ feed}$$

$$Turnover\ frequency\ (hr^{-1}) = \frac{d(moles\ of\ carbon\ produced)}{dt} \times \frac{1}{moles\ of\ protons}$$

9.3. Results

Scheme 5 shows our proposed reaction pathway to produce HMF from cellulose in polar aprotic solvents. Cellulose initially undergoes reaction to produce levoglucosan under dilute acidic conditions at temperatures in the range of 140-190^{o}C. It has been reported that levoglucosan can be produced from cellulose in the organic solvent sulfolane (36% yield after 2 minutes at 330 °C), but relatively higher temperatures (200-330 °C) were required to carry out the reaction and a catalyst was not used.[316] The same authors showed relatively high yields of levoglucosenone (38%) and furfural (20%) under acidic conditions.[317] Our experiments show that acid is necessary to produce levoglucosan as confirmed by blank studies (without acid catalyst) with cellulose in THF, which resulted in negligible cellulose conversion (no detectable products) at 170 °C after 6 hours. The levoglucosan then undergoes a double dehydration step to produce HMF. The water produced in this reaction can react with levoglucosan to produce glucose.[318] HMF can also undergo rehydration with water over an acid catalyst to produce levulinic acid and formic acid. Once glucose is formed, it can also undergo dehydration to produce HMF, as well as undergo degradation to produce humic species. Furfural was also detected in carbon yields lower than 7%. It has been reported that furfural is a by-product of levoglucosan[319] and/or glucose[104] decomposition. Separate decomposition studies with HMF in THF and sulfuric acid showed that HMF is relatively stable in the non-aqueous environment with conversions below 8% at 190 °C after 180 minutes. Other studies have also mentioned that THF prevents further degradation of furfural and HMF.[320, 321]

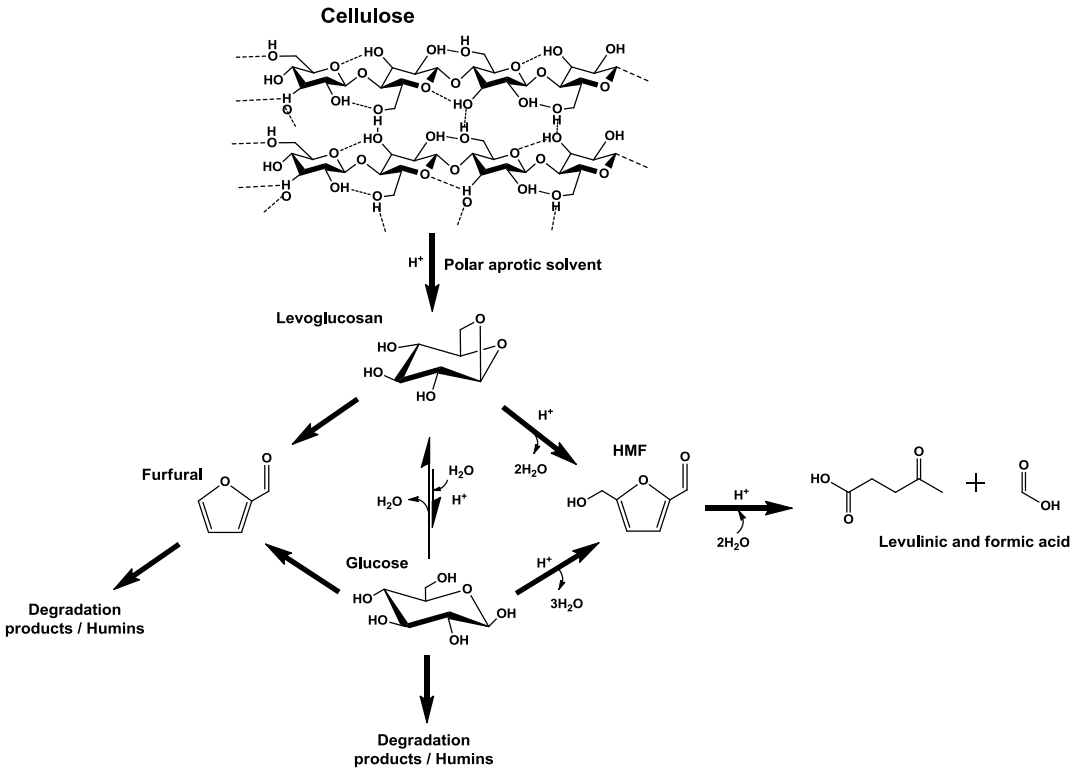

Scheme 5. Proposed reaction scheme for HMF production from cellulose in polar aprotic solvents under acidic conditions.

The polar aprotic solvents including GVL, acetone and THF showed considerable higher yields of HMF from cellulose compared to ethyl acetate, water and ethanol, as shown in Figure 54. The HMF yield increased in the following order: ethanol < water < ethyl acetate << GVL < acetone ~ THF. Reactions in water and ethanol, both protic solvents, resulted in the lowest HMF yields. Despite being a polar aprotic solvent, the yields obtained in ethyl acetate were only somewhat higher compared to the protic solvents. We believe that this behavior is due to the instability of ethyl acetate under the applied reaction conditions where water (from the dehydration reaction) reacts with ethyl acetate to form ethanol and acetic acid. Both of these by-products were detected with HPLC when ethyl acetate was used as a solvent. Acetone has been

shown to be a valuable solvent for HMF production from carbohydrates;[322, 323] however, acetone is not stable under acidic conditions, as it undergoes aldol-type reactions to form dimers and trimers.[322]

Previous work has shown GVL to be a promising solvent for biomass processing.[59, 324, 325] Alonso *et al.* used a monophase system comprised of a solution of 90 wt% GVL and 10 wt% water as the solvent with Amberlyst 70 to selectively produce levulinic acid from cellulose with yields close to 70%.[326] Increasing the amount of water in the solvent decreased the reaction rate. GVL/water solutions were also used to convert the hemicellulose and cellulose fractions of lignocellulosic biomass to furfural and levulinic acid respectively.[104, 327] However, it has also been reported that GVL reacts with water under acidic conditions[328] and also undergoes oxidation to form degradation products in the presence of molecular oxygen.[329] In this respect, we carried out stability studies with GVL and sulfuric acid under inert atmosphere, and we detected traces of levulinic acid and pentenoic acid[330] after 60 minutes at 170 °C. Identical studies with THF resulted in no identifiable degradation products.

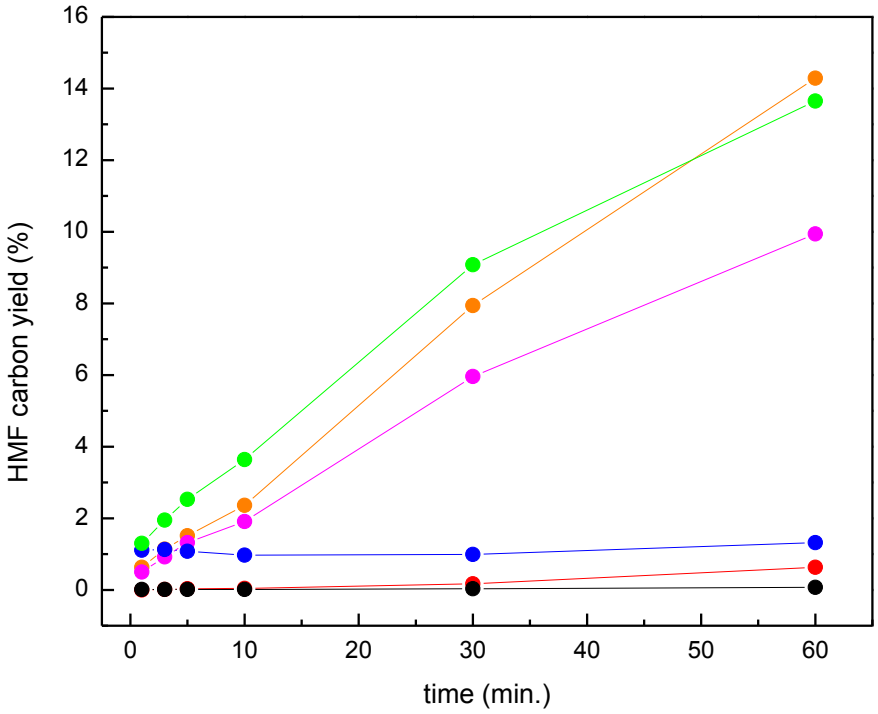

Figure 54. Cellulose decomposition in polar protic and aprotic solvents under acidic conditions. HMF production as a function of reaction time at 170 °C. Cellulose loading was 5 wt% and solvent volume was 60 mL. Catalyst concentration was 5 mM sulfuric acid. Water (●); THF (●); GVL (●); Ethyl acetate (●); Acetone (●); Ethanol (●).

THF was selected as the reaction solvent for more detailed studies. Biphasic mixtures of THF and water have been used in a wide array of biomass conversion processes, including furfural production from hemicellulose, HMF production from glucose and the use of co-solvent systems to produce the aforementioned products from maple wood.[320] Cellulose decomposition with dilute sulfuric acid was carried out in four different solvent systems (pure THF, pure water, a 1:1 THF/water mixture, and a 9:1 THF/water mixture), as shown in Figure 55. The major products detected were levoglucosan, glucose, HMF and levulinic acid. Higher carbon yields of levoglucosan (7% after 60 minutes) were observed in pure THF compared to the other reaction mixtures. Levoglucosan is most likely the primary decomposition product of cellulose in THF.

Stoichiometry requires that water be a reactant for the production of glucose from cellulose.[331] We also identified trace amounts of other anhydrosugars including levoglucosenone, 1,4:3,6-dianhydro-α-D-glucopyranose and 1,6-anhydro-β-D-glucofuranose, which are byproducts of levoglucosan dehydration and isomerization reactions.[317] These byproducts are identical to those detected from gas-phase cellulose pyrolysis.[286] Glucose is also observed when THF is the reaction solvent.

Separate experiments with levoglucosan in THF under acidic conditions confirmed that HMF and levulinic acid can be produced directly from levoglucosan (Figure A.16 in the Appendix). Hu *et al.* also reported that levoglucosan undergoes dehydration to form HMF in the presence of Amberlyst 70 in organic solvents, however it is important to note that their reaction systems were not completely free of water due to the ion resin which was not dried prior to the reaction (*ca.* 57% water content).[319] The HMF yield was higher when glucose was used as a feedstock compared to levoglucosan, but by no more than 3%. Levoglucosan (21% after 30 minutes) was also observed as a product from glucose dehydration when THF was used as a solvent (Figure A.17 in the Appendix). In contrast, only trace levels of levoglucosan were observed when water was used as a solvent for glucose dehydration. Similar high yields of levoglucosan have been observed for glucose dehydration with Amberlyst 15 in the polar aprotic solvent *N*,*N*-dimethylformamide.[332] The rate of glucose conversion in THF was higher than that in water (above 90% conversion after 5 minutes in THF), implying the formation of unknown reaction intermediates when THF was used as a solvent. This shows the significance of the solvent effect on the reaction chemistry.

The carbon yields of HMF and levulinic acid increased as the water content in the solvent decreased (Figure 55(c)). The initial turnover frequencies (TOF) for cellulose conversion and HMF formation per sulfuric acid site were calculated from the data in Figure A.18 (Appendix) and Figure 55 respectively. The TOF for cellulose conversion in THF was more than twenty fold higher than the TOF in pure water and the TOF for HMF formation in THF was more than forty times higher than in water (Figure A.19 in the Appendix). It is notable to mention that a fraction of the cellulose (up to 50%) can also produce insoluble humins in pure water and this was not accounted for in the TOF calculations. This would only alter the results by a factor of two at the most. Nevertheless, it is clear that water has a significant inhibition effect on cellulose decomposition, as well as the dehydration reaction. We believe that the acid sites are less reactive in the presence of water due to solvation of the proton by water molecules. For example, the Gibbs free energy for solvation of a proton changes from –265.9 kcal mol^{-1} in liquid water to –260.2 kcal mol^{-1} in an aprotic solvent such as acetonitrile.[333] Thus, the proton catalyst is stabilized in an aprotic solvent to a less extent than in water (by 5.7 kcal mol^{-1}), leading to higher reactivity of the proton, provided that the solvent has a more moderate effect on the transition state for the acid-catalyzed reaction relative to the reactant. This higher reactivity of the Brønsted acid catalyst in an aprotic solvent allows for the use of low acid concentrations to carry out the reaction, as mentioned in previous studies with GVL.[334] The TOF for cellulose conversion decreases from 190 hr^{-1} to 52 hr^{-1} as the solvent changes from 0% H_2O to 10% H_2O. It has previously been shown that minimizing the water concentration in the reactor leads to a number of advantages[104, 334]: (1) enhanced rate of furfural/HMF production from

monosaccharides; (2) facilitated product recovery; (3) mitigation of degradation reactions, and (4) opportunity to use solid catalysts with improved stability in the reaction media.

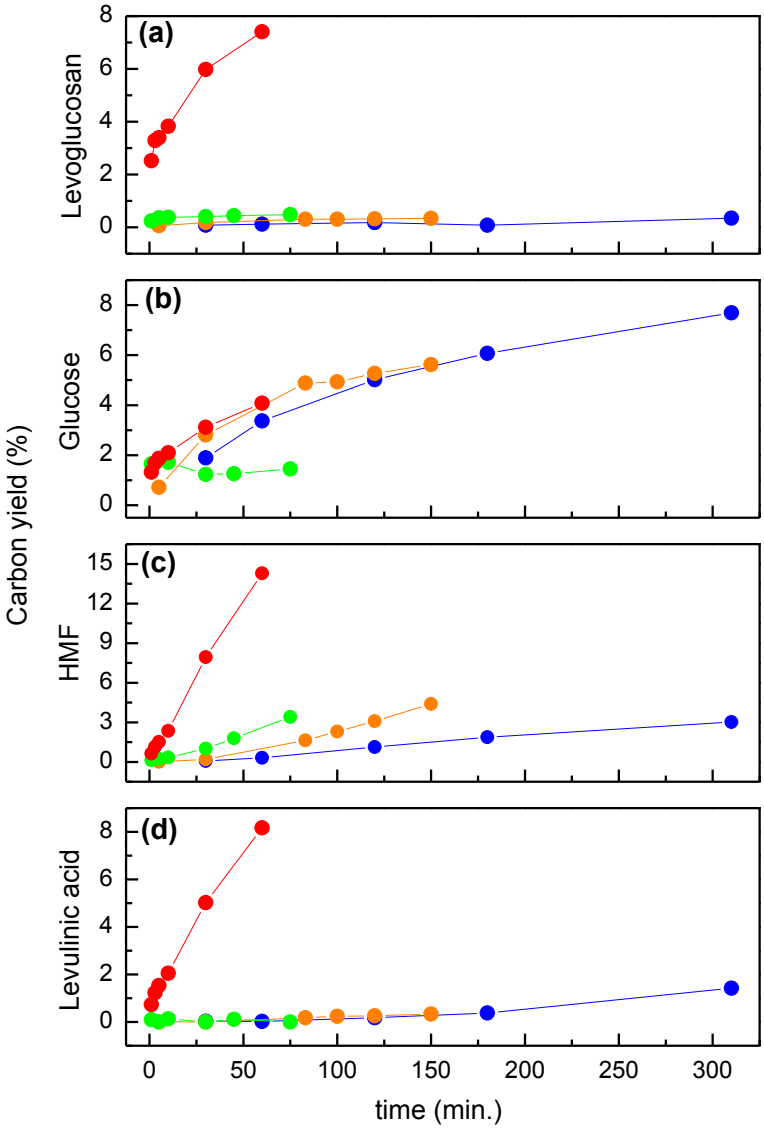

Figure 55. Cellulose decomposition in THF/water mixtures under acidic conditions. Carbon yield of major products as a function of reaction time at 170 °C. (**a**) levoglucosan, (**b**) glucose, (**c**) HMF, (**d**) levulinic acid. Cellulose loading was 5 wt% and reaction volume was 60 mL. Catalyst concentration was 5 mM sulfuric acid. Water (●), Water:THF 1:1 v/v (●), Water:THF 1:9 v/v (●), THF (●).

The product selectivity can be modified by adjusting the reaction temperature. The levoglucosan yield increased with increasing temperature as shown in Figure A.20(a) in the Appendix (39% yield after 1 minute at 210 °C). The HMF yield went through a maximum at 190 °C (Figure A.20(c) in the Appendix). It is also notable to mention that in pure THF at relatively low temperatures (*i.e.* 170 °C), the HMF yield increases with increased initial concentration of cellulose (compare between Figure 55(c) and Figure A.20(c) in the Appendix). Figure 56 shows the carbon yield of all the detectable products and their relative carbon selectivity at 190 °C. The HMF yield increased steadily with time reaching 44% after 120 minutes at 190 °C (Figure 56(a)). The HMF yield then remained constant, even after 4 hours, and the relative HMF selectivity increased with time to 65% (Figure 56(b)). At 190 °C levoglucosan went through a maximum yield of 25% after 30 minutes. The glucose yield (18% maximum) decreased with reaction time at 190 and 210 °C. The cumulative detectable products carbon yield at 190 °C went through a maximum of 88% after 60 minutes, decreasing to 67% after 4 hours, suggesting that undesired humins form in this reaction. The levulinic acid yield also decreased with reaction time at 190 and 210 °C (23% maximum). This differs from our previous studies in aqueous systems (Chapter 5) where levulinic acid was found to be stable with time. Separate decomposition studies with levulinic acid in THF and sulfuric acid showed that levulinic acid is relatively stable in THF with conversions below 5% at 190 °C after 240 minutes. Hence, the decrease in levulinic acid yield suggests that levulinic acid decomposes by reacting with byproducts formed during the cellulose decomposition reaction. The concentration of water produced under these reaction conditions can reach up to 0.2 wt% in THF with quantitative yields of HMF (assuming water is only produced *via* dehydration reactions and water is only

consumed *via* rehydration to produce levulinic acid). Accordingly, based on the data in Figure 56, the water concentration after 120 minutes is 0.08 wt%. Consequently, developing techniques to remove water from the reaction system could further suppress side reactions and improve HMF selectivity.

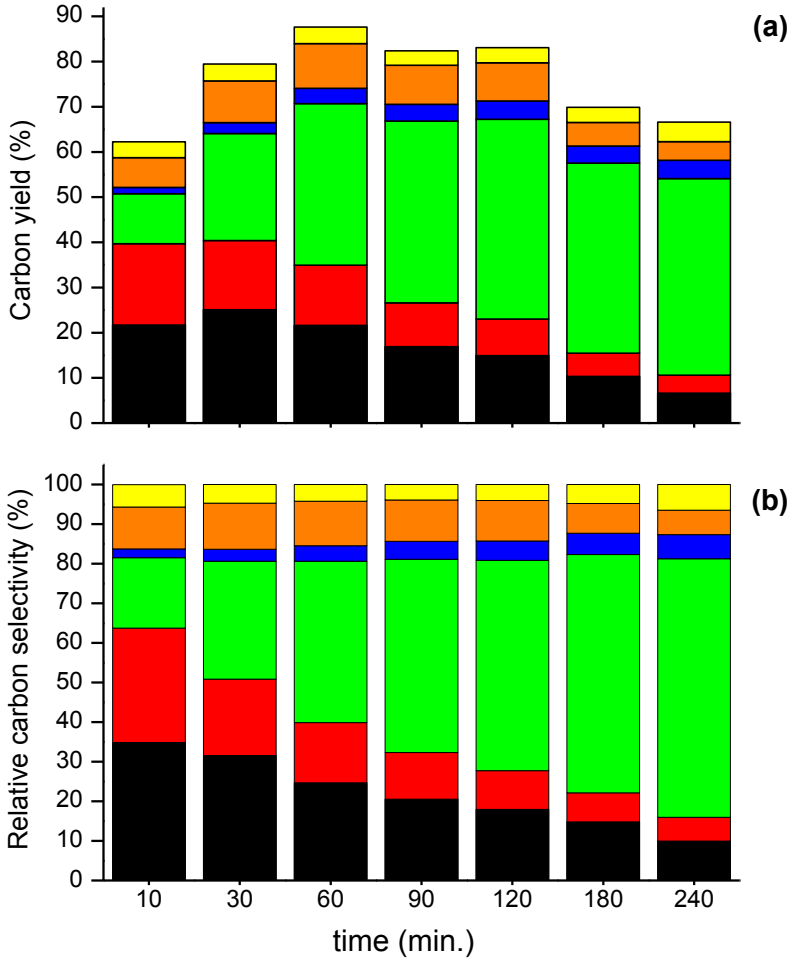

Figure 56. Cellulose decomposition in THF under acidic conditions at 190 °C. (**a**) Carbon yield of detectable products; (**b**) Relative carbon selectivity of detectable products. Cellulose loading was 1 wt% and reaction volume was 60 mL. Catalyst concentration was 5 mM sulfuric acid. ■ levoglucosan; ■ glucose; ■ HMF; ■ furfural; ■ levulinic acid; ■ formic acid.

CHAPTER 10

Conclusions and Future work (III)

10.1. Conclusions

In Chapter 9 we discussed the conversion of cellulose to HMF in polar aprotic solvents (*i.e.* THF) under dilute acid conditions. In this sequence of reactions, levoglucosan is the first major decomposition product of cellulose, followed by dehydration to produce HMF. Glucose, levulinic acid and formic acid are products from side reactions with water, which is a by-product of dehydration. The maximum obtainable yield of HMF we achieved is 44%, with a combined yield of 53% for HMF and levulinic acid. These results are comparable to those obtained in ILs or biphasic systems.[16] The system that we propose here has several distinct advantages compared to other existing processes to produce HMF from cellulose, including a 20 times reduction in acid usage, a 20 times higher reaction rate (compared to aqueous systems), the potential to use less expensive feedstocks (lignocellulosic biomass), operation at lower reaction temperatures, and improved stability of the HMF product in the solvent. Furthermore, the reactants and products can be separated from the solvent using conventional petrochemical separation technology. This type of system also does not require the use of Lewis acids to promote isomerization of glucose to fructose as a preliminary step to produce HMF.

10.2. Future work

This study opens new directions to develop highly efficient and commercially feasible processes to convert cellulosic biomass into platform chemicals using polar aprotic solvents. As this is a relatively new field, there are still many unanswered fundamental questions pertaining to the role of polar aprotic solvents in biomass upgrading. Future advances in this field are contingent on developing a more detailed mechanistic understanding of how solvents affect acid-

catalyzed chemistry combined with studying levoglucosan chemistry. The following are a number of key questions to be addressed in future research:

- How do polar aprotic solvents affect the reaction chemistry (*i.e.* kinetics and product selectivity)?
- Why are cyclic ethers, such as GVL[16] and THF, more favorable than other polar aprotic solvents for biomass upgrading?
- Why do we observe a higher catalytic activity in polar aprotic solvents compared to water?
- How are the acid protons affected by the solvent?

In order to further suppress side reactions and improve HMF selectivity, it would be desirable to develop techniques to remove water from the reaction system. Shimizu *et al.* were able to enhance the HMF production from fructose in dimethyl sulfoxide (DMSO) solvent by implementing water removal techniques, such as carrying out the reaction under mild evacuation and decreasing the particle size of the acid resin.[335] This former technique is feasible when the reaction solvent has a higher boiling point compared to water (*i.e.* DMSO boiling point is 189 °C). Zhang *et al.* noticed a 10% increase in HMF yield when they added 5A molecular sieves during the dehydration of glucose in ionic liquids catalyzed by germanium(IV) chloride.[336] It is notable to mention that these studies were carried out at relatively low temperatures of 120 ºC, which facilitated the use of these water adsorbents. Further work is essential to develop water removal techniques that are applicable under harsher reaction conditions.

Future research in this field should also focus on realizing the commercial potential of these processes for biomass upgrading. As part of this effort, it would be desirable to use a continuous regime to convert biomass into fuels and chemicals. As most biomass feeds are solids, it is critical to develop catalytic processes for the direct conversion of solid biomass into

fuels and chemicals. It would be desirable to design a robust catalytic reactor system that can process different types of solid biomass, carry out different reactions (*i.e.* hydrolysis, hydrodeoxygenation and dehydration) and use solid catalysts. We have designed and built a continuous high pressure reactor system to produce versatile renewable biochemicals from solid biomass feedstocks, as shown in Figure 57. The feed will be a slurry mixture consisting of the solid feed, solvent (*i.e.* water or polar aprotic solvent) and a catalyst (homogeneous or heterogeneous).

Future work with this system should center on answering elementary questions pertaining to the effect of different feedstocks on the reaction chemistry, the nature of the reaction and the types of catalysts (homogeneous or heterogeneous). Being that this is a slurry bubble column, it will be imperative to study the hydrodynamics of the system to ensure ideal mixing patterns in the reactor. Kinetic studies are also essential to develop reactor-kinetic models and derive apparent rate parameters.

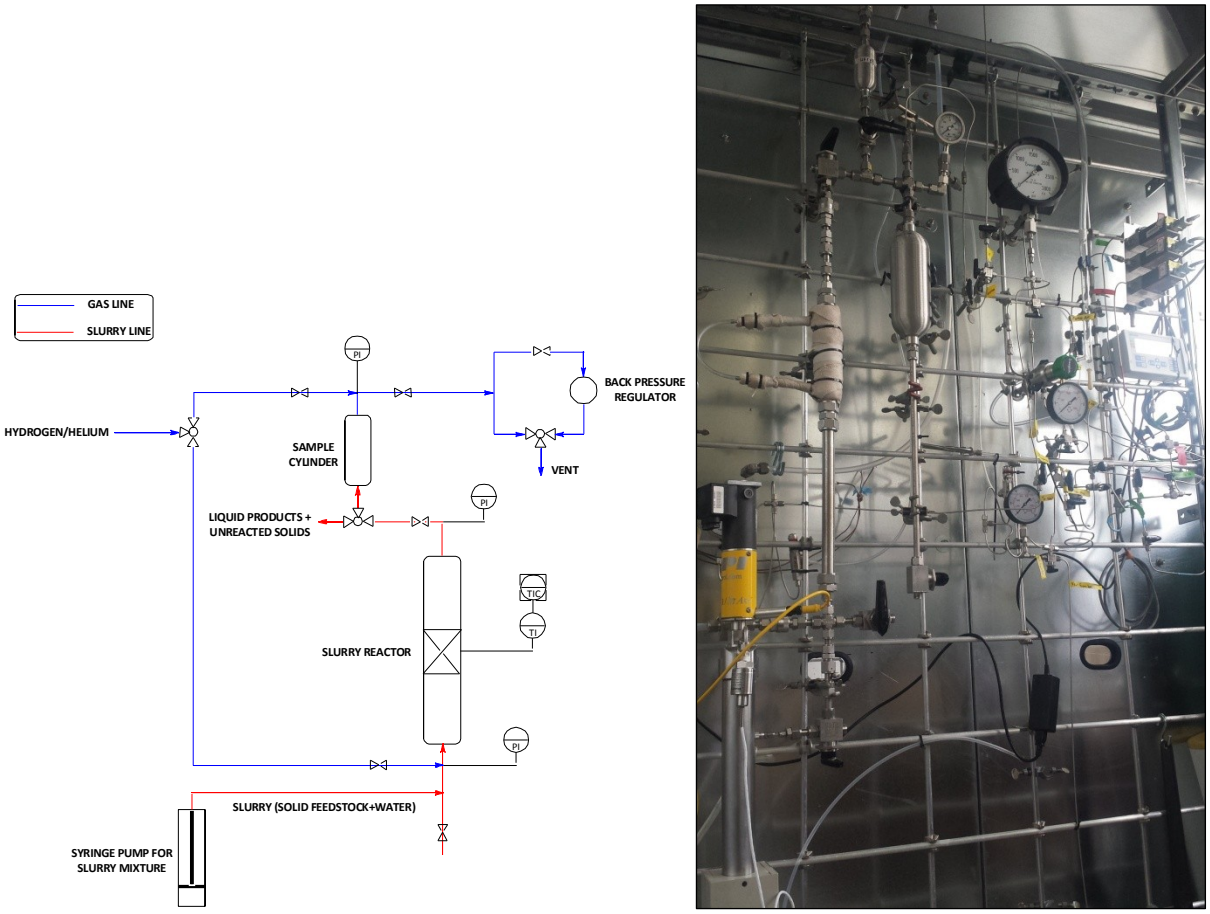

Figure 57. Schematic and photo of high pressure continuous slurry reactor for the production of fuels and chemicals from solid biomass derived compounds.

NOMENCLATURE

Abbreviation	Definition
BET	Brunauer–Emmett–Teller
CSTR	Continuously stirred-tank reactor
DHMTHF	2,5-dihydroxy-methyltetrahydrofuran
DI	De-ionized
DMA	Dimethylacetamide
DMF	2,5-dimethylfuran
DMSO	Dimethyl sulfoxide
DRIFTS	Diffuse reflectance infrared fourier transform spectroscopy
DSC	Differential scanning calorimetry
EQP	Equivalence point
FDCA	2,5-furandicarboxylic acid
FTIR	Fourier transform infrared spectroscopy
Furfural	2-furancarboxaldehyde
GVL	γ-valerolactone
HCl	Hydrochloric acid
HMF	5-hydroxymethylfurfural
HNO_3	Nitric acid
HPLC	High-pressure liquid chromatography
ICP	Inductively coupled plasma

MAS	Magic angle spinning
MIBK	Methyl isobutyl ketone
MTHF	2-methyltetrahydrofuran
NMR	Nuclear magnetic resonance
ODE	Ordinary differential equation
PFR	Plug flow reactor
PSIG	Pounds per square inch gauge
PZC	Point of zero charge
SnP	Tin phosphate
TCD	Thermal conductivity detector
TGA	Thermogravimetric analysis
THF	Tetrahydrofuran
TOC	Total organic carbon
TOF	Turnover frequency
TPD	Temperature-programmed desorption
UHP	Ultra high purity
XPS	X-ray photoelectron spectroscopy
XRD	X-ray diffraction
$Yb(OTf)_3$	Ytterbium (III) trifluoromethanesulfonate hydrate
ZrP	Zirconium phosphate

APPENDIX

Table A.1. Aqueous phase titration of solid acid catalysts at constant Brønsted sites and constant total acid sites (according to NH_3-TPD).[c]

	At constant Brønsted sites [a]	At constant total acid sites [b]
Catalyst	Titrated sites (mmoles)	Titrated sites (mmoles)
ZrP	0.090	0.137
SiO_2-Al_2O_3	0.077	0.102
HY	0.053	0.061
WO_X/ZrO_2	0.092	0.082
γ-Al_2O_3	0.012	0.011

[a] Brønsted sites were kept constant at 0.015 mmoles according to NH_3-TPD.
[b] Total acid sites were kept constant at 0.030 mmoles according to NH_3-TPD.
[c] Reprinted from ref.[140], Copyright(2011), with permission from Elsevier.

Table A.2. Acid concentrations of fresh and regenerated catalysts after exposure to water at 160 °C according to NH_3-TPD.[a]

	Fresh Catalyst	Regenerated Catalyst
Catalyst	Total acid sites (mmol g^{-1})	Total acid sites (mmol g^{-1})
ZrP	1.413	1.705
SiO_2-Al_2O_3	0.432	0.590
WO_X/ZrO_2	0.324	0.385

[a] Reprinted from ref.[140], Copyright(2011), with permission from Elsevier.

Table A.3. Product distribution from non-catalyzed hydrothermal decomposition of cellulose in a stirred batch reactor at 170 °C with recycling of solids. Initial solids loading for each cycle was 29 wt%. Each cycle reaction time was 4 h.[b]

Cycle	Cumulative cellulose conversion (%)	Cumulative carbon selectivity (%)			Cumulative carbon yield (%)		
		Usable organics [a]	Water-soluble humins	Solid humins	Usable organics [a]	Water-soluble humins	Solid humins
1	7.4	70.5	20.5	9.1	5.2	1.5	0.7
2	18.1	70.1	16.9	13.0	12.7	3.1	2.3
3	25.8	62.0	14.5	23.5	16.0	3.7	6.1
4	31.1	59.3	15.1	25.6	18.4	4.7	7.9
5	36.2	57.0	14.7	28.3	20.6	5.3	10.2
6	41.8	53.8	14.4	31.8	22.5	6.0	13.3

[a] includes: glucose, fructose, cellobiose, levoglucosan, HMF, furfural, levulinic acid, formic acid

[b] Reproduced from ref.[255] by permission of The Royal Society of Chemistry.

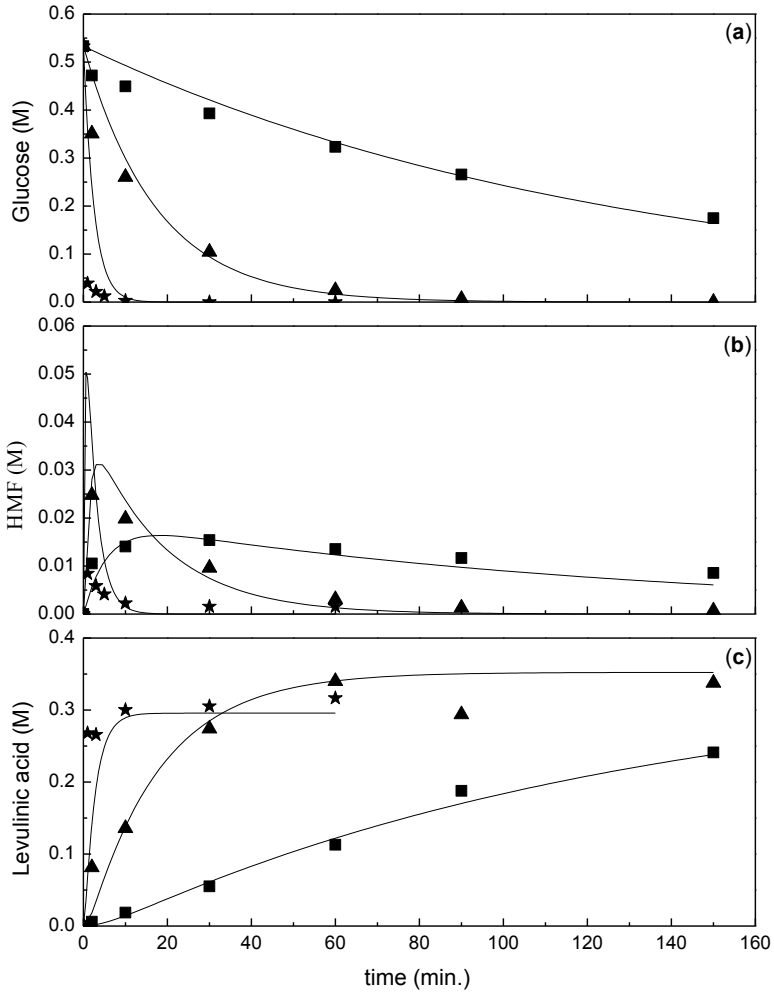

Figure A.1. Aqueous-phase acid-catalyzed glucose dehydration in a stirred batch reactor. Kinetic model fit for (**a**) glucose dehydration, (**b**) HMF formation and (**c**) levulinic acid formation for 10 wt% glucose and 0.5 M HCl. T (°C) = 140 (■), 160 (▲), 180 (★); Model prediction (—). Reprinted from ref.[175], Copyright(2012), with permission from John Wiley and Sons.

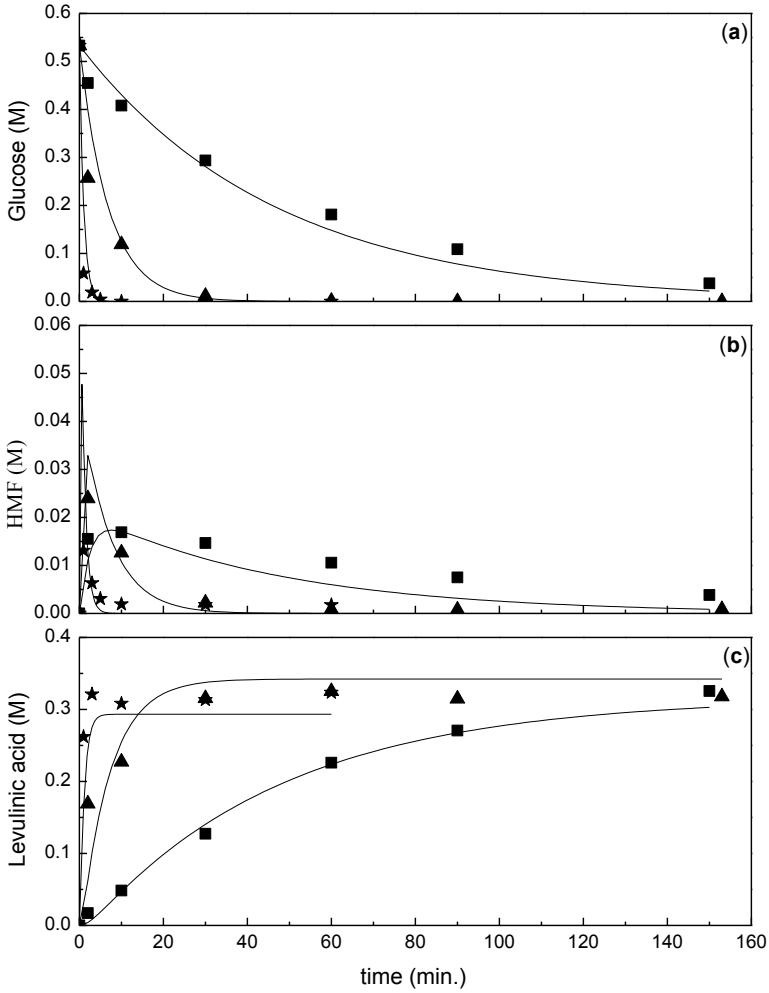

Figure A.2. Aqueous-phase acid-catalyzed glucose dehydration in a stirred batch reactor. Kinetic model fit for (**a**) glucose dehydration, (**b**) HMF formation and (**c**) levulinic acid formation for 10 wt% glucose and 1.0 M HCl. T (°C) = 140 (■), 160 (▲), 180 (★); Model prediction (—). Reprinted from ref.[175], Copyright(2012), with permission from John Wiley and Sons.

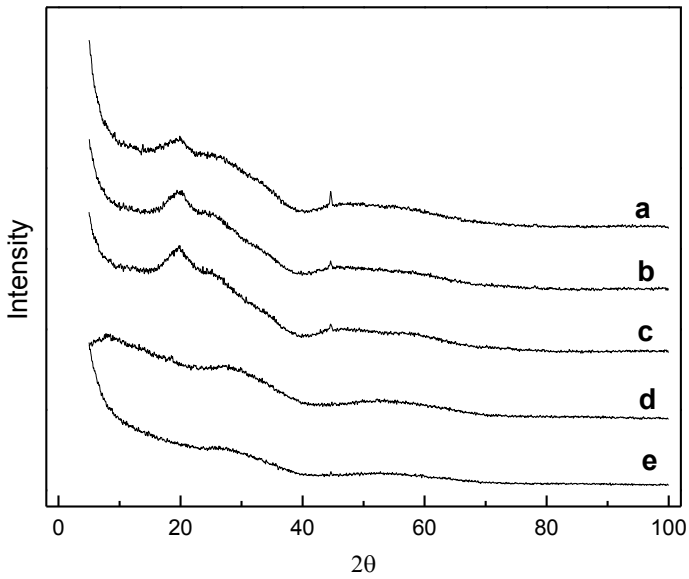

Figure A.3. X-ray diffraction patterns of the different solid acid catalysts. Catalysts: (**a**) ZrP1, (**b**) ZrP2, (**c**) ZrP3, (**d**) SnP1, (**e**) SnP2. Reprinted from ref.[205], Copyright(2013), with permission from Elsevier.

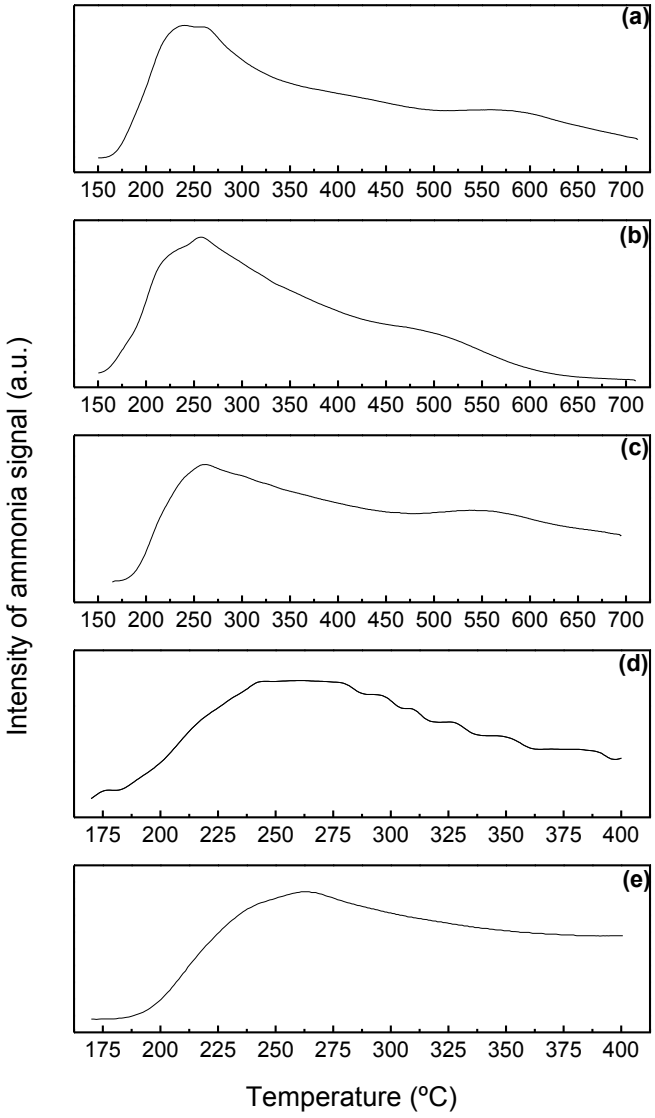

Figure A.4. NH_3-TPD profiles of the different solid acid catalysts. Catalysts: (**a**) ZrP1, (**b**) ZrP2, (**c**) ZrP3, (**d**) SnP1, (**e**) SnP2. Reprinted from ref.[205], Copyright(2013), with permission from Elsevier.

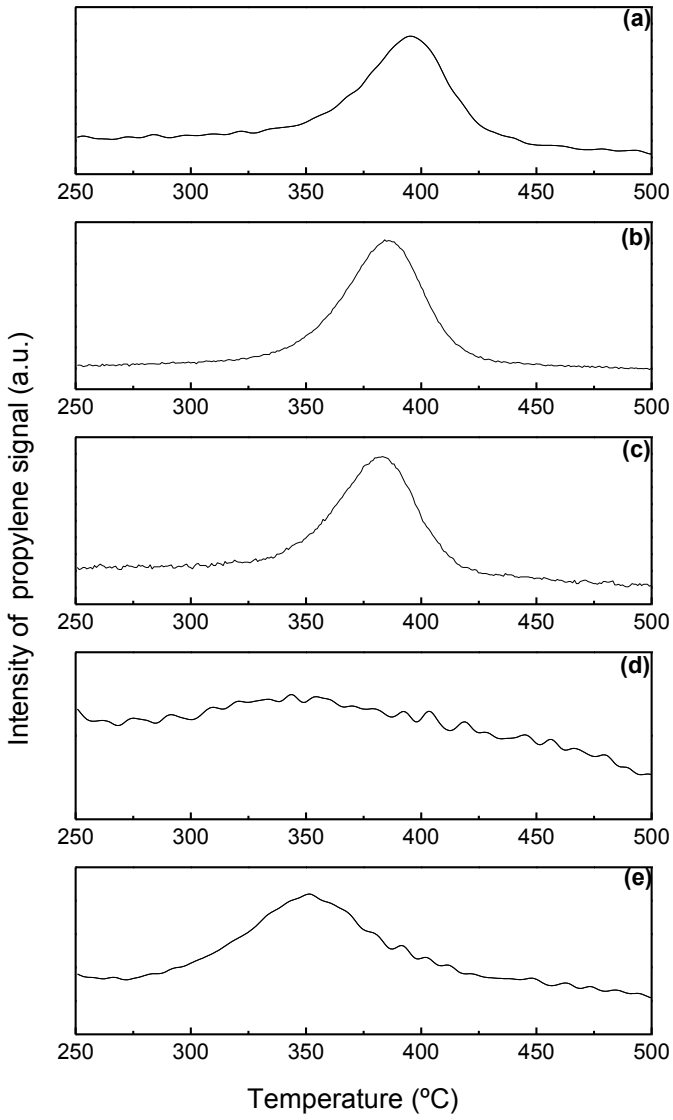

Figure A.5. TPD profiles of propylene (m/z = 39) from TGA-MS for the different solid acid catalysts. Catalysts: (**a**) ZrP1, (**b**) ZrP2, (**c**) ZrP3, (**d**) SnP1, (**e**) SnP2. Reprinted from ref.[205], Copyright(2013), with permission from Elsevier.

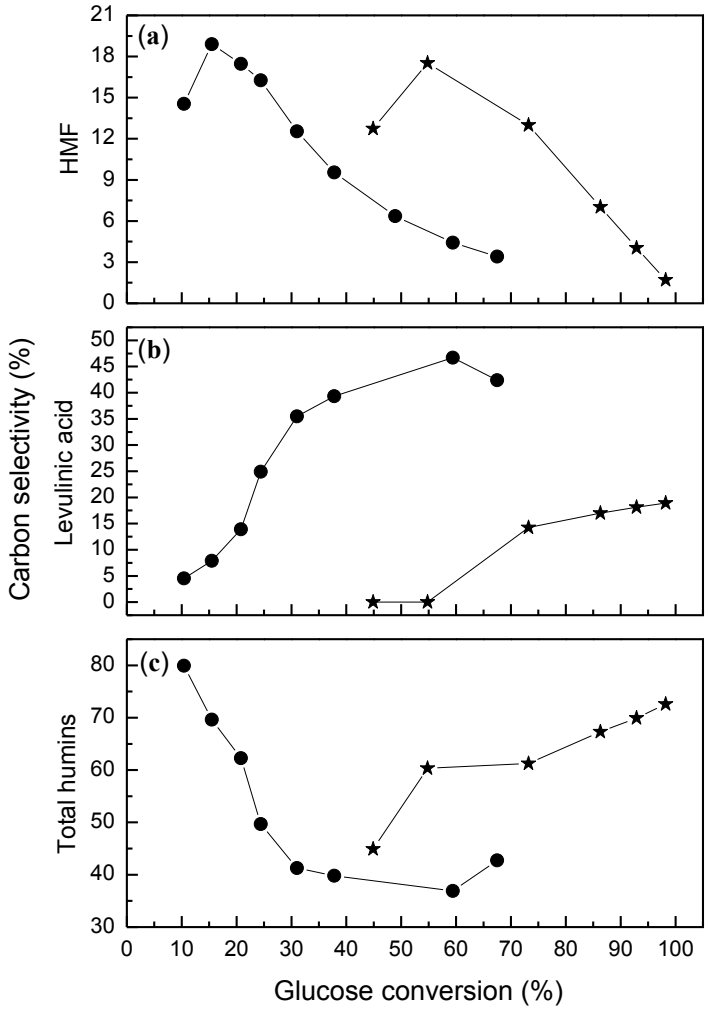

Figure A.6. Aqueous phase glucose dehydration in a stirred batch reactor with homogeneous acid catalysts at 160 °C. Effect of type of acid site on carbon selectivity for (**a**) HMF; (**b**) levulinic acid; (**c**) humins. Feed was 10 wt% glucose aqueous solution and acid concentration was 0.1 M. Acid catalyst type = Brønsted: HCl (●), Lewis: $Yb(OTf)_3$ (★). Reproduced from ref.[255] by permission of The Royal Society of Chemistry.

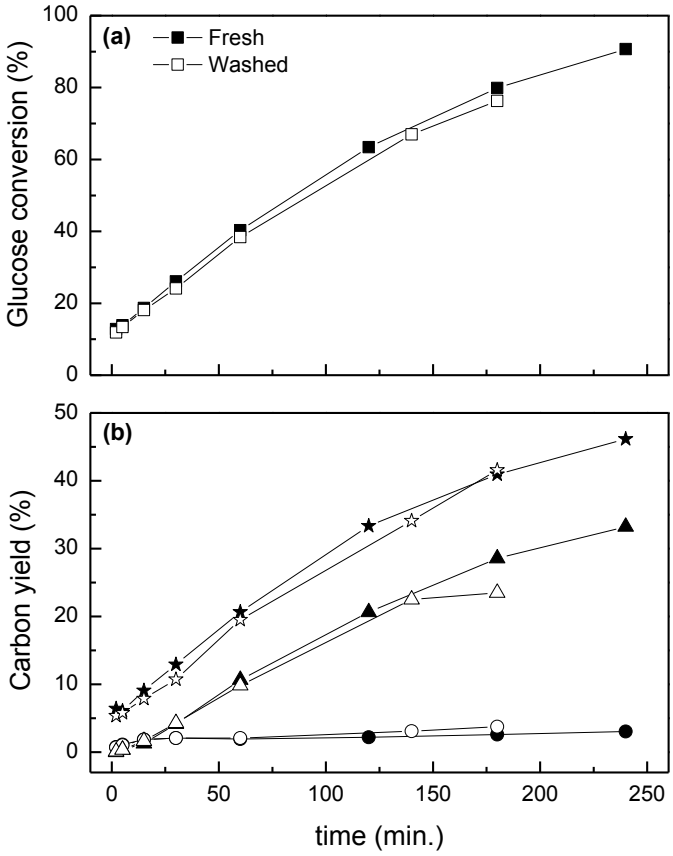

Figure A.7. Stability test with Amberlyst 70 for aqueous phase acid-catalyzed glucose dehydration in a stirred batch reactor at 160 °C. (**a**) glucose conversion; (**b**) carbon yield of major products: HMF (●), levulinic acid (▲), soluble and solid humins (★). Feed was 10 wt% glucose aqueous solution. Catalyst concentration was 0.1 M total acid sites (taken from manufacturer). Closed symbols denote reaction with fresh catalyst. Open symbols denote reaction with washed catalyst. Reproduced from ref.[255] by permission of The Royal Society of Chemistry.

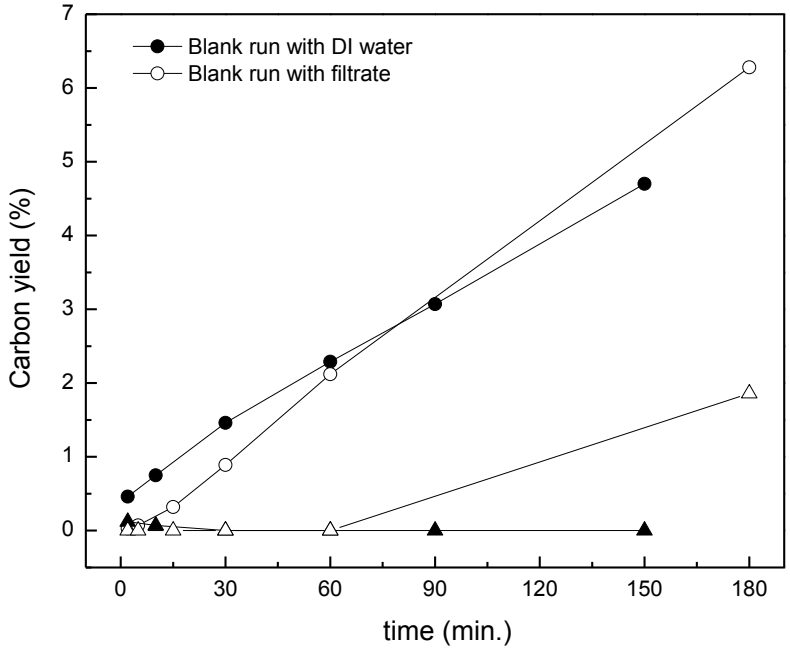

Figure A.8. Non-catalyzed aqueous phase glucose dehydration in a stirred batch reactor at 160 °C. Carbon yield of major products as a function of reaction time: HMF (●), levulinic acid (▲). Feed was 10 wt% glucose aqueous solution. Closed symbols denote reaction with clean DI water as solvent. Open symbols denote reaction with aqueous filtrate after exposure to Amberlyst 70 at hydrothermal conditions. Reproduced from ref.[255] by permission of The Royal Society of Chemistry.

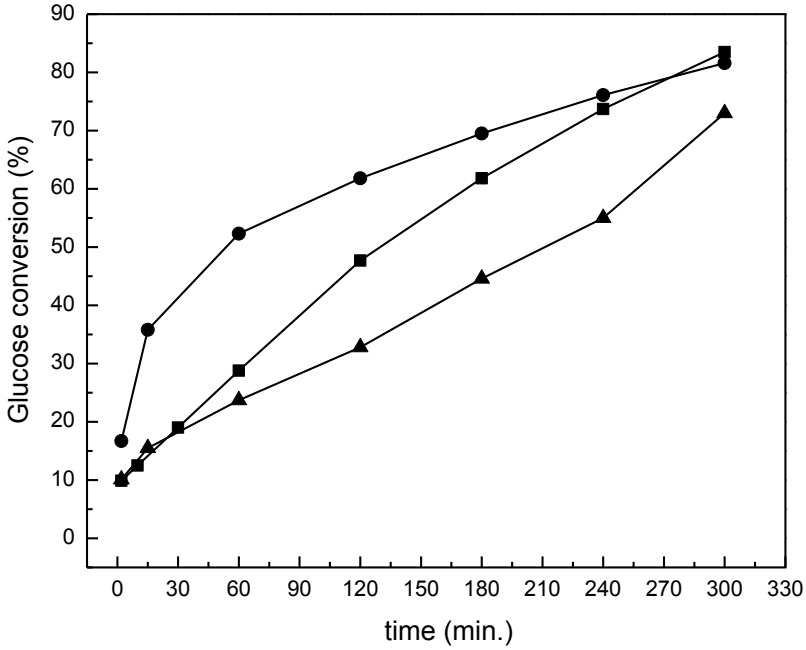

Figure A.9. Recycle test with Amberlyst 70 for aqueous phase acid-catalyzed glucose dehydration in a stirred batch reactor at 160 °C. Glucose conversion as a function of reaction time for: fresh catalyst (■), recycled catalyst (●), regenerated catalyst (▲). Feed was 10 wt% glucose aqueous solution. Catalyst concentration of fresh batch was 0.1 M total acid sites (taken from manufacturer). Reproduced from ref.[255] by permission of The Royal Society of Chemistry.

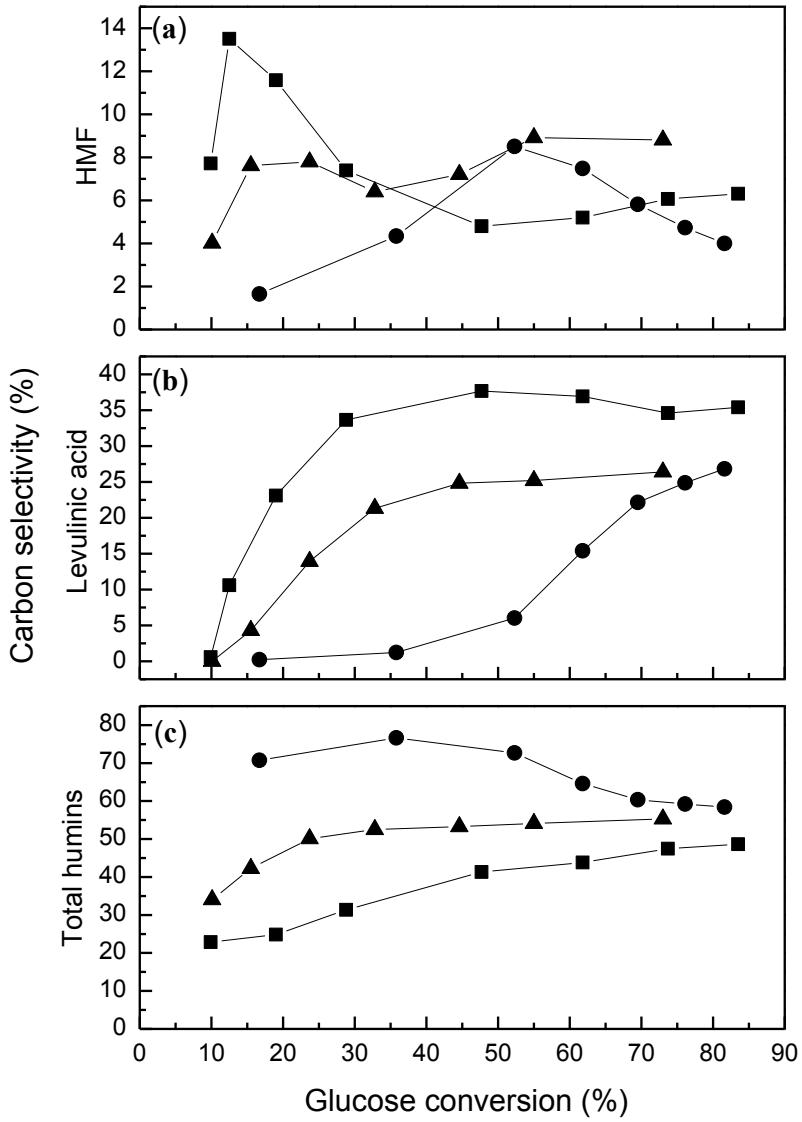

Figure A.10. Recycle test with Amberlyst 70 for aqueous phase acid-catalyzed glucose dehydration in a stirred batch reactor at 160 °C. Effect on carbon selectivity for (**a**) HMF; (**b**) levulinic acid; (**c**) total humins. Feed was 10 wt% glucose aqueous solution. Catalyst concentration of fresh batch was 0.1 M total acid sites (taken from manufacturer). Fresh catalyst (■), recycled catalyst (●), regenerated catalyst (▲). Reproduced from ref.[255] by permission of The Royal Society of Chemistry.

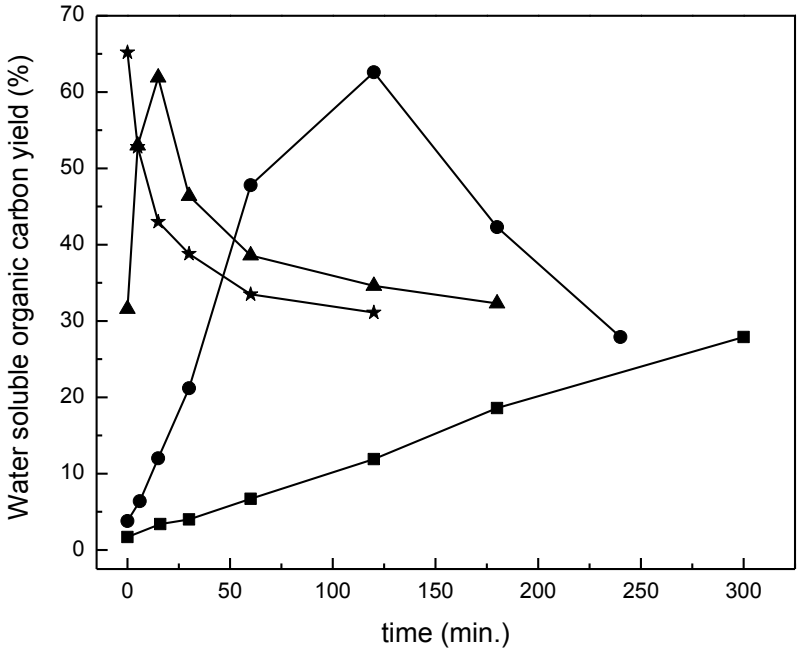

Figure A.11. Hydrothermal decomposition of cellulose without a solid acid catalyst in a stirred batch reactor. Total water-soluble organic carbon yield as a function of reaction time. Initial cellulose loading was 4 wt% of total. T (°C) = 190 (■), 220 (●), 250 (▲), 270(★). Reproduced from ref.[255] by permission of The Royal Society of Chemistry.

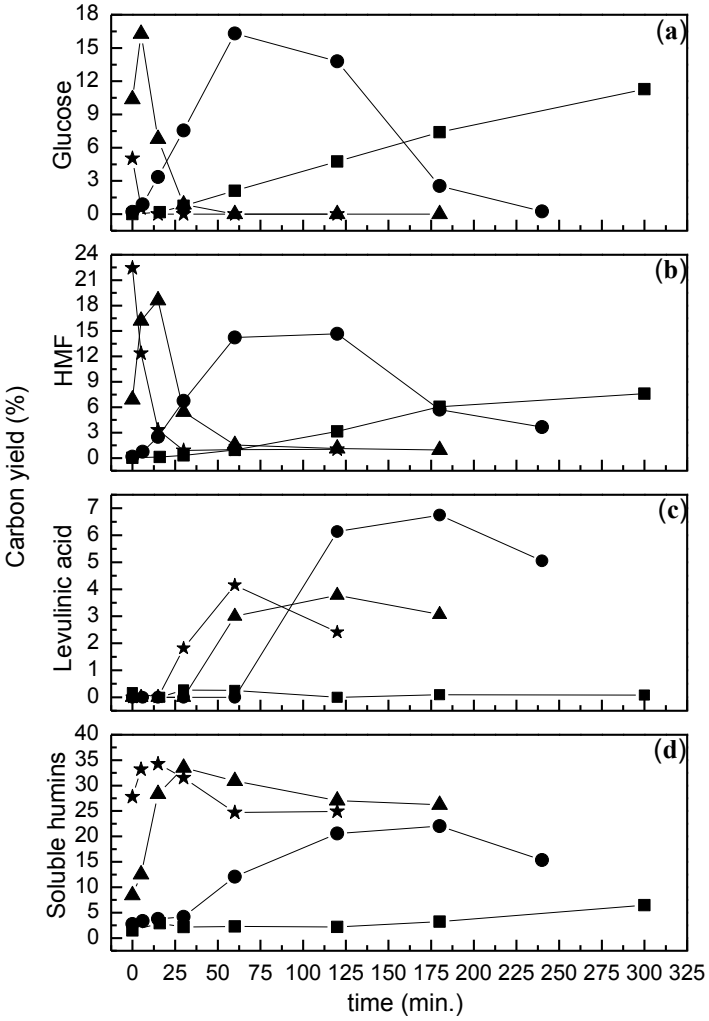

Figure A.12. Hydrothermal decomposition of cellulose without a solid acid catalyst in a stirred batch reactor. Water-soluble organic carbon yield for (**a**) glucose, (**b**) HMF, (**c**) levulinic acid, (**d**) soluble humins. Initial cellulose loading was 4 wt% of total. T (°C) = 190 (■), 220 (●), 250 (▲), 270(★). Reproduced from ref.[255] by permission of The Royal Society of Chemistry.

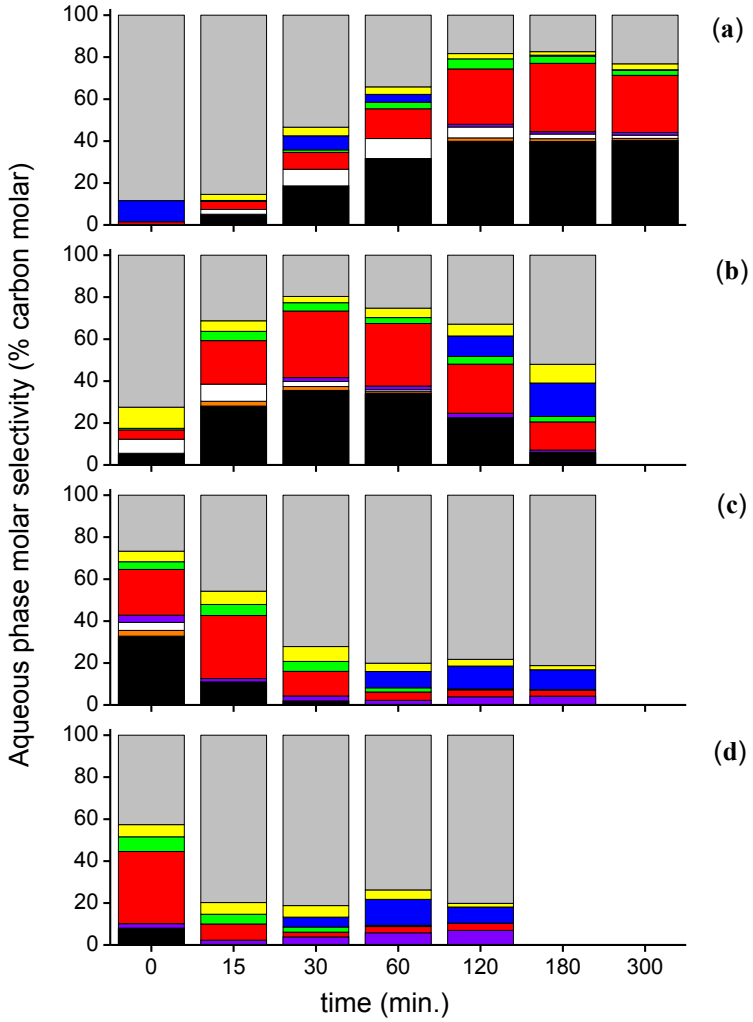

Figure A.13. Water-soluble organic carbon product selectivity for the aqueous phase cellulose decomposition without a solid acid catalyst in a stirred batch reactor for T (°C) = (**a**) 190 (**b**) 220, (**c**) 250, (**d**) 270. Initial cellulose loading was 4 wt% of total. ■ glucose; ■ fructose; □ cellobiose; ■ levoglucosan; ■ HMF; ■ furfural; ■ levulinic acid; ■ formic acid; ■ humins. Reproduced from ref.[255] by permission of The Royal Society of Chemistry.

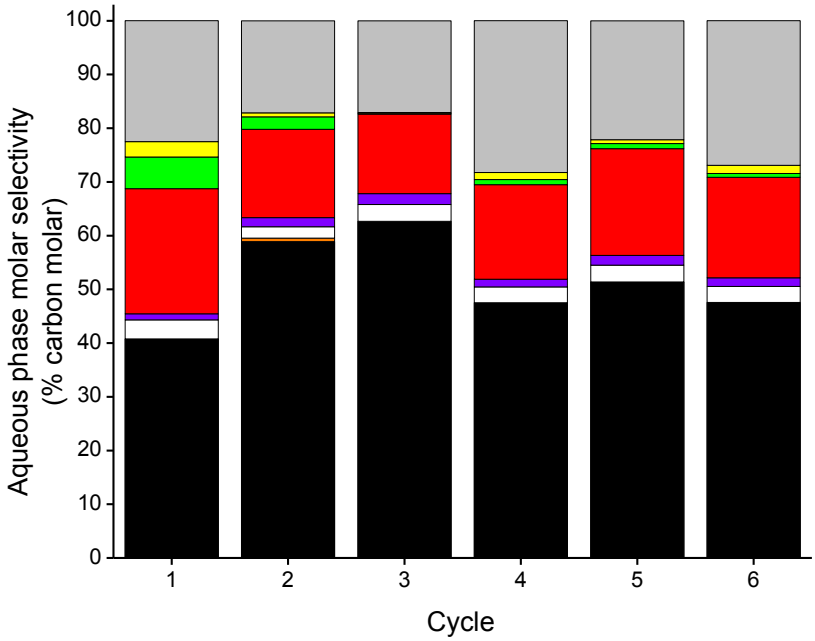

Figure A.14. Water-soluble organic carbon product selectivity for each recycle run from non-catalyzed hydrothermal decomposition of cellulose in a stirred batch reactor at 170 °C. Initial solids loading for each cycle was 29 wt%. Each cycle reaction time was 4 h. ■ glucose; ■ fructose; □ cellobiose; ■ levoglucosan; ■ HMF; ■ furfural; ■ levulinic acid; ■ formic acid; ■ humins. Reproduced from ref.[255] by permission of The Royal Society of Chemistry.

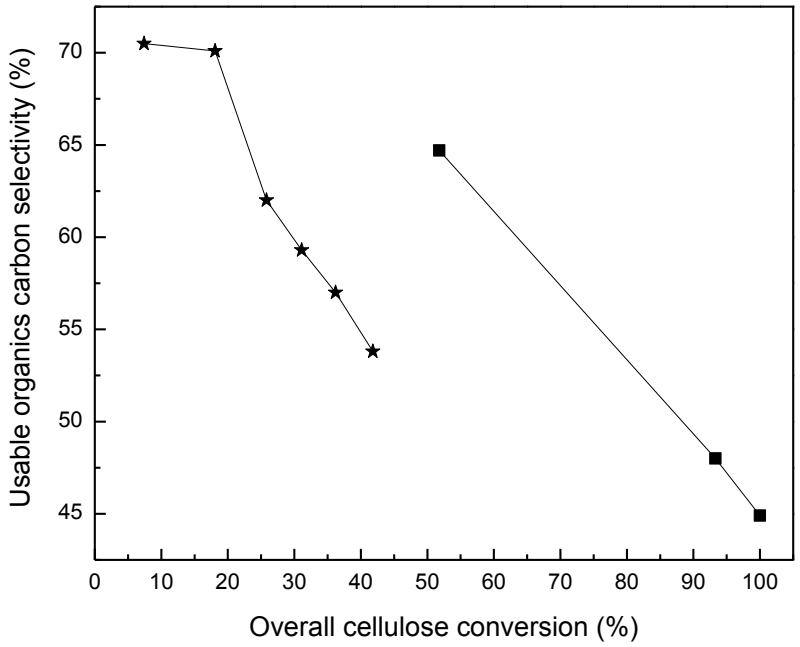

Figure A.15. Cumulative carbon selectivity of usable organics obtained from hydrothermal decomposition of cellulose with recycling of solids. Initial solids loading for each cycle was 29 wt%. Reaction conditions: 220 °C for 30 min. each cycle (■); 170 °C for 4 h each cycle (★). Reproduced from ref.[255] by permission of The Royal Society of Chemistry.

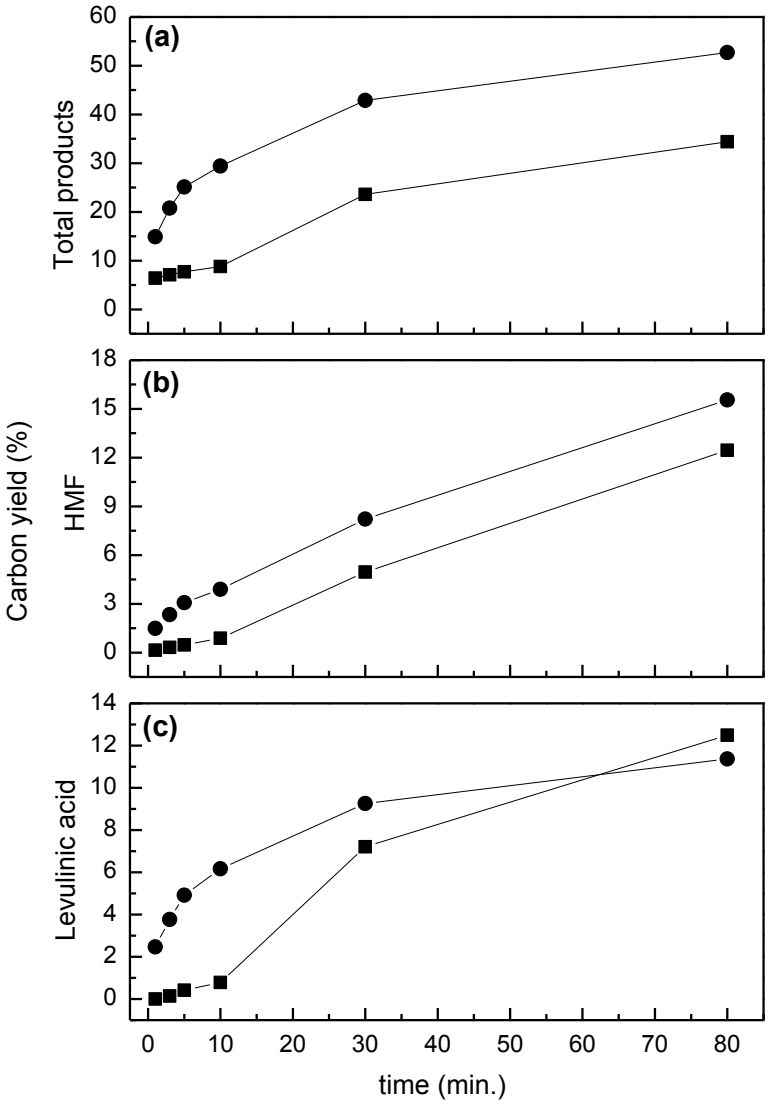

Figure A.16. Dehydration studies in THF with levoglucosan (■) and glucose (●) feedstocks under acidic conditions at 170 °C. Carbon yields as a function of reaction time: (**a**) Total detectable products, (**b**) HMF, (**c**) levulinic acid. Feedstock loading was 2 wt% and reaction volume was 60 mL. Catalyst concentration was 5 mM sulfuric acid.

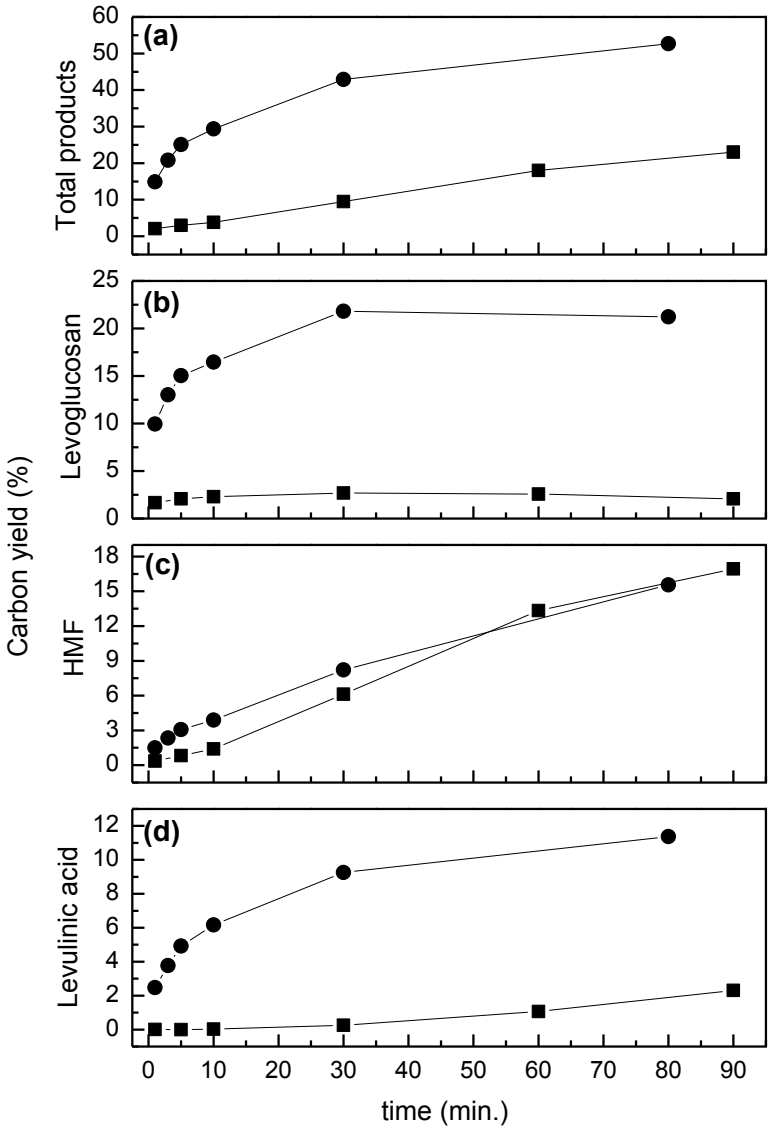

Figure A.17. Effect of solvent in glucose dehydration studies under acidic conditions at 170 °C. Carbon yields as a function of reaction time: (**a**) Total detectable products, (**b**) levoglucosan, (**c**) HMF, (**d**) levulinic acid. Feedstock loading was 2 wt% and reaction volume was 60 mL. Catalyst concentration was 5 mM sulfuric acid. Water (■), THF (●).

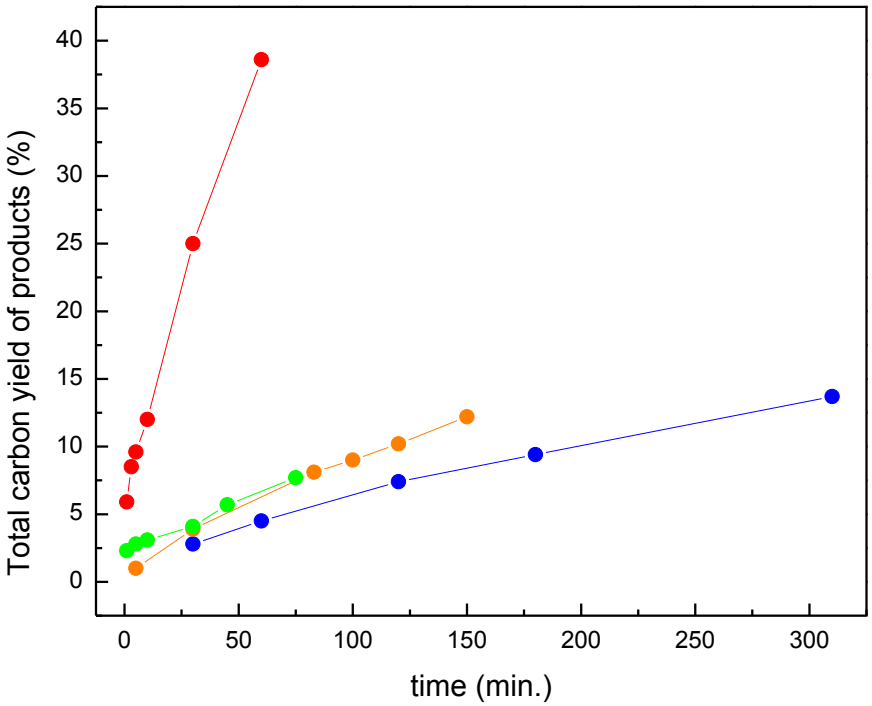

Figure A.18. Cellulose decomposition in THF/water mixtures under acidic conditions. Total carbon yield of detectable products as a function of reaction time at 170 °C. Cellulose loading was 5 wt% and reaction volume was 60 mL. Catalyst concentration was 5 mM sulfuric acid. Water (●), Water:THF 1:1 v/v (●), Water:THF 1:9 v/v (●), THF (●).

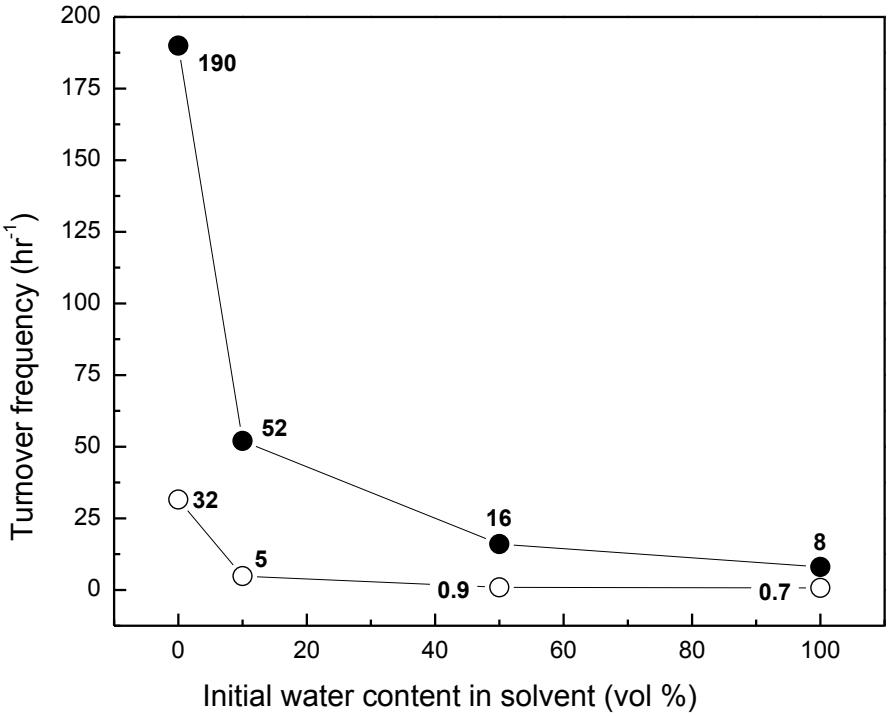

Figure A.19. Cellulose decomposition in THF/water mixtures under acidic conditions. Initial turnover frequency as a function of initial water content in the solvent at 170 °C. Cellulose loading was 5 wt% and reaction volume was 60 mL. Catalyst concentration was 5 mM sulfuric acid. Based on the total moles of carbon from the detectable products (●); Based on the moles of carbon of HMF produced (○).

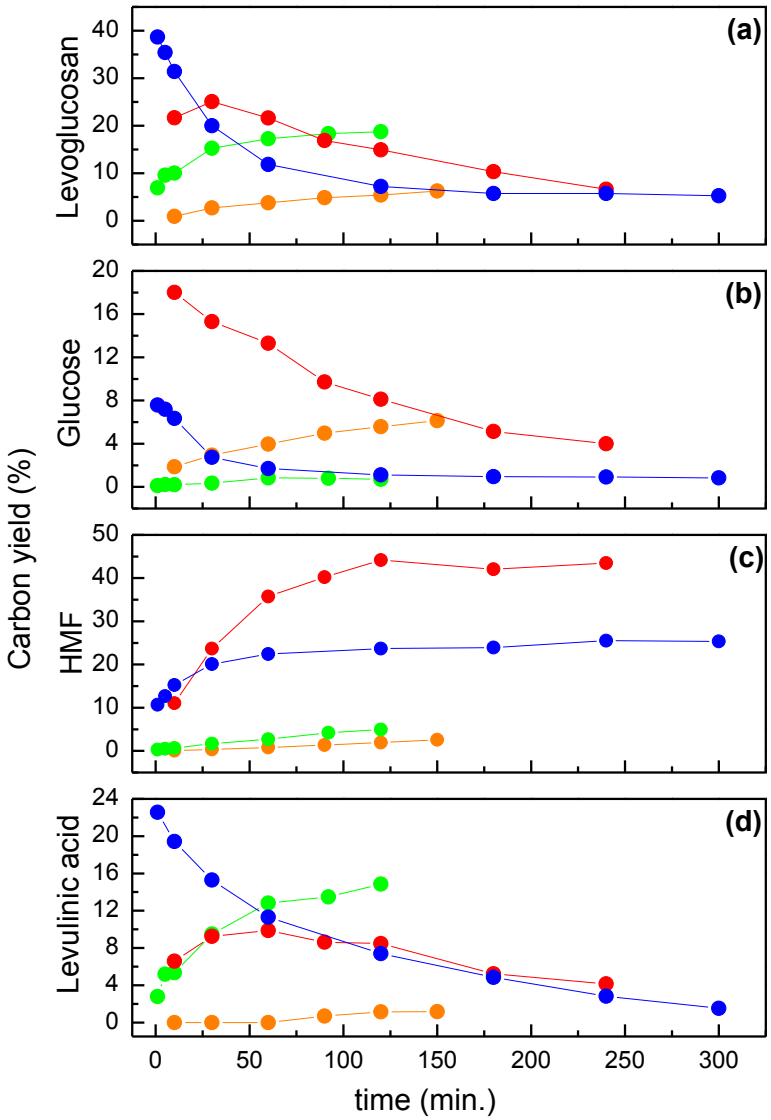

Figure A.20. Effect of temperature on cellulose decomposition in THF under acidic conditions. Carbon yield of major products as a function of reaction time. (**a**) levoglucosan, (**b**) glucose, (**c**) HMF, (**d**) levulinic acid. Cellulose loading was 1 wt% and reaction volume was 60 mL. Catalyst concentration was 5 mM sulfuric acid. T (°C) = 140 (●), 170 (●), 190 (●), 210 (●).

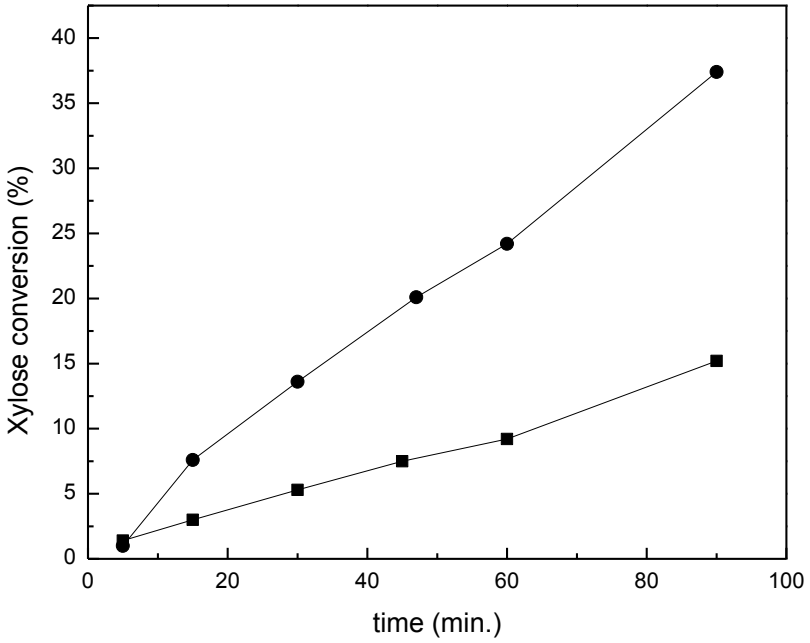

Figure A.21. Comparison between heating methods for aqueous phase xylose dehydration with zirconium phosphate. Xylose conversion as a function of time at 160 °C. ZrP loading was 1.18 wt%. Feed was 10 wt% xylose aqueous solution. Conventional heating (■); Microwave heating (●). Reprinted from ref.[140], Copyright(2011), with permission from Elsevier.

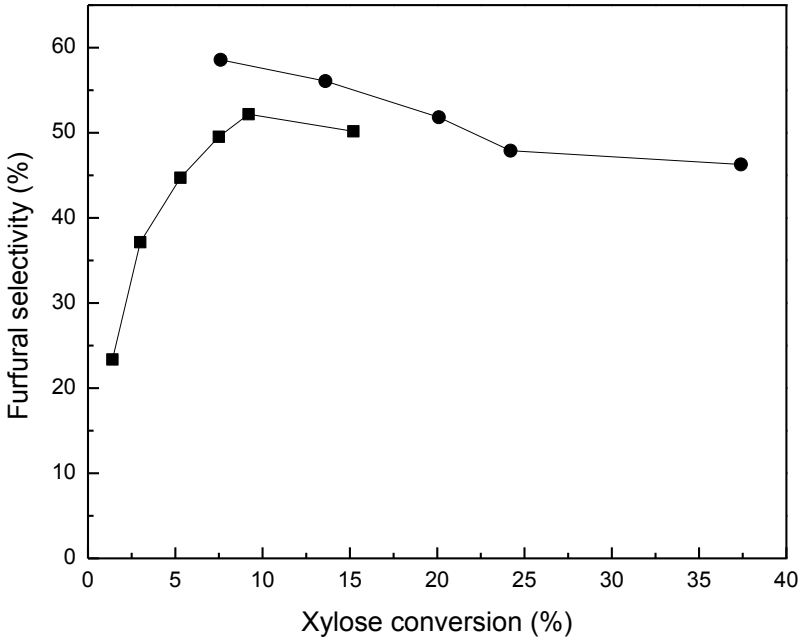

Figure A.22. Comparison between heating methods for aqueous phase xylose dehydration with zirconium phosphate. Furfural selectivity as a function of xylose conversion at 160 °C. ZrP loading was 1.18 wt%. Feed was 10 wt% xylose aqueous solution. Conventional heating (■); Microwave heating (●). Reprinted from ref.[140], Copyright(2011), with permission from Elsevier.

REFERENCES

1. Perego, C.; Bianchi, D., Biomass upgrading through acid-base catalysis. *Chemical Engineering Journal* **2010,** *161* (3), 314-322.

2. Huber, G. W.; Dumesic, J. A., An overview of aqueous-phase catalytic processes for production of hydrogen and alkanes in a biorefinery. *Catalysis Today* **2006,** *111* (1-2), 119-132.

3. Lynd, L. R.; Cushman, J. H.; Nichols, R. J.; Wyman, C. E., Fuel Ethanol from Cellulosic Biomass. *Science* **1991,** *251*, 1318-1323.

4. Davda, R. R.; Shabaker, J. W.; Huber, G. W.; Cortright, R. D.; Dumesic, J. A., A review of catalytic issues and process conditions for renewable hydrogen and alkanes by aqueous-phase reforming of oxygenated hydrocarbons over supported metal catalysts. *Applied Catalysis B: Environmental* **2005,** *56* (1-2), 171-186.

5. Chheda, J. N.; Dumesic, J. A., An overview of dehydration, aldol-condensation and hydrogenation processes for production of liquid alkanes from biomass-derived carbohydrates. *Catalysis Today* **2007,** *123* (1-4), 59-70.

6. Chheda, J. N.; Huber, G. W.; Dumesic, J. A., Liquid-Phase Catalytic Processing of Biomass-Derived Oxygenated Hydrocarbons to Fuels and Chemicals. *Angew. Chem. Int. Ed.* **2007,** *46* (38), 7164-7183.

7. Simonetti, D. A.; Dumesic, J. A., Catalytic Strategies for Changing the Energy Content and Achieving C-C Coupling in Biomass-Derived Oxygenated Hydrocarbons. *ChemSusChem* **2008,** *1* (8-9), 725-733.

8. Simonetti, D. A.; Dumesic, J. A., Catalytic Production of Liquid Fuels from Biomass-Derived Oxygenated Hydrocarbons: Catalytic Coupling at Multiple Length Scales. *Catal. Rev.* **2009,** *51* (3), 441-484.

9. Alonso, D. M.; Bond, J. Q.; Dumesic, J. A., Catalytic conversion of biomass to biofuels. *Green Chemistry* **2010,** *12* (9), 1493-1513.

10. Serrano-Ruiz, J. C.; West, R. M.; Dumesic, J. A., Catalytic Conversion of Renewable Biomass Resources to Fuels and Chemicals. *Annual Review of Chemical and Biomolecular Engineering* **2010,** *1*, 79-100.

11. Serrano-Ruiz, J. C.; Dumesic, J. A., Catalytic routes for the conversion of biomass into liquid hydrocarbon transportation fuels. *Energy & Environmental Science* **2011,** *4* (1), 83-99.

12. Huber, G. W.; Iborra, S.; Corma, A., Synthesis of Transportation Fuels from Biomass: Chemisrty, Catalysts, and Engineering. *Chemical Reviews* **2006,** *106* (9), 4044-4098.

13. Petrus, L.; Noordermeer, M. A., Biomass to biofuels, a chemical perspective. *Green Chemistry* **2006,** *8*, 861-867.

14. Corma, A.; Iborra, S.; Velty, A., Chemical routes for the transformation of biomass into chemicals. *Chem Rev* **2007,** *107*, 2411-2502.

15. Fitzpatrick, S. W., The Biofine technology: a "bio-refinery" concept based on thermochemical conversion of cellulosic biomass. *ACS Symposium Series* **2006,** *921*, 271-287.

16. Luterbacher, J. S.; Rand, J. M.; Alonso, D. M.; Han, J.; Youngquist, J. T.; Maravelias, C. T.; Pfleger, B. F.; Dumesic, J. A., Nonenzymatic Sugar Production from Biomass Using Biomass-Derived γ-Valerolactone. *Science* **2014,** *343* (6168), 277-280.

17. Zhou, C.-H.; Xia, X.; Lin, C.-X.; Tong, D.-S.; Beltramini, J., Catalytic conversion of lignocellulosic biomass to fine chemicals and fuels. *Chemical Society Reviews* **2011,** *40* (11), 5588-5617.

18. Cabiac, A.; Guillon, E.; Chambon, F.; Pinel, C.; Rataboul, F.; Essayem, N., Cellulose reactivity and glycosidic bond cleavage in aqueous phase by catalytic and non catalytic transformations. *Applied Catalysis A: General* **2011,** *402* (1-2), 1-10.

19. Hara, M., Biomass conversion by a solid acid catalyst. *Energy & Environmental Science* **2010,** *3* (5), 601-607.

20. Pang, J.; Wang, A.; Zheng, M.; Zhang, T., Hydrolysis of cellulose into glucose over carbons sulfonated at elevated temperatures. *Chemical Communications* **2010,** *46* (37), 6935-6937.

21. Dee, S. J.; Bell, A. T., A Study of the Acid-Catalyzed Hydrolysis of Cellulose Dissolved in Ionic Liquids and the Factors Influencing the Dehydration of Glucose and the Formation of Humins. *ChemSusChem* **2011,** *4* (8), 1166-1173.

22. Dee, S.; Bell, A. T., Effects of reaction conditions on the acid-catalyzed hydrolysis of miscanthus dissolved in an ionic liquid. *Green Chemistry* **2011,** *13* (6), 1467-1475.

23. Gross, A. S.; Bell, A. T.; Chu, J.-W., Thermodynamics of Cellulose Solvation in Water and the Ionic Liquid 1-Butyl-3-Methylimidazolim Chloride. *The Journal of Physical Chemistry B* **2011,** *115* (46), 13433-13440.

24. Binder, J. B.; Raines, R. T., Fermentable sugars by chemical hydrolysis of biomass. *Proceedings of the National Academy of Sciences* **2010,** *107* (10), 4516-4521.

25. Zhu, S., Use of ionic liquids for the efficient utilization of lignocellulosic materials. *Journal of Chemical Technology & Biotechnology* **2008,** *83* (6), 777-779.

26. Rinaldi, R.; Schuth, F., Design of solid catalysts for the conversion of biomass. *Energy and Environmental Science* **2009,** *2*, 610-626.

27. Tong, X.; Ma, Y.; Li, Y., Biomass into chemicals: Conversion of sugars to furan derivatives by catalytic processes. *Applied Catalysis A: General* **2010,** *385* (1-2), 1-13.

28. Moreau, C.; Belgacem, M. N.; Gandini, A., Recent catalytic advances in the chemistry of substituted furans from carbohydrates and in the ensuing polymers. *Top. Catal.* **2004,** *27*, 11-30.

29. Roman-Leshkov, Y.; Chheda, J. N.; Dumesic, J. A., Phase modifiers promote efficient production of hydroxymethylfurfural from fructose. *Science* **2006,** *312*, 1933-1937.

30. Roman-Leshkov, Y.; Barrett, C. J.; Liu, Z. Y.; Dumesic, J. A., Production of dimethylfuran for liquid fuels from biomass-derived carbohydrates. *Nature* **2007,** *447* (7147), 982-985.

31. Chheda, J. N.; Roman-Leshkov, Y.; Dumesic, J. A., Production of 5-hydroxymethylfurfural and furfural by dehydration of biomass-derived mono- and poly-saccharides. *Green Chemistry* **2007,** *9* (4), 342-350.

32. West, R.; Liu, Z.; Peter, M.; Dumesic, J., Liquid Alkanes with Targeted Molecular Weights from Biomass-Derived Carbohydrates. *ChemSusChem* **2008,** *1* (5), 417-424.

33. Roman-Leshkov, Y.; Dumesic, J. A., Solvent Effects on Fructose Dehydration to 5-Hydroxymethylfurfural in Biphasic Systems Saturated with Inorganic salts. *Topics in Catalysis* **2009,** *52* (3), 297-303.

34. Huber, G. W.; Cortright, R. D.; Dumesic, J. A., Renewable Alkanes by Aqueous-Phase Reforming of Biomass-Derived Oxygenates. *Angewandte Chemie International Edition* **2004,** *43* (12), 1549-1551.

35. Xing, R.; Subrahmanyam, A. V.; Olcay, H.; Qi, W.; van Walsum, G. P.; Pendse, H.; Huber, G. W., Production of jet and diesel fuel range alkanes from waste hemicellulose-derived aqueous solutions. *Green Chemistry* **2010,** *12* (11), 1933-1946.

36. Kottke, R. H., Furan Derivatives. In *Kirk-Othmer Encyclopedia of Chemical Technology*, John Wiley & Sons: 2000; Vol. 12, pp 259-286.

37. Lecomte, J.; Finiels, A.; Moreau, C., A new selective route to 5-hydroxymethylfurfural from furfural and furfural derivatives over microporous solid acidic catalysts. *Industrial Crops and Products* **1999,** *19* (3), 235-241.

38. Sain, B.; Chaudhuri, A.; Borgohain, J. N.; Baruah, B. P.; Ghose, J. L., Furfural and Furfural-based Industrial Chemicals. *Journal of Scientific and Industrial Research* **1982,** *41*, 431-438.

39. Huber, G. W.; Chheda, J. N.; Barrett, C. J.; Dumesic, J. A., Production of Liquid Alkanes by Aqueous-Phase Processing of Biomass-Derived Carbohydrates. *Science* **2005,** *308* (5727), 1446-1450.

40. Bayan, S.; Beati, E., Furfural and its derivatives as motor fuels. *La Chimica e L'Industria* **1941,** *23*, 432-434.

41. Gullón, P.; Romaní, A.; Vila, C.; Garrote, G.; Parajó, J. C., Potential of hydrothermal treatments in lignocellulose biorefineries. *Biofuels, Bioproducts and Biorefining* **2012,** *6* (2), 219-232.

42. Dutta, S.; De, S.; Saha, B., A Brief Summary of the Synthesis of Polyester Building-Block Chemicals and Biofuels from 5-Hydroxymethylfurfural. *ChemPlusChem* **2012,** *77* (4), 259-272.

43. Tuck, C. O.; Perez, E.; Horvath, I. T.; Sheldon, R. A.; Poliakoff, M., Valorization of Biomass: Deriving More Value from Waste. *Science* **2012,** *337* (6095), 695-699.

44. Jae, J.; Zheng, W.; Lobo, R. F.; Vlachos, D. G., Production of Dimethylfuran from Hydroxymethylfurfural through Catalytic Transfer Hydrogenation with Ruthenium Supported on Carbon. *Chemsuschem* **2013,** *6* (7), 1158-1162.

45. Williams, C. L.; Chang, C.-C.; Phuong, D.; Nikbin, N.; Caratzoulas, S.; Vlachos, D. G.; Lobo, R. F.; Fan, W.; Dauenhauer, P. J., Cycloaddition of Biomass-Derived Furans for Catalytic Production of Renewable p-Xylene. *ACS Catalysis* **2012,** *2* (6), 935-939.

46. Nikbin, N.; Do, P. T.; Caratzoulas, S.; Lobo, R. F.; Dauenhauer, P. J.; Vlachos, D. G., A DFT study of the acid-catalyzed conversion of 2,5-dimethylfuran and ethylene to p-xylene. *Journal of Catalysis* **2013,** *297*, 35-43.

47. Chang, C.-C.; Green, S. K.; Williams, C. L.; Dauenhauer, P. J.; Fan, W., Ultra-selective cycloaddition of dimethylfuran for renewable p-xylene with H-BEA. *Green Chemistry* **2013**.

48. Wang, D.; Osmundsen, C. M.; Taarning, E.; Dumesic, J. A., Selective Production of Aromatics from Alkylfurans over Solid Acid Catalysts. *Chemcatchem* **2013,** *5* (7), 2044-2050.

49. Brandvold, T. A. Carbohydrate route to para-xylene and terephthalic acid. US 8,314,267 B2, 2012.

50. Alamillo, R.; Tucker, M.; Chia, M.; Pagan-Torres, Y.; Dumesic, J., The selective hydrogenation of biomass-derived 5-hydroxymethylfurfural using heterogeneous catalysts. *Green Chemistry* **2012,** *14* (5), 1413-1419.

51. Leonard, R., Levulinic Acid as a Basic Chemical Raw Material. *Industrial & Engineering Chemistry* **1956,** *48* (8), 1330-1341.

52. Bozell, J. J.; Moens, L.; Elliott, D. C.; Wang, Y.; Neuenscwander, G. G.; Fitzpatrick, S. W.; Bilski, R. J.; Jarnefeld, J. L., Production of levulinic acid and use as a platform chemical for derived products. *Resources, Conservation and Recycling* **2000,** *28*, 227-239.

53. Elliott, D. C.; Frye, J. G. Hydrogenated 5-carbon compound and method of making. 5883266, 1999.

54. Bozell, J. J., Connecting Biomass and Petroleum Processing with a Chemical Bridge. *Science* **2010,** *329* (5991), 522-523.

55. Heeres, H.; Handana, R.; Chunai, D.; Borromeus Rasrendra, C.; Girisuta, B.; Jan Heeres, H., Combined dehydration/(transfer)-hydrogenation of C6-sugars (D-glucose and D-fructose) to γ-valerolactone using ruthenium catalysts. *Green Chemistry* **2009,** *11* (8), 1247-1255.

56. Deng, L.; Zhao, Y.; Li, J.; Fu, Y.; Liao, B.; Guo, Q.-X., Conversion of Levulinic Acid and Formic Acid into γ-Valerolactone over Heterogeneous Catalysts. *ChemSusChem* **2010,** *3* (10), 1172-1175.

57. Horvath, I. T.; Mehdi, H.; Fabos, V.; Boda, L.; Mika, L. T., γ-Valerolactone-a sustainable liquid for energy and carbon-based chemicals. *Green Chemistry* **2008,** *10* (2), 238-242.

58. Lange, J.-P.; Price, R.; Ayoub, P. M.; Louis, J.; Petrus, L.; Clarke, L.; Gosselink, H., Valeric Biofuels: A Platform of Cellulosic Transportation Fuels. *Angewandte Chemie International Edition* **2010,** *49* (26), 4479-4483.

59. Bond, J. Q.; Alonso, D. M.; Wang, D.; West, R. M.; Dumesic, J. A., Integrated Catalytic Conversion of γ-Valerolactone to Liquid Alkenes for Transportation Fuels. *Science* **2010,** *327* (5969), 1110-1114.

60. Leger, F.; Hibbert, H., The conversion of furfuryl alcohol to levulinic acid. *Canadian Journal of Research, Section B: Chemical Sciences* **1938,** *16* (B), 68-69.

61. Timokhin, B. V.; Baransky, V. A.; Eliseeva, G. D., Levulinic acid in organic synthesis. *Russian Chemical Reviews* **1999,** *68* (1), 73-84.

62. Farone, W. A.; Cuzens, J. E. Method for the Production of Levulinic Acid and its Derivatives. 6054611, 2000.

63. Cha, J. Y.; Hanna, M. A., Levulinic acid production based on extrusion and pressurized batch reaction. *Industrial Crops and Products* **2002,** *16* (2), 109-118.

64. Fang, Q.; Hanna, M. A., Experimental studies for levulinic acid production from whole kernel grain sorghum. *Bioresource Technology* **2002,** *81* (3), 187-192.

65. Yan, L.; Yang, N.; Pang, H.; Liao, B., Production of Levulinic Acid from Bagasse and Paddy Straw by Liquefaction in the Presence of Hydrochloride Acid. *CLEAN – Soil, Air, Water* **2008,** *36* (2), 158-163.

66. Peng, L.; Lin, L.; Zhang, J.; Zhuang, J.; Zhang, B.; Gong, Y., Catalytic Conversion of Cellulose to Levulinic Acid by Metal Chlorides. *Molecules* **2010,** *15* (8), 5258-5272.

67. Girisuta, B. Levulinic Acid from Lignocellulosic Biomass. University of Groningen, Groningen, 2007.

68. Rackemann, D. W.; Doherty, W. O. S., The conversion of lignocellulosics to levulinic acid. *Biofuels, Bioproducts and Biorefining* **2011,** *5* (2), 198-214.

69. Williams, D. L.; Dunlop, A. P., Kinetics of Furfural Destruction in Acidic Aqueous Media. *Industrial and Engineering Chemistry* **1948,** *40* (2), 239-241.

70. Rose, I. C.; Epstein, N.; Watkinson, A. P., Acid-Catalyzed 2-Furaldehyde (Furfural) Decomposition Kinetics. *Ind. Eng. Chem. Res.* **2000,** *39*, 843-845.

71. Jing, Q.; LÜ, X., Kinetics of Non-catalyzed Decomposition of D-xylose in High Temperature Liquid Water. *Chinese Journal of Chemical Engineering* **2007,** *15* (5), 666-669.

72. Garrett, E. R.; Dvorchik, B. H., Kinetics and Mechanisms of the Acid Degradation of the Aldopentoses to Furfural. *Journal of Pharmaceutical Sciences* **1969,** *58* (7), 813-820.

73. Montane, D.; Salvado, J.; Torras, C.; Farriol, X., High-temperature dilute-acid hydrolysis of olive stones for furfural production. *Biomass and Bioenergy* **2002,** *22*, 295-304.

74. Zeitsch, K. J. Process for the manufacture of furfural. WO 0047569, 2000.

75. Vlachos, D. G.; Caratzoulas, S., The roles of catalysis and reaction engineering in overcoming the energy and the environment crisis. *Chemical Engineering Science* **2010,** *65* (1), 18-29.

76. Trimble, F.; Dunlop, A. P., Recovery of Furfural from Aqueous Solutions. *Industrial and Engineering Chemistry, Analytical Edition* **1940,** *12* (12), 721-722.

77. Conway, J. B.; Philip, J. B., Ternary System: Furfural-Methyl Isobutyl Ketone-Water at 25 ^{o}C. *Industrial and Engineering Chemistry* **1953,** *45* (5), 1083-1085.

78. Cope, A. C. Production and Recovery of Furans. US 2917520, 1959.

79. Rivalier, P.; Duhamet, J.; Moreau, C.; Durand, R., Development of a continuous catalytic heterogeneous column reactor with simultaneous extraction of an intermediate product by an organic solvent circulating in countercurrent manner with the aqueous phase. *Catalysis Today* **1995,** *24* (1-2), 165-171.

80. Sako, T.; Sugeta, T.; Nakazawa, N.; Okubo, T.; Sato, M.; Taguchi, T.; Hiaki, T., Kinetic Study of Furfural Formation Accompanying Supercritical Carbon Dioxide Extraction. *Journal of Chemical Engineering of Japan* **1992,** *25* (4), 372-377.

81. Qi, X.; Watanabe, M.; Aida, T. M.; Smith, R. L., Jr., Catalytic dehydration of fructose into 5-hydroxymethylfurfural by ion-exchange resin in mixed-aqueous system by microwave heating. *Green Chemistry* **2008,** *10*, 799-805.

82. Zhao, Z.; Li, C. Preparation of 5-hydroxymethyl furfural in ionic liquid under microwave radiation. 101456851 (A), 2009.

83. Gedye, R.; Smith, F.; Westaway, K.; Ali, H.; Baldisera, L.; Laberge, L.; Rousell, J., The Use of Microwave Ovens for Rapid Organic Synthesis. *Tetrahedron Letters* **1986,** *27* (3), 279-282.

84. Das, S. K., Application of Microwave Irradiation in the Synthesis of Carbohydrates. *Synlett* **2004,** *6*, 915-932.

85. Hoz, A.; Diaz-Ortiz, A.; Moreno, A., Microwaves in organic synthesis. Thermal and non-thermal microwave effects. *Chemical Society Reviews* **2005,** *34*, 164-178.

86. Qi, X.; Watanabe, M.; Aida, T. M.; Smith, R. L., Jr., Efficient process for conversion of fructose to 5-hydroxymethylfurfural with ionic liquids. *Green Chemistry* **2009,** *11*, 1327-1331.

87. Qi, X.; Watanabe, M.; Aida, T. M.; Smith, R. L., Jr., Efficient Catalytic Conversion of Fructose into 5-Hydroxymethylfurfural in Ionic Liquids at Room Temperature. *ChemSusChem* **2009,** *2*, 944-946.

88. Zakrzewska, M. E.; Bogel-Lukasik, E.; Bogel-Lukasik, R., Solubility of Carbohydrates in Ionic Liquids. *Energy Fuels* **2010,** *24*, 737-745.

89. Gronnow, M. J.; White, R. J.; Clark, J. H.; Macquarrie, D. J., Energy Efficiency in Chemical Reactions: A Comparative Study of Different Reaction Techniques. *Organic Process Research & Development* **2005,** *9* (4), 516-518.

90. Weingarten, R.; Cho, J.; Conner, W. C.; Huber, G. W., Kinetics of Furfural Production by Dehydration of Xylose in a Biphasic Reactor with Microwave Heating. *Green Chemistry* **2010,** *12* (8), 1423-1429.

91. Dunlop, A. P., Furfural Formation and Behavior. *Industrial and Engineering Chemistry* **1948,** *40* (2), 204-209.

92. Root, D. F.; Saeman, J. F.; Harris, J. F.; Neill, W. K., Kinetics of the Acid-Catalyzed Conversion of Xylose to Furfural. *Forest Products Journal* **1959,** *9*, 158-165.

93. Oefner, P. J.; Lanziner, A. H.; Bonn, G.; Bobleter, O., Quantitative Studies on Furfural and Organic Acid Formation during Hydrothermal, Acidic and Alkaline Degradation of D-Xylose. *Monatshefte fur Chemie* **1992,** *123* (6), 547-556.

94. Conner, W. C.; Tompsett, G. A., How Could and Do Microwaves Influence Chemistry at Interfaces? *Journal of Physical Chemistry B* **2008,** *112*, 2110-2118.

95. Antal, M. J.; Leesomboon, T.; Mok, W. S.; Richards, G. N., Mechanism of formation of 2-furaldehyde from D-xylose. *Carbohydrate Research* **1991,** *217*, 71-85.

96. Dias, A. S.; Pillinger, M.; Valente, A. A., Liquid phase dehydration of d-xylose in the presence of Keggin-type heteropolyacids. *Applied Catalysis A: General* **2005,** *285* (1-2), 126-131.

97. Dias, A. S.; Pillinger, M.; Valente, A. A., Dehydration of xylose into furfural over micro-mesoporous sulfonic acid catalysts. *Journal of Catalysis* **2005,** *229* (2), 414-423.

98. Dias, A. S.; Pillinger, M.; Valente, A. A., Mesoporous silica-supported 12-tungstophosphoric acid catalysts for the liquid phase dehydration of d-xylose. *Microporous and Mesoporous Materials* **2006,** *94* (1-3), 214-225.

99. Dias, A.; Lima, S.; Brandão, P.; Pillinger, M.; Rocha, J.; Valente, A., Liquid-phase Dehydration of D-xylose over Microporous and Mesoporous Niobium Silicates. *Catalysis Letters* **2006,** *108* (3), 179-186.

100. Lima, S.; Antunes, M. M.; Fernandes, A.; Pillinger, M.; Ribeiro, M. F.; Valente, A. A., Acid-Catalysed Conversion of Saccharides into Furanic Aldehydes in the Presence of Three-Dimensional Mesoporous Al-TUD-1. *Molecules* **2010,** *15* (6), 3863-3877.

101. Dias, A. S.; Lima, S.; Carriazo, D.; Rives, V.; Pillinger, M.; Valente, A. A., Exfoliated titanate, niobate and titanoniobate nanosheets as solid acid catalysts for the liquid-phase dehydration of d-xylose into furfural. *Journal of Catalysis* **2006,** *244* (2), 230-237.

102. Dias, A.; Lima, S.; Pillinger, M.; Valente, A., Modified versions of sulfated zirconia as catalysts for the conversion of xylose to furfural. *Catalysis Letters* **2007,** *114* (3), 151-160.

103. Lima, S.; Fernandes, A.; Antunes, M.; Pillinger, M.; Ribeiro, F.; Valente, A., Dehydration of Xylose into Furfural in the Presence of Crystalline Microporous Silicoaluminophosphates. *Catalysis Letters* **2010,** *135* (1), 41-47.

104. Gürbüz, E. I.; Gallo, J. M. R.; Alonso, D. M.; Wettstein, S. G.; Lim, W. Y.; Dumesic, J. A., Conversion of Hemicellulose into Furfural Using Solid Acid Catalysts in gamma-Valerolactone. *Angewandte Chemie-International Edition* **2013,** *52* (4), 1270-1274.

105. Gallo, J. M. R.; Alonso, D. M.; Mellmer, M. A.; Yeap, J. H.; Wong, H. C.; Dumesic, J. A., Production of Furfural from Lignocellulosic Biomass Using Beta Zeolite and Biomass-Derived Solvent. *Topics in Catalysis* **2013,** *56* (18-20), 1775-1781.

106. Agirrezabal-Telleria, I.; Requies, J.; Guemez, M. B.; Arias, P. L., Dehydration of D-xylose to furfural using selective and hydrothermally stable arenesulfonic SBA-15 catalysts. *Applied Catalysis B-Environmental* **2014,** *145*, 34-42.

107. Karinen, R.; Vilonen, K.; Niemela, M., Biorefining: Heterogeneously Catalyzed Reactions of Carbohydrates for the Production of Furfural and Hydroxymethylfurfural. *ChemSusChem* **2011,** *4* (8), 1002-1016.

108. Brown, G. E.; Henrich, V. E.; Casey, W. H.; Clark, D. L.; Eggleston, C.; Felmy, A.; Goodman, D. W.; Gratzel, M.; Maciel, G.; McCarthy, M. I.; Nealson, K. H.; Sverjensky, D. A.; Toney, M. F.; Zachara, J. M., Metal Oxide Surfaces and Their Interactions with Aqueous Solutions and Microbial Organisms. *Chemical Reviews* **1998,** *99* (1), 77-174.

109. James, R. O., Characterization of Colloids in Aqueous Systems. *Advances in Ceramics* **1987,** *21*, 349-410.

110. Franks, G. V.; Gan, Y., Charging Behavior at the Alumina-Water Interface and Implications for Ceramic Processing. *Journal of the American Ceramic Society* **2007,** *90* (11), 3373-3388.

111. Parks, G. A., The Isoelectric Points of Solid Oxides, Solid Hydroxides, and Aqueous Hydroxo Complex Systems. *Chemical Reviews* **1965,** *65* (2), 177-198.

112. Kosmulski, M., The pH-Dependent Surface Charging and the Points of Zero Charge. *Journal of Colloid and Interface Science* **2002,** *253* (1), 77-87.

113. Kosmulski, M., pH-dependent surface charging and points of zero charge II. Update. *Journal of Colloid and Interface Science* **2004,** *275* (1), 214-224.

114. Kosmulski, M., pH-dependent surface charging and points of zero charge: III. Update. *Journal of Colloid and Interface Science* **2006,** *298* (2), 730-741.

115. Kosmulski, M., pH-dependent surface charging and points of zero charge. IV. Update and new approach. *Journal of Colloid and Interface Science* **2009,** *337* (2), 439-448.

116. Kosmulski, M., Compilation of PZC and IEP of sparingly soluble metal oxides and hydroxides from literature. *Advances in Colloid and Interface Science* **2009,** *152* (1-2), 14-25.

117. Barton, D. G.; Shtein, M.; Wilson, R. D.; Soled, S. L.; Iglesia, E., Structure and Electronic Properties of Solid Acids Based on Tungsten Oxide Nanostructures. *The Journal of Physical Chemistry B* **1999,** *103* (4), 630-640.

118. Kasprzyk-Hordern, B., Chemistry of alumina, reactions in aqueous solution and its application in water treatment. *Advances in Colloid and Interface Science* **2004,** *110* (1-2), 19-48.

119. Glazneva, T. S.; Kotsarenko, N. S.; Paukshtis, E. A., Surface Acidity and Basicity of Oxide Catalysts: From Aqueous Suspensions to In Situ Measurements. *Kinetics and Catalysis* **2008,** *49* (6), 859-867.

120. Forni, L., Comparison of the Methods for the Determination of Surface Acidity of Solid Catalysts *Catalysis Reviews* **1973,** *8* (1), 65-115.

121. Benesi, H. A.; Winquist, B. H. C., Surface acidity of solid catalysts. In *Advances In Catalysis*, Academic Press, Inc.: New York, 1978; Vol. 27, pp 97-182.

122. Moliner, M.; Román-Leshkov, Y.; Davis, M. E., Tin-containing zeolites are highly active catalysts for the isomerization of glucose in water. *Proceedings of the National Academy of Sciences* **2010,** *107* (14), 6164-6168.

123. Kulkarni, A. P.; Muggli, D. S., The effect of water on the acidity of TiO2 and sulfated titania. *Applied Catalysis A: General* **2006,** *302* (2), 274-282.

124. Ranjan, R.; Thust, S.; Gounaris, C. E.; Woo, M.; Floudas, C. A.; Keitz, M. v.; Valentas, K. J.; Wei, J.; Tsapatsis, M., Adsorption of fermentation inhibitors from lignocellulosic biomass hydrolyzates for improved ethanol yield and value-added product recovery. *Microporous and Mesoporous Materials* **2009,** *122* (1-3), 143-148.

125. Okuhara, T., Water-Tolerant Solid Acid Catalysts. *Chemical Reviews* **2002,** *102* (10), 3641-3666.

126. Grenall, A., Montmorillonite Cracking Catalyst. *Industrial and Engineering Chemistry* **1949,** *41* (7), 1485-1489.

127. Plank, C. J., Activity of Silica-Alumina Cracking Catalysts. *Analytical Chemistry* **1952,** *24* (8), 1304-1306.

128. Holm, V. C. F.; Bailey, G. C.; Clark, A., Acidity Studies of Silica-Alumina Catalysts. *The Journal of Physical Chemistry* **1959,** *63* (2), 129-133.

129. Matsumura, Y.; Hagiwara, S.; Takahashi, H., Automatic Potentiometric Titration of Surface Acidity of Carbon Black. *Carbon* **1976,** *14*, 163-167.

130. Neffe, S., Evaluation of the pH-metric method for the determination of acidic groups on the surface of oxidized carbons. *Carbon* **1987,** *25* (3), 441-443.

131. Tanabe, K., *Solid Acids and Bases: their catalytic properties*. Kodansha Scientific Books: Tokyo, 1970; p 175.

132. Kamiya, Y.; Sakata, S.; Yoshinaga, Y.; Ohnishi, R.; Okuhara, T., Zirconium phosphate with a high surface area as a water-tolerant solid acid. *Catalysis Letters* **2004,** *94* (1-2), 45-47.

133. Rao, K. N.; Sridhar, A.; Lee, A. F.; Tavener, S. J.; Young, N. A.; Wilson, K., Zirconium phosphate supported tungsten oxide solid acid catalysts for the esterification of palmitic acid. *Green Chemistry* **2006,** *8* (9), 790-797.

134. Pavlova, S. N.; Sadykov, V. A.; Zabolotnaya, G. V.; Kochubey, D. I.; Maximovskaya, R. I.; Zaikovskii, V. I.; Kriventsov, V. V.; Tsybulya, S. V.; Burgina, E. B.; Volodin, A. M.; Chaikina, M. V.; Kuznetsova, N. N.; Lunin, V. V.; Agrawal, D.; Roy, R., The novel acid catalysts -- framework zirconium phosphates: the bulk and surface structure. *Journal of Molecular Catalysis A: Chemical* **2000,** *158* (1), 319-323.

135. Ross-Medgaarden, E. I.; Knowles, W. V.; Kim, T.; Wong, M. S.; Zhou, W.; Kiely, C. J.; Wachs, I. E., New insights into the nature of the acidic catalytic active sites present in ZrO2-supported tungsten oxide catalysts. *Journal of Catalysis* **2008,** *256* (1), 108-125.

136. Zhou, W.; Ross-Medgaarden, E. I.; Knowles, W. V.; Wong, M. S.; Wachs, I. E.; Kiely, C. J., Identification of active Zr-WO_x clusters on a ZrO_2 support for solid acid catalysts. *Nature Chemistry* **2009,** *1* (9), 722-728.

137. Shimizu, K.; Venkatraman, T. N.; Song, W., NMR study of tungstated zirconia catalyst: acidic properties of tungstated zirconia and influence of tungsten loading. *Applied Catalysis A: General* **2002,** *224* (1-2), 77-87.

138. Harmer, M. A.; Farneth, W. E.; Sun, Q., High Surface Area Nafion Resin/Silica Nanocomposites: A New Class of Solid Acid Catalyst. *Journal of the American Chemical Society* **1996,** *118* (33), 7708-7715.

139. Molnar, A., Nafion-Silica Nanocomposites: A New Generation of Water-Tolerant Solid Acids of High Efficiency. *Current Organic Chemistry* **2008,** *12*, 159-181.

140. Weingarten, R.; Tompsett, G. A.; Conner Jr, W. C.; Huber, G. W., Design of solid acid catalysts for aqueous-phase dehydration of carbohydrates: The role of Lewis and Brønsted acid sites. *Journal of Catalysis* **2011,** *279* (1), 174-182.

141. Woolery, G. L.; Kuehl, G. H.; Timken, H. C.; Chester, A. W.; Vartuli, J. C., On the nature of framework Brønsted and Lewis acid sites in ZSM-5. *Zeolites* **1997,** *19* (4), 288-296.

142. Brunner, E., Characterization of solid acids by spectroscopy. *Catalysis Today* **1997,** *38* (3), 361-376.

143. Kondo, J. N.; Nishitani, R.; Yoda, E.; Yokoi, T.; Tatsumi, T.; Domen, K., A comparative IR characterization of acidic sites on HY zeolite by pyridine and CO probes with silica-alumina and γ-alumina references. *Physical Chemistry Chemical Physics* **2010,** *12* (37), 11576-11586.

144. Török, B.; Kiricsi, I.; Molnár, Á.; Olah, G. A., Acidity and Catalytic Activity of a Nafion-H/Silica Nanocomposite Catalyst Compared with a Silica-Supported Nafion Sample. *Journal of Catalysis* **2000,** *193* (1), 132-138.

145. Onda, A.; Ochi, T.; Yanagisawa, K., Selective hydrolysis of cellulose into glucose over solid acid catalysts. *Green Chemistry* **2008,** *10*, 1033-1037.

146. Li, N.; Tompsett, G. A.; Huber, G. W., Renewable High-Octane Gasoline by Aqueous-Phase Hydrodeoxygenation of C5 and C6 Carbohydrates over Pt/Zirconium Phosphate Catalysts. *ChemSusChem* **2010,** *3* (10), 1154-1157.

147. Niu, F.; Hofmann, H., Activity and deactivation behavior of various zeolite catalysts. *Applied Catalysis A: General* **1995,** *128* (1), 107-118.

148. Corma, A.; Garcia, H., Lewis Acids: From Conventional Homogeneous to Green Homogeneous and Heterogeneous Catalysis. *Chemical Reviews* **2003,** *103* (11), 4307-4365.

149. Siril, P. F.; Cross, H. E.; Brown, D. R., New polystyrene sulfonic acid resin catalysts with enhanced acidic and catalytic properties. *Journal of Molecular Catalysis A: Chemical* **2008,** *279* (1), 63-68.

150. Alonso, D. M.; Bond, J. Q.; Serrano-Ruiz, J. C.; Dumesic, J. A., Production of liquid hydrocarbon transportation fuels by oligomerization of biomass-derived C_9 alkenes. *Green Chemistry* **2010,** *12*, 992-999.

151. Harmer, M. A.; Sun, Q., Solid acid catalysis using ion-exchange resins. *Applied Catalysis A: General* **2001,** *221* (1-2), 45-62.

152. Chai, S.-H.; Wang, H.-P.; Liang, Y.; Xu, B.-Q., Sustainable production of acrolein: investigation of solid acid-base catalysts for gas-phase dehydration of glycerol. *Green Chemistry* **2007,** *9* (10), 1130-1136.

153. Islam, A. M.; Saad, S. M.; Aboul-Fetouh, M. S.; Sakran, M. A., Study of Furfural Fromation by Acid Hydrolysis of Rice-Hulls. *Holzforschung* **1973,** *27* (4), 117-123.

154. Kunitake, T.; Yamaguchi, K.; Aso, C., Polymerization of aromatic aldehydes, 9. Cationic copolymerization of furfural and vinyl ethers. *Die Makromolekulare Chemie* **1973,** *172* (1), 85-96.

155. Lourvanij, K.; Rorrer, G. L., Reactions of aqueous glucose solutions over solid-acid Y-zeolite catalyst at 110-160 .degree.C. *Industrial & Engineering Chemistry Research* **1993,** *32* (1), 11-19.

156. Lourvanij, K.; Rorrer, G. L., Dehydration of glucose to organic acids in microporous pillared clay catalysts. *Applied Catalysis A: General* **1994,** *109* (1), 147-165.

157. Lourvanij, K.; Rorrer, G. L., Reaction Rates for the Partial Dehydration of Glucose to Organic Acids in Solid-Acid, Molecular-Sieving Catalyst Powders. *Journal of Chemical Technology & Biotechnology* **1997,** *69* (1), 35-44.

158. Choudhary, V.; Pinar, A. B.; Sandler, S. I.; Vlachos, D. G.; Lobo, R. F., Xylose Isomerization to Xylulose and its Dehydration to Furfural in Aqueous Media. *ACS Catalysis* **2011,** *1* (12), 1724-1728.

159. Choudhary, V.; Caratzoulas, S.; Vlachos, D. G., Insights into the isomerization of xylose to xylulose and lyxose by a Lewis acid catalyst. *Carbohydrate Research* **2013,** *368*, 89-95.

160. Choudhary, V.; Sandler, S. I.; Vlachos, D. G., Conversion of Xylose to Furfural Using Lewis and Bronsted Acid Catalysts in Aqueous Media. *ACS Catalysis* **2012,** *2* (9), 2022-2028.

161. Xing, R.; Qi, W.; Huber, G. W., Production of furfural and carboxylic acids from waste aqueous hemicellulose solutions from the pulp and paper and cellulosic ethanol industries. *Energy & Environmental Science* **2011,** *4* (6), 2193-2205.

162. Cinlar, B. Acid Catalyzed Carbohydrate Degradation and Dehydration. Iowa State University, Ames, 2010.

163. Fitzpatrick, S. W. Lignocellulose Degradation to Furfural and Levulinic Acid. 4897497, 1990.

164. Fitzpatrick, S. W. Production of Levulinic Acid From Carbohydrate-Containing Materials. 5608105, 1997.

165. Saeman, J. F., Kinetics of Wood Saccharification - Hydrolysis of Cellulose and Decomposition of Sugars in Dilute Acid at High Temperature. *Industrial & Engineering Chemistry* **1945,** *37* (1), 43-52.

166. Heimlich, K. R.; Martin, A. N., A Kinetic Study of Glucose Degradation in Acid Solution. *Journal of the American Pharmaceutical Association, Scientific Edition* **1960,** *49* (9), 592-597.

167. McKibbins, S. W.; Harris, J. F.; Saeman, J. F.; Neill, W. K., Kinetics of the acid-catalyzed conversion of D-glucose to 5-hydroxymethyl-2-furaldehyde and levulinic acid. *Forest Products Journal* **1962,** *12*, 17-23.

168. Singh, B.; Dean, G. R.; Cantor, S. M., The Role of 5-(Hydroxymethyl)-furfural in the Discoloration of Sugar Solutions. *Journal of the American Chemical Society* **1948,** *70* (2), 517-522.

169. Chang, C.; Ma, X.; Cen, P., Kinetics of Levulinic Acid Formation from Glucose Decomposition at High Temperature. *Chinese Journal of Chemical Engineering* **2006,** *14* (5), 708-712.

170. Girisuta, B.; Janssen, L. P. B. M.; Heeres, H. J., A kinetic study on the decomposition of 5-hydroxymethylfurfural into levulinic acid. *Green Chemistry* **2006,** *8* (8), 701-709.

171. Girisuta, B.; Janssen, L. P. B. M.; Heeres, H. J., Green Chemicals: A Kinetic Study on the Conversion of Glucose to Levulinic Acid. *Chemical Engineering Research and Design* **2006,** *84* (5), 339-349.

172. Girisuta, B.; Janssen, L. P. B. M.; Heeres, H. J., Kinetic Study on the Acid-Catalyzed Hydrolysis of Cellulose to Levulinic Acid. *Industrial & Engineering Chemistry Research* **2007,** *46* (6), 1696-1708.

173. Jing, Q.; LÜ, X., Kinetics of Non-catalyzed Decomposition of Glucose in High-temperature Liquid Water. *Chinese Journal of Chemical Engineering* **2008,** *16* (6), 890-894.

174. Shen, J. C.; Wyman, C. E., Hydrochloric Acid-Catalyzed Levulinic Acid Formation from Cellulose: Data and Kinetic Model to Maximize Yields. *Aiche Journal* **2012,** *58* (1), 236-246.

175. Weingarten, R.; Cho, J.; Xing, R.; Conner, W. C.; Huber, G. W., Kinetics and Reaction Engineering of Levulinic Acid Production from Aqueous Glucose Solutions. *Chemsuschem* **2012,** *5* (7), 1280-1290.

176. Horvat, J.; Klaic, B.; Metelko, B.; Sunjic, V., Mechanism of levulinic acid formation. *Tetrahedron Letters* **1985,** *26* (17), 2111-2114.

177. Horvat, J.; Klaic, B.; Metelko, B.; Sunjic, V., Mechanism of levulinic acid formation in acid catalysed hydrolysis of 2-hydroxymethylfurane and 5-hydroxymethylfurane-2-carbaldehyde. *Croatica Chemica Acta* **1986,** *59* (2), 429-438.

178. Baugh, K. D.; McCarty, P. L., Thermochemical pretreatment of lignocellulose to enhance methane fermentation: I. Monosaccharide and furfurals hydrothermal decomposition and product formation rates. *Biotechnology and Bioengineering* **1988,** *31* (1), 50-61.

179. Bienkowski, P. R.; Ladisch, M. R.; Narayan, R.; Tsao, G. T.; Eckert, R., Correlation of glucose (dextrose) degradation at 90 to 190^{o}C in 0.4 to 20% acid. *Chemical Engineering Communications* **1987,** *51* (1), 179-192.

180. Kato, K.; Doihara, T.; Sakai, F.; Takahashi, N., Thermal degradation of D-glucose. Identification of furfural and acetaldehyde. *Kenkyu Hokoku - Nippon Senbai Kosha Chuo Kenkyusho* **1966,** *108*, 361-364.

181. Ohnishi, A.; Kato, K.; Takagi, E., Curie-Point Pyrolysis of Cellulose. *Polymer Journal* **1975,** *7* (4), 431-437.

182. Krishna, R.; Kallury, M. R.; Ambidge, C.; Tidwell, T. T.; Boocock, D. G. B.; Agblevor, F. A.; Stewart, D. J., Rapid hydrothermolysis of cellulose and related carbohydrates. *Carbohydrate Research* **1986,** *158* (1), 253-261.

183. Luijkx, G. C. A.; Rantwijk, F. v.; Bekkum, H. v., Hydrothermal formation of 1,2,4-benzenetriol from 5-hydroxymethyl-2-furaldehyde and D-fructose. *Carbohydrate Research* **1993,** *242* (1), 131-139.

184. Smith, P. C.; Grethlein, H. E.; Converse, A. O., Glucose decomposition at high temperature, mild acid, and short residence times. *Solar Energy* **1982,** *28* (1), 41-48.

185. Dam, H. E. v.; Kieboom, A. P. G.; Bekkum, H. v., The conversion of fructose and glucose in acidic media: Formation of hydroxymethylfurfural. *Starch* **1986,** *38* (3), 95-101.

186. Xiang, Q.; Lee, Y.; Torget, R., Kinetics of glucose decomposition during dilute-acid hydrolysis of lignocellulosic biomass. *Applied Biochemistry and Biotechnology* **2004,** *115* (1), 1127-1138.

187. Harris, D. W.; Feather, M. S., Studies on the mechanism of the interconversion of D-glucose, D-mannose, and D-fructose in acid solution. *Journal of the American Chemical Society* **1975,** *97* (1), 178-181.

188. Binder, J. B.; Cefali, A. V.; Blank, J. J.; Raines, R. T., Mechanistic insights on the conversion of sugars into 5-hydroxymethylfurfural. *Energy & Environmental Science* **2010,** *3* (6), 765-771.

189. Román-Leshkov, Y.; Moliner, M.; Labinger, J. A.; Davis, M. E., Mechanism of Glucose Isomerization Using a Solid Lewis Acid Catalyst in Water. *Angewandte Chemie International Edition* **2010,** *49* (47), 8954-8957.

190. Nikolla, E.; Román-Leshkov, Y.; Moliner, M.; Davis, M. E., "One-Pot" Synthesis of 5-(Hydroxymethyl)furfural from Carbohydrates using Tin-Beta Zeolite. *ACS Catalysis* **2011,** *1* (4), 408-410.

191. Kuster, B. F. M.; Temmink, H. M. G., The dehydration of D-fructose (formation of 5-hydroxymethyl-2-furaldehyde and levulinic acid): Part IV. The influence of pH and weak-acid anions on the dehydration of D-fructose *Carbohydrate Research* **1977,** *54* (2), 185-191.

192. Perez Locas, C.; Yaylayan, V. A., Isotope Labeling Studies on the Formation of 5-(Hydroxymethyl)-2-furaldehyde (HMF) from Sucrose by Pyrolysis-GC/MS. *Journal of Agricultural and Food Chemistry* **2008,** *56* (15), 6717-6723.

193. Anet, E. F. L. J., Degradation of carbohydrates. Part 2. The action of acid and alkali on 3-deoxyhexosones. *Australian Journal of Chemistry* **1961,** *14* (2), 295-301.

194. Assary, R. S.; Redfern, P. C.; Hammond, J. R.; Greeley, J.; Curtiss, L. A., Computational Studies of the Thermochemistry for Conversion of Glucose to Levulinic Acid. *The Journal of Physical Chemistry B* **2010,** *114* (27), 9002-9009.

195. Chidambaram, M.; Bell, A. T., A two-step approach for the catalytic conversion of glucose to 2,5-dimethylfuran in ionic liquids. *Green Chemistry* **2010,** *12* (7), 1253-1262.

196. Antal, M. J.; Mok, W. S. L.; Richards, G. N., Kinetic studies of the reactions of ketoses and aldoses in water at high temperature. Part 1. Mechanism of formation of 5-(hydroxymethyl)-2-furaldehyde from D-fructose and sucrose. *Carbohydrate Research* **1990,** *199* (1), 91-109.

197. Assary, R. S.; Redfern, P. C.; Greeley, J.; Curtiss, L. A., Mechanistic Insights into the Decomposition of Fructose to Hydroxy Methyl Furfural in Neutral and Acidic Environments Using High-Level Quantum Chemical Methods. *The Journal of Physical Chemistry B* **2011,** *115* (15), 4341-4349.

198. Caratzoulas, S.; Vlachos, D. G., Converting fructose to 5-hydroxymethylfurfural: a quantum mechanics/molecular mechanics study of the mechanism and energetics. *Carbohydrate Research* **2011,** *346* (5), 664-672.

199. Kato, K.; Komorita, H., Pyrolysis of Cellulose. Part V. Isolation and identification of 3-Deoxyglycosones produced from D-glucose, D-xylose and alpha-cellulose by heating. *Agricultural and Biological Chemistry* **1968,** *32* (6), 715-720.

200. Srokol, Z.; Bouche, A.-G.; van Estrik, A.; Strik, R. C. J.; Maschmeyer, T.; Peters, J. A., Hydrothermal upgrading of biomass to biofuel; studies on some monosaccharide model compounds. *Carbohydrate Research* **2004,** *339* (10), 1717-1726.

201. Fagan, R. D.; Grethlein, H. E.; Converse, A. O.; Porteous, A., Kinetics of the acid hydrolysis of cellulose found in paper refuse. *Environmental Science & Technology* **1971,** *5* (6), 545-547.

202. Hayes, D. J.; Fitzpatrick, S.; Hayes, M. H. B.; Ross, J. R. H., *The Biofine Process – Production of Levulinic Acid, Furfural, and Formic Acid from Lignocellulosic Feedstocks*. Wiley-VCH Verlag GmbH: 2008; p 139-164.

203. Pagán-Torres, Y. J.; Wang, T.; Gallo, J. M. R.; Shanks, B. H.; Dumesic, J. A., Production of 5-Hydroxymethylfurfural from Glucose Using a Combination of Lewis and Brønsted Acid Catalysts in Water in a Biphasic Reactor with an Alkylphenol Solvent. *ACS Catalysis* **2012,** *2* (6), 930-934.

204. Wang, T.; Pagán-Torres, Y.; Combs, E.; Dumesic, J.; Shanks, B., Water-Compatible Lewis Acid-Catalyzed Conversion of Carbohydrates to 5-Hydroxymethylfurfural in a Biphasic Solvent System. *Topics in Catalysis* **2012**, 1-6.

205. Weingarten, R.; Kim, Y. T.; Tompsett, G. A.; Fernandez, A.; Han, K. S.; Hagaman, E. W.; Conner, W. C.; Dumesic, J. A.; Huber, G. W., Conversion of glucose into levulinic acid with solid metal(IV) phosphate catalysts. *Journal of Catalysis* **2013,** *304*, 123-134.

206. Jow, J.; Rorrer, G. L.; Hawley, M. C.; Lamport, D. T. A., Dehydration of D-Fructose to Levulinic Acid over LZY Zeolite Catalyst. *Biomass* **1987,** *14* (3), 185-194.

207. Wang, P.; Zhan, S.; Yu, H., Production of Levulinic Acid from Cellulose Catalyzed by Environmental-Friendly Catalyst. *Advanced Materials Research* **2010,** *96*, 183-187.

208. Rataboul, F.; Essayem, N., Cellulose Reactivity in Supercritical Methanol in the Presence of Solid Acid Catalysts: Direct Synthesis of Methyl-levulinate. *Industrial & Engineering Chemistry Research* **2011,** *50* (2), 799-805.

209. Peng, L.; Lin, L.; Zhang, J.; Shi, J.; Liu, S., Solid acid catalyzed glucose conversion to ethyl levulinate. *Applied Catalysis A: General* **2011,** *397* (1-2), 259-265.

210. Clearfield, A.; Thakur, D. S., The Acidity of Zirconium Phosphates in Relation to Their Activity in the Dehydration of Cyclohexanol. *Journal of Catalysis* **1980,** *65* (1), 185-194.

211. Ginestra, A. L.; Patrono, P.; Berardelli, M. L.; Galli, P.; Ferragini, C.; Massucci, M. A., Catalytic Activity of Zirconium Phosphate and Some Derived Phases in the Dehydration of Alcohols and Isomerization of Butenes. *Journal of Catalysis* **1987,** *103* (2), 346-356.

212. Johnstone, R. A. W.; Liu, J.-Y.; Whittaker, D., Mechanism of cyclohexanol dehydration catalysed by zirconium phosphate. *Journal of the Chemical Society, Perkin Transactions 2* **1998,** *6*, 1287-1288.

213. Patel, S. M.; Chudasama, U. V.; Ganeshpure, P. A., Metal (IV) phosphates as solid acid catalysts for selective cyclodehydration of 1,n-diols. *Green Chemistry* **2001,** *3*, 143-145.

214. Clearfield, A.; Thakur, D. S., Zirconium and Titanium Phosphates as Catalysts: A Review. *Applied Catalysis* **1986,** *26* (1), 1-26.

215. Ginestra, A. L.; Patrono, P., Acidic Properties of Germanium, Titanium, Zirconium and Tin Phosphates and Arsenates. *Materials Chemistry and Physics* **1987,** *17* (1), 161-179.

216. Patel, S. M.; Chudasama, U. V.; Ganeshpure, P. A., Cyclodehydration of 1,4-Butanediol Catalyzed by Metal(IV) Phosphates. *Reaction Kinetics and Catalysis Letters* **2002,** *76* (2), 317-325.

217. Jimenez-Jimenez, J.; Merida-Robles, J.; Rodriguez-Castellon, E.; Jimenez-Lopez, A.; Lopez Granados, M.; del Val, S.; Melian Cabrera, I.; Fierro, J. L. G., Oxidation of o-xylene on mesoporous Ti-phosphate-supported VOx catalysts and promoter effect of K^+ on selectivity. *Catalysis Today* **2005,** *99* (1-2), 179-186.

218. Srilakshmi, C.; Ramesh, K.; Nagaraju, P.; Lingaiah, N.; Prasad, P. S. S., Studies on preparation, characterization and ammoxidation functionality of zirconium phosphate-supported V_2O_5 catalysts. *Catalysis Letters* **2006,** *106* (3-4), 115-122.

219. Carlini, C.; Giuttari, M.; Maria Raspolli Galletti, A.; Sbrana, G.; Armaroli, T.; Busca, G., Selective saccharides dehydration to 5-hydroxymethyl-2-furaldehyde by heterogeneous niobium catalysts. *Applied Catalysis A: General* **1999,** *183* (2), 295-302.

220. Armaroli, T.; Busca, G.; Carlini, C.; Giuttari, M.; Raspolli Galletti, A. M.; Sbrana, G., Acid sites characterization of niobium phosphate catalysts and their activity in fructose dehydration to 5-hydroxymethyl-2-furaldehyde. *Journal of Molecular Catalysis A: Chemical* **2000,** *151* (1-2), 233-243.

221. Benvenuti, F.; Carlini, C.; Patrono, P.; Raspolli Galletti, A. M.; Sbrana, G.; Massucci, M. A.; Galli, P., Heterogeneous zirconium and titanium catalysts for the selective synthesis of 5-hydroxymethyl-2-furaldehyde from carbohydrates. *Applied Catalysis A: General* **2000,** *193* (1-2), 147-153.

222. Carlini, C.; Patrono, P.; Galletti, A. M. R.; Sbrana, G., Heterogeneous catalysts based on vanadyl phosphate for fructose dehydration to 5-hydroxymethyl-2-furaldehyde. *Applied Catalysis A: General* **2004,** *275* (1-2), 111-118.

223. Gu, M.; Yu, D.; Zhang, H.; Sun, P.; Huang, H., Metal (IV) Phosphates as Solid Catalysts for Selective Dehydration of Sorbitol to Isosorbide. *Catalysis Letters* **2009,** *133* (1), 214-220.

224. Li, N.; Tompsett, G. A.; Zhang, T.; Shi, J.; Wyman, C. E.; Huber, G. W., Renewable gasoline from aqueous phase hydrodeoxygenation of aqueous sugar solutions prepared by hydrolysis of maple wood. *Green Chemistry* **2011,** *13* (1), 91-101.

225. Asghari, F. S.; Yoshida, H., Dehydration of fructose to 5-hydroxymethylfurfural in sub-critical water over heterogeneous zirconium phosphate catalysts. *Carbohydrate Research* **2006,** *341* (14), 2379-2387.

226. West, R. M.; Braden, D. J.; Dumesic, J. A., Dehydration of butanol to butene over solid acid catalysts in hing water environments. *Journal of Catalysis* **2009,** *262*, 134-143.

227. Pagán-Torres, Y. J.; Gallo, J. M. R.; Wang, D.; Pham, H. N.; Libera, J. A.; Marshall, C. L.; Elam, J. W.; Datye, A. K.; Dumesic, J. A., Synthesis of Highly Ordered Hydrothermally Stable Mesoporous Niobia Catalysts by Atomic Layer Deposition. *ACS Catalysis* **2011,** *1* (10), 1234-1245.

228. Hattori, T.; Ishiguro, A.; Murakami, Y., Acidity of crystalline zirconium phosphate. *Journal of Inorganic and Nuclear Chemistry* **1978,** *40* (6), 1107-1111.

229. Sinhamahapatra, A.; Sutradhar, N.; Roy, B.; Tarafdar, A.; Bajaj, H. C.; Panda, A. B., Mesoporous zirconium phosphate catalyzed reactions: Synthesis of industrially important chemicals in solvent-free conditions. *Applied Catalysis A: General* **2010,** *385* (1-2), 22-30.

230. Spielbauer, D.; Mekhemer, G. A. H.; Riemer, T.; Zaki, M. I.; Knözinger, H., Structure and Acidic Properties of Phosphate-Modified Zirconia. *The Journal of Physical Chemistry B* **1997,** *101* (23), 4681-4688.

231. Kresnawahjuesa, O.; Gorte, R. J.; Olivera, D. d.; Lau, L. Y., A simple, inexpensive, amd reliable method for measuring Brønsted-acid site densities in solid acids *Catalysis Letters* **2002,** *82* (3-4), 155-160.

232. Tittensor, J. G.; Gorte, R. J.; Chapman, D. M., Isopropylamine adsorption for the characterization of acid sites in silica-alumina catalysts. *Journal of Catalysis* **1992,** *138* (2), 714-720.

233. Gorte, R. J., What do we know about the acidity of solid acids? *Catalysis Letters* **1999,** *62* (1), 1-13.

234. Mishra, H. K.; Parida, K. M., Studies on sulphated zirconia: synthesis, physico-chemical characterisation and n-butane isomerisation activity. *Applied Catalysis A: General* **2002,** *224* (1-2), 179-189.

235. Ciesla, U.; Stucky, G.; Schiith, F.; L. Bonneviot, F. B. C. D. S. G.; Kaliaguine, S., Improvement of the Thermal Stability of Mesostructured Metal Oxides with Zirconia as the Example. In *Studies in Surface Science and Catalysis*, Elsevier: 1998; Vol. Volume 117, pp 527-534.

236. Pinto, R. R.; Borges, P.; Lemos, M. A. N. D. A.; Lemos, F.; Védrine, J. C.; Derouane, E. G.; Ribeiro, F. R., Correlating NH_3-TPD and ^1H MAS NMR measurements of zeolite acidity: proposal of an acidity scale. *Applied Catalysis A: General* **2005,** *284* (1-2), 39-46.

237. Batamack, P.; Dorémieux-Morin, C.; Vincent, R.; Fraissard, J., Wide-line ^{1}H NMR: a new application for the study of Brønsted acidity strength of solids with HY zeolite as example. *Chemical Physics Letters* **1991,** *180* (6), 545-550.

238. Batamack, P.; Dorémieux-Morin, C.; Vincent, R.; Fraissard, J., Broad-line proton NMR: a new application for studying the Broensted acid strength of solids. *The Journal of Physical Chemistry* **1993,** *97* (38), 9779-9783.

239. Heeribout, L.; Semmer, V.; Batamack, P.; Dorémieux-Morin, C.; Vincent, R.; Fraissard, J., Brønsted acid strength of solids studied by ^{1}H NMR: establishing the scale; influence of Lewis acid sites. In *Studies in Surface Science and Catalysis*, Elsevier: 1996; Vol. Volume 101, pp 831-840.

240. Semmer, V.; Batamack, P.; Dorémieux-Morin, C.; Vincent, R.; Fraissard, J., The Acid Strength of Sulfated Zirconia Measured by Two ^{1}H NMR Techniques in the Presence of Water: 4 K Broad-Line and 300 K High Resolution MAS. *Journal of Catalysis* **1996,** *161* (1), 186-193.

241. Heeribout, L.; Semmer, V.; Batamack, P.; Dorémieux-Morin, C.; Fraissard, J., Brønsted acid strength of zeolites studied by ^{1}H NMR: scaling, influence of defects. *Microporous and Mesoporous Materials* **1998,** *21* (4-6), 565-570.

242. Semmer-Herlédan, V.; Heeribout, L.; Batamack, P.; Dorémieux-Morin, C.; Fraissard, J.; Gola, A.; Benazzi, E., Comparison of the acid strength of dealuminated H-faujasites determined by ^{1}H NMR after water adsorption. *Microporous and Mesoporous Materials* **2000,** *34* (2), 157-169.

243. Sun, Y.; Afanasiev, P.; Vrinat, M.; Coudurier, G., Porous zirconium phosphates prepared by surfactant-assisted precipitation. *Journal of Materials Chemistry* **2000,** *10* (10), 2320-2324.

244. Liu, W.; Song, Z.; Ikegawa, T.; Nishiguchi, H.; Ishihara, T.; Takita, Y., Two step synthesis and characterization of thermally stable hexagonal zirconium phosphate. *Materials Letters* **2004,** *58* (26), 3328-3331.

245. Zhao, G. L.; Yuan, Z. Y.; Chen, T. H., Synthesis of amorphous supermicroporous zirconium phosphate materials by nonionic surfactant templating. *Materials Research Bulletin* **2005,** *40* (11), 1922-1928.

246. Jiménez-Jiménez, J.; Maireles-Torres, P.; Olivera-Pastor, P.; Rodríguez-Castellón, E.; Jiménez-López, A.; Jones, D. J.; Rozière, J., Surfactant-Assisted Synthesis of a Mesoporous Form of Zirconium Phosphate with Acidic Properties. *Advanced Materials* **1998,** *10* (10), 812-815.

247. Segawa, K.-I.; Kurusu, Y.; Nakajima, Y.; Kinoshita, M., Characterization of crystalline zirconium phosphates and their isomerization activities. *Journal of Catalysis* **1985,** *94* (2), 491-500.

248. Segawa, K.-I.; Nakajima, Y.; Nakata, S.-I.; Asaoka, S.; Takahashi, H., ^{31}P-MASNMR Spectroscopic studies with zirconium phosphate catalysts. *Journal of Catalysis* **1986,** *101* (1), 81-89.

249. Yuan, Z.-Y.; Ren, T.-Z.; Azioune, A.; Pireaux, J.-J.; Su, B.-L., Marvelous self-assembly of hierarchically nanostructured porous zirconium phosphate solid acids with high thermal stability. *Catalysis Today* **2005,** *105* (3-4), 647-654.

250. Puziy, A. M.; Poddubnaya, O. I.; Ziatdinov, A. M., On the chemical structure of phosphorus compounds in phosphoric acid-activated carbon. *Applied Surface Science* **2006,** *252* (23), 8036-8038.

251. Colón, J. L.; Thakur, D. S.; Yang, C.-Y.; Clearfield, A.; Martin, C. R., X-Ray Photoelectron Spectroscopy and Catalytic Activity of α–Zirconium Phosphate and Zirconium Phosphate Sulfophenylphosphonate. *Journal of Catalysis* **1990,** *124* (1), 148-159.

252. Holm, M. S.; Pagan-Torres, Y. J.; Saravanamurugan, S.; Riisager, A.; Dumesic, J. A.; Taarning, E., Sn-Beta catalysed conversion of hemicellulosic sugars. *Green Chemistry* **2012,** *14* (3), 702-706.

253. Chambon, F.; Rataboul, F.; Pinel, C.; Cabiac, A.; Guillon, E.; Essayem, N., Cellulose hydrothermal conversion promoted by heterogeneous Brønsted and Lewis acids: Remarkable efficiency of solid Lewis acids to produce lactic acid. *Applied Catalysis B: Environmental* **2011,** *105* (1-2), 171-181.

254. Holm, M. S.; Saravanamurugan, S.; Taarning, E., Conversion of Sugars to Lactic Acid Derivatives Using Heterogeneous Zeotype Catalysts. *Science* **2010,** *328* (5978), 602-605.

255. Weingarten, R.; Conner Jr, W. C.; Huber, G. W., Production of levulinic acid from cellulose by hydrothermal decomposition combined with aqueous phase dehydration with a solid acid catalyst. *Energy and Environmental Science* **2012,** *5*, 7559-7574.

256. Tran, M. T.; Gnep, N. S.; Szabo, G.; Guisnet, M., Influence of the calcination temperature on the acidic and catalytic properties of sulphated zirconia. *Applied Catalysis A: General* **1998,** *171* (2), 207-217.

257. Kellum, G. E.; Hahn, J. R., Surface area-hydroxyl correlation employing trimethylsiloxy-treated ammonium silicates. *Analytical Chemistry* **1968,** *40* (6), 952-956.

258. Tichit, D.; El Alami, D.; Figueras, F., Preparation and anion exchange properties of zirconia. *Applied Catalysis A: General* **1996,** *145* (1-2), 195-210.

259. Chuah, G. K.; Jaenicke, S.; Cheong, S. A.; Chan, K. S., The influence of preparation conditions on the surface area of zirconia. *Applied Catalysis A: General* **1996,** *145* (1-2), 267-284.

260. Yadav, G. D.; Nair, J. J., Sulfated zirconia and its modified versions as promising catalysts for industrial processes. *Microporous and Mesoporous Materials* **1999,** *33* (1-3), 1-48.

261. Jung, K. T.; Bell, A. T., The effects of synthesis and pretreatment conditions on the bulk structure and surface properties of zirconia. *Journal of Molecular Catalysis A: Chemical* **2000,** *163* (1-2), 27-42.

262. Griffith Edward, J., Factors Influencing the Chain Lengths of Inorganic Polyphosphates. In *Phosphorus Chemistry*, American Chemical Society: 1992; Vol. 486, pp 86-101.

263. Ahmed, A. I.; El-Hakam, S. A.; Samra, S. E.; El-Khouly, A. A.; Khder, A. S., Structural characterization of sulfated zirconia and their catalytic activity in dehydration of ethanol. *Colloids and Surfaces A: Physicochemical and Engineering Aspects* **2008,** *317* (1â€“3), 62-70.

264. Toor, S. S.; Rosendahl, L.; Rudolf, A., Hydrothermal liquefaction of biomass: A review of subcritical water technologies. *Energy* **2011,** *36* (5), 2328-2342.

265. Vàrhegyi, G.; Szabo, P.; Mok, W. S.-L.; Antal, M. J., Kinetics of the thermal decomposition of cellulose in sealed vessels at elevated pressures. Effects of the presence of water on the reaction mechanism. *Journal of Analytical and Applied Pyrolysis* **1993,** *26*, 159-174.

266. Deguchi, S.; Tsujii, K.; Horikoshi, K., Crystalline-to-amorphous transformation of cellulose in hot and compressed water and its implications for hydrothermal conversion. *Green Chemistry* **2008,** *10* (2), 191-196.

267. Yu, Y.; Wu, H., Understanding the Primary Liquid Products of Cellulose Hydrolysis in Hot-Compressed Water at Various Reaction Temperatures. *Energy & Fuels* **2010,** *24* (3), 1963-1971.

268. Chen, H.; Yu, B.; Jin, S., Production of levulinic acid from steam exploded rice straw via solid superacid. *Bioresource Technology* **2011,** *102* (3), 3568-3570.

269. Van de Vyver, S.; Thomas, J.; Geboers, J.; Keyzer, S.; Smet, M.; Dehaen, W.; Jacobs, P. A.; Sels, B. F., Catalytic production of levulinic acid from cellulose and other biomass-derived carbohydrates with sulfonated hyperbranched poly(arylene oxindole)s. *Energy & Environmental Science* **2011,** *4* (9), 3601-3610.

270. Lai, D.-m.; Deng, L.; Guo, Q.-x.; Fu, Y., Hydrolysis of biomass by magnetic solid acid. *Energy & Environmental Science* **2011,** *4* (9), 3552-3557.

271. Redmon, B. C. Process for the Production of Levulinic Acid. 2738367, 1956.

272. Schraufnagel, R. A.; Rase, H. F., Levulinic Acid from Sucrose Using Acidic Ion-Exchange Resins. *Product R&D* **1975,** *14* (1), 40-44.

273. Hegner, J.; Pereira, K. C.; DeBoef, B.; Lucht, B. L., Conversion of cellulose to glucose and levulinic acid via solid-supported acid catalysis. *Tetrahedron Letters* **2010,** *51* (17), 2356-2358.

274. Potvin, J.; Sorlien, E.; Hegner, J.; DeBoef, B.; Lucht, B. L., Effect of NaCl on the conversion of cellulose to glucose and levulinic acid via solid supported acid catalysis. *Tetrahedron Letters* **2011,** *52* (44), 5891-5893.

275. Patil, S. K. R.; Lund, C. R. F., Formation and Growth of Humins via Aldol Addition and Condensation during Acid-Catalyzed Conversion of 5-Hydroxymethylfurfural. *Energy & Fuels* **2011,** *25* (10), 4745-4755.

276. Abatzoglou, N.; Bouchard, J.; Chornet, E., Dilute acid depolymerization of cellulose in aqueous phase: Experimental evidence of the significant presence of soluble oligomeric intermediates. *The Canadian Journal of Chemical Engineering* **1986,** *64*, 781-786.

277. Rinaldi, R.; Palkovits, R.; Schuth, F., Depolymerization of Cellulose Using Solid Catalysts in Ionic Liquids. *Angewandte Chemie-International Edition* **2008,** *47* (42), 8047-8050.

278. Minowa, T.; Fang, Z.; Ogi, T.; Vàrhegyi, G., Decomposition of Cellulose and Glucose in Hot-Compressed Water under Catalyst-Free Conditions. *Journal of Chemical Engineering of Japan* **1998,** *31* (1), 131-134.

279. Miyazawa, T.; Ohtsu, S.; Funazukuri, T., Hydrothermal degradation of polysaccharides in a semi-batch reactor: product distribution as a function of severity parameter. *Journal of Materials Science* **2008,** *43* (7), 2447-2451.

280. Asghari, F. S.; Yoshida, H., Conversion of Japanese red pine wood (Pinus densiflora) into valuable chemicals under subcritical water conditions. *Carbohydrate Research* **2010,** *345* (1), 124-131.

281. Kumar, V.; Kothari, S. H., Effect of compressional force on the crystallinity of directly compressible cellulose excipients. *International Journal of Pharmaceutics* **1999,** *177* (2), 173-182.

282. Park, S.; Baker, J. O.; Himmel, M. E.; Parilla, P. A.; Johnson, D. K., Cellulose crystallinity index: measurement techniques and their impact on interpreting cellulase performance. *Biotechnology for Biofuels* **2010,** *3*, 1-10.

283. Akiya, N.; Savage, P. E., Roles of Water for Chemical Reactions in High-Temperature Water. *Chemical Reviews* **2002,** *102* (8), 2725-2750.

284. Yu, Y.; Lou, X.; Wu, H., Some Recent Advances in Hydrolysis of Biomass in Hot-Compressed Water and Its Comparisons with Other Hydrolysis Methodsâ€ *Energy & Fuels* **2008,** *22* (1), 46-60.

285. Bradbury, A. G. W.; Sakai, Y.; Shafizadeh, F., A kinetic model for pyrolysis of cellulose. *Journal of Applied Polymer Science* **1979,** *23* (11), 3271-3280.

286. Lin, Y. C.; Cho, J.; Tompsett, G. A.; Westmoreland, P. R.; Huber, G. W., Kinetics and Mechanism of Cellulose Pyrolysis. *J. Phys. Chem. C* **2009,** *113* (46), 20097-20107.

287. Cho, J.; Davis, J. M.; Huber, G. W., The Intrinsic Kinetics and Heats of Reactions for Cellulose Pyrolysis and Char Formation. *ChemSusChem* **2010,** *3* (10), 1162-1165.

288. Almendros, G.; Sanz, J.; Sobrados, I., Characterization of synthetic carbohydrate-derived humic-like polymers. *From Science of the Total Environment* **1989,** *81-82*, 91-98.

289. Tompsett, G. A.; Subrahmanyam, A. V.; Wang, W.; Jae, J.; Agarwal, V.; Narkeviciute, I.; Hu, W.; Shen, J.; Zhang, T.; Auerbach, S. M.; Wyman, C. E.; Huber, G. W., Characterization and Catalytic Fast Pyrolysis of Hydrolysis Humic Residue. *in preparation* **2012**.

290. Upadhye, A. A.; Qi, W.; Huber, G. W., Conceptual process design: A systematic method to evaluate and develop renewable energy technologies. *AIChE Journal* **2011,** *57* (9), 2292-2301.

291. Douglas, J. M., *Conceptual Design of Chemical Processes*. McGraw-Hill: 1988.

292. Fitzpatrick, S. W. Production of formic acid from hydrolysis of carbohydrate-containing compounds such as paper pulp and wood feedstocks. 0234638 A1, 2010.

293. *Commercialization of the Biofine Technology for levulinic acid production from paper sludge*; BioMetics, Inc.: 2002.

294. Chickos, J. S.; Jr., W. E. A., Enthalpies of Vaporization of Organic and Organometallic Compounds, 1880-2002. *Journal of Physical and Chemical Reference Data* **2003,** *32* (2), 519-878.

295. Proskouriakoff, A., Some Salts of Levulinic Acid. *Journal of the American Chemical Society* **1933,** *55* (5), 2132-2134.

296. Alonso, D. M.; Wettstein, S. G.; Bond, J. Q.; Root, T. W.; Dumesic, J. A., Production of Biofuels from Cellulose and Corn Stover Using Alkylphenol Solvents. *ChemSusChem* **2011,** *4* (8), 1078-1081.

297. Serrano-Ruiz, J. C.; Braden, D. J.; West, R. M.; Dumesic, J. A., Conversion of cellulose to hydrocarbon fuels by progressive removal of oxygen. *Applied Catalysis B: Environmental* **2010,** *100* (1-2), 184-189.

298. McLeese, D. W.; Zitko, V.; Sergeant, D. B.; Burridge, L.; Metcalfe, C. D., Lethality and accumulation of alkylphenols in aquatic fauna. *Chemosphere* **1981,** *10* (7), 723-730.

299. Warhurst, A. M. *An environmental assessment of alkylphenol ethoxylates and alkylphenols*; 1995.

300. Ertl, G.; Knozinger, H.; Weitkamp, J., *Handbook of Heterogeneous Catalysis*. 1997; Vol. 3.

301. Case, P. A.; Heiningen, A. R. P. v.; Wheeler, M. C., Liquid hydrocarbon fuels from cellulosic feedstocks via thermal deoxygenation of levulinic acid and formic acid salt mixtures. *Green Chemistry* **2012,** *14*, 85-89.

302. Daorattanachai, P.; Namuangruk, S.; Viriya-empikul, N.; Laosiripojana, N.; Faungnawakij, K., 5-Hydroxymethylfurfural production from sugars and cellulose in acid- and base-catalyzed conditions under hot compressed water. *Journal of Industrial and Engineering Chemistry* **2012,** *18* (6), 1893-1901.

303. Yin, S. D.; Pan, Y. L.; Tan, Z. C., Hydrothermal Conversion of Cellulose to 5-Hydroxymethyl Furfural. *Int. J. Green Energy* **2011,** *8* (2), 234-247.

304. Li, C.; Zhao, Z. K.; Wang, A.; Zheng, M.; Zhang, T., Production of 5-hydroxymethylfurfural in ionic liquids under high fructose concentration conditions. *Carbohydrate Research* **2010,** *345* (13), 1846-1850.

305. Binder, J. B.; Raines, R. T., Simple Chemical Transformation of Lignocellulosic Biomass into Furans for Fuels and Chemicals. *Journal of the American Chemical Society* **2009,** *131* (5), 1979-1985.

306. Zhao, H.; Holladay, J. E.; Brown, H.; Zhang, Z. C., Metal Chlorides in Ionic Liquid Solvents Convert Sugars to 5-Hydroxymethylfurfural. *Science* **2007,** *316* (5831), 1597-1600.

307. Su, Y.; Brown, H. M.; Huang, X.; Zhou, X.-d.; Amonette, J. E.; Zhang, Z. C., Single-step conversion of cellulose to 5-hydroxymethylfurfural (HMF), a versatile platform chemical. *Applied Catalysis A: General* **2009,** *361* (1–2), 117-122.

308. van Putten, R. J.; van der Waal, J. C.; de Jong, E.; Rasrendra, C. B.; Heeres, H. J.; de Vries, J. G., Hydroxymethylfurfural, A Versatile Platform Chemical Made from Renewable Resources. *Chemical Reviews* **2013,** *113* (3), 1499-1597.

309. Sen, S. M.; Binder, J. B.; Raines, R. T.; Maravelias, C. T., Conversion of biomass to sugars via ionic liquid hydrolysis: process synthesis and economic evaluation. *Biofuels, Bioproducts and Biorefining* **2012,** *6* (4), 444-452.

310. Rinaldi, R.; Schuth, F., Acid Hydrolysis of Cellulose as the Entry Point into Biorefinery Schemes. *Chemsuschem* **2009,** *2* (12), 1096-1107.

311. Zakrzewska, M. E.; Bogel-Łukasik, E.; Bogel-Łukasik, R., Ionic Liquid-Mediated Formation of 5-Hydroxymethylfurfural—A Promising Biomass-Derived Building Block. *Chemical Reviews* **2011,** *111* (2), 397-417.

312. Tan, S. S. Y.; MacFarlane, D. R., Ionic Liquids in Biomass Processing. In *Ionic Liquids*, Kirchner, B., Ed. Springer-Verlag Berlin: Berlin, 2009; Vol. 290, pp 311-339.

313. Zhang, Z.; Liu, W.; Xie, H.; Zhao, Z. K., An Unexpected Reaction between 5-Hydroxymethylfurfural and Imidazolium-Based Ionic Liquids at High Temperatures. *Molecules* **2011,** *16* (10), 8463-8474.

314. Vigier, K. D.; Benguerba, A.; Barrault, J.; Jerome, F., Conversion of fructose and inulin to 5-hydroxymethylfurfural in sustainable betaine hydrochloride-based media. *Green Chemistry* **2012,** *14* (2), 285-289.

315. Liu, F.; Barrault, J.; Vigier, K. D.; Jerome, F., Dehydration of Highly Concentrated Solutions of Fructose to 5-Hydroxymethylfurfural in a Cheap and Sustainable Choline Chloride/Carbon Dioxide System. *Chemsuschem* **2012,** *5* (7), 1223-1226.

316. Kawamoto, H.; Hatanaka, W.; Saka, S., Thermochemical conversion of cellulose in polar solvent (sulfolane) into levoglucosan and other low molecular-weight substances. *Journal of Analytical and Applied Pyrolysis* **2003,** *70* (2), 303-313.

317. Kawamoto, H.; Saito, S.; Hatanaka, W.; Saka, S., Catalytic pyrolysis of cellulose in sulfolane with some acidic catalysts. *J. Wood Sci.* **2007,** *53* (2), 127-133.

318. Helle, S.; Bennett, N. M.; Lau, K.; Matsui, J. H.; Duff, S. J. B., A kinetic model for production of glucose by hydrolysis of levoglucosan and cellobiosan from pyrolysis oil. *Carbohydrate Research* **2007,** *342* (16), 2365-2370.

319. Hu, X.; Wu, L.; Wang, Y.; Mourant, D.; Lievens, C.; Gunawan, R.; Li, C.-Z., Mediating acid-catalyzed conversion of levoglucosan into platform chemicals with various solvents. *Green Chemistry* **2012,** *14* (11), 3087-3098.

320. Cai, C. M.; Zhang, T.; Kumar, R.; Wyman, C. E., THF co-solvent enhances hydrocarbon fuel precursor yields from lignocellulosic biomass. *Green Chemistry* **2013**.

321. Yang, Y.; Hu, C. W.; Abu-Omar, M. M., Conversion of carbohydrates and lignocellulosic biomass into 5-hydroxymethylfurfural using $AlCl_3$ $6H_2O$ catalyst in a biphasic solvent system. *Green Chemistry* **2012,** *14* (2), 509-513.

322. Bicker, M.; Hirth, J.; Vogel, H., Dehydration of fructose to 5-hydroxymethylfurfural in sub- and supercritical acetone. *Green Chemistry* **2003,** *5* (2), 280-284.

323. Bicker, M.; Kaiser, D.; Ott, L.; Vogel, H., Dehydration of D-fructose to hydroxymethylfurfural in sub- and supercritical fluids. *Journal of Supercritical Fluids* **2005,** *36* (2), 118-126.

324. Wettstein, S. G.; Alonso, D. M.; Chong, Y. X.; Dumesic, J. A., Production of levulinic acid and gamma-valerolactone (GVL) from cellulose using GVL as a solvent in biphasic systems. *Energy & Environmental Science* **2012,** *5* (8), 8199-8203.

325. Wettstein, S. G.; Bond, J. Q.; Alonso, D. M.; Pham, H. N.; Datye, A. K.; Dumesic, J. A., RuSn bimetallic catalysts for selective hydrogenation of levulinic acid to gamma-valerolactone. *Applied Catalysis B-Environmental* **2012,** *117*, 321-329.

326. Alonso, D. M.; Gallo, J. M. R.; Mellmer, M. A.; Wettstein, S. G.; Dumesic, J. A., Direct conversion of cellulose to levulinic acid and gamma-valerolactone using solid acid catalysts. *Catalysis Science & Technology* **2013,** *3* (4), 927-931.

327. Alonso, D. M.; Wettstein, S. G.; Mellmer, M. A.; Gürbüz, E. I.; Dumesic, J. A., Integrated conversion of hemicellulose and cellulose from lignocellulosic biomass. *Energy & Environmental Science* **2013,** *6* (1), 76-80.

328. Horvath, I. T.; Mehdi, H.; Fabos, V.; Boda, L.; Mika, L. T., gamma-Valerolactone - a sustainable liquid for energy and carbon-based chemicals. *Green Chemistry* **2008,** *10* (2), 238-242.

329. Gallo, J. M. R.; Alonso, D. M.; Mellmer, M. A.; Dumesic, J. A., Production and upgrading of 5-hydroxymethylfurfural using heterogeneous catalysts and biomass-derived solvents. *Green Chemistry* **2013,** *15* (1), 85-90.

330. Bond, J. Q.; Wang, D.; Alonso, D. M.; Dumesic, J. A., Interconversion between γ-valerolactone and pentenoic acid combined with decarboxylation to form butene over silica/alumina. *Journal of Catalysis* **2011,** *281* (2), 290-299.

331. Kobayashi, H.; Yabushita, M.; Komanoya, T.; Hara, K.; Fujita, I.; Fukuoka, A., High-Yielding One-Pot Synthesis of Glucose from Cellulose Using Simple Activated Carbons and Trace Hydrochloric Acid. *Acs Catalysis* **2013,** *3* (4), 581-587.

332. Ohara, M.; Takagaki, A.; Nishimura, S.; Ebitani, K., Syntheses of 5-hydroxymethylfurfural and levoglucosan by selective dehydration of glucose using solid acid and base catalysts. *Applied Catalysis A: General* **2010,** *383* (1–2), 149-155.

333. Kelly, C. P.; Cramer, C. J.; Truhlar, D. G., Single-ion solvation free energies and the normal hydrogen electrode potential in methanol, acetonitrile, and dimethyl sulfoxide. *Journal of Physical Chemistry B* **2007,** *111* (2), 408-422.

334. Alonso, D. M.; Wettstein, S. G.; Dumesic, J. A., Gamma-valerolactone, a sustainable platform molecule derived from lignocellulosic biomass. *Green Chemistry* **2013,** *15* (3), 584-595.

335. Shimizu, K.-i.; Uozumi, R.; Satsuma, A., Enhanced production of hydroxymethylfurfural from fructose with solid acid catalysts by simple water removal methods. *Catalysis Communications* **2009,** *10* (14), 1849-1853.

336. Zhang, Z. H.; Wang, Q. A.; Xie, H. B.; Liu, W. J.; Zhao, Z. B., Catalytic Conversion of Carbohydrates into 5-Hydroxymethylfurfural by Germanium(IV) Chloride in Ionic Liquids. *Chemsuschem* **2011,** *4* (1), 131-138.